



COPYRIGHT AND USE OF THIS THESIS

This thesis must be used in accordance with the provisions of the Copyright Act 1968.

Reproduction of material protected by copyright may be an infringement of copyright and copyright owners may be entitled to take legal action against persons who infringe their copyright.

Section 51 (2) of the Copyright Act permits an authorized officer of a university library or archives to provide a copy (by communication or otherwise) of an unpublished thesis kept in the library or archives, to a person who satisfies the authorized officer that he or she requires the reproduction for the purposes of research or study.

The Copyright Act grants the creator of a work a number of moral rights, specifically the right of attribution, the right against false attribution and the right of integrity.

You may infringe the author's moral rights if you:

- fail to acknowledge the author of this thesis if you quote sections from the work
- attribute this thesis to another author
- subject this thesis to derogatory treatment which may prejudice the author's reputation

For further information contact the University's Copyright Service.

sydney.edu.au/copyright

A novel role for Adenomatous Polyposis Coli protein in the transport of mitochondria

A thesis submitted by
Kate May Mills

In total fulfilment of the requirements for the degree of
Doctor of Philosophy



THE UNIVERSITY OF
SYDNEY




Westmead Millennium Institute
for Medical Research

Westmead Millennium Institute
Faculty of Medicine
The University of Sydney
AUGUST 2015

Copyright Statement

To the best of my knowledge and belief, this thesis contains no material which has been accepted for the award of any other degree or diploma by another university or institute and contains no material previously published or written by another person, except where due reference has been made.



Kate May Mills

28 AUGUST 2015

Abstract

Adenomatous Polyposis Coli (APC) is a multifunctional tumour suppressor protein and a negative regulator of the β -catenin Wnt signalling pathway. APC also contributes to numerous other pathways for normal cell growth and differentiation including cell migration, mitosis, and DNA repair and replication. Mutations in the APC gene occur in ~80% of colorectal cancers (CRCs) and typically give rise to a truncated protein lacking C-terminal sequences which display altered mobility, subcellular localisation and function. APC gene mutation is one of the earliest events in the progression of inherited and sporadic CRC and initiates subsequent deregulation of key cellular pathways. Previous studies from this laboratory identified a new subcellular localisation for APC at the mitochondria, an intriguing finding given that many crucial aspects of mitochondrial function are also reported to be deregulated in carcinogenesis. In particular, the efficient distribution of mitochondria throughout the cell is essential for their ability to perform site-specific tasks including effective ATP dispersal, and there is a growing body of evidence which suggests that alterations in this process contribute to cancer progression. This thesis seeks to investigate the hypothesis that APC plays a role in the anterograde transport of mitochondria, and that this process is disrupted by CRC-associated APC mutations.

The above hypothesis is first tested and initially validated in Chapter 3, where observations from immunofluorescence microscopy of fixed cells revealed that the typical uniform spread of mitochondria throughout the cytoplasm was disrupted following siRNA-mediated loss of wild-type APC. These cells displayed a strong perinuclear accumulation of mitochondria after APC silencing, indicative of disruption to mitochondrial transport. Further analysis of other membrane bound organelles following loss of wild-type APC indicated that this phenomena was specific to mitochondria, and not a by-product of microtubule destabilisation. These findings were consolidated by the use of immunoprecipitation and proximity ligation assay protein-binding studies that revealed APC interacts at the mitochondria with Miro and Milton, crucial protein components of the primary mitochondrial transport complex.

Chapter 4 explores the implications of APC mutation on mitochondrial transport and identifies the C-terminal region of APC, commonly lost in CRC, as the Miro/Milton

binding domain. In support of this notion, analysis of fixed cells by immunofluorescence microscopy showed that C-terminal deletion of APC in mutant cell lines severely impaired mitochondrial localisation at the cell periphery. This correlated with binding studies which indicated that the association of mutant APC with Miro/Milton was compromised. Both mitochondrial distribution and the APC-Miro/Milton interaction could be recovered in CRC cell lines upon reconstitution of wild-type APC, thereby providing a direct link between APC and Miro/Milton-mediated mitochondrial localisation.

In Chapter 5, mitochondria are tracked in real time in live cells to investigate the mechanism by which APC regulates transport to the cell periphery. Compared to mitochondria in control cells, a striking decrease in anterograde motility was observed following silencing of wild-type APC. The velocity or rate of mitochondrial transport, on the other hand, remained unaffected once transport had commenced, indicating a specific role for APC in the initiation of mitochondrial transport. This finding correlates with experiments in fixed cells which demonstrated that loss of APC reduced mitochondrial localisation at dynamic regions of the cell membrane, suggesting that APC may act as a mitochondrial chaperone to deliver targeted ATP supplies to the cell periphery, possibly for cell migration. The nature of the APC-Miro/Milton interaction is examined in more detail in Chapter 6, where a series of proximity ligation assay-based protein binding studies show that both loss of wild-type APC, and APC C-terminal deletion, disrupts the association between Miro and Milton. These preliminary findings suggest that APC may stabilise the Miro/Milton interaction, potentially acting in a scaffolding capacity.

The identification of a new role for APC in the transport of mitochondria opens up a new route through which CRC-associated APC mutations may contribute to the carcinogenic process. Pathways contributing to mitochondrial dysfunction are increasingly being targeted in the treatment of numerous cancer types, and these findings could offer an additional range of protein drug targets.

Acknowledgments

Undertaking this PhD study has been an extremely challenging journey. Fortunately, it has also enabled me to meet many wonderful people whose advice, assistance and constant support have helped to get me over the finish line.

First and foremost I would like to thank my supervisor A/Prof Beric Henderson. Thank you for giving me the opportunity to undertake this PhD under your guidance in the Gene Expression group. More importantly, thanks for your constant, unwavering support throughout this journey and your ability to keep a cool head, especially when mine was not so cool. You have taught me the value of persistence and good science, and for that I am grateful. I would also like to thank my co-supervisor Dr Mariana Brocardo. Your advice, kind words and ability to help me remember the bigger picture has made the past four years more bearable.

Thank you to my fellow lab members past and present Estefania, Kamila Cara, Christina, Crystal, Manisha, Myth, Michael and Kirsty for the support, the laughs and most importantly the morning teas! I've truly enjoyed getting to know each and every one of you over the past few years. A special thanks to my fellow inmates, I mean PhD students, Dr Cara and Dr Christina, for joining me throughout this entire journey. Your ability to know exactly when to employ emergency coffee and sympathy is uncanny. I'm so grateful I got to share this experience with you.

Finally, to my friends and family, thank you for putting up with my constant whinging and helping to keep me sane. I appreciate all of you so much. Thank you for checking up on me and understanding when I cancelled on plans for the 2nd, 3rd and 4th time in a row. I am particularly thankful, to formatting wizard Tina. Your encouragement and help to make this thesis look presentable saved me from a Microsoft Word-induced rage. Lastly, to my Mum and Dad – I am eternally grateful. Thank you for your love, support and for making sure I was kept fed, watered and sheltered. I could not have done this without you.

Table of Contents

Abstract	i
Acknowledgments	iii
List of Figures	xii
List of Tables.....	xvii
List of Abbreviations.....	xviii
Chapter 1: Introduction	1
1.1 Background	2
1.2 The APC tumour suppressor protein.....	3
1.2.1 APC protein localisation, interactions and function.....	4
1.2.1.1 Regulation of APC localisation.....	5
1.2.1.2 The role of APC in Wnt Signalling	7
1.2.1.3 APC and cytoskeletal organisation	9
1.2.1.4 The role of APC in other cellular functions	12
1.2.2 APC dysfunction in colorectal cancer	13
1.2.2.1 Deregulation of Wnt signalling and proliferation	14
1.2.2.2 Cell migration.....	14
1.2.2.3 Chromosome segregation and CIN	15
1.2.2.4 Apoptosis.....	16
1.3 Mitochondria.....	16
1.3.1 Mitochondrial function.....	17
1.3.1.1 ATP production by oxidative phosphorylation	17
1.3.1.2 Calcium buffering	19
1.3.1.3 Regulation of apoptosis	19
1.3.2 Mitochondrial transport.....	20
1.3.2.1 Miro/Milton/KIF5 mitochondrial transport.....	21
1.3.2.2 Other mitochondrial transport mechanisms	25
1.3.2.3 The functional relevance of mitochondrial transport	28
1.3.3 Mitochondrial Fission/Fusion Dynamics	28
1.3.3.1 Mechanisms of fission/fusion.....	29
1.3.3.2 The functional relevance of mitochondrial fission/fusion dynamics.....	32
1.3.4 Mitochondrial dysfunction in disease.....	33
1.3.4.1 Neurodegenerative disease	34

1.3.4.2	Cancer.....	35
1.4	Rationale for study.....	36
Chapter 2: General Materials and Methods.....		38
2.1	Materials.....	39
2.1.1	Cell Lines.....	39
2.1.2	Antibodies and Dyes.....	39
2.1.3	Small interfering RNA (siRNA).....	41
2.1.4	Plasmids.....	42
2.1.5	Drugs.....	42
2.1.6	Other Reagents.....	43
2.2	Methods.....	45
2.2.1	Bacterial culture.....	45
2.2.1.1	Overnight bacterial culture.....	45
2.2.1.2	Freezing bacterial cultures as glycerol stocks.....	45
2.2.1.3	Preparation of XL10-gold or BL-21 competent cells.....	45
2.2.1.4	Heat shock transformation of XL10-gold or BL-21 cells.....	46
2.2.2	Preparation of plasmid DNA.....	46
2.2.2.1	Plasmid midi-preps.....	46
2.2.2.2	Quantification of plasmid concentration.....	47
2.2.3	Cell culture.....	47
2.2.3.1	Propagation of cell lines.....	47
2.2.3.2	Freezing cells.....	48
2.2.3.3	Reviving cells from liquid nitrogen stocks.....	48
2.2.3.4	Transfection of cell lines with plasmids or siRNA.....	48
2.2.3.5	Drug Treatments.....	50
2.2.3.6	Wound Healing Assays.....	50
2.2.4	Preparation of slides for immunofluorescence microscopy.....	51
2.2.4.1	Application of Dyes by Molecular Probes®.....	51
2.2.4.2	Standard fixation.....	51
2.2.4.3	Immunostaining.....	51
2.2.5	Acquisition by DeltaVision microscopy.....	52
2.2.5.1	Fixed Cell.....	52
2.2.5.2	Live Cell.....	52
2.2.6	Localisation assays.....	52

2.2.6.1	Preparation of cells	52
2.2.6.2	Analysis of localisation	52
2.2.7	Mitochondrial distribution and morphology assays	53
2.2.7.1	Preparation of cells	53
2.2.7.2	Analysis of mitochondrial distribution.....	53
2.2.7.3	Analysis of mitochondrial morphology.....	55
2.2.8	Duolink Proximity Ligation Assay (PLA)	55
2.2.8.1	Rationale.....	55
2.2.8.2	Preparation and fixation of cells for Duolink PLA	56
2.2.8.3	Duolink PLA	57
2.2.8.4	Duolink PLA with ectopically expressed GFP-tagged constructs	57
2.2.8.5	Immunostaining after Duolink PLA.....	58
2.2.8.6	Analysis and quantification of Duolink PLA.....	58
2.2.9	SDS-PAGE and Western Blot analysis of proteins.....	58
2.2.9.1	Protein extraction	58
2.2.9.2	Quantification of protein cell lysates	59
2.2.9.3	Resolving proteins by SDS-PAGE.....	59
2.2.9.4	Resolving proteins by SDS-Agarose gel electrophoresis.....	60
2.2.9.5	Western blot transfer – Acrylamide Gel.....	60
2.2.9.6	Western blot transfer – Agarose Gel	61
2.2.9.7	Immunoblotting	61
2.2.9.8	Immunodetection by ECL	62
2.2.10	Detection of protein interactions by immunoprecipitation (IP)	62
2.2.10.1	Protein extraction for immunoprecipitation	62
2.2.10.2	Preparation of protein A-sepharose beads.....	62
2.2.10.3	Addition of primary antibody.....	62
2.2.10.4	Addition of beads	63
2.2.10.5	Resolving and developing immunoprecipitation.....	63
2.2.11	Statistics and Graphs	63
2.2.11.1	Statistical Analysis	63
2.2.11.2	Graphs	63

Chapter 3: APC associates with the Miro/Milton mitochondrial transport complex.....	69
3.1 Introduction.....	71
3.2 Methods.....	73
3.2.1 Cell culture	73
3.2.2 Cell fixation and staining for immunofluorescence microscopy.....	73
3.2.3 Immunofluorescence cell image acquisition and processing	73
3.2.4 Quantification of cell organelle distribution	74
3.2.4.1 Quantification of mitochondrial distribution.....	74
3.2.5 Drug treatments	75
3.2.6 Immunoprecipitation assays	75
3.2.7 Western blot analysis.....	76
3.2.8 Duolink Proximity Ligation Assay (PLA)	76
3.2.9 Graphs and statistics	77
3.3 Results.....	78
3.3.1 Loss of wild-type APC alters the cellular distribution of mitochondria but not of other microtubule-associated organelles	78
3.3.2 Loss of wild-type APC induces a redistribution of mitochondria from the cell membrane to the perinuclear region.....	78
3.3.3 Destruction of the microtubule network by nocodazole induces a redistribution of mitochondria towards the perinuclear region, similar to that caused by loss of APC.....	82
3.3.4 Mitochondrial redistribution following loss of APC is specific, and not due to microtubule destabilisation.....	84
3.3.5 Mitochondria and APC co-localise with a number of potential co-factors including the Miro/Milton mitochondrial transport complex	85
3.3.6 Specificity of Miro-1 and Milton-2 antibodies.....	89
3.3.7 APC interacts with the Miro/Milton mitochondrial transport complex	89
3.3.8 APC/Miro and APC/Milton complexes localise to the mitochondria ...	92
3.4 Discussion	96
3.4.1 APC has a novel and specific role in the subcellular localisation of mitochondria.....	96
3.4.2 Evidence for APC transport of mitochondria along microtubules	97
3.4.3 APC interacts with the Miro/Milton mitochondrial transport complex to move mitochondria in the anterograde direction.....	99
3.4.4 Summary	100

3.5	Supplementary Figures	101
-----	-----------------------------	-----

Chapter 4: Cancer mutations disrupt binding of APC to Miro/Milton and		
impair mitochondrial transport.....		105
4.1	Introduction.....	107
4.2	Methods.....	109
4.2.1	Cell culture	109
4.2.2	Cell fixation and staining for immunofluorescence microscopy.....	109
4.2.3	Immunofluorescence cell image acquisition and processing	110
4.2.4	Quantification of mitochondrial distribution.....	110
4.2.5	Immunoprecipitation assays	110
4.2.6	Western blot analysis.....	111
4.2.7	Duolink Proximity Ligation Assay (PLA)	111
4.2.8	Graphs and statistics	112
4.3	Results.....	113
4.3.1	APC dependent relocalisation of mitochondria is disrupted by truncating APC mutations in colorectal cancer cell lines.....	113
4.3.2	Mitochondrial localisation towards the plasma membrane is rescued by reconstitution of wild-type APC in mutant APC HT-29 cells.....	115
4.3.3	C-terminal truncating mutations disrupt APC binding to Miro/Milton	117
4.3.4	The Miro-binding region maps to the C-terminal amino acids (2650-2843) of APC	121
4.3.5	The APC C-terminal sequence also binds to Milton.....	125
4.3.6	Overexpression of the C-terminal region of APC partially disrupts mitochondrial transport.	126
4.3.7	Overexpression of APC(2650-2843) does not disrupt the interaction between endogenous APC and Miro.	127
4.4	Discussion	129
4.4.1	Truncating APC mutations disrupt the interaction between APC and the Miro/Milton complex inhibiting mitochondrial transport	129
4.4.2	Identification of a C-terminal sequence that mediates binding of APC to Miro/Milton	131
4.4.3	Disruption of mitochondrial transport by APC truncation may contribute to the CRC tumour cell phenotype.....	132
4.4.3.1	Mis-regulated ATP targeting by disruption of mitochondrial transport may contribute to CRC carcinogenesis	133

4.4.3.2	Disruption of mitochondrial transport may contribute to aberrant calcium signalling in CRC carcinogenesis.....	134
4.4.3.3	Perinuclear clustering of mitochondria may contribute to aberrant gene transcription in CRC carcinogenesis.....	135
4.4.4	Summary	135
4.5	Supplementary Figures	137

Chapter 5: APC stimulates the initiation of mitochondrial transport to the cell

	periphery	144
5.1	Introduction.....	146
5.2	Methods.....	148
5.2.1	Cell culture	148
5.2.2	Wound Healing.....	148
5.2.3	Cell fixation and staining for immunofluorescence microscopy.....	148
5.2.4	Fixed cell immunofluorescence cell image acquisition and processing.....	149
5.2.5	Live cell imaging acquisition and analysis.....	149
5.2.6	Western blot analysis.....	151
5.2.7	Graphs and statistics	151
5.3	Results.....	152
5.3.1	Loss of APC slows cell migration	152
5.3.2	Mitochondrial localisation at extended cellular protrusions of actively migrating cells is significantly reduced upon loss of APC....	153
5.3.3	Optimisation of imaging mitochondria movement in living cells.....	156
5.3.3.1	Visualisation of mitochondria and image capture.....	156
5.3.3.2	Optimisation of transfection in cells at 90% confluence.....	157
5.3.4	Measurements of mitochondrial velocity in sub-confluent NIH 3T3 cells are comparable to those in the literature	158
5.3.5	Loss of APC decreases initiation of mitochondrial transport.....	159
5.3.6	Loss of APC does not slow the rate of mitochondrial transport	163
5.4	Discussion	165
5.4.1	APC appears to stimulate the initiation, rather than the velocity, of anterograde mitochondrial transport	165
5.4.2	APC stimulates transport of mitochondria to cell membrane protrusions and the leading edge: Implications for cell migration.	167
5.4.2.1	APC may target mitochondrial ATP to cellular protrusions and the leading edge to supply energy for cell migration	168

5.4.3	APC mutation may contribute to aberrant cell migration in CRC through disruption of mitochondrial transport	169
5.5	Supplementary Figures	172
5.6	Supplementary Videos	174

Chapter 6: APC promotes the formation of the mitochondrial transport complex

	by stabilising Miro/Milton	176
6.1	Introduction	178
6.2	Methods	180
6.2.1	Cell culture	180
6.2.2	Drug Treatments	180
6.2.3	Cell fixation and staining for immunofluorescence microscopy	180
6.2.4	Immunofluorescence cell image acquisition and processing	181
6.2.5	Live cell imaging acquisition and analysis	181
6.2.6	Immunoprecipitation assays	181
6.2.7	Western blot analysis	181
6.2.8	Duolink Proximity Ligation Assay (PLA)	182
6.2.9	Graphs and statistics	182
6.3	Results	183
6.3.1	Full-length APC is not required for the ability of Milton to interact with KIF5	183
6.3.2	Loss of APC diminishes the GFP Miro-1/Milton interaction	185
6.3.3	APC truncation correlates with loss of the Miro/Milton interaction ...	187
6.3.4	Loss of APC does not alter the expression or mitochondrial localisation of Miro or Milton	189
6.3.5	Calcimycin treatment inhibits mitochondrial transport without altering the localisation of Miro, Milton and APC at the mitochondria	189
6.3.6	Calcimycin treatment does not alter APC localisation at microtubule clusters	192
6.3.7	Calcimycin treatment does not alter the APC-Miro interaction	193
6.4	Discussion	195
6.4.1	Evidence to support a role for APC in regulating the interaction between Miro and Milton	195
6.4.1.1	Possible involvement of APC in Miro/Milton post-translational modification pathways	198

6.4.2	APC regulation of the Miro/Milton mitochondrial transport complex is not calcium dependent.	199
6.5	Supplementary Figures	201
Chapter 7: General Overview and Discussion		206
7.1	APC is a novel regulator of the Miro/Milton mitochondrial pathway	207
7.1.1	APC may interact with a post-translationally modified form of Miro.	209
7.2	APC truncation disrupts mitochondrial transport	210
7.3	Disruption of mitochondrial transport may contribute to CRC	211
7.4	Other Implications for APC in mitochondrial transport	212
7.4.1	Regulation of CNS structure and function.	212
7.4.2	Regulation of development	213
7.5	APC as a potential regulator of other mitochondrial transport pathways	213
7.5.1	APC and RanBP2	213
7.5.2	APC and other kinesin pathways.....	215
7.5.3	Myosin.....	215
7.6	APC in mitochondrial morphology.....	216
7.6.1	APC knockdown causes changes in mitochondrial morphology	216
7.6.2	Binding studies	217
7.7	Future direction, clinical implications and conclusion	217
7.8	Supplementary Figures	219
References		225

List of Figures

Chapter 1

Figure 1.1: Functional domains and protein binding sites of the APC tumour suppressor.	4
Figure 1.2: APC localisation to distinct sub-cellular compartments is altered by C-terminal truncating mutations.	5
Figure 1.3: The Wnt signalling pathway.....	8
Figure 1.4: Functional roles of mitochondria.....	18
Figure 1.5: Miro/Milton mitochondrial transport complex binding and modification domains.	22
Figure 1.6: Mechanisms of mitochondrial fission and fusion.....	29
Figure 2.1: Mitochondrial distribution scoring method.	54
Figure 2.2: Mitochondrial morphology scoring method.	55
Figure 2.3: Rationale for Duolink PLA	56
Figure 3.1: Loss of APC alters transport of select microtubule associated organelles. ..	80
Figure 3.2: Loss of wild-type APC induces a redistribution of mitochondria in U2OS, HDF1314 and NIH 3T3 cells.	81
Figure 3.3: Nocodazole but not latrunculin A treatment induces a redistribution of mitochondria in U2OS cells.	83
Figure 3.4: Loss of microtubule cap protein EB1 does not induce mitochondrial redistribution in HDF1314 cells.....	84
Figure 3.5: Mitochondrial colocalisation with potential co-factors in U2OS cells.....	86
Figure 3.6: APC colocalisation with potential co-factors in U2OS cells.....	88
Figure 3.7: APC interacts with the Miro/Milton mitochondrial transport complex in U2OS and Hela cells	91
Figure 3.8: APC interacts with Miro at mitochondria in U2OS and Hela cells.....	94
Figure 3.9: APC interacts with Milton at mitochondria in U2OS and Hela cells.....	95
Figure 4.1: Loss of truncated APC in colon cancer cell lines does not induce redistribution of mitochondria.....	115
Figure 4.2: Reconstitution of GFP APC-WT expression in HT-29 cells restores mitochondrial distribution to the cell periphery.....	116

Figure 4.3: Truncated APC does not interact with the Miro/Milton complex in colon cancer cell lines	119
Figure 4.4: Overexpression of GFP APC-WT in SW480 cells restores the APC/Miro interaction as measured by Duolink.....	120
Figure 4.5: The Miro-binding domain of APC maps to the C-terminal sequences by Duolink.....	123
Figure 4.6: The C-terminal sequences of APC are confirmed to interact with Miro by immunoprecipitation and localise to the mitochondria.....	124
Figure 4.7: The C-terminal sequences of APC also interact with Milton by Duolink PLA.	125
Figure 4.8: The overexpression of APC(2650-2843) partially disrupts mitochondrial distribution.	126
Figure 4.9: Overexpression of APC(2650-2843) does not interrupt the endogenous APC/Miro interaction.....	128
Figure 4.10: Model.....	130
Figure 5.1: Loss of APC slows cell migration in NIH 3T3 cells	152
Figure 5.2: APC and mitochondria co-localise with components of the cell cytoskeleton at cell membrane protrusions in NIH 3T3 cells.	154
Figure 5.3: Loss of APC reduces mitochondrial localisation at cellular protrusions....	155
Figure 5.4: Loss of APC reduced the initiation of anterograde mitochondrial transport in NIH 3T3 cells.....	161
Figure 5.5: Loss of APC disrupts mitochondrial motility.....	163
Figure 5.6: Loss of APC has no effect on mitochondrial velocity once transport is initiated.....	164
Figure 6.1: Evidence that APC is not required for the ability of Milton to interact with KIF5	185
Figure 6.2: Loss of APC disrupts the interaction between GFP Miro-1 and Milton in U2OS cells by Duolink	187
Figure 6.3: Miro does not interact with Milton in SW480 mutant APC cells	188
Figure 6.4: Loss of APC does not alter mitochondrial localisation or expression of Miro or Milton in U2OS cells	190
Figure 6.5: Treatment with calcimycin (20 μ M) inhibits mitochondrial transport.....	191
Figure 6.6: Calcimycin treatment does not alter mitochondrial localisation or expression of Miro, Milton or APC in U2OS cells	192

Figure 6.7: Calcimycin treatment does not alter APC localisation at microtubule clusters in U2OS cells	193
Figure 6.8: Calcimycin treatment does not alter the APC-Miro interaction by Duolink	194
Figure 6.9: The Miro/Milton mitochondrial transport complex.....	197
Figure 7.1: APC truncation impairs formation of the Miro/Milton/KIF5 motor complex, preventing anterograde transport of mitochondria.....	208
Supplementary Figure S2.1: Duolink Negative controls	66
Supplementary Figure S2.2: Duolink Positive Control - APC interacts with β -Catenin	67
Supplementary Figure S2.3: Ectopic Duolink positive control - GFP APC(1379-2080) interacts with β -Catenin.	68
Supplementary Figure S3.1: Loss of APC effects transport of select microtubule associated organelles.....	101
Supplementary Figure S3.2: Loss of wild-type APC induces a redistribution of mitochondria in U2OS stained with HSP70	101
Supplementary Figure S3.3: Miro-1 and Milton-2 antibodies are not homolog specific.	102
Supplementary Figure S3.4: Additional immunoprecipitation blots - GFP Miro-1 and GFP Milton-2 can be immunoprecipitated using an APC antibody	102
Supplementary Figure S3.5: APC interacts with Miro and Milton in U2OS and Hela Cells - Expanded Duolink Data	103
Supplementary Figure S3.6: Loss of APC decreases the APC/Miro Duolink PLA signal in U2OS cells.	104
Supplementary Figure S4.1: APC and regulators of mitochondrial dynamics in colon cancer cell lines.....	137
Supplementary Figure S4.2: APC antibodies can immunoprecipitate Miro and Milton in wild-type inducible HEK293 cells, but not mutant inducible HEK293 cells	138
Supplementary Figure S4.3: Truncated APC does not interact with the Miro/Milton complex - Expanded Duolink PLA data	139
Supplementary Figure S4.4: Reconstitution of GFP APC-WT into SW480 cells restores the APC/Miro interaction by Duolink - Expanded Duolink PLA Data	140
Supplementary Figure S4.5: GFP APC-WT but not GFP APC-1309 interacts with Miro in U2OS cells by Duolink PLA.....	141

Supplementary Figure S4.6: The C-terminal sequences of APC interact with Miro – Expanded Duolink PLA Data	142
Supplementary Figure S4.7: The C-terminal sequences of APC interact with Milton – Expanded Duolink PLA Data	143
Supplementary Figure S4.8: Overexpression of APC C-terminal sequences does not interrupt the endogenous APC/Miro interaction – Expanded Duolink PLA Data.....	143
Supplementary Figure S5.1: Mitochondria co-localise with components of the cell cytoskeleton at cell membrane protrusions in HDF1314 cells.....	172
Supplementary Figure S5.2: Mitochondrial tracking in sub-confluent NIH 3T3 cells.	173
Supplementary Figure S5.3: Loss of APC does not alter mitochondrial transport velocity in 3T3 cells.....	173
Supplementary Figure S6.1: Milton interacts with KIF5 in APC wild-type and mutant cell lines by Duolink– expanded Duolink data	201
Supplementary Figure S6.2: Loss of APC disrupts the interaction between GFP Miro-1 and Milton in U2OS cells – expanded Duolink data.....	202
Supplementary Figure S6.3: Immunoprecipitation assays suggest that loss of APC in U2OS cells may disrupt the interaction between Miro and Milton	203
Supplementary Figure S6.4: GFP Miro-1 does not interact with Milton in SW480 mutant APC cells – expanded Duolink data	203
Supplementary Figure S6.5: Miro does not interact with Milton in SW480 mutant APC cells by IP – longer time points.....	204
Supplementary Figure S6.6: Calcimycin treatment does not alter the APC-Miro interaction – Expanded Duolink Data.....	205
Supplementary Figure S7.1: APC and Milton may bind to a post-translationally modified form of Miro.....	219
Supplementary Figure S7.2: Loss of RanBP2 induces redistribution of mitochondria in U2OS and SW480 cells.....	220
Supplementary Figure S7.3: RanBP2 does not interact with Miro by Duolink PLA. ..	221
Supplementary Figure S7.4: APC/RanBP2 immunocomplexes do not localise to mitochondria.	222
Supplementary Figure S7.5: Loss of wild-type, but not truncated APC induces fragmentation of mitochondria.....	223
Supplementary Figure S7.6: APC does not interact with key regulators of mitochondrial fission and fusion by Duolink PLA.....	224

List of Tables

Chapter 1

Table 1.1: Interactions of APC with Wnt proteins.....	8
Table 1.2: Cytoskeletal interactions of APC.....	10
Table 1.3: Miro/Milton complex co-factors.....	23
Table 1.4: Mechanisms of mitochondrial transport	26
Table 1.5: Regulation of the core mitochondrial fission/fusion machinery.....	31
Table 2.1: Cell lines and source	39
Table 2.2: Primary antibodies	40
Table 2.3: Secondary antibodies	41
Table 2.4: Dyes	41
Table 2.5: siRNA target sequences	41
Table 2.6: Plasmids and sources	42
Table 2.7: Drug target action	42
Table 2.8: Reagents.....	43
Table 2.9: Cell line specific parameters for scoring mitochondrial distribution.	54
Table 2.10: Separating Gel for SDS-Page.....	60
Table 2.11: Stacking Gel for SDS-Page.....	60
Table 5.1: Selection of mitochondrial marker for live cell imaging.....	157
Table 5.2: Selection of transfection reagent for live cell imaging in wound healing assays	158
Table 5.3: Optimised mitochondrial tracking in sub-confluent NIH 3T3 cells.....	159
Table 5.4: Effect of APC loss on parameters of mitochondrial transport in migrating NIH 3T3 cells.....	162

List of Abbreviations

°C	degrees celsius
2-YT	2-yeast tryptone
A ₂₆₀	absorbance a 260nm
A ₂₈₀	absorbance at 280nm
ADOA	autosomal dominant optic atrophy
ADP	adenosine diphosphate
APC	adenomatous polyposis coli
APS	ammonium persulphate
Arm	armadillo
ATP	adenosine triphosphate
BCL-2	B-cell lymphoma 2
BSA	bovine serum albimim
CaCl	calcium chloride
CCCP	carbonyl cyanide <i>m</i> -chlorophenyl hydrazone
C.I.	confidence interval
CIN	chromosome instability
CK1 α	casesin kinase 1 alpha
CMT	Charcot-Marie-Tooth
CO ₂	carbon dioxide
CRC	colorectal cancer
CtBP	C-terminal binding protein
DFN	displacement from nucleus
DLG1	disks large homolog 1

DMEM	Dulbecco's Modified Eagles Medium
DMSO	dimethyl sulphoxide
DPBS	phosphate buffered saline
DRP1	dynamin related protein 1
<i>E. coli</i>	Escherichia coli
EB1	end binding protein 1
EDTA	ethylenediaminetetra-acetic acid
ER	endoplasmic reticulum
FAP	familial adenomatous polyposis
FBS	fetal bovine serum
g	gram
GFP	green fluorescent protein
GSK-3 β	glycogen synthase kinase 3 beta
h	hour
H ₂ O	water
HDAC	histone deacetylase
HIF-1 α	hypoxia induced factor 1 alpha
HUMMR	hypoxia up-regulated mitochondrial movement regulator
IF	immunofluorescence
IMM	inner mitochondrial membrane
IMS	intermembrane space (mitochondrial)
IP	immunoprecipitation
IQGAP1	IQ motif containing GTPase activating protein 1
IQR	interquartile range
KAP3A	kinesin-associating protein 3A

kDa	kiloDaltons
KIF	kinesin family member
LEF	lymphoid enhancer-binding factor
M	molar
mAb	monoclonal antibody
MAP	microtubule associated protein
MCR	mutation cluster region
MCU	mitochondrial calcium uniporter
Mfn1/2	mitofusin 1/2
mg	microgram
MgCl	magnesium chloride
MgSO ₄	magnesium sulphate
min	minutes
Min (APC min/+)	mouse model for CRC containing APC 1-850/WT
ml	millilitre
mM	millimolar
MnCl	manganese (II) chloride
MOMP	mitochondrial outer membrane permeabilisation
NaCl	sodium chloride
NES	nuclear export factor
NFκB	nuclear factor kappa-light-chain-enhancer of activated B cells
NLS	nuclear localisation signal
nM	nanomolar
nm	nanometre
Nup	nucleoporin

OGA	O-GlcNAcase
O-GlcNAc	O-linked N-acetylglucosamine
OGT	O-GlcNAc transferase
OMM	outer mitochondrial membrane
OPA1	optic atrophy 1
pAb	polyclonal antibody
PD	parkinson's disease
PDH	pyruvate dehydrogenase
PDK1	pyruvate dehydrogenase kinase 1
PEI	polyethylenimine
PINK1	PTEN-induced putative kinase 1
PLA	proximity ligation assay
PP2A	protein phosphatase 2 A
Rac1	ras-related C3 botulinum toxin substrate 1
RanBP2	ran-binding protein 2
RbCl	rubidium chloride
ROS	reactive oxygen species
RPA32	replication protein A 32kDa subunit
rpm	revolutions per minute
RT	room temperature
s	seconds
SD	standard deviation
SDS	sodium dodecyl sulphate
SDS-PAGE	sodium dodecyl sulphate-polyacrylamide gel electrophoresis
siRNA	small interfering RNA

TBE	tris borate EDTA buffer
TBS	tris buffered saline
TBST	tris buffered saline supplemented with 0.2% tween-20
TCF	T-cell factor
VEGF	vascular endothelial growth factor
WB	western blot
WT	wild type
<i>xg</i>	times g force
μg	microgram
μl	microlitre
μM	micromolar
μm	micrometre



CHAPTER 1

Introduction



1.1 Background

Colorectal Cancer (CRC) is the second most common cancer diagnosed in Australia and in 2012 approximately 16,000 new cases were reported (1). CRC primarily affects patients over the age of 75 and results in ~ 4,000 deaths each year (1). The high incidence and mortality rate of CRC is also observed world-wide with 1,369,000 and 694,000 cases respectively reported in 2012 (2). Development of colon cancer results from an accumulation of gene mutations (activating mutations in oncogenes and inactivating mutations in tumour suppressor genes) that promote genomic instability and cellular transformation. Mutation of the gene encoding the tumour suppressor, adenomatous polyposis coli (APC), occurs in 80% of CRC and is one of the earliest events in the progression of sporadic colon cancer (3-5). APC was first identified as the mutated protein responsible for familial adenomatous polyposis (FAP), an autosomal dominant disease carrying a germ line APC mutation and characterised by the formation of colorectal polyps. This inherited mutation primes the other APC gene allele for a 'second hit' in the form of a somatic mutation, which can predispose patients to a high risk of early CRC (6-8).

It is not surprising that APC mutation is a driving force behind carcinogenesis given its multiple roles in the deregulation of key cell growth and differentiation pathways, which are disrupted following loss of C-terminal functional domains. This includes altered APC function as a negative regulator of the Wnt signalling pathway, where it contributes to β -catenin degradation (9, 10). APC truncation also impacts its numerous other functions at locations throughout the cell, including the nucleus, plasma membrane, centrosome and the mitochondria (11, 12).

The subcellular localisation of APC at the mitochondria was initially identified in this laboratory, and it was shown that APC mutants preferentially accumulate at mitochondria to stabilise Bcl-2 and protect cells against apoptosis (13). The notion that APC, a potent tumour suppressor, localised to the mitochondria was intriguing given the growing body of evidence implicating mitochondrial dysfunction in the carcinogenic process (reviewed in 14). Like APC, the ability of mitochondria to utilise elements of the cytoskeleton to shuttle around the cell and perform site-specific tasks is key to many of its essential cellular processes, which include the delivery of ATP to bio-

energetically demanding regions, and modulation of calcium signals (reviewed in 15, 16, 17). With this in mind, it is perhaps unsurprising that alterations to transport of mitochondria have been linked to cancer progression (18, 19).

The primary aim of this thesis was to test the novel hypothesis that APC plays a functional role in regulating transport of the mitochondria. Therefore, this literature review provides background on our current understanding of APC biology, localisation and function, and describes how CRC-associated APC truncations contribute to deregulation of normal cellular processes which lead to tumourigenesis. The second part of this chapter will cover key aspects of mitochondria biology, with an emphasis on mitochondrial transport and function and how these are altered and/or contribute to the development of cancer.

1.2 The APC tumour suppressor protein

APC is a large (310 kDa, 2843 amino acids) protein comprised of multiple protein interaction sites and functional domains that contribute to normal cell function. These include regulation of Wnt signalling and cytoskeletal organisation. In particular, the coiled armadillo repeat (Arm) domain is a primary binding site for several important APC partners, whilst the ‘basic’ domain and C-terminal regions mediate both direct and indirect associations with the cytoskeleton (Figure 1.1). These wide range of protein contact sites are critical to the intracellular shuttling of APC, and it has been proposed that the Arm domain drives the mobility and targeting of APC within the cell whilst the C-terminal half of APC is important for its scaffolding role in assembly of large protein complexes (Section 1.2.1, and reviewed in 12).

APC mutations commonly occur in a central region known as the mutation cluster region (MCR) (Figure 1.1) and give rise to a truncated protein which lacks the C-terminal sequence (20). In FAP patients, MCR mutations typically cause the most severe phenotypes, presenting >5000 polyps (21). In sporadic CRCs the most common truncation is located in the MCR at amino acid 1309 (Figure 1.1). These mutations cause an alteration in APC localisation and function, which compromises APC’s tumour suppressive function and drives CRC carcinogenesis (see Section 1.2.2).

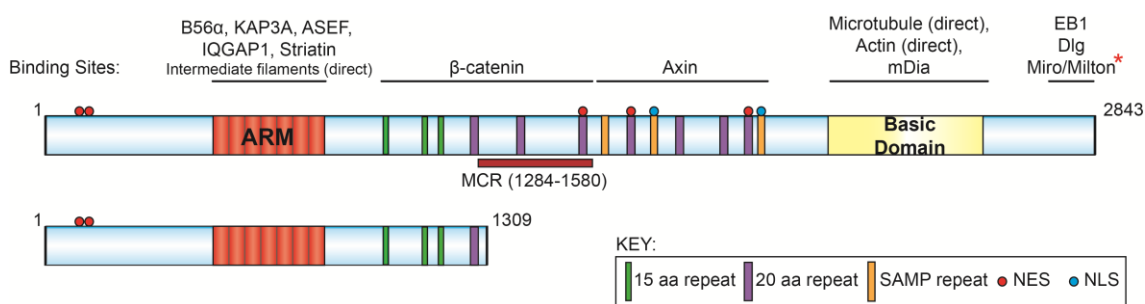


Figure 1.1: Functional domains and protein binding sites of the APC tumour suppressor.

Wild type APC is comprised of 2834 amino acids and contains numerous functional domains and protein binding sites. APC truncating mutations often occur in the mutation cluster region (MCR), most commonly at amino acid 1309. Loss of C-terminal functional domains is a driving force behind CRC carcinogenesis. (*) The APC C-terminal association with Miro/Milton will be investigated in this thesis.

1.2.1 APC protein localisation, interactions and function

The dynamic nature of APC enables it to shuttle throughout the cell, performing numerous tasks at distinct subcellular locations outside of its best known role in β -catenin degradation (via regulation of Wnt signalling). Highlighted in Figure 1.2, these site-specific tasks include organisation of microtubules and actin filaments at the cell membrane, regulation of the DNA repair and damage response in the nucleus and regulating microtubule dynamics at the centrosome (11, 12). The recent finding that APC also targets to the mitochondria (13), was the foundation of this study. Based on the multidirectional targeting of APC, compounded by its ability to regulate the cytoskeleton and numerous protein interactions, APC can be considered as a mobile scaffolding protein.

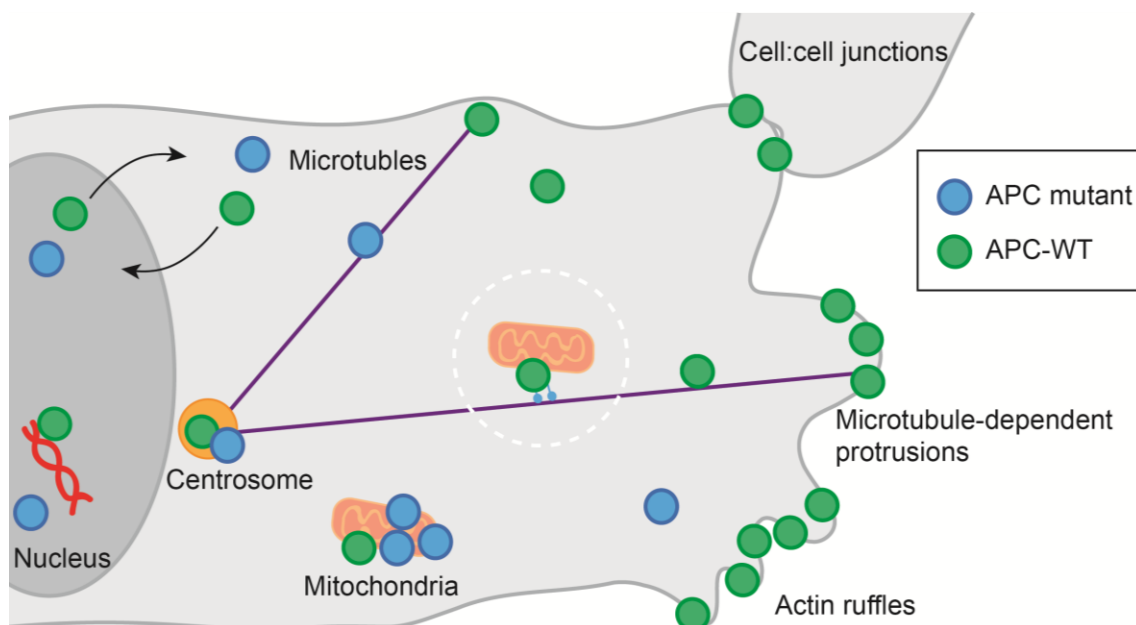


Figure 1.2: APC localisation to distinct sub-cellular compartments is altered by C-terminal truncating mutations.

Wild-type APC can be detected at microtubule dependent protrusions and actin ruffles where it accumulates strongly, as well as microtubules, cell:cell junctions, mitochondria, the centrosome and the nucleus. C-terminal truncating mutations alter APC localisation, and disrupt its site-specific functions. This study focuses on the recently defined mitochondrial localisation of APC and investigates a novel role in microtubule-dependent mitochondrial transport.

1.2.1.1 Regulation of APC localisation

As alluded to above and outlined in Figure 1.2, APC is a dynamic, highly mobile protein that shuttles between multiple regions in the cell including the nucleus, plasma membrane, mitochondria and centrosome where it performs a variety of site-specific tasks. This localisation is mediated through a number of pathways which are facilitated by both internal signalling sequences and protein-protein interactions (Figure 1.1). For example, the N-terminal region of APC comprises critical signal sequences through which it is translocated in and out of the nucleus. The nuclear export signal (NES) binds to the major export receptor CRM1, to facilitate transport through the nuclear pore complex from the nucleus to the cytoplasm (22, 23), whilst the nuclear localisation signal (NLS) facilitates transport into the nucleus through its association with Importin receptors (24). An additional Arm-domain mediated pathway for APC nuclear import

has been identified, and is stimulated by an association with B56 α (25). Arm-domain targeting of APC to both the centrosome and mitochondria has also been reported, though this is not well defined (13 and Lui and Henderson, unpublished).

Targeting of APC to the cell membrane is also partially dependent on the Arm domain and its association with the kinesin-2 adaptor protein, KAP3A. This association was shown to be necessary, but not sufficient, for APC accumulation at microtubule plus-ends (26). Deletion mapping further showed that the minimal APC sequence required to target APC to cellular protrusions is APC(1-2226), and that this is partly aided by an interaction with β -catenin (27). Whilst this mechanism has yet to be fully elucidated, it may be regulated in part by GSK-3 β -dependent phosphorylation of APC and β -catenin, which has been shown to promote detachment of APC from microtubules (28), and β -catenin destruction (Section 1.2.1.2). These studies provide a logical explanation for the innovative live cell timelapse work of Mimori–Kiyosue and colleagues (29), which showed that APC travels in clusters along microtubules of living cells. Striatin, another Arm-domain binding protein has also been reported to target APC to the cell periphery, specifically to cell-cell junctions (30) in an actin-dependent manner. The main context for interpreting these studies revolved around explaining how APC is recruited to the cell periphery, including the ends of microtubules, membrane protrusions/clusters and actin ruffles. However, as will be discussed later (Section 1.4), this thesis will investigate the potential novel role of APC as a chaperone for the microtubule-dependent transport of mitochondria to the membrane.

CRC-associated APC truncations typically impact its role as a mobile scaffold by altering its subcellular localisation (see Figure 1.2), in particular cytoskeletal retention at the plasma membrane is lost (10, 12, 27). Other important APC targeting domains, such as the primary NES and the Arm domain, are located within the N-terminus and thus retained in most cancer mutant forms of APC (Figure 1.1), which have been shown to be highly mobile within the cell (31). Truncated APC mutants have also been shown to accumulate preferentially and more strongly than wild-type APC at mitochondria (13). APC must be correctly targeted to specific compartments or structures within the cell in order to fulfil its specific roles in normal cell growth and differentiation (Section 1.2.1.2 - 1.2.1.4). Hence alteration in APC localisation, combined with loss of co-factor binding, can disrupt this ability to act as a mobile scaffold, contributing to

carcinogenesis through loss tumour suppressive activity. This is discussed in detail in Section 1.2.3.

1.2.1.2 The role of APC in Wnt Signalling

Wnt Signalling

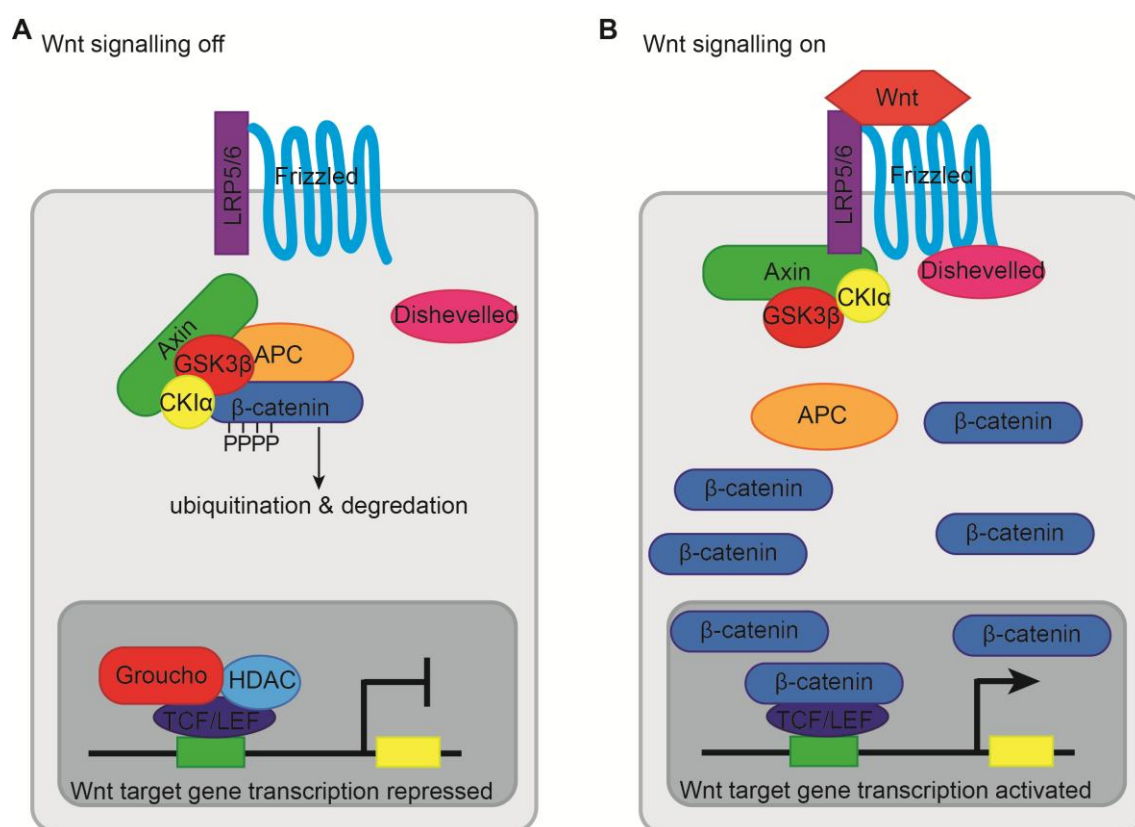
APC is a negative regulator of Wnt signalling, a pathway that relays signals from the plasma membrane to the nucleus (via β -catenin), leading to the activation of specific genes important for embryogenesis, normal cell growth and differentiation (5, 10, 32, 33). This pathway is reviewed in detail elsewhere (9, 32, 34, 35), and summarised in Figure 1.3. Briefly, under normal cellular conditions, Wnt signalling is turned off and APC, Axin, glycogen synthase kinase (GSK-3 β) and casein kinase 1 α (CKI α) form a complex (the ‘destruction complex’) that phosphorylates β -catenin, marking it for ubiquitination and ultimately degradation. However, upon association of a Wnt ligand with the Frizzled / LRP5/6 receptor complex at the plasma membrane, the destruction complex is inactivated, and Wnt signalling activated. This occurs through the recruitment and phosphorylation of regulatory protein Dishevelled to the receptor complex, in turn signalling LRP5/6 phosphorylation and the recruitment of Axin to the cell membrane. Free from degradation, β -catenin accumulates in the cytoplasm, where it can translocate to the nucleus, and interact with and trans-activate members of the T cell factor (TCF)/lymphoid enhancer factor (LEF) family of transcription factors, TCF1, TCF3, TCF4 and LEF1 to promote transcription of Wnt target genes.

APC interactions with Wnt proteins

To regulate β -catenin degradation, APC closely associates with core proteins in the destruction complex including β -catenin, Axin and GSK-3 β , along with B56 α , a subunit of the negative regulatory protein phosphatase 2A (PP2A) (36). These associations are outlined in Table 1.1.

Table 1.1: Interactions of APC with Wnt proteins.

Protein Partner	Binding Domain(s)	Reference
β -catenin	15 and 20 amino acid repeat domains. These domains are subject to GSK-3 β and CKI α phosphorylation to enhance β -catenin binding.	(37-39)
Axin	SAMP domains (conserved 16 amino acid repeats) 20R2 domain (20 amino acid repeat number 2)	(40-42)
GSK-3 β	The central region of APC	(37)
B56 α	Arm domain	(25)

**Figure 1.3: The Wnt signalling pathway.**

(A) In the absence of a Wnt ligand, β -catenin levels are tightly regulated by the multi-protein destruction complex, which phosphorylates β -catenin, targeting it for proteosomal degradation. (B) Activation of the Frizzled / LRP5/6 receptor complex by a Wnt ligand turns Wnt signalling on, causing dissociation of the destruction complex and subsequent translocation of β -Catenin into the nucleus to stimulate transcription of Wnt target genes.

The role of APC in the destruction complex

APC was initially proposed to function as a scaffold for assembly of the β -catenin destruction complex, whereby its interactions with β -catenin and Axin were suggested to offer stability to the complex and promote phosphorylation of β -catenin by the Axin-bound kinases GSK-3 β and CKI α . More recently several other models have been proposed. One model suggests that APC enhances the turnover of β -catenin at the destruction complex, wherein phosphorylation of its 20 amino acid repeats increases its affinity for binding to β -catenin, thereby displacing it from Axin. This would leave Axin free to interact with another β -catenin molecule (43, 44). An alternate model proposes that APC promotes β -catenin ubiquitination (45, 46), whilst another suggests that APC regulates Axin localisation by restricting Dishevelled-mediated Axin recruitment to the plasma membrane (47). A number of reviews (9, 10) discuss these models in much greater detail. It is possible that these mechanisms are not mutually exclusive, and that APC contributes to β -catenin degradation through multiple pathways.

Other mechanisms by which APC regulates transcription of Wnt target genes

APC is also reported to inhibit TCF-dependent transcription of Wnt target genes through several alternate pathways. Studies from this laboratory and others suggested that APC can regulate accumulation of β -catenin in the nucleus by facilitating its nuclear export back to the cytoplasm for degradation (11, 22, 48, 49). Furthermore, studies also indicate that APC can directly interact with the transcription repressor, C-terminal binding protein (CtBP), to form a complex with additional co-factors, blocking TCF mediated transcription (50, 51).

1.2.1.3 APC and cytoskeletal organisation

As previously mentioned, APC closely associates with cytoskeletal networks through both direct binding and indirect associations with binding partners (see Table 1.2 and Figure 1.1), which assist in mediating its localisation at the cell membrane and, in turn, its site-specific cytoskeletal regulatory functions. In particular, APC accumulates at the distal ends of microtubules where it contributes to microtubule stabilisation at the cell cortex, and also at actin ruffles where it contributes to actin organisation and polymerisation (52-54). The ability of APC to associate with microtubules, actin and a wide range of regulatory partners at the plasma membrane facilitates cross-talk and co-

ordination between the two networks (54). This is essential in the regulation of cell polarity and highlights its unique role as a mobile scaffold. APC has also been reported to organise intermediate filaments during cell migration (55) through a direct Arm-dependent association. The mechanism for this process has not yet been determined.

Table 1.2: Cytoskeletal interactions of APC.

Cytoskeletal Element	Adaptor	APC Domain	Reference
Actin	Direct	Basic domain	(56)
	ASEF	Arm domain	(57)
	IQGAP1	Arm domain	(58)
	Dlg	C-terminal region	(59)
	Striatin	Arm domain	(30)
Microtubule	Direct	Basic domain	(60)
	KAP3A	Arm domain	(26)
	EB1	C-terminal region	(61)
	RanBP2	APC (1211-1859)	(62)
Intermediate filaments	Direct	Arm domain	(55)

APC and microtubule protrusion formation

The localisation of APC in clusters at the distal ends of microtubules contributes to the stability and lifespan of microtubules *in vivo* and *in vitro* (28, 60, 63). Stabilised microtubules drive the formation of microtubule-dependent protrusions that are important for directing cell migration (reviewed in 64). This is reflected by studies showing that loss of APC correlates with decreased protrusion formation (27) and directed cell migration (65) *in vitro*. Inactivation of APC was also demonstrated to block cell migration *in vivo* along the crypt-villus axis in APC flox mice (66).

The capacity of APC to stabilise microtubules is mediated directly through the ‘basic’ domain, and indirectly through an association with the +tip protein, end binding protein 1 (EB1) (28, 63, 67). The literature suggests that the APC-EB1 interaction stabilises microtubules by capping microtubule plus ends, for which several co-factors have been implicated including Amer2, mDia and KIF17 (68-70). Intriguingly, the APC-EB1 association has also been reported to promote microtubule assembly and polymerisation from the centrosome *in vitro* and *in vivo* (71), though precisely how this occurs requires further investigation.

APC and actin organisation and polymerisation

APC also localises to actin ruffles and lamellipodia at the cell membrane to organise actin filaments and promote polymerisation, crucial for cell migration. One way APC achieves this is through an interaction with IQ motif containing GTPase activating protein 1 (IQGAP1), which is proposed to crosslink microtubules and actin filaments, thereby stabilising actin and promoting cell migration (58). Another study has indicated that a direct association with actin can also crosslink microtubules and actin filaments by competing for APC 'basic' domain binding (72).

APC has been implicated in the organisation of the actin cytoskeleton through stimulation of ASEF, a Rac-specific guanine nucleotide exchange factor, which it activates by binding to the ASEF N-terminal region and relieving negative regulation (57, 73). In turn ASEF stimulates Rac reorganisation of the actin cytoskeletal network, promoting formation of lamellipodia and membrane ruffling (57). Furthermore, in MDCK cells, ASEF stimulation is reported to decrease E-cadherin cell-cell adhesion, thereby promoting cell migration (73). A study by Okada and colleagues (56), indicates that the 'basic' domain of APC is also directly involved in actin nucleation. APC is reported to dimerise and recruit actin monomers for polymerisation, further highlighting its multifunctional role as a protein scaffold.

APC and cell polarity

Establishing cell polarity is important for determining direction of cell migration, and requires the stabilisation and anchoring of microtubules to the basal cortex in addition to centrosome reorientation. In migrating cells, the dynein/dynactin complex has been shown to be essential in exerting mechanical forces on stabilised microtubules to induce centrosome reorientation (64). APC's ability to capture, stabilise and crosslink microtubules with actin is important for microtubule anchorage to the actin-rich cortex (74). Moreover, microtubule bound APC has been shown to interact with the polarity anchoring protein disks large homolog 1 (DLG1) via its C-terminal region (59) at the basal plasma membrane. This process has been implicated in cell polarisation of astrocytes (75). It has been demonstrated that DLG1 associates with the dynein/dynactin complex to induce centrosome reorientation (76), though this process is poorly understood. The wide range of cytoskeletal connections APC is able to make at the cell

membrane (Table 1.2), and co-factors involved, could very well promote the microtubule anchoring ability of the APC-DLG1 association.

Away from the cell membrane, APC has also been implicated in centrosome reorientation and positioning at the nuclear envelope where it was proposed to tether microtubules through an interaction with Nup153 (77). Collin and colleagues (77) suggest that the APC/Nup153 complex serves as an anchor for microtubules emanating from the centrosome. An interaction with the mobile Nup, Ran binding protein 2 (RanBP2/Nup358), was also implicated in cell polarity by binding and driving APC towards the cell cortex in a kinesin-dependent manner (62), presumably where it can promote microtubule stabilisation and anchoring.

APC at the centrosome and mitotic spindle

APC has been linked to other facets of centrosomal function including duplication, centrosome microtubule nucleation and mitosis and chromosome segregation (12, 78). APC accumulates strongly at the centrosome, and while its role in interphase is poorly understood, during mitosis APC helps stabilise formation and orientation of the mitotic spindle. APC has been detected at kinetochores and the mitotic spindle during mitosis (79) and, it was suggested that APC is involved in mediating the attachment of kinetochores to the plus ends of the spindle microtubules, an essential step in mitosis and for the integrity of chromosome segregation (80).

1.2.1.4 The role of APC in other cellular functions

APC and DNA replication and repair

In the nucleus, APC binds to A/T rich DNA sequences through a number of central and C-terminal amino acid regions (81). Furthermore, several studies indicate that APC is involved in DNA replication contributing to cell cycle progression from G1 to S phase (82, 83). Whilst it is unclear whether the ability of APC to directly bind DNA contributes to this, an interaction with replication protein A subunit 32 (RPA32) at chromatin is known to be involved. APC promotes the ATR kinase-dependent phosphorylation of RPA32 and other co-factors, particularly in response to DNA replication stress, which can contribute to the re-initiation of S-phase progression (82). A specific function for APC in DNA repair has also been described whereby binding to

DNA polymerase β and Fen-1 causes the blockage of base excision repair, the most common pathway for damaged DNA abasic repair (84).

APC and the mitochondria

APC has long been associated with regulation of apoptosis (12, 85), for instance through blocking Wnt-mediated repression of caspase 3 and 7 expression (86). In 2008, APC was first reported to display a specific localisation at the mitochondria, and was found to interact with the anti-apoptotic protein, Bcl-2 (13). Whilst the significance of the wild-type APC-Bcl-2 interaction is not clear, APC truncating mutants were shown to preferentially accumulate at mitochondria and stabilise Bcl-2 levels, protecting cells against apoptosis. This is discussed further in Section 1.2.2.4. APC localisation at the mitochondria was later confirmed in a study by Qian and colleagues (87), which also implicated APC in regulation of apoptosis. Caspase-cleaved forms of APC were shown to bind to distinct isoforms of the hTID-1 apoptotic regulator, and differentially modulate apoptosis. This thesis will focus on a new role for APC at mitochondria, implicating it in mitochondrial transport and as a consequence the regulation of ATP dispersal and calcium buffering within the cell (Section 1.4).

1.2.2 APC dysfunction in colorectal cancer

As discussed previously (Section 1.2.1.1), a primary effect of APC truncation is an alteration in subcellular localisation, which results in a net loss of APC cytoskeletal retention, and an increase in APC motility (11). It is also possible that mutant APC acquires additional cancer-promoting activities. Studies *in vivo* and *in vitro* show that APC mutations exert a dominant-negative effect in systems where only one APC allele is mutated, or when mutant APC is overexpressed. This may be due to the ability of APC to dimerise through its N-terminal region, thereby allowing mutant APC to bind to and inhibit wild-type APC in a dominant negative manner (88, 89). Alternatively, in cells with heterozygous alleles the truncated forms of APC might compete with wild-type APC to initiate assembly of protein complexes but fail to complete the process due to an inability to bind C-terminal-specific partners.

1.2.2.1 Deregulation of Wnt signalling and proliferation

The most well known characteristic of cells expressing mutant APC is defective control of Wnt signalling. Loss of both the SAMP and 20R2 Axin binding domains, compromises formation of the destruction complex and stabilises β -catenin, which accumulates and translocates to the nucleus to form stable constitutively active complexes with the TCF/LEF1 transcription factors. This leads to the unregulated transcription of proliferative oncogenic Wnt target genes such as c-myc, cyclin D1 and fibronectin, which drives cell transformation and cancer (reviewed in 10, 33, 37, 90, 91). Exactly how the β -catenin destruction complex is compromised has yet to be fully determined. One possibility is that the complex formed is insufficient to induce β -catenin degradation thereby inhibiting the required phosphorylation or ubiquitination. The contribution of deregulated Wnt signalling in tumourigenesis has been reviewed extensively (5, 10, 32, 33, 92), and its clinical importance is highlighted by the continuous research and development into indentifying new drug targets for this pathway (93).

1.2.2.2 Cell migration

Loss of APC cytoskeletal retention at actin ruffles and the distal ends of microtubules following C-terminal truncation impacts on the site-specific scaffolding functions of APC at the cell membrane (27, 31, 94), despite the fact that the APC N-terminal half retains the capacity to bind microtubule/actin regulators such as IQGAP1 and ASEF, and the kinesin complex (KAP3A). A major effect of APC mutation is the disruption of cell polarity which in non-adherent cells means a lack of centrosome positioning to allow for direction of motion during cell migration. This disruption is most likely due to loss of microtubule stabilisation and anchoring at the basal cortex (74, 95), and to APC mutants which act in a dominant negative manner to cause a more random movement of cells (96). For example, the overexpression of truncated APC fragments in Vero cells (APC wild-type) was found to impair centrosome orientation (58). Furthermore, cells expressing mutant APC against a background of one or two wild-type copies of APC displayed a distinct loss of directional preference in numerous experimental models (96). In particular, enterocytes in the small intestine of APC (Min/+) mice (a mouse model for CRC containing APC 1-850/WT) experienced a sharp decrease in migration along the crypt-villi axis in comparison to control mice (96). Cell retention at the base

of colonic crypts has been observed on multiple occasions in colonic adenomas of humans and APC (Min/+) mice (97-99). Retention in the colonic crypt is favourable for carcinogenic transformation given that this region is highly proliferative, and therefore the opportunity to acquire further selective advantages is increased.

Somewhat paradoxically, studies by Kawasaki and colleagues (73, 100) found that mutant APCs were more efficient than wild-type APC in stimulating the activity of the Rac1-exchange factor ASEF. This was proposed to trigger Rac-dependent cytoskeletal reorganisation and loss of E-cadherin at cell:cell junctions, in turn promoting cell migration. In a separate study, restoration of wild-type APC expression in SW480 (APC 1-1337) CRC cells caused recovery of E-cadherin at the cell:cell junctions, correlating with an increase in cell adhesion (101). These studies suggest that APC mutants not only mediate tumourigenesis by causing loss of function, but in specific instances can cause a gain of function. It is however hard to predict the effect ASEF stimulation might have on the speed of cell migration in the context of the colonic crypt, where directionality of movement is also vital.

1.2.2.3 Chromosome segregation and CIN

Defects in chromosome segregation are most often caused by chromosome misalignment, or inefficient chromosome separation during mitosis and result in aneuploidy (multiple copies of chromosomes). This phenotype has been demonstrated to promote chromosomal instability (CIN) (102, 103), a hallmark of many CRCs, and has been shown to correlate with APC mutation in the embryonic stem cells of APC (Min/+) mice (79, 104). Aberrant chromosome segregation can result from defective spindle formation and attachment to kinetochores during mitosis in APC-mutant cells (80, 104). One study proposed that overexpression of APC(1-1450) in HEK 293 cells (APC wild-type) interrupts spindle-kinetochore attachments and interferes with chromosome segregation in a dominant-negative fashion (80), an effect mediated by competitive inhibition of the interaction between endogenous wild-type APC and EB1 (105). These defects allow cells to bypass the normal spindle checkpoint and result in chromosome mis-segregation, chromosome instability and cancer (102, 103).

1.2.2.4 Apoptosis

Cells expressing mutant APC often are more resistant to the apoptotic impact of different drugs. In particular, in mutant APC CRC cell lines treated with HDAC inhibitors or 5-FU, this apoptotic resistance is reversible upon reconstitution of wild-type APC (106, 107). These findings have been attributed to a number of APC pathways, both Wnt-dependent and –independent.

Increased accumulation of β -catenin following APC truncation affects apoptosis at a transcriptional level. Wnt signalling has been shown to induce the expression of pro-survival proteins Survivin and Akt (modulates Bax, BAD and caspase 9), and repress expression of pro-apoptotic caspases 3 and 7, thereby promoting cell survival (86, 107, 108). Furthermore, constitutively active β -catenin was reported to translocate to the mitochondria and associate with pro-survival protein Bcl-2, somehow promoting cell survival (109, 110). Previous studies in this laboratory showed that APC truncating mutants accumulate strongly at the mitochondria in comparison to wild-type, where they associate with and possibly stabilise Bcl-2 (13). Knockdown of APC in SW480 (APC 1-1337) cells was shown to cause mitochondrial outer membrane permeabilisation and stimulate apoptosis, which correlated with a loss of Bcl-2. This is intriguing particularly as APC(1-1337) retains β -catenin binding, however, it is yet to be determined if these two pathways are linked.

1.3 Mitochondria

Mitochondria are highly dynamic cell organelles encased by a unique double membrane structure consisting of the highly folded cristae of the inner mitochondrial membrane (IMM) and a simpler outer mitochondrial membrane (OMM). In addition to this, mitochondria have their own genome (mtDNA) and protein synthesis machinery to translate proteins essential for their specific cellular functions, of which ATP synthesis is the most well known (17, 111). As highlighted in Section 1.3.1, mitochondria perform a range of other critical cellular functions including regulation of calcium buffering and apoptosis, and are a reactive site for numerous metabolic pathways such as the Krebs cycle. Like APC, the motile, dynamic nature of mitochondria is critical for

targeting to different subcellular locations to perform site-specific tasks. This subsection aims to highlight the mechanisms and importance of tightly regulated mitochondrial dynamics (transport and morphology) (Sections 1.3.2 and 1.3.3), and will outline how disruptions to these pathways can promote tumourigenesis and other disease phenotypes (Section 1.3.4).

1.3.1 Mitochondrial function

The most prominent role of mitochondria is ATP synthesis whereby mitochondria convert nutrient derived molecules into energy by oxidative phosphorylation (Section 1.3.1.1). The mitochondria also house crucial metabolic enzymes in the IMM and mitochondrial matrix, thereby mediating other metabolic pathways including the citric acid cycle (Krebs cycle), fatty acid oxidation, the urea cycle and heme and iron sulphur cluster synthesis. Parts of the steroid, ketone, cardiolipin, dolichol and ubiquinone synthesis pathways are also housed in the mitochondria (17, 112-116). Aside from metabolism, mitochondria also regulate calcium buffering (Section 1.3.1.2) and apoptosis (Section 1.3.1.3). This section will briefly summarise some of these functions in order to provide a better context for understanding the implications of disrupted mitochondrial dynamics.

1.3.1.1 ATP production by oxidative phosphorylation

Mitochondria convert fuel in the form of NADH and FADH₂ derived from nutrient catabolism into energy (ATP) through a process known as oxidative phosphorylation (117-120). The machinery required for this process is embedded in the IMM and comprises the multi-protein electron transport chain complexes (Complexes I-IV), electron carriers (Coenzyme Q and Cytochrome C) and ATP synthase. Briefly, electrons from NADH and FADH₂ are transferred into Complex I and Complex II respectively, after which they move through the electron transport chain, undergoing a series of redox reactions to release free energy until they reach Complex IV and reduce oxygen to water (see Figure 1.4A). The free energy released is used to pump protons through Complexes I, III and IV, in turn creating a proton gradient. Protons diffusing back along the gradient power ATP synthase, in turn driving the phosphorylation of ADP into ATP (Figure 1.4A).

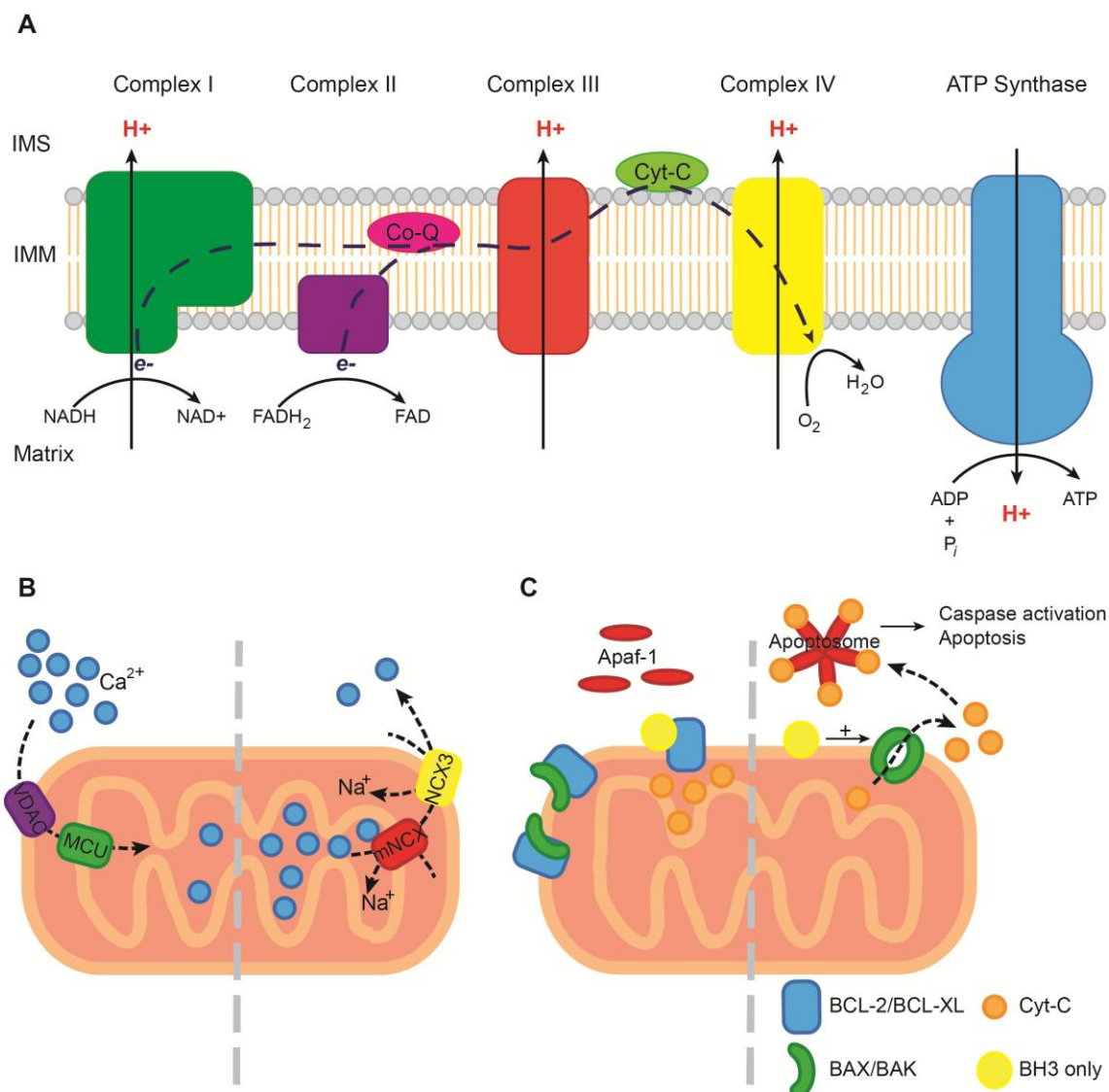


Figure 1.4: Functional roles of mitochondria

(A) ATP production. Electrons enter the electron transport chain following the oxidation of NADH and FADH₂ at Complex I and Complex II, respectively, and are shuttled by the electron carriers Coenzyme Q (Co-Q) and Cytochrome C (Cyt-C) to Complexes III and IV respectively, and used to reduce oxygen to water. As the electrons move through the electron transport chain they undergo a series of redox reactions, releasing free energy which is harnessed to pump protons through Complexes I, III and IV across the inner mitochondrial membrane (IMM) into the intermembrane space (IMS), creating an electrochemical gradient across the membrane. This energy is utilised to generate ATP through the movement of protons back along the gradient into the matrix through ATP synthase, which phosphorylates ADP.

(B) Calcium buffering. Calcium uptake into the mitochondria is chiefly regulated by the voltage dependent anion-selective channel (VDAC) and the mitochondrial calcium uniporter (MCU) over the OMM and IMM, respectively. Calcium release is primarily mediated by the mitochondrial Na⁺/Ca⁺ exchanger (mNCX) and the Na⁺/Ca⁺ exchanger isoform 3 (NCX3) for the IMM and OMM, respectively.

(C) Intrinsic apoptosis. In the absence of

apoptotic signalling, pro-apoptotic mediators BAK/BAX and their activating BH3-only proteins are sequestered at the mitochondria by anti-apoptotic mediators including BCL-2 and BCL-XL. When apoptosis is stimulated, anti-apoptotic sequestration is relieved allowing BAK/BAX, stimulated by BH3-only proteins to dimerise, form permeable pores and release apoptotic signalling proteins. Release of Cytochrome C (Cyt-C) in particular, activates Apaf-1, stimulating the formation of the apoptosome and in turn cleavage of executioner caspases.

1.3.1.2 Calcium buffering

The ability of mitochondria to sequester and release calcium is essential for regulating calcium availability and signalling in the cytoplasm. Uptake of calcium into the mitochondria also regulates cellular ATP synthesis by increasing H⁺ extrusion over the IMM, and can trigger apoptosis by opening the permeability transition pore (15, 121-123). Influx of calcium into the mitochondria is primarily mediated by the voltage dependent anion-selective channel (VDAC) and the mitochondrial calcium uniporter (MCU) over the OMM and IMM, respectively, as highlighted in Figure 1.4B (124-126). The MCU is a gated, highly selective ion channel which relies on the negative membrane potential generated by the electron transport chain to facilitate calcium uptake. Reflecting the low affinity/high capacity nature of the MCU, mitochondria have a specific role in buffering calcium microdomains, localised sites within the cytoplasm with a high calcium ion concentration, usually formed in the vicinity of Ca²⁺ ion channels (for example at the plasma membrane). This is different to the calcium uptake mechanisms of the ER, which more effectively buffer lower levels of calcium (127). Calcium release on the other hand, is chiefly mediated by the mitochondrial Na⁺/Ca⁺ exchanger (mNCX) and the Na⁺/Ca⁺ exchanger isoform 3 (NCX3) for the IMM and OMM respectively (Figure 1.4B and 128, 129).

1.3.1.3 Regulation of apoptosis

Mitochondria are crucial in the regulation of the intrinsic apoptotic pathway, which relies on proteins released from the mitochondria into the cytoplasm to initiate apoptosis. Mitochondrial outer membrane permeabilisation (MOMP) is a key event in this process, which is tightly regulated by the interplay between Bcl-2 family proteins (reviewed in 16, 130, 131-133). Briefly, the Bcl-2 protein family consists of anti-

apoptotic mediators such as Bcl-2 and Bcl-XL, and the pro-apoptotic mediators including Bax and Bak and their activating BH3-only proteins. Once activated, pro-apoptotic mediators Bax and Bak cluster to form protein permeable pores in the OMM, facilitating the release of apoptotic signalling proteins from the intermembrane space (IMS). The pro-survival Bcl-2 proteins are thought to inhibit this process directly by sequestering Bax and Bak, and indirectly by sequestering BH3-only proteins. Whilst the mechanism by which Bax and Bak form these permeable pores has yet to be fully elucidated, current evidence suggests that they homo-dimerise, then multimerise with lipids from the OMM to form a pore complex (132). This process is summarised in Figure 1.4C. As described previously (Section 1.2.3.4), APC may influence this process through its ability to stabilise Bcl-2 at mitochondria (13), perhaps indirectly reducing Bax dimerisation, and as a result MOMP.

Pro-apoptotic proteins released from the mitochondria activate caspase-dependent apoptotic pathways, where hundreds of target endonuclease and protease substrates are cleaved, causing cell death. The most well documented of these is Cytochrome C, which binds to the procaspase-activating adaptor Apaf-1 causing it to form a heptameric structure known as the apoptosome, which kick-starts a signalling cascade to activate the executioner caspases-3 and -7 (see Figure 1.4C and review 134). Over an extended period of time, MOMP has also been shown to cause cell death independently of caspase activation. This is most likely due to a progressive loss of mitochondrial function following loss of OMM integrity, including release of soluble components of the electron transport chain (135, 136).

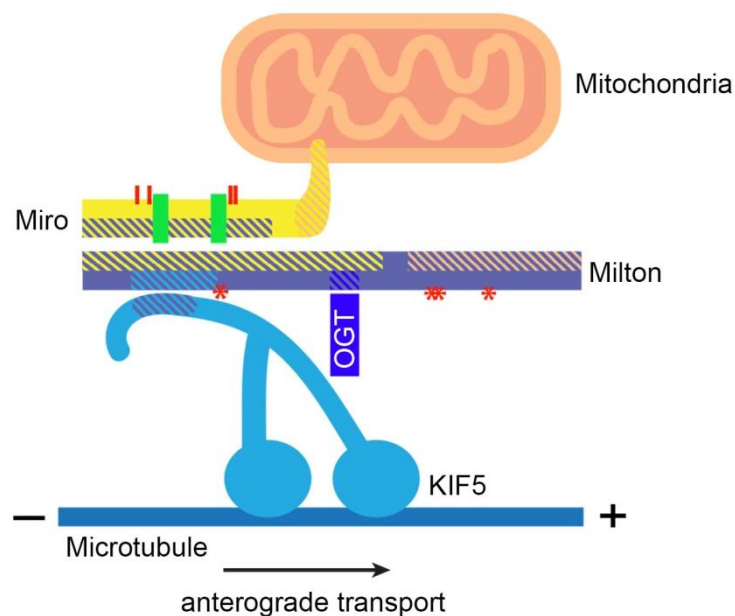
1.3.2 Mitochondrial transport

Mitochondria move across cytoskeletal networks, frequently engaging in rapid bi-directional movement, interspersed between periods of stationary docking. This dynamic transport is key to the ability of mitochondria to redistribute in response to cellular signals, enabling them to perform highly site-specific tasks, such as ATP provision and modulation of calcium buffering (see Section 1.2.3.3). Mitochondrial transport has most often been studied in neuronal cells due to their unique cellular architecture, which requires long distance transport through the axon from the cell body towards the synaptic terminal (137, 138). Disruption to this process has been shown to

contribute to a number of neurological conditions (139-141). More recent studies however, highlight the crucial nature of mitochondrial transport in other cell types, particularly in the context of regulated cell migration (18, 19, 142).

1.3.2.1 Miro/Milton/KIF5 mitochondrial transport

The Miro/Milton/KIF5 transport complex is the primary means of microtubule-dependent mitochondrial transport within the cell. Miro and Milton were originally identified by genetic screening of *Drosophila* retinal neurons devoid of axonal and terminal mitochondria (143, 144). Miro and Milton have since been shown to be evolutionarily conserved in mammals, with two orthologues identified for each protein, Miro-1/Miro-2 and Milton-1/Milton-2 that are expressed in a wide variety of cell and tissue types (143, 145-147). Miro is a mitochondrial transmembrane protein, to which Milton associates at the surface of the OMM. Milton then functions as an adaptor to link the mitochondria to the KIF5 kinesin motor to facilitate anterograde transport along microtubules (148-150). Milton is reported to associate with all three KIF5 subtypes, the neuronal-specific KIF5A/KIF5C and the ubiquitous KIF5B, demonstrating the importance of this complex for basic cellular function. This importance is further highlighted by the absence of mitochondria in the axons and synaptic terminal of *Drosophila* harbouring mutant Miro, Milton or KIF5 (143, 144, 151). Moreover, live cell studies show that disruption of Miro and Milton by siRNA silencing or use of a dominant-negative significantly diminishes the pool of motile mitochondria (152-154).



Miro/Milton binding domains

Key	Binding	Domain	Reference
	Miro/Milton	dMiro: 1-574, dMilton: 1-750 hMilton-2: 476-700, hMiro-1: N-terminal region	(149, 150)
	Milton/KIF5	dMilton: 138-450, dKIF5: 810-891 hMilton-2: 124-283, hKIF5C: 336-957	(149, 155)
	Milton/OGT	hMilton-1: 658-672	(156)
	Miro/Mito	hMiro-1/2: 593-615	(148)
	Milton/Mito	dMilton: 847-1116	(149)

Miro/Milton sites of post-translational modification

Key	Modification	Site	Reference
	Phosphorylation	Ser 156/182 (hMiro-1/dMiro), Ser 324 (dMiro), Thr 325 (dMiro)	(152, 157)
	O-GlcNA- cetylation	Ser 447 (hMilton-1), Ser 829 (hMilton-1), Ser 830 (hMilton-1), Ser 938 (hMilton-1)	(156)
	Calcium binding (EF hands)	184-219 (hMiro-1), 304-339 (hMiro-1)	

Figure 1.5: Miro/Milton mitochondrial transport complex binding and modification domains.

The schematic outlines sites of protein interaction and post-translational modification in the Miro/Milton complex, as currently defined in the literature (see figure key for explanations). The + ends of microtubules are stable caps at the growing ends that become tethered at the plasma membrane in interphase cells. Anterograde transport of proteins means outward movement from nucleus toward the plasma membrane.

The Miro/Milton complex is regulated by metabolic fluctuations in calcium levels (153, 158, 159) and glucose availability (156), which target the action of Miro and Milton, respectively. These and other regulatory post-translational modifications are discussed below, and the current knowledge pertaining to the Miro/Milton/KIF5 complex modification and binding domains is outlined in Figure 1.5. Intriguingly, Milton can also localise at mitochondria independently of Miro, for which a target domain has been identified (149). It is possible that this Milton/mitochondria association contributes to complex stability, however this has not been investigated. Furthermore it is unclear from the literature if Miro and Milton interact directly and without the assistance of other co-factors. A number of co-factors (detailed in Table 1.3) have already been reported to associate with the core components of the Miro/Milton/KIF5 complex including hypoxia up-regulated mitochondrial movement regulator (HUMMR), Alex3 and Mitofusin 2 (Mfn2). When inactivated, by shRNA (HUMMR and Alex3) or expression of dominant negative mutants (Mfn2) these proteins were shown to suspend anterograde (membrane-directed) transport of mitochondria, highlighting their ability to regulate the transport complex and in turn providing a regulatory link to hypoxic, non-canonical Wnt and mitochondrial fusion–dependent pathways (160-162).

Table 1.3: Miro/Milton complex co-factors.

Co-factor	Association	Mechanism	Reference
HUMMR	Miro-1/2	Induced by HIF-1 α to facilitate anterograde mitochondrial transport under hypoxic conditions.	(160)
Alex3	Miro-1/2 Milton-2	Associates with Miro/Milton in a Ca ²⁺ -dependent manner to promote mitochondrial transport. Targeted for proteosomal degradation via the non-canonical Wnt signalling pathway.	(161, 163)
Mfn2	Miro-1/2 Milton-1/2	A regulator of mitochondrial fusion demonstrated to associate with Miro/Milton and promote mitochondrial transport.	(162)

Calcium Sensitivity

The role of mitochondria in the site-specific buffering of intracellular calcium (Section 1.3.1.2) is highlighted by the Miro-regulated, calcium-dependent suppression of

mitochondrial transport (158, 164). When intracellular calcium levels are elevated, calcium binds to Miro's EF-hand motifs (helix-loop-helix structural domains that bind calcium), causing a conformational change that facilitates mitochondrial detachment from microtubules (153, 158, 159). The mechanism by which this conformational change disrupts mitochondrial transport is somewhat controversial. Wang and Schwarz (153) report that calcium binding to the EF-hand motifs (see Figure 1.5) results in Miro binding and blocking the KIF5 motor domain, causing the entire complex to dissociate from the microtubule. On the other hand, findings by MacAskill and colleagues (159) suggest that Miro binds KIF5 independently of Milton, and that elevated calcium disrupts this interaction causing Miro/Milton detachment from KIF5. Some of these differences may be attributed to the use of different cell types and Miro/Milton homologs in these studies. However, further investigation is required to fully elucidate the mechanism by which Miro-calcium binding alters the complex.

Post-translational modification

Mitochondrial transport is also subject to post-translational regulation whereby Miro and Milton are modified by Pten-induced kinase-1 (PINK1)/Parkin pathways and O-linked N-acetylglucosamine transferase (OGT), respectively (Figure 1.5). The PINK1/Parkin pathway targets Miro for proteosomal degradation, thereby blocking mitochondrial transport. The mechanism is unclear. PINK1 was originally reported to phosphorylate Miro-1/2 at Ser 156, priming it for ubiquitination and subsequent proteosomal degradation in a Parkin-dependent manner (152), however this was later disputed by others (165). A number of other PINK1-dependent phosphorylation sites have since been identified in *Drosophila* Miro (Ser 324, Thr 325) (157). It is possible that if these phosphorylation sites are conserved in human Miro orthologues, Parkin ubiquitination may occur by this means. A recent study by Birsa and colleagues (166) contributes further to this controversy, by suggesting an alternate mechanism whereby Parkin-dependent ubiquitination of Miro is sufficient to inhibit mitochondrial transport prior to its degradation. Whilst degradation was delayed for several hours following ubiquitination, this modification did not affect the integrity of Miro/Milton binding (166).

OGT has been demonstrated to bind directly to, and catalyse the O-GlcNAcylation of Milton, in turn disrupting mitochondrial transport. As OGT is stimulated by glucose

flux, this modification is proposed to assist in ATP production by pausing mitochondrial movement to enable uptake in glucose microdomains (156). O-GlcNAcylation of Milton does not affect formation of the Miro/Milton/KIF5 complex, and the mechanism by which mitochondrial transport is disrupted is unknown (156).

1.3.2.2 Other mitochondrial transport mechanisms

Numerous mechanisms independent of the Miro/Milton complex are also used to transport mitochondria throughout the cell. For the most part, these mechanisms are not functionally redundant and contribute to different facets of mitochondrial transport. For example, a number of mechanisms identified for microtubule-based transport have been found to be specific to neuronal cells (Table 1.4). Furthermore, the actin and intermediate filament networks have also been implicated in mitochondrial transport, enabling mitochondria to reach regions of the cell not accessible by microtubules. Other mitochondrial motor protein complexes involved in regulating microtubular anterograde transport of mitochondria are described in Table 1.4. In the retrograde direction however, only cytoplasmic dynein has been implicated. Interestingly, both Miro (167, 168) and Milton (169) have been shown to interact with the dynein motor and contribute to retrograde movement. A number of MAP proteins, outlined in Table 1.4 have also been shown to regulate mitochondrial transport.

Mitochondrial transport across the actin and intermediate filament networks is poorly defined. Mitochondrial transport is primarily actin-based in yeast, however there is increasing evidence implicating this mode of transport in higher eukaryotes. In particular, the actin-based motor proteins Myosins V, VI and XIX have been shown to regulate mitochondrial transport (Table 1.4). Actin-dependent transport may be important for facilitating transport to microtubule-scarce regions of the cell and perhaps shuttling detached mitochondria back to microtubules. This notion is in line with findings that actin-based transport is primarily short range (170-172). The role of intermediate filaments in transporting mitochondria is even less clear. Cells with defective keratin and neurofilament networks have been shown to display aberrant mitochondrial distribution (173, 174) and mitochondrial transmembrane protein Plectin 1b has been proposed to link mitochondria to these intermediate filament networks (175).

Table 1.4: Mechanisms of mitochondrial transport

Cytoskeleton	Motor	Adaptor/Cofactors	Mechanism	References
Microtubule (anterograde motor transport)	KIF5A/B/C	Miro/Milton (Mfn2, Alex3)	Mitochondrial transmembrane protein Miro attaches to the KIF5 motor complex through the adaptor protein Milton.	Section 1.3.2.1
	KIF5B/C	RanBP2	RanBP2 associates directly with KIF5 and relieves its auto-inhibition, thereby stimulating motor activity.	(176, 177)
	KIF5B	Syntabulin	Syntabulin targets to the OMM, and directly binds KIF5 to drive mitochondrial transport in neuronal processes.	(178)
	KIF1B α	KBP	KBP localises to mitochondria and binds directly to the motor domain of KIF1B α where it is suggested to increase kinesin motor activity.	(179, 180)
	KLP6	KBP	Kinesin KLP6 stimulates mitochondrial transport through an undefined mechanism, possibly facilitated by its association with KBP.	(181)
Microtubule (retrograde motor transport)	Cytoplasmic Dynein	Miro Milton	Cytoplasmic dynein drives retrograde mitochondrial transport.	(182)

Table continued over page.

Cytoskeleton	Motor	Adaptor/Cofactors	Mechanism	References
Microtubule (other)	-	MAP1B	MAP1B negatively regulates retrograde mitochondrial transport possibly by competing for motor proteins in neuronal axons.	(183)
	-	Tau	Tau negatively regulates anterograde mitochondrial transport possibly by competing for motor proteins in neuronal axons.	(183, 184)
	-	Syntaphilin	Syntaphilin is a Ca ²⁺ induced anchor, used to immobilise mitochondria by displacing KIF5 from Miro/Milton. Specific for axonal mitochondrial transport.	(185, 186)
Actin	Myosin V	?	Myosin V disrupts anterograde and retrograde transport, possibly by competing with microtubule motor proteins for mitochondrial cargo.	(187)
	Myosin VI	?	Myosin VI disrupts anterograde and retrograde transport, possibly by competing with microtubule motor proteins for mitochondrial cargo.	(187)
	Myosin XIX	Direct	Myosin XIX associates directly with mitochondria to facilitate actin-based transport.	(188)
Intermediate filament	-	Plectin 1b	Plectin 1b, a mitochondrial transmembrane protein, links mitochondria to intermediate filaments. Loss of Plectin 1b caused defects in mitochondrial dynamics which may be due defects in mitochondrial transport.	(175)

1.3.2.3 The functional relevance of mitochondrial transport

Regulation of mitochondrial transport is essential for the site-specific functionality of mitochondria, namely its dispersal of synthesised ATP (Section 1.3.1.1), and buffering of calcium (Section 1.3.1.2). Targeting of mitochondria to subcellular regions with high bioenergetic demands is a much more effective method of ATP supply compared to the random diffusion of ATP through the cytoplasm, and has been reported to be particularly relevant at the cell membrane for cell migration, and the synaptic terminal of neurons for the generation of action potentials (18, 19, 142, 189). Likewise, close proximity to calcium micro-domains and the cell periphery is required to facilitate rapid calcium uptake (15, 127, 190). Aberrant mitochondrial transport has been linked to a number of neurodegenerative diseases including Alzheimer's, and Parkinson's diseases (139), and more recently, increased risk of metastasis in cancer (18, 19). These disease phenotypes are reviewed in more detail in Section 1.3.4.

1.3.3 Mitochondrial Fission/Fusion Dynamics

Mitochondrial morphology is not static. Rather, mitochondria continuously undergo fission and fusion events in response to numerous cellular signals allowing them to exist as both tubular networks and discrete puncta. These processes are primarily regulated by the opposing actions of the core fission/fusion machinery (described in Section 1.3.3.1), and are important for many aspects of normal cellular function including mitophagy and maintenance of mtDNA fidelity (see Section 1.3.3.2). Fission/Fusion dynamics are intimately linked with mitochondrial transport dynamics. For example, defective mitochondrial transport can affect the ability of mitochondria to move together for fusion, and apart for fission. Furthermore, excessive fission or fusion has been demonstrated to respectively increase or decrease the speed of mitochondrial transport (19). As such, it is unsurprising that aberrant mitochondrial fission/fusion dynamics have been linked to similar neurodegenerative and cancer disease phenotypes as defective mitochondrial transport. This is described in more detail in Section 1.3.4.

1.3.3.1 Mechanisms of fission/fusion

Mitochondrial fission and fusion is maintained by the actions of a set of dynamin related GTPase proteins, comprised of fusion mediators Mitofusin1/2 (Mfn1/2) and Optic atrophy 1 (OPA1), and fission mediator Dynamin related protein 1 (DRP1). These proteins are in turn regulated by various effector proteins and signals in response to cellular demands (Table 1.5). The mechanisms of mitochondrial fission/fusion have been reviewed extensively (191-195) and are summarised below.

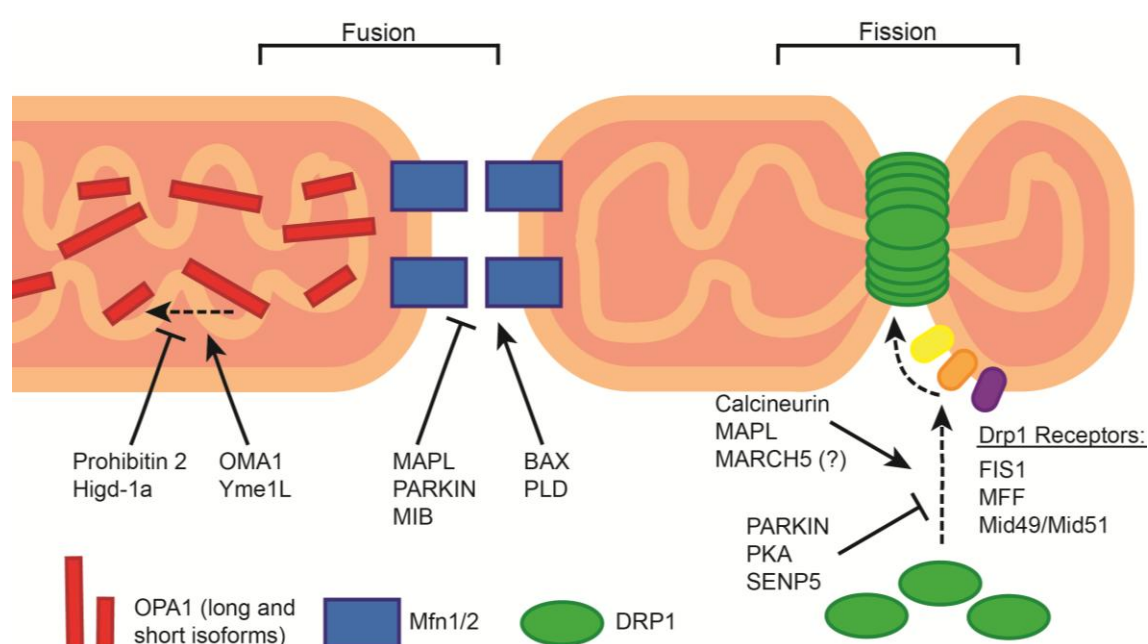


Figure 1.6: Mechanisms of mitochondrial fission and fusion.

The schematic outlines core mechanisms of mitochondrial fission/fusion. Fusion requires coordination between the OMM and IMM. Mfn1/2 on opposing OMMs dimerise and promote fusion. OPA1 regulates IMM fusion which requires both long, and shorter cleaved isoforms to be effective. Fission is regulated by DRP1, a cytoplasmic protein which requires mitochondrial recruitment via a receptor protein. When fission is stimulated, DRP1 oligomerises and forms a ring structure which constricts around the mitochondria. Regulatory proteins indicated on the schematic are summarised in Table 1.5.

Fusion

Effective mitochondrial fusion requires coordination of both the OMM and IMM, primarily relying on Mfn1/2 and OPA1, respectively (196). The two mitofusins, Mfn1 and Mfn2, are anchored in the OMM (197, 198), where they homo- or hetero-dimerise with Mfn1/2 anchored in the OMM of opposing mitochondria, acting as a tether (see Figure 1.6). The mitofusins then attach to the opposing mitochondrial membranes, after which a GTPase-dependent conformational change causes OMM fusion (191, 199). Mfn2 also contributes to mitochondrial tethering to the ER (200), and to mitochondrial transport (Table 1.3). Regulation of Mfn1/2 activity is outlined in Table 1.5. The fission regulator OPA1 is responsible for IMM fusion and cristae remodelling (191, 201, 202). Whilst the mechanism is unclear, OPA1 is reported to undergo alternate splicing (Table 1.5) to produce a range of protein isoforms required for effective fusion (203-205).

Fission

Key to the regulation of mitochondrial fission is the GTPase protein, DRP1. DRP1 is primarily cytoplasmic, but when activated it translocates to the mitochondria where it oligomerises, forming a helical ring structure which, when hydrolysed, constricts mitochondria to induce fission (206, 207). Numerous other proteins have been reported to contribute to fission, however these mainly function to regulate DRP1 activation or localisation at the OMM in response to different cellular signals. These effectors are summarised in Table 1.5 and primarily act through post-translational modification or as DRP1 receptors. ER tubules have also been proposed to contribute to fission by wrapping around mitochondria at fission sites (208). Other players, including Endophilin B, MTP18 and GDAP1 have been implicated in controlling mitochondrial fission but their role is less clear (209-211).

Table 1.5: Regulation of the core mitochondrial fission/fusion machinery

Target	Cofactor(s)	Regulation	Mechanism	References
Mfn 1/2	MUL1 Parkin	Ubiquitination	Targets Mfn2 to the proteasome for degradation, inhibiting fusion.	(212-214)
	MIB	?	Blocks Mfn1 through an unknown mechanism, inhibiting fusion.	(215)
	BAX	?	Targets Mfn2 to promote fusion through an unknown mechanism.	(216)
	Phospholipase D	?	Targets Mfn1/2 to promote fusion through an unknown mechanism.	(217)
OPA1	OMA1 Yme1L	Proteolytic cleavage	Regulates cleavage of long forms of OPA1 into short forms.	(218, 219)
	Prohibitin-2 Higd-1a	Protection from proteolytic cleavage	Protects against accelerated cleavage of long forms of OPA1.	(220, 221)
DRP1	FIS1	Receptor	Recruits DRP1 to the OMM, promoting fission. Also proposed to inactivate Mid51.	(222, 223)
	MF1	Receptor	Recruits DRP1 to the OMM, promoting fission.	(224)
	Mid49/Mid51 (MIEF2/1)	Receptor	Recruits DRP1 to the OMM where it inhibits DRP1's GTPase function, blocking fission.	(223, 225, 226).
	MARCH5 (MITOL)	Ubiquitination	Unclear, may positively regulate fission by promoting DRP1 at fission sites, rather than marking for proteasomal degradation.	(227, 228)
	PARKIN	Ubiquitination	Targets DRP1 to the proteasome for degradation, inhibiting fission.	(229)
	PKA	Phosphorylation	Blocks DRP1 translocation to the mitochondria, inhibiting fission.	(230, 231).
	Calcineurin	Dephosphorylation	Stimulates DRP1 translocation to the mitochondria, promoting fission.	(232)
	MUL1	SUMOylation	Stabilises DRP1 at the OMM, promoting fission.	(233, 234)
	SENP5	DeSUMOylation	Blocks DRP1 translocation to the mitochondria, inhibiting fission.	(235)

1.3.3.2 The functional relevance of mitochondrial fission/fusion dynamics

Mitochondrial fission and fusion dynamics have been implicated in mtDNA fidelity, mitophagy, apoptosis and other processes including regulation of ATP production (236), speed of mitochondrial transport (19) and mitochondrial inheritance during mitosis (237). The importance of mitochondrial fission/fusion dynamics is highlighted by the numerous disease pathologies which present when these dynamics are compromised, primarily in neurodegenerative diseases such as Charcot-Marie-Tooth (CMT) and Parkinson's disease (Section 1.3.4)

mtDNA fidelity (mitochondrial homogenisation)

The fusion of mitochondria is essential in maintaining a homogenous mitochondrial population (238). When mitochondria undergo fusion, their contents including mtDNA, metabolites and enzymes are able to be exchanged (239, 240). This is particularly important for mtDNA which encodes crucial enzymes in the electron transport chain, and is prone to damaging mutations as a result of its close proximity to sites of ROS production. Unlike nuclear DNA, the mtDNA genome is polyploid, therefore thousands of copies are present per cell. Furthermore, mutations are usually recessive and can accumulate at high levels without effecting mitochondrial function (241, 242). Mixing of mitochondrial contents therefore allows for damaged mtDNA to be exchanged for complimentary healthy mtDNA (239, 240). However, defective mitochondria with severely damaged mtDNA are quarantined and primed for mitophagy, as detailed below.

Mitophagy and autophagy

Mitophagy is a specific type of autophagy which targets mitochondria for degradation, often assisting in mitochondrial quality control through the quarantine and removal of dysfunctional mitochondria (243). Mitochondrial fission is essential for separating defective mitochondria from the healthy population, a process which is regulated through the PINK/Parkin mitophagy pathway. In this pathway, PINK1 is targeted to damaged, depolarised mitochondria and recruits Parkin to the OMM, where it poly-ubiquitinates OMM proteins targeting them for degradation (244, 245), and subsequently stimulating mitophagy (246). Mfn2 in particular is targeted by Parkin in this process, decreasing fusion and tipping the balance towards fission (247).

Fission/Fusion dynamics have also been reported to play a role in cell survival during starvation-induced autophagy. Starvation induces PKA activation, stimulating the phosphorylation of DRP1, consequently inhibiting mitochondrial translocation, and fission (230, 231). The subsequent mitochondrial elongation has been reported to protect mitochondria from autophagosomes, possibly through steric hindrance, thereby allowing autophagic cells to maintain ATP production and hence, viability (248).

Apoptosis

Mechanisms mediating induction of apoptosis and mitochondrial fission/fusion dynamics often intersect as these pathways share many common proteins (see Table 1.5). As such, it is hard to elucidate if mitochondrial morphology plays a role in the apoptotic response, or if any apoptotic changes are secondary effects caused by modulation of common machinery. For example, the apoptotic response is associated with extensive mitochondrial fission which occurs immediately prior to release of Cytochrome C. Alterations to DRP1 activity by stimulating its translocation to the OMM inducing mitochondrial fragmentation, or through expression of a dominant-negative mutant inducing mitochondrial elongation have been demonstrated to respectively increase and decrease the sensitivity of cells to apoptotic stimuli (230, 249, 250). However, extensive mitochondrial fission has been observed in many cases not pertaining to apoptosis (summarised in 251). Moreover, it is unclear whether mitochondrial fission is required for the apoptotic process, or is simply a by-product of other apoptotic pathways mediated by DRP1. This is presently a subject of controversy within the literature (252, 253). This topic and further examples pertaining to other proteins in the fission/fusion machinery are reviewed in more detail elsewhere (251, 254).

1.3.4 Mitochondrial dysfunction in disease

The mitochondria are a cornerstone of normal cell function, playing the central role in cellular metabolism (Section 1.3.1). As a result, mitochondrial dysfunction has wide-reaching effects. Neurodegenerative diseases in particular are often associated with aberrant mitochondrial function due to the high bioenergetic demands, and the unique morphology of neuronal cells (Section 1.3.4.1). Mitochondrial dysfunction has also been increasingly linked to numerous cancer types (Section 1.3.4.2). Other pathologies

associated with defective mitochondrial function include the mitochondrial cytopathies, like MELAS syndrome, which is characterised by defects in the electron transport chain, and Type II diabetes (255-257).

1.3.4.1 Neurodegenerative disease

In neurodegenerative disease pathologies, disrupted mitochondrial transport, extensive fragmentation and loss of mtDNA fidelity (a common effect of aberrant fission/fusion dynamics – Section 1.3.3.2) are commonly observed (139-141). Neurons are highly sensitive to these defects due to their high metabolic demands, long post-mitotic life spans and far reaching processes over which mitochondria need to be shuttled. Dysfunctional mitochondria affect many aspects of normal neuronal function, for example at synaptic terminals where mitochondria are required to supply ATP for neurotransmission, and buffer calcium influxes for maintenance of neuroplasticity (258).

The neuromuscular disorder, Charcot-Marie-Tooth (CMT) subtype 2A for example, is specifically caused by a point mutation in *Mfn2*, which causes mitochondrial fragmentation and mtDNA damage leading to motor axon degeneration (259). Another neurological disease, autosomal dominant optic atrophy (ADOA) type 1, is often caused by a mutation in *OPA1* and affects retinal ganglion cells in the optic nerve (260). The retinal ganglion cells of patients with ADOA display extensive mitochondrial fragmentation and are more sensitive to apoptosis, leading to degeneration which impairs sight and can lead to blindness. A growing body of evidence also indicates that mitochondrial dysfunction is a key feature of Parkinson's disease (PD) and, certain subtypes have been linked to mutations in proteins that influence mitochondrial transport and morphology. Mutations in *PINK/Parkin* (see Section 1.3.2.1, Table 1.5), are often observed in autosomal recessive juvenile PD, and directly impact mitochondrial distribution and quality control (257, 261). Aberrant expression of mitochondrial fission/fusion proteins and altered kinesin dynamics have also been observed in Alzheimer's and Huntington's diseases (139, 257, 261).

1.3.4.2 Cancer

Defective mitochondria were first linked to carcinogenesis as the cause of the “Warburg effect”, a commonly observed phenotype whereby tumour cells display increased rates of ATP generation by glycolysis in the cytosol as an alternate method to production by oxidative phosphorylation (262). Since then, many aspects of mitochondrial dysfunction have been found to contribute to tumorigenesis, and due to the interlinked nature of metabolic and mitochondrial regulatory pathways often aberrations in one pathway can cause a knock-on effect resulting in defects in numerous others. Excessive mtDNA genome mutation and defective mitophagy, mitochondrial biogenesis, and metabolic signalling have all been observed in tumour cells. The complex interplay between these pathways frequently results in aberrant ROS production, ATP production and metabolic signalling, often switching on pathways that promote growth, cell survival and even alterations in nuclear DNA fidelity. These pathways are reviewed extensively in the literature (14, 263, 264).

A growing body of evidence suggests that defective mitochondrial transport and fission/fusion dynamics play a significant role in cancer formation. The heterogenic nature of tumours means that preference for particular defects could depend on many factors including tissue type, stage of carcinogenesis and location within the tumour. As previously discussed, mitochondrial transport and fission/fusion dynamics are intimately linked, for simplicity however they have been split in the subsections below.

Mitochondrial transport

Recent studies have linked perturbations in mitochondrial transport to aberrant cell migration, a hallmark of cancer cells (18, 19). These studies indicate that mitochondria in metastatic breast, and prostate cancer cell lines preferentially cluster at the leading edge of migrating cells, and contribute to increased migration speed, directional persistence and invasion, which can be attenuated by disrupting the mitochondrial transport complex (18). Mitochondria localised at the cell periphery in metastatic breast cancer cells were directly implicated in supplying the ATP required for the polymerisation of F-actin, and lamellipodia formation in cell migration (19). On the other hand, mitochondrial localisation away from the cell periphery, in the perinuclear region, is also reported to be favourable for carcinogenesis. In a study by Al-Mehdi and

colleagues (265), mitochondrial clustering around the nucleus was observed to create an oxidant-rich nuclear environment by releasing ROS. This elevated nuclear ROS was then shown to cause oxidative base DNA damage, stimulating the transcription of growth signalling proteins like vascular endothelial growth factor (VEGF).

Mitochondrial fission/fusion dynamics

Aberrant expression of mitochondrial fission and fusion proteins have been observed in numerous cancer types (14, 140, 266). However, the outcome of defective morphological dynamics can vary. For example, up-regulation of DRP1 tips the morphological balance towards fission, and has been reported in several cancer types where it was linked to increased mitochondrial motility, and a loss of mtDNA fidelity, electron transport chain defects, and subsequently increased ROS production, which are all favourable in cancer progression. However, electron transport chain defects reduce ATP production and extensive mitochondrial fission is reported to promote apoptosis; neither is favourable for tumourigenesis (19, 140, 266). On the other hand, hypoxia-induced mitochondrial fusion is also reported to be favourable to cancer progression, with links to cancer cell survival and higher rates of ATP production (14, 140, 267). The paradoxical nature of mitochondrial fission/fusion dynamics in carcinogenesis is likely due to the heterogeneity in tumour cells, suggesting that the preferred mitochondrial morphology for cancer growth is determined on a cell-by-cell basis.

1.4 Rationale and summary of study

Evidence in the literature supports a mitochondrial transporter or chaperone role for APC; (1) APC is a large mobile scaffold than can not only stimulate assembly of protein complexes (e.g. the β -catenin destruction complex), but also influence the localisation of other proteins (e.g. β -catenin) (Section 1.2.1). (2) APC associates with mitochondria in both mutant and full-length forms (Section 1.2.1.4). (3) Mitochondria are highly dynamic and transported to the plasma membrane by kinesin complexes that sometimes include known APC-binding partners, such as RanBP2 (Section 1.3.2). (4) Both APC and mitochondria have been linked to cell migration and shown to be directed along microtubules to the membrane (Sections 1.2.1.3, 1.3.2.3). When considered together,

these and other facets of the biology of APC and mitochondria suggested a potential role for APC in the transport of mitochondria.

The hypothesis, that APC plays a novel role in the anterograde transport of mitochondria was investigated and shown to be true. In Chapter 3, loss of APC wild-type is demonstrated to cause uniformly spread mitochondria to redistribute towards the perinuclear region, a finding consolidated by identification of mitochondrial transport proteins Miro and Milton as novel APC binding partners. Chapter 4 identifies the C-terminal region of APC as the Miro/Milton binding domain and focuses on the implications of CRC-associated APC truncation on its mitochondrial transport capabilities. APC mutation is found to correlate strongly with defective mitochondrial transport to the cell periphery, which is restorable by expression of wild-type APC. The dynamics of APC-dependent mitochondrial transport are addressed in Chapter 5, where live cell imaging is used to determine that APC is specifically involved in the initiation of anterograde mitochondrial transport. The nature of the association between APC and Miro/Milton is investigated further in Chapter 6, where preliminary studies suggest that APC stabilises the interaction between Miro and Milton, perhaps in a scaffolding capacity.



CHAPTER 2

General Materials and Methods



2.1 Materials

2.1.1 Cell Lines

All cell lines used in this study are outlined in Table 2.1. All cell lines were obtained from the American Type Culture Collection (ATCC) unless otherwise stated.

Table 2.1: Cell lines and source

Cell Line	APC Status	Source
U2OS	Wild type	Human epithelial osteosarcoma
HDF1314	Wild type	Human dermal fibroblast
NIH 3T3	Wild type	Mouse embryonic fibroblast
Hela	Wild type	Human epithelial cervical cancer
SW480	(1-1337)	Human epithelial colorectal adenocarcinoma
HT-29	(1-853/1-1555)	Human epithelial colorectal adenocarcinoma
HCT116	Wild type	Human epithelial colorectal adenocarcinoma
LIM 1215	Wild type	Human epithelial colorectal adenocarcinoma
Inducible HEK 293 (1-2843)	Wild type, inducible wild type.	Human embryonic kidney. Inducible APC cells created and supplied by (268).
Inducible HEK 293 (1-1309)	Wild type, inducible (1-1309)	Human embryonic kidney. Inducible APC cells created and supplied by (268)

2.1.2 Antibodies and Dyes

Primary antibodies, secondary antibodies and dyes used in this study are outlined in Table 2.2, Table 2.3 and Table 2.4, respectively.

Table 2.2: Primary antibodies

Antibody Target	Clonality	Dilution			IP	Supplier
		IF	WB	Duo		
α -Actin	Monoclonal	1:1000	-	-		Sigma-Aldrich
APC (Ab1)	Monoclonal	-	1:100	-		Calbiochem
APC (Ab5)	Monoclonal	-	-	-	Y	Calbiochem
APC (Ab7)	Monoclonal	1:100	-	1:400		Calbiochem
APC (C20)	Polyclonal	-	-	-	Y	Santa Cruz
APC (H290)	Polyclonal	1:400	1:500	1:2000		Santa Cruz
β -Catenin	Monoclonal	1:100	1:2000	1:1000		BD Biosciences
β -Catenin	Polyclonal	1:100	-	1:1,000		Santa Cruz
BRCA1	Polyclonal	-	-	1:300		Calbiochem
DRP1	Monoclonal	1:800	1:1000	1:10000		BD Biosciences
EB1	Monoclonal	1:200	1:500	-		BD Biosciences
58k	Monoclonal	1:150	-	-		Abcam
Fis1	Polyclonal	1:400	-	1:2000		Gift*
GFP	Monoclonal	1:1000	1:1000	1:100000		Roche
GFP	Polyclonal	1:1000	1:1000	-	Y	Invitrogen
HSP70	Monoclonal	1:1000	1:1000	-		Pierce
IgGr	Polyclonal	-	-	-	Y	Sigma-Aldrich
IgGm	Monoclonal	-	-	-	Y	Sigma-Aldrich
IQGAP1	Polyclonal	1:200	-	1:400		Santa Cruz
KAP3A	Monoclonal	1:200	-	-		BD Biosciences
KIF5	Monoclonal	-	-	1:600		Millipore
LAMP-1	Monoclonal	1:100	-	-		BD Biosciences
Milton 2 (TRAK2)	Polyclonal	1:100	1:100	1:500	Y	Sigma-Aldrich
Miro 1 (RHOT1)	Polyclonal	1:100	1:500	1:300		Sigma-Aldrich
Mfn2	Polyclonal	1:500	1:1000	1:2000		Gift*
OPA1	Monoclonal	1:500	1:1000	1:5000		BD Biosciences
PCNA	Monoclonal	-	-	1:500		BD Biosciences
RanBP2	Monoclonal	1:100	1:500	1:2000	Y	Santa Cruz
RanBP2	Polyclonal	1:500	-	1:2000		Santa Cruz
Topo II	Monoclonal	-	1:500	-		Calbiochem
α tubulin	Monoclonal	1:1000	1:1500	-		Sigma-Aldrich
γ -tubulin	Monoclonal	1:200	-	-		Abcam

IF: Immunofluorescence, WB: Western Blot, Duo: Duolink, IP: Immunoprecipitation. Antibodies marked with (*) were generously gifted by Dr Mike Ryan.

Table 2.3: Secondary antibodies

Antibody	Dilution		Supplier
	IF	WB	
AlexaFluor® 405 anti-mouse	1:400	-	Molecular Probes
AlexaFluor® 405 anti-rabbit	1:400	-	Molecular Probes
AlexaFluor® 488 anti-mouse	1:500	-	Molecular Probes
AlexaFluor® 488 anti-rabbit	1:500	-	Molecular Probes
AlexaFluor® 594 anti-mouse	1:2000	-	Molecular Probes
AlexaFluor® 594 anti-rabbit	1:2000	-	Molecular Probes
HRP-conjugated anti-mouse	-	1:10000	Sigma-Aldrich
HRP-conjugated anti-rabbit	-	1:10000	Sigma-Aldrich

IF: Immunofluorescence, WB: Western Blot.

Table 2.4: Dyes

Dye	Dilution, IF	Supplier
CMX-Ros	1:10000	Molecular Probes
ER Tracker	1:500	Molecular Probes
Hoechst 33258 (200 µg/ml)	1:200	Sigma-Aldrich

IF: Immunofluorescence

2.1.3 Small interfering RNA (siRNA)

Small interfering RNAs (siRNA) used are outlined in Table 2.5.

Table 2.5: siRNA target sequences

Target Gene	siRNA	Target Sequence	Source
scrambled sequence	control siRNA	AAT TCT CCG AAC GTG TCA CGT	QIAGEN- custom made
scrambled sequence	control siRNA	Non-targeting nucleotides	Santa Cruz (sc-367007)
APC	APC2	AAC GAG CAC AGC GAA GAA TAG	QIAGEN- custom made
APC	APCd	AGG GGC AGC AAC TGA TGA AAA	QIAGEN- custom made
APC (mouse)	mAPC	AAG GAC TGG TAT TAT GCT CAA	QIAGEN- custom made
APC (mouse)	mAPC-red (AlexaFluor® 555)	AAG GAC TGG TAT TAT GCT CAA	QIAGEN- custom made
EB1	EB1	Pool of 3-5 siRNA nucleotides	Santa Cruz (sc-35258)
RanBP2	RanBP2	Pool of 3-5 siRNA nucleotides	Santa Cruz (sc-36381)

2.1.4 Plasmids

Plasmid DNA constructs used in this study are outlined in Table 2.6 below.

Table 2.6: Plasmids and sources

Gene	Construct	Tag	Source
APC	APC WT	pCMV	Dr Bert Vogelstein* (91)
	APC WT	GFP	Dr Angela Barth *(269).
	APC (1-1309)	pCMV	Dr Bert Vogelstein* (91)
	APC (1-1309)	EGFP	Dr Myth Mok (Chinese University of Hong Kong)
	APC (1-302)	EGFP	Dr Manisha Sharma (27)
	APC (334-900)	EGFP	Dr Manisha Sharma (27)
	APC (1379-2080)	GFP	Dr Mariann Bienz* (49)
	APC (2226-2644)	EGFP	Dr Manisha Sharma (27)
	APC (2650-2843)	EGFP	Dr Manisha Sharma (27)
Mito targeting sequence (COX8)	Mito	GFP2	Evrogen (Moscow, Russia)
Miro (RHOT)	Miro-1	EGFP	Dr Mike Ryan* (270)
	Miro-2	EGFP	Dr Mike Ryan* (270)
Milton (TRAK)	Milton-1	EGFP	Dr Mike Ryan* (270)
	Milton-2	EGFP	Dr Mike Ryan* (270)

WT: Wild type. Sources marked with (*) kindly supplied plasmids as gifts.

2.1.5 Drugs

Drug treatments performed in this study are outlined in Table 2.7.

Table 2.7: Drug target action

Drug	Target Action	Dosage /Time	Solvent	Supplier
Calcimycin (A23187)	Cation ionophore selective for Ca^{2+} , Mn^{2+} and Mg^{2+} . Used in this study to increase intracellular Ca^{2+} concentrations.	20 μM /5 min	DMSO	Sigma-Aldrich
Latrunculin A	Binds actin monomers to prevent polymerisation into F-actin.	0.5 nM /1 h	DMSO	Sigma-Aldrich
Nocodazole	Binds to β -tubulin sub-units to prevent polymerisation into microtubules.	33 μM /1 h	DMSO	Sigma-Aldrich
Tetracycline	An antibiotic used in this study to induce APC fragment expression in inducible HEK cell lines.	4.5 nM /16h	H ₂ O	Sigma-Aldrich

2.1.6 Other Reagents

Other reagents used in this study are outlined in Table 2.8.

Table 2.8: Reagents

Reagent	Supplier
Acetic acid	Fisher Scientific
Acetone	Merck
Acrylamide solution 40%	Merck
Agar	Amresco
Agarose	Amresco
Ammonium persulphate (APS)	Sigma-Aldrich
Ampicillin	Calbiochem
Bacto-agar	Oxoid
Bacto-tryptone	Oxoid
Bacto-yeast extract	Amresco
Blastocidin	Sigma-Aldrich
Boric Acid	Astral Scientific
Bovine serum albumin (BSA)	Sigma-Aldrich
Bromophenol blue	Sigma-Aldrich
Calcium chloride (CaCl ₂)	Sigma-Aldrich
Chromotography paper	Whatman
Deoxycholate	Biomedicals Inc.
Dulbecco's Modified Eagle Medium (DMEM)	Sigma-Aldrich
Duolink α -rabbit probes	O-link Biosciences
Duolink α -mouse probes	O-link Biosciences
Duolink amplification Red	O-link Biosciences
Duolink amplification Green	O-link Biosciences
Duolink Mounting Media	O-link Biosciences
Dimethyl Sulphoxide (DMSO)	Amresco
ECL Western blotting detection reagents	GE Healthcare
Ethanol (absolute)	Merck
Ethylenediaminetetra-acetic acid (EDTA)	Amresco
Fetal bovine serum (FBS)	ThermoTrace
Fugene HD	Promega
Glucose (20%)	Amresco
Glutamine (200 mM)	SAFC biosciences
Glycerol	Amresco
Glycine	Amresco
HEPES buffer (1 M)	SAFC Biosciences
Hydrochloric acid (HCl)	AJAX chemicals

Hygromycin B	Sigma-Aldrich
Isopropanol	Amresco
K2 Transfection	Biontex
Kanamycin	Boehringer Mannheim
Lipofectamine	Life Technologies
Manganese (II) chloride (MnCl ₂)	AJAX chemicals
Magnesium chloride (MgCl ₂)	AJAX chemicals
Magnesium sulphate (MgSO ₄)	AJAX chemicals
β-mercaptoethanol	Sigma-Aldrich
Methanol (absolute)	Fronine
Nitrocellulose membrane	Millipore
Nonidet P-40 (NP-40)	Roche
Opti-MEM™ reduced serum medium	Life Technologies
Penicillin G (500 U/mL)/Streptomycin sulphate (5000 µg/ml)	CSL Biosciences
Polyethylenimine (PEI)	Sigma-Aldrich
Phosphate Buffered Saline (PBS, distilled)	Lonza Biowhittaker
Poly-L-lysine	Sigma-Aldrich
Ponceau S	Sigma-Aldrich
Potassium acetate	AJAX chemicals
Potassium chloride (KCl)	AnalaR
Potassium phosphate (KH ₂ PO ₄)	Sigma-Aldrich
Precision Plus Dual colour standards	BioRad
Protease inhibitor cocktail tablets (complete)	Roche
Protein-A-sepharose beads	GE Healthcare
Rubidium chloride (RbCl)	Sigma-Aldrich
Skim milk powder	Diploma
Sodium chloride (NaCl)	Sigma-Aldrich
Sodium dodecyl sulphate (SDS; 20%)	Amresco
(Di)Sodium phosphate (Na ₂ HPO ₄)	AJAX Chemicals
TEMED	Amresco
Tris	Amresco
Triton-X-100	Astral Scientific
Trypsin	JRH Biosciences
Tween-20	Astral Scientific
Vectashield mounting medium	Vector Laboratories
Water (distilled)	Baxter Laboratories

2.2 Methods

2.2.1 Bacterial culture

2.2.1.1 Overnight bacterial culture

2-yeast tryptone (2-YT) medium or agar was prepared as per Appendix 2.1. Agar plates were streaked with a bacterial glycerol stock (prepared as 2.2.1.2) in a sterile environment using an inoculation loop, and then incubated for 14-16 h at 37°C. A single colony from the agar plate was used to inoculate 2-YT media containing the appropriate antibiotic (ampicillin or kanamycin, 50 µg/ml), and incubated at 37°C for 14-16 h at 250 rpm (revolutions per minute).

2.2.1.2 Freezing bacterial cultures as glycerol stocks

Bacterial glycerol stocks were created by adding 300 µl of sterile glycerol (50%) to 700 µl of an overnight *E.coli* culture in a cryovial, then vortexed. Cultures were snap-frozen on dry ice and stored at -80°C.

2.2.1.3 Preparation of XL10-gold or BL-21 competent cells

A single colony of XL10-gold or BL-21 cells was incubated in 5 ml 2-YT medium without antibiotic at 37°C and shaken at 250 rpm for 14-16 h. This was used to inoculate 250 ml 2-YT medium supplemented with MgSO₄ (20 mM) and further incubated at 37°C, 250 rpm until the OD_{600nm} = 0.8 – 1.0. The cells were centrifuged at 1,000 *xg*/5 min/4°C, prior to discarding the supernatant and resuspending in 100 ml cold TFB1 buffer (Appendix 2.1). Following 5 min incubation on ice, cells were once more centrifuged at 1000 *xg*/5 min/4°C. The supernatant was discarded and the cells resuspended in 10 ml TFB2 buffer (Appendix 2.1). Cells were incubated on ice for a further 15-50 min then either transformed immediately or aliquoted and stored at -80°C for later use.

2.2.1.4 Heat shock transformation of XL10-gold or BL-21 cells

β -mercaptoethanol (4 μ l) was added to 100 μ l of XL10-gold or BL-21 cells (prepared as 2.2.1.3) prior to a 10 min incubation on ice with gentle agitation every 2 min. Plasmid DNA (50 ng) was then added to the cells and mixed gently before further incubation on ice for 30 min. Cells were subjected to a 90 s heat pulsation in a water bath at 42°C and then cooled on ice for 2 min. Warmed 2-YT medium (900 μ l) was added to the cells which were then incubated at 37°C, shaking at 250 rpm for 1 h. Cells were centrifuged at 358 xg for 2 min, and most of the medium removed, leaving ~100 μ l. The cell pellet was resuspended in this remaining medium, plated onto 2-YT agar plates containing the appropriate antibiotic (ampicillin or kanamycin, 50 μ g/ml) and incubated at 37°C for 14-16 h.

2.2.2 Preparation of plasmid DNA

2.2.2.1 Plasmid midi-preps

Plasmid DNA preparations were obtained using the PureYield™ Plasmid Midi-Kit (Promega) according to the manufacturer's instructions. Briefly, a 50 ml overnight culture (see 2.2.1.1) was centrifuged at 10,000 xg for 10 min and the supernatant discarded. The bacterial pellet was then resuspended in Cell Resuspension Solution (3 ml), after which Cell Lysis Solution (3 ml) was added. The bacterial solution was gently mixed by inversion and incubated at RT for 4 min. Neutralisation Solution (5 ml) was added to the lysed cells and mixed gently by inversion, before incubation at RT for 3 min in an upright position.

The following centrifugation steps utilising the PureYield™ Clearing and Binding Columns were performed using a centrifuge with a swinging bucket rotor. A PureYield™ Clearing Column was placed in a 50 ml Falcon tube and the lysate poured into the column, where it was allowed to filter through for 5 min prior to centrifugation at 1,500 xg for 5 min. A PureYield™ Binding Column was placed in a new 50 ml Falcon tube and the filtered lysate was poured into the column before further centrifugation at 1,500 xg for 5 min. Endotoxin Removal Wash (5 ml) was added to the Binding Column which was then subjected to centrifugation at 1,500 xg for 5 min

before the flow-through was discarded. Column Wash (20 ml) was added to the Binding Column and centrifuged at 1,500 xg for 5 min, after which the flow-through was discarded and the column re-centrifuged at 1,500 xg for 10 min to remove excess liquid.

To elute the DNA, the PureYield™ Binding Column was placed into a new 50 ml Falcon and nuclease-free water (600 μ l) was dropped onto the middle of the column membrane. This was subjected to centrifugation at 1500 xg for 5 min, after which the DNA-containing filtrate was transferred into an Eppendorf tube for storage at -20°C.

2.2.2.2 *Quantification of plasmid concentration*

Plasmid DNA concentration was determined using the Warburg-Christian method on a Beckman DU-64 spectrophotometer. 5 μ l DNA was diluted in 45 μ l nuclease-free water and ultraviolet radiation absorbance at 260nm (A260) and 280nm (A280) was measured. A ratio between A260:A280 in the range of 1.8-2.0 indicates that the plasmid DNA is highly purified. The DNA concentration was determined from the A260 value using the formula described below.

$$\text{DNA concentration (ng/}\mu\text{l)} = \text{A260} \times \text{dilution factor} \times 50 \text{ ng/}\mu\text{l constant}$$

2.2.3 Cell culture

All cell lines used in this thesis are described in Table 2.1 and were subject to routine mycoplasma testing. All cell culture was performed in a laminar flow hood.

2.2.3.1 *Propagation of cell lines*

All cell lines were grown as adherent cells in 25 cm², 75 cm² or 150 cm² flasks, unless otherwise stated. U2OS, HeLa, SW480, HT-29, HCT116, LIM 1215, HDF1314 and NIH 3T3 cells were maintained in supplemented DMEM (Appendix 2.1) and cultured at 37°C with 5% CO₂. HEK293 (APC-WT) and HEK293 (APC-1309) cells were maintained in supplemented DMEM containing 15 g/ml blasticidin and 150 g/ml hygromycin B and cultured at 37°C with 5% CO₂.

To propagate cell lines, the culture media was removed and the cells were washed with distilled phosphate buffered saline (PBS, Appendix 2.1). Cells were detached from the flask and collected following a 5-10 min incubation period at 37°C with 5% CO₂ in trypsin, after which they were placed in new cell culture medium. The cells were then either added to a new flask for continued propagation or seeded into the appropriate vessel for experiments (specifics outlined in the methods section for each chapter). Cells were discarded after passage 22.

2.2.3.2 Freezing cells

Cells grown to 80% confluence at a low passage number were collected using trypsin (as per 2.2.3.1), and centrifuged at 500 *xg* for 5 min after which the cell pellet was resuspended in Fetal Bovine Serum (FBS) supplemented with 10% DMSO. The cell suspension was aliquoted into cryovials on ice, and placed at -80°C for freezing prior to storage in liquid nitrogen

2.2.3.3 Reviving cells from liquid nitrogen stocks

Stocks were thawed at 37°C in a sterile water bath and added to 5 ml Dulbecco's Modified Eagle Medium (DMEM) which had been pre-warmed to 37°C. The cells were subjected to centrifugation at 500 *xg* for 5 min, after which the cell pellet was resuspended in 5 ml supplemented DMEM, transferred into a 25 cm² flask and placed in an incubator at 37°C with 5% CO₂.

2.2.3.4 Transfection of cell lines with plasmids or siRNA

A number of transfection methods were used in this study to transfect the siRNA and plasmid DNA (described in Table 2.5 and Table 2.6 respectively), into cells which had been seeded at least 12 h prior. Transfection of siRNAs was typically performed on cells at ~50% confluence with Lipofectamine (Lipofectamine 2000), whilst transfection of plasmid DNA was typically performed on cells at ~70% confluence with polyethylenimine (PEI). Following treatment with transfection reagents, cells were incubated at 37°C and 5% CO₂, for 72 h for siRNA transfection or 48 h for plasmid DNA transfection. The typical concentration for plasmid DNA transfection was 1-2

µg/ml, however under certain conditions this amount was reduced. This is discussed further in the relevant results chapters.

The protocol for both Lipofectamine and PEI is identical. Lipofectamine or PEI was diluted in serum-free OptiMEM™ medium and incubated for 5 min at RT. In a separate tube, siRNA or plasmid DNA was diluted in serum-free OptiMEM™ medium. The Lipofectamine or PEI mixture was then slowly added to the siRNA/Plasmid DNA mixture and incubated at RT for 20 min, before it was diluted in DMEM and added to the cell culture. Following a 6 h incubation period at 37°C and 5% CO₂, the culture medium was removed and replaced with supplemented DMEM. Reagent volumes used for typical transfection are outlined below.

PEI and Lipofectamine Transfection Reagents

<u>Tube 1</u>	<u>Tube 2</u>	<u>DMEM</u>
3 µg siRNA <i>OR</i> 1-2 µg Plasmid DNA	3 µl Lipofectamine <i>OR</i> PEI	1 ml
100 µl serum-free OptiMEM™	100 µl serum-free OptiMEM™	

The above protocol describes the components required for a single well in a standard 6-well tissue culture plate. Reagents were scaled up and down according to size of vessel.

The protocol for transfection of plasmid DNA with Fugene HD is as follows; Fugene HD and plasmid DNA were diluted in serum-free OptiMEM™ medium, incubated at RT for 20 min, diluted in DMEM and added to the cell culture. The medium was changed after a 6 h incubation period at 37°C and 5% CO₂, and replaced with supplemented DMEM. Reagent volumes used for typical transfection are outlined below.

Fugene Transfection Reagents

<u>Tube 1</u>	<u>DMEM</u>
1-2 µg Plasmid DNA	2 ml
4 µl Fugene	
100 µl serum-free OptiMEM™	

The above protocol describes the components required for a single well in a standard 6-well tissue culture plate. Reagents were scaled up and down according to size of vessel.

The protocol for transfection of plasmid DNA with the K2 transfection system is as follows; The K2 multiplier reagent was diluted in supplemented DMEM, added to the cell culture and incubated for 2 h at 37°C and 5% CO₂. K2 transfection reagent was diluted in serum-free OptiMEM™ medium and, in a separate tube, plasmid DNA was diluted in serum-free OptiMEM™ medium. The K2 mixture and the plasmid DNA mixture were then slowly mixed together and incubated at RT for 20 min, before being added to the cell culture containing the multiplier reagent. Following a 24 h incubation period at 37°C and 5% CO₂, the medium was removed and replaced with supplemented DMEM. Reagent volumes used for typical transfection are outlined below.

K2 Transfection Reagents

<u>Tube 1</u>	<u>Tube 2</u>	<u>DMEM</u>
1-2 µg Plasmid DNA	3 µl K2 transfection reagent	1 ml
100 µl serum-free OptiMEM™	100 µl serum-free OptiMEM™	30 µl multiplier

The above protocol describes the components required for a single well in a standard 6-well tissue culture plate. Reagents were scaled up and down according to size of vessel.

2.2.3.5 Drug Treatments

All drugs were aliquoted and stored according to the manufacturer's instructions and diluted to the desired concentration just prior to administration. To determine the dosage, drug concentrations were optimised by titration using functional concentrations and treatment times from the literature. The optimal concentration and treatment time for each drug used in this study is described in Table 2.7 and experimental specifics outlined where relevant in the results chapters.

2.2.3.6 Wound Healing Assays

Confluent cells grown on coverslips coated with Poly-L-Lysine (1 mg/ml) were wounded with a 0.8 mm (PrecisionGlide, BD) needle and washed twice with PBS prior to the addition of new DMEM. Subsequent fixation/immunostaining or live cell imaging was performed 5 h after wounding.

2.2.4 Preparation of slides for immunofluorescence microscopy

2.2.4.1 Application of Dyes by Molecular Probes®

Application of dyes by Molecular Probes® (Life Technologies) occurred prior to fixation. Cells were incubated for 15 min at 37°C and 5% CO₂ with the desired dye diluted (Table 2.4) in DMEM warmed to RT, at a volume sufficient to cover the slide. Cells were either fixed immediately afterwards, or if they were to be subjected to live cell microscopy, washed 3 times with PBS, covered in supplemented DMEM and immediately processed.

2.2.4.2 Standard fixation

Cells for analysis by immunofluorescence microscopy were grown on glass cover-slips (Menzel-gläser) in 6-well tissue culture plate (Nunc) or, if Duolink PLA was required (see Section 2.2.8), in 8-well chamber slides with silicone wells (Lab-Tek). Prior to fixation, the cell medium was removed from the well and the slide washed 3 times with PBS. A sufficient volume of chilled (-20°C) methanol:acetone (1:1) was applied to cover the slide which was then incubated at -20°C for 5 min. After fixation, the slide was washed 3 times with PBS.

2.2.4.3 Immunostaining

This protocol is for fixed cells grown on coverslips in a 6-well tissue culture plate; for the Duolink counter-staining protocol, see Section 2.2.8.5. Cells were blocked with 3% bovine serum albumin (BSA) - PBS (1 ml/well) for 40 min, after which cells were incubated for 1 h with the desired primary antibodies (Table 2.2) diluted in 3% BSA-PBS in a volume sufficient to cover the slide. Slides were then washed 3 times with PBS before incubation with secondary antibodies and/or Hoechst dye diluted (Table 2.3, Table 2.4) in 3% BSA-PBS for 1 h. Coverslips were washed 3 times with PBS and mounted on glass slides using Vectashield mounting media and sealed with clear nail polish. For basic immunofluorescence microscopy analysis, slides were viewed using an upright Olympus Fluorescent BX40 system at 40x and 60x magnification. For more advanced analysis and image capture, the inverted Olympus IX71 DeltaVision core deconvolution microscope was used (see Section 2.2.5). Slides were stored at 4°C.

2.2.5 Acquisition by DeltaVision microscopy

The Olympus IX71 DeltaVision core deconvolution microscope equipped with a CoolSNAP HQ² camera was used for advanced image capture and live cell imaging at 40x, 60x and 100x magnification.

2.2.5.1 Fixed cell

Collected images were further resolved using SoftWorx deconvolution software (Version 3.7.1; Applied Precision) and where required, sequential transverse optical sections (z-stack images) were taken which could be rendered into 3-D projections (more detail in relevant chapters). Analysis of immunofluorescence images for localisation assays, mitochondrial distribution and morphology, and Duolink PLA is described in Sections 2.2.6, 2.2.7 and 2.2.8 respectively.

2.2.5.2 Live cell

For live cell experiments, cells were seeded in 2-well chamber slides coated with Poly-L-lysine and grown until they reached the desired confluence. To visualize mitochondria, cells were either transfected with pGFP2-mito or stained with CMX-Ros. Cells subject to imaging were maintained inside the chamber at 37°C and 5% CO₂. The protocol for live cell imaging, including optimisation and post-acquisition analysis is described in greater detail in Chapter 5.

2.2.6 Localisation assays

2.2.6.1 Preparation of cells

Cells grown on glass cover-slips in 6-well tissue culture plates were fixed, immunostained and imaged as outlined in Section 2.2.4 and 2.2.5.

2.2.6.2 Analysis of localisation

The DeltaVision imaging software, SoftWorx was used to assess colocalisation between different proteins and mitochondrial markers (mitochondrial dye CMX-Ros or antibody HSP-70) stained with alternate colours. Colocalisation was deemed positive if the

staining patterns of the proteins or markers showed at least a partial overlap and, as red and green fluorophores (i.e. AlexaFluor® 594 and AlexaFluor® 488 respectively) were typically used, this was usually identified by the production of a yellow colour in the merged image.

2.2.7 Mitochondrial distribution and morphology assays

2.2.7.1 Preparation of cells

Cells grown on glass cover-slips in 6-well tissue culture plates were fixed, immunostained and imaged as outlined in Sections 2.2.4 and 2.2.5. During immunostaining, mitochondria were marked using CMX-Ros or α -HSP70. If possible, the nucleus and cell membrane were also stained using Hoescht or a cytoplasmic marker (i.e. α -tubulin or IQGAP1) respectively. If however, this was outside the limitations of 3-colour staining, the DIC channel (white light) was used to detect the nucleus and cell membrane.

2.2.7.2 Analysis of mitochondrial distribution

To quantify mitochondrial distribution, the localisation of mitochondria in cells was scored by eye into one of three 'zones' starting at the nucleus and radiating out to the cell membrane. These zones constituted 33% (zone 1), 66% (zone 2) and 100% (zone 3) of the cytoplasmic area and mitochondria were scored according to which zone they extended into (see Figure 2.1 for examples across a number of cell lines).

Differences in morphological features across the cell lines analysed meant that in some cells, certain parameters had to be put in place for mitochondrial scoring. These are described in Table 2.9. Furthermore as SW480 is a biclonal cell line expressing two morphologically distinct cell types that are round or elongated, additional parameters to those outlined in Table 2.9 were observed. Elongated cells typically presented a higher number of mitochondria in zone 3 compared to round cells and appeared more sensitive to toxicity associated with certain experimental procedures such as siRNA treatment. To avoid selecting out a single population whilst scoring, it was ensured that equal numbers of round and elongated cells were scored, and results pooled.

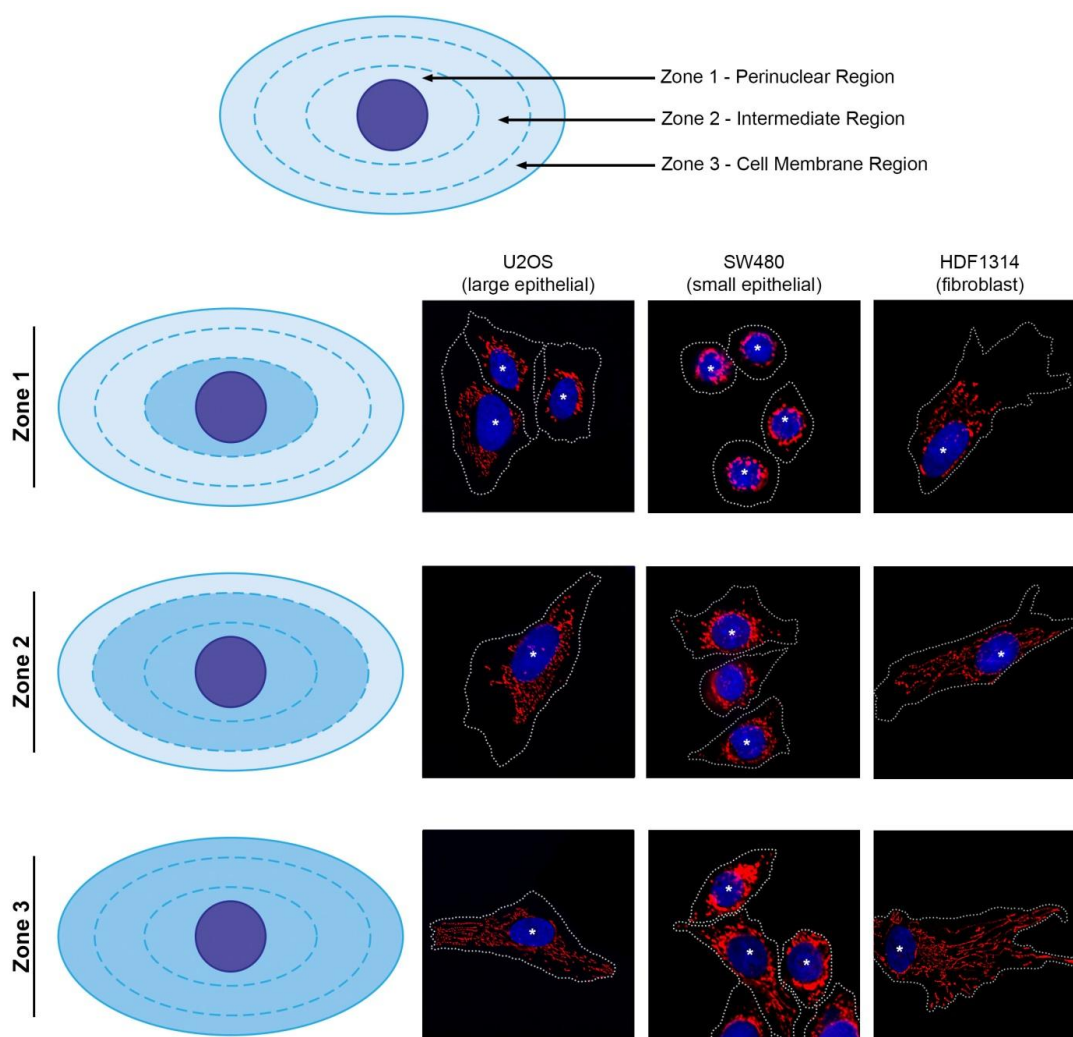


Figure 2.1: Mitochondrial distribution scoring method.

Cells were scored into one of three cellular ‘zones’ according to how far they radiated from the nucleus to the cell membrane. Cells relevant to each zone are marked (*). For cell line specific parameters see Table 2.9.

Table 2.9: Cell line specific parameters for scoring mitochondrial distribution.

Cell Type	Cell Lines	Mitochondrial Distribution Scoring Parameters
Large epithelial	U2OS, HeLa	N/A
Small epithelial	SW480, HT-29, HCT116, LIM 1215	Scoring zones are very narrow due to size of cell. Mitochondria that do not touch the nucleus are at least considered 'zone 2'. In 'zone 3' cells, the mitochondria typically touch the cell membrane.
Fibroblast	HDF1414, NIH 3T3	Mitochondria must enter the cell extensions and protrusions typically observed in fibroblasts to be considered 'zone 3'.

2.2.7.3 Analysis of mitochondrial morphology

To analyse mitochondrial morphology, cells were classified according to the size of the majority of mitochondria within the cell. Individual mitochondria were determined by eye to be either a puncta ($\sim < 2 \mu\text{m}$) or a rod ($\sim \geq 2 \mu\text{m}$) according to their length (Figure 2.2). Cells presenting a mitochondrial population where $\sim > 66\%$ were puncta was classified as “punctate”, whilst cells with $\sim > 66\%$ of the population as rods was classified as “rods”. Cells which fell into neither category (i.e. $< 66\%$ puncta and $< 66\%$ rods) were classified as “mixed”. Examples can be seen in Figure 2.2 below.

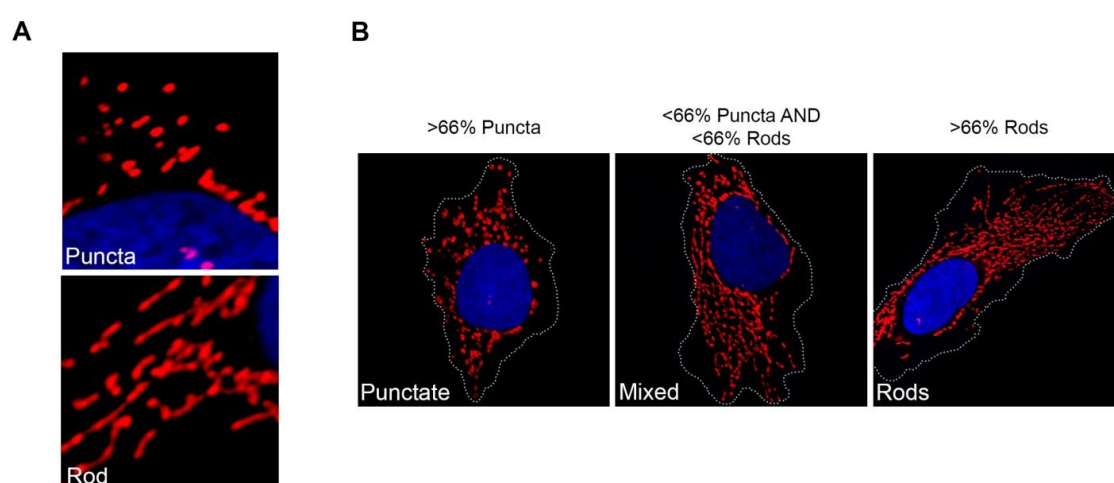


Figure 2.2: Mitochondrial morphology scoring method.

The morphology of individual mitochondria was classified as puncta or rods (A). Cells were classified according to the majority mitochondrial population (B).

2.2.8 Duolink Proximity Ligation Assay (PLA)

2.2.8.1 Rationale

Duolink PLA utilises specifically designed “PLA” probes, species-specific secondary antibodies joined to a short oligonucleotide sequence, which attach to the primary antibodies of target proteins. If the target proteins are in close proximity ($< 40 \text{ nm}$), following the addition of ligase, PLA probes are able to hybridise. Addition of polymerase then facilitates rolling-circle amplification of the probe oligonucleotides which attach to a complementary fluorophore to generate a quantifiable signal for visualisation of protein-protein interactions in the cell. This is represented in Figure 2.3.

For each interaction, the primary antibodies used were also tested on their own for background control.

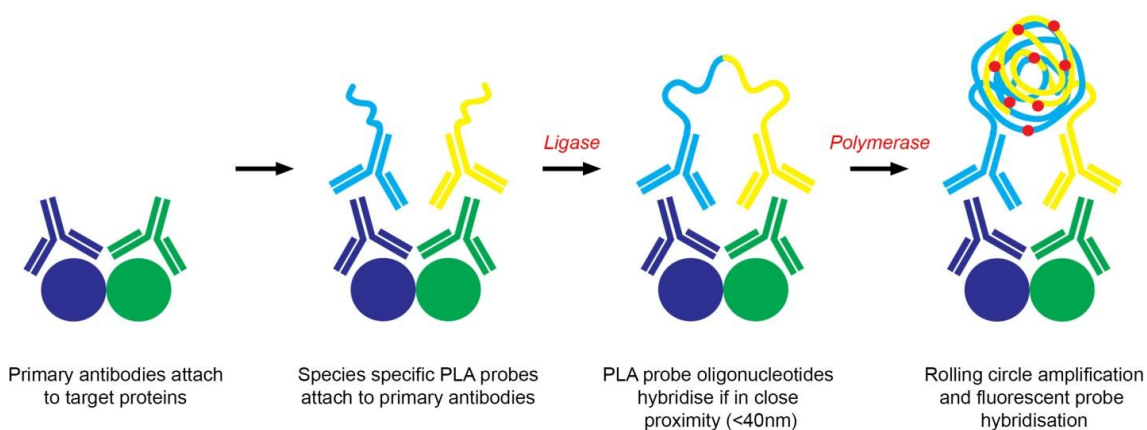


Figure 2.3: Rationale for Duolink PLA

Circles represent target proteins of interest attached to the respective primary antibody (purple and green symbols). Blue and yellow symbols represent secondary PLA probes with oligonucleotides attached. Red dots are fluorophores.

Prior to this study, the Duolink technique had not been previously used in this lab, hence a number of control experiments were undertaken to confirm the reliability and specificity of the assay. For negative controls, neither the APC/BRCA1 interaction (shown to be negative by IP) nor the Miro/PCNA interaction (proteins localised to separate cell compartments), produced PLA signals above background level in U2OS cells (Supplementary Figure S2.1). For a positive control, the APC/ β -Catenin interaction was successfully shown to produce PLA signals above background across a number of cell lines (Supplementary Figure S2.2). A positive control for ectopically expressed GFP-tagged constructs was also undertaken whereby U2OS cells transfected with the β -Catenin binding domain, pGFP-APC(1379-2080), were shown to produce GFP/ β -Catenin PLA signals, ~6.8-fold higher than cells transfected with pGFP alone (Supplementary Figure S2.3).

2.2.8.2 Preparation and fixation of cells for Duolink PLA

Cells were grown to 80% confluence on 8-well chamber slides (Lab-Tek) coated with Poly-L-Lysine (1 mg/ml) then fixed with methanol:acetone (1:1) as per Section 2.2.4.2. Chamber wells were removed from the slides prior to commencement of Duolink PLA (2.2.8.3).

2.2.8.3 Duolink PLA

Duolink was performed using the Duolink In-Situ PLA kit (O-link Biosciences) as per the manufacturer's instructions. Aside from the primary antibodies, all reagents used were provided by the Duolink In-Situ PLA kit and all incubations were carried out at 37°C in a light-proof humidity chamber. Cells were incubated in Duolink Blocking Buffer for 40 min, followed by incubation with the desired primary antibodies (Table 2.2), diluted in Duolink Diluent for a further 60 min. The slides were submerged in a Coplin jar and gently washed in Duolink Buffer A (Appendix 2.1) by rocking (2 x 5 min). Cells were then incubated with Duolink PLA probes (1:5) diluted in Duolink diluent for 60 min, before further washing with Duolink Buffer A (2 x 5 min).

Ligation was facilitated by incubation with ligase (1:40), diluted in a Duolink Ligation Reaction Solution for 30 min. Slides were washed with Duolink Buffer A (2 x 2 min). Polymerisation was facilitated by incubation with polymerase (1:80), diluted in Duolink Polymerisation Reaction Solution (contains fluorophores which hybridise to amplified signal) for 100 min. Slides were then washed using Duolink Buffer B (Appendix 2.1) (2 x 10 min). If further immunostaining (2.2.8.4) was not required, slides were washed in Duolink Buffer B 0.01% (1 x 2 min), mounted using the Duolink Mounting Media containing DAPI, sealed with nail polish and stored at -20°C until further processing (2.2.8.5).

2.2.8.4 Duolink PLA with ectopically expressed GFP-tagged constructs

When required, transfection of GFP-tagged constructs was undertaken as described in Section 2.2.3.4, however the amount of plasmid DNA transfected was scaled down to 30-50% of its usual concentration. This was to reduce the high levels of background which occur when cells are flooded with GFP. Duolink PLA was performed as described in 2.2.8.3, using an antibody against GFP to detect interactions with the transfected construct and an endogenous target protein. The GFP signal for transfected cells was usually dampened when using Duolink PLA; therefore, following completion of the assay, the Duolink counterstaining protocol (Section 2.2.8.5) was employed using the same species GFP antibody, to identify transfected cells expressing modest levels of GFP. All Duolink PLA's with cells expressing ectopic GFP-tagged constructs were performed in parallel with cells expressing GFP alone.

2.2.8.5 Immunostaining after Duolink PLA

Upon completion of Duolink PLA (Section 2.2.8.3), the slide was washed in Duolink Buffer A (2 x 2 min). The desired primary antibody was then diluted (Table 2.2) in Duolink diluent and added to the appropriate well where it was incubated in a light-free environment for 1 h. The slide was again washed in Duolink Buffer A (2 x 2 min) before the appropriate secondary antibody (Table 2.3) diluted in Duolink diluent was added to the appropriate well and incubated in a light-free environment for 1 h. The slide was then washed in Duolink Buffer A (2 x 2 min), followed by 0.01 % Duolink Buffer B (1 x 2 min) after which the slides were mounted using Duolink mounting media as per 2.2.8.3.

2.2.8.6 Analysis and quantification of Duolink PLA

Slides were analysed by immunofluorescence microscopy using the DeltaVision core microscope with fluorescent images captured at 40x and 60x magnification as described in 2.2.5. Captured images showed PLA signals, visualized as dots, in clear focus. In some cell lines (SW480 and HT-29) it was not possible to achieve this on a single focal plane, so z-stack images were acquired. The PLA signal for each cell was scored manually using an overlay of the DIC channel (white light) to define the periphery of each cell whilst scoring the dots within.

Where localisation of PLA signals to mitochondria needed to be verified, sequential transverse optical sections (z-stack images) of cells stained with CMX-Ros were acquired in 0.2 μm incremental steps. Images were then rendered into 3-D projections using SoftWorx software. PLA signals were considered to be localised to mitochondria if >50% overlapped with mitochondrial staining.

2.2.9 SDS-PAGE and Western Blot analysis of proteins

2.2.9.1 Protein extraction

Cells were washed with PBS, then detached and collected from the flask using trypsin (Section 2.2.3.1). The cell suspension was then pelleted by centrifugation at 500 xg , for 5 min at 4°C, washed in PBS and re-centrifuged. Next, cells were resuspended in either

RIPA or HUNT buffer (approximately 80 μ l for a confluent 25 cm² flask; for recipes see Appendix 2.1) and incubated on ice for 30 min to promote cell lysis. Insoluble components were removed by centrifugation at 14,000 xg for 12 min at 4°C, after which the supernatant was collected.

2.2.9.2 Quantification of protein cell lysates

The Bradford assay was used to quantify the protein concentration of cell extracts. BSA standards (0, 2, 4, 6 μ g/ml) were diluted in Protein Assay Dye Reagent (1x) (Bio-Rad), and measured at 595 nm with a DU 800 spectrophotometer to create a standard curve. Samples were diluted in the Protein Assay Dye Reagent (1x) (1 μ l/ml) and measured at 595 nm. The standard curve was used to determine the protein concentration of the sample.

2.2.9.3 Resolving proteins by SDS-PAGE

Cell lysates or immunoprecipitation samples (see Section 2.2.10) were suspended in 4x Laemmli buffer and denatured by boiling for 6 min at 95°C. Proteins were resolved by sodium dodecyl sulphate-polyacrylamide gel electrophoresis (SDS-PAGE) using a Mini-Protean II® Electrophoresis System (Bio-Rad). The gel apparatus was prepared by pouring freshly made separating gel (Table 2.10) between two glass plates, leaving ~1.5 cm at the top for coverage with 100% isopropanol. The percentage of acrylamide used for the separating gel varied depending on the size of the protein of interest. Following gel polymerization (~20 min), the isopropanol was removed and freshly made stacking gel (Table 2.11) was used to fill the rest of the apparatus. A comb was inserted into the stacking gel at the top of the apparatus to create wells for loading the protein samples, which was then removed after polymerization (~20 min). The samples were loaded into the gel (for concentrations see relevant chapters) and resolved via electrophoresis at 100 V for 2 h in running buffer (Appendix 2.1), or until the sample ran to the end of the gel. Precision Plus Dual Colour Standards (Bio-Rad) were used as molecular size standards.

Table 2.10: Separating Gel for SDS-Page

Reagent	10% A	7.5% A	5% A
Poly-Acrylamide Stock (4:1, 40%) (ml)	10	7.5	5
H ₂ O (ml)	14.55	17.05	21.6
1 M Tris, pH 8.7 (ml)	15	15	15
20% SDS (μl)	200	200	200
10% APS (μl)	200	200	200
TEMED (μl)	40	40	40

A: Acrylamide

Table 2.11: Stacking Gel for SDS-Page

Reagent	
Poly-Acrylamide Stock (4:1, 40%) (ml)	1.25
H ₂ O (ml)	7.4
1 M Tris, pH 6.8 (ml)	1.25
20% SDS (μl)	50
10% APS (μl)	100
TEMED (μl)	20

2.2.9.4 Resolving proteins by SDS-Agarose gel electrophoresis

As APC is a very large protein (~320 kDa), occasionally it was resolved using SDS-agarose gel electrophoresis rather than traditional SDS-PAGE methods. To prepare the gel, 2.5% agarose was melted in Tris Borate EDTA buffer (TBE, Appendix 2.1), after which 10% SDS was added and the solution poured into a gel apparatus until full. A comb was inserted immediately into the top of the apparatus, which was removed following gel polymerization (~20 min). The samples, denatured in Laemmli buffer (Appendix 2.1) as in Section 2.2.9.3, were loaded into the gel (for concentrations see relevant chapters), and resolved via electrophoresis at 100 V in running buffer (see 2.2.9.3) until the Plus Dual Colour Standards marker was separated (~40 min).

2.2.9.5 Western blot transfer – Acrylamide gel

Following SDS-PAGE (Section 2.2.9.3), the gel and components of the transfer apparatus were equilibrated in transfer buffer (Appendix 2.1). To construct the transfer apparatus, the gel and a nitrocellulose membrane (Millipore) were sandwiched between two pieces of chromatography paper (Whatman 3MM) and two sponges and placed

inside a Mini-Trans-Blot® cell (Bio-Rad) according to the manufacturer's instructions. The Mini-Trans-Blot® cell, along with an ice-block and magnetic stirrer, were placed into the transfer chamber which was filled with transfer buffer. The proteins on the gel were transferred to the membrane at 100 V for 1-3 h, depending on the protein size. Protein transfer was confirmed using Ponceau S stain (1 min incubation with membrane, Appendix 2.1), after which the membrane was stored in PBS at 4°C until immunoblotting.

2.2.9.6 Western blot transfer – Agarose gel

Following SDS-Agarose separation (Section 2.2.9.4), the gel and components of the transfer apparatus were equilibrated in Tris Buffered Saline (TBS, Appendix 2.1) supplemented with 10% SDS. The transfer apparatus was assembled as follows: from bottom to top – 3 cm paper towel, 3 x chromatography paper (Whatman 3MM), nitrocellulose membrane (Millipore), agarose gel, 2 x chromatography paper. The transfer apparatus was then placed over a tank containing TBS supplemented with 10% SDS and covered with a salt bridge made from chromatography paper which was anchored into each side of the tank. The gel was transferred onto the membrane overnight at RT.

2.2.9.7 Immunoblotting

Membranes were rinsed with TBS supplemented with 0.2% Tween-20 (TBST) and blocked for 1 h in 3% skim milk powder made up with TBST (3% skim milk/TBST). The membrane was incubated with the desired primary antibodies diluted to the relevant concentrations (Table 2.2) in 3% skim milk/TBST, for 1 h at RT. This was followed by 3 x 10 min washes with TBST. The secondary HRP-conjugated antibody was diluted to the relevant concentration (Table 2.3) in 3% skim milk/TBST and applied to the membrane for 1 h at RT after which the membrane was subjected to 3 x 10 min washes with TBST.

2.2.9.8 Immunodetection by ECL

ECL reagents (GE Healthcare) were combined (1:1), added to the membrane and incubated for 1 min. Excess reagent was removed and the membrane developed by film or detected on a ChemiDoc MP imaging system (BioRad).

For film development, the membrane was covered in cling film and placed in an X-omatic cassette (Dupont cronex), where it was exposed to film (X-OMat BT, Kodak or Amersham Hyperfilm ECL, GE Healthcare) at various time intervals. Films were developed using a CP1000 X-Ray film processor (AGFA).

For ChemiDoc development, the membrane was placed inside the ChemiDoc MP imaging system and developed using the ECL detection protocol at various time intervals.

2.2.10 Detection of protein interactions by immunoprecipitation (IP)

2.2.10.1 *Protein extraction for immunoprecipitation*

Cells were harvested and lysed as per Section 2.2.9.1, and cell lysates quantified for protein concentration using the Bradford assay as per Section 2.2.9.2.

2.2.10.2 *Preparation of protein A-sepharose beads*

Protein A-Sepharose beads (GE Healthcare) were washed 3 times in the relevant IP lysis buffer (RIPA or HUNT, see Section 2.2.9.1). Once the beads had sedimented after the final wash, the lysis buffer was removed until the volume of beads to buffer was 1:1.

2.2.10.3 *Addition of primary antibody*

Cell lysates (700 µg – 2 mg protein) suspended in ~700 µl of lysis buffer were incubated with 2 µg of the primary antibody of interest or IgG control overnight, at 4°C, with continuous end over end mixing. It was ensured that enough lysate was reserved for the input (~10% of IP samples), which was suspended in 4x Laemmli buffer (Appendix 2.1), boiled at 95°C for 6 min and stored at -20°C until further processing.

2.2.10.4 *Addition of beads*

30 μ l of Protein A-sepharose bead suspension (2.2.10.2) was added to the cell lysate mixture (2.2.10.3) and incubated for 2 h at 4°C, with continuous end over end mixing to allow protein attachment to the beads. The beads were pelleted by centrifugation at 500 xg for 2 min at 4°C after which the supernatant was removed. The beads were then washed in 700 μ l lysis buffer on ice and re-centrifuged at 500 xg for 1 min at 4°C. The wash procedure was repeated twice more. The supernatant was removed following the final wash and the beads resuspended in 30 μ l of 4x Laemmli buffer (2.2.9.3) and boiled at 95°C for 8 min to remove the immunocomplexes from the beads and to denature the protein. The mixture was centrifuged at 16,000 xg for 1 min and the supernatant removed and subjected to gel electrophoresis (Section 2.2.10.5).

2.2.10.5 *Resolving and developing immunoprecipitation*

Immunoprecipitation samples (2.2.10.4) and the input (2.2.10.3) were loaded into an agarose or acrylamide gel then resolved and developed as per Section 2.2.9.

2.2.11 Statistics and Graphs

All experimental data was compiled in Microsoft Excel.

2.2.11.1 *Statistical analysis*

Microsoft Excel was used to complete basic statistical analysis such as mean, median and standard deviation. GraphPad Prism (version 5.0) was utilised to perform statistical comparisons between different samples using an unpaired T-test, for data with normal distribution, or a Mann-Whitney U-test, for data without normal distribution.

2.2.11.2 *Graphs*

Bar graphs were generated using Microsoft Excel and typically showed mean \pm standard deviation. Box-and-whisker plots and dot plots were generated in GraphPad Prism 5. For box-and-whisker plots the data presented is median (line), upper/lower quartile (box), min/max (error bars with 95% C.I).

Appendix 2.1 General Buffers and Culture Medium

2-YT Medium

2-YT Medium consisted of Bacto-tryptone 15 g, Bacto-yeast extract 10 g and NaCl 5 g. Components were dissolved in 1 L distilled water and autoclaved.

2-YT Agar

For preparation of agar plates, 15 g bacto-agar was added to 2-YT medium prior to autoclaving and left to cool to 50°C. In a sterile environment, antibiotic was then added before the solution was poured into sterile petri dishes (~20 ml/dish) and set at room temperature (RT).

4x Laemmli Buffer

125 mM Tris-HCl pH 6.8, 20% glycerol, 10% β -Mercaptoethanol, 5% SDS and 0.005% Bromophenol Blue.

Duolink Buffer A

0.01 M Tris pH 8.0, 0.15 M NaCl and 0.05% Tween 20. Buffers made up with sterile H₂O, filtered and stored at 4°C.

Duolink Buffer B

1 M Tris pH 7.5 and 0.1 M NaCl. Buffers made up with sterile H₂O, filtered and stored at 4°C.

HUNT Buffer

50 mM Tris pH 7.5, 100 mM NaCl and 0.5% NP-40. Made up in PBS with fresh cocktail protease inhibitor (Roche) added just prior to use.

Phosphate Buffered Saline (PBS)

137 mM NaCl, 2.7 mM KCl, 10 mM Na₂HPO₄, 1.8 mM KH₂PO₄. Made up with H₂O and adjusted to pH 7.4

Ponceau S Stain

5% Acetic Acid and 0.01 g Ponceau S, made up with H₂O.

RIPA Buffer

1% NP-40, 0.5% deoxycholate and 0.1% SDS. Made up in PBS with fresh cocktail protease inhibitor (Roche) added just prior to use.

Running Buffer

Tris 2.5 mM, glycine 25 mM, and SDS 0.001%. Made up with H₂O.

Supplemented DMEM

Dulbecco's Modified Eagle Medium (DMEM) supplemented with 20 mM HEPES, 4 mM L-Glutamine, 10 % FBS, 100 units/ml Penicillin and 100 µg/ml Streptomycin. Medium was stored at 4°C and brought to RT prior to use.

Transfer Buffer

Tris 25 mM, glycine 192 mM, methanol 20%. Made up with H₂O.

Tris Borate EDTA Buffer (TBE 10x)

890 mM Tris, 890 mM Boric Acid and 20 mM EDTA. Made up with H₂O and adjusted to pH 8.3. Dilute with H₂O for a 1x stock.

Tris Buffered Saline (TBS)

50 mM Tris and 150 mM NaCl. Made up with H₂O and adjusted to pH 7.6

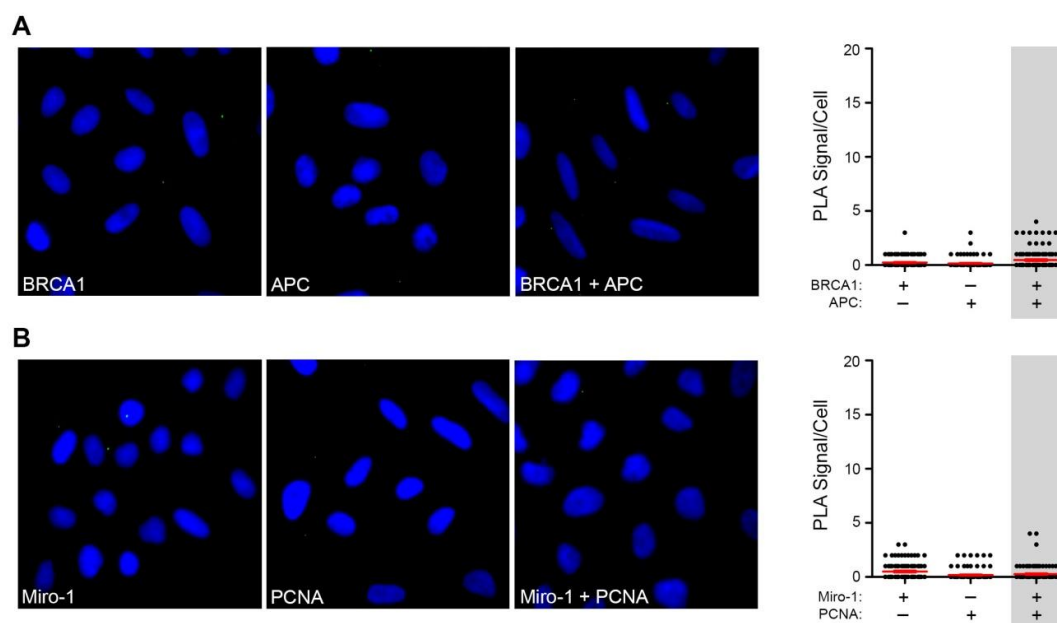
TFB1 Buffer

30 mM Potassium acetate, 10 mM CaCl₂, 50 mM MnCl₂, 100 mM RbCl and 15% glycerol. Made up with sterile H₂O and stored at 4°C.

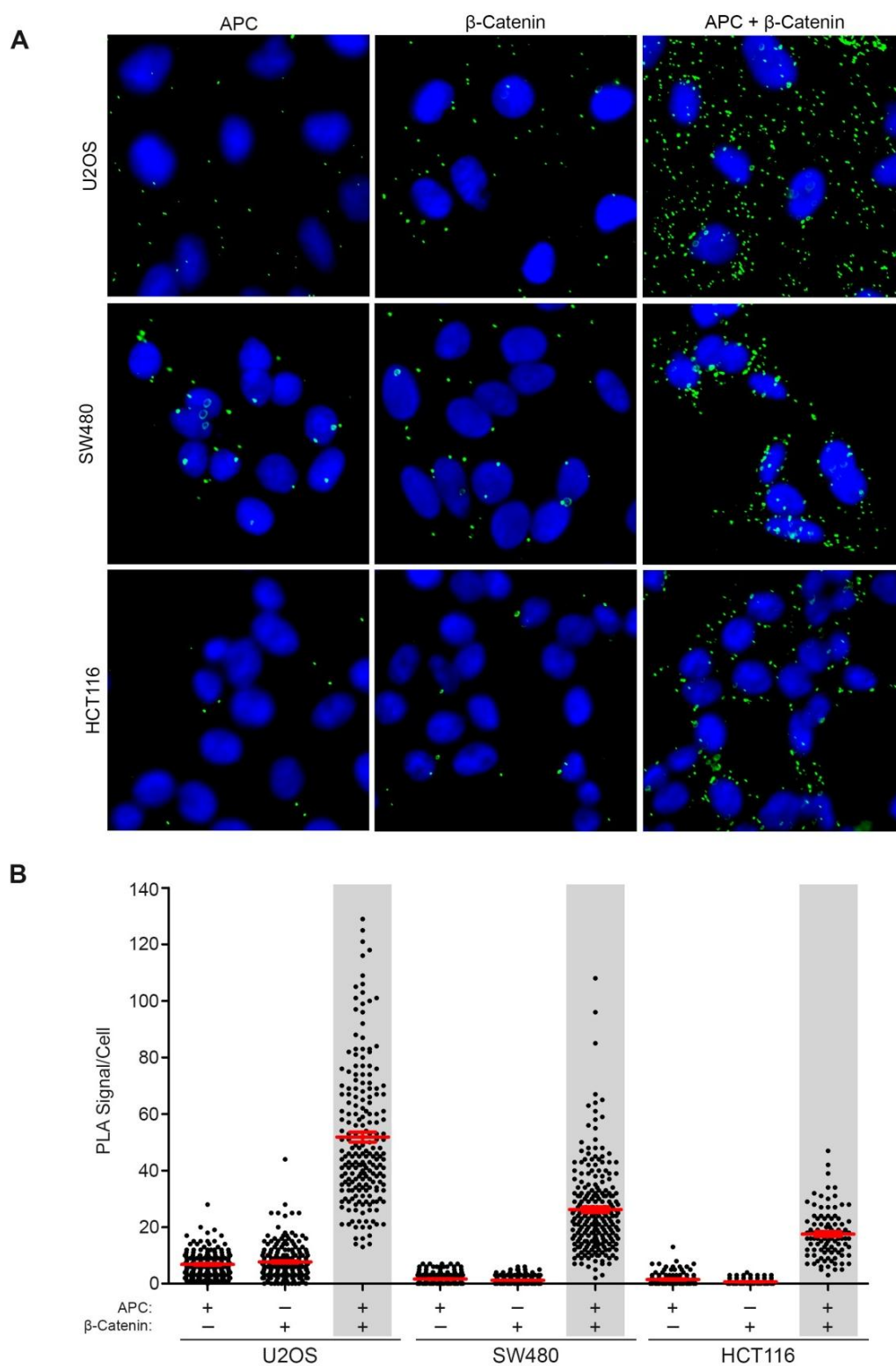
TFB2 Buffer

8.8 mM HEPES, 75 mM CaCl₂, 10 mM RbCl and 15% glycerol. Made up with sterile H₂O and stored at 4°C.

Appendix 2.2 Supplementary Figures

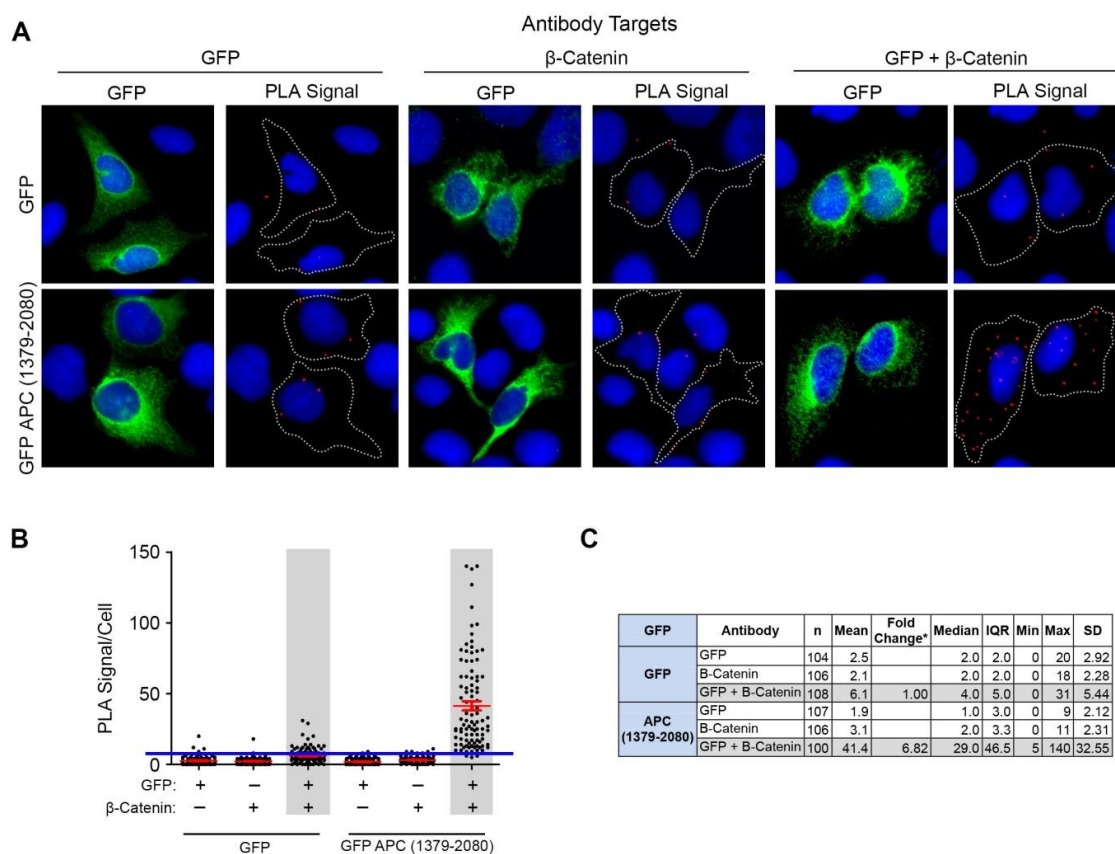
**Supplementary Figure S2.1: Duolink Negative controls**

(A-B) U2OS cells were subject to Duolink PLA using antibodies against (A) BRCA1 and APC (mAb), or (B) Miro-1 and PCNA to visualise interactions between the proteins of interest. Representative images are shown and scoring quantification of PLA signals per cell as seen in the dot-plots (mean \pm S.D), reveal negative interactions between BRCA1/APC and Miro-1/PCNA.



Supplementary Figure S2.2: Duolink Positive Control - APC interacts with β-Catenin

(A-B) U2OS, SW480 and HCT116 cells were subjected to Duolink PLA using antibodies against APC (APC2, pAb) and β-Catenin (mAb) to visualise interactions between the two proteins. (A) Representative images are shown and scoring quantification of PLA signals is visualised in the (B) dot-plot (mean \pm S.D).



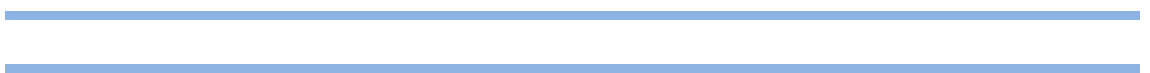
Supplementary Figure S2.3: Ectopic Duolink positive control - GFP APC(1379-2080) interacts with β -Catenin.

(A-C) U2OS cells transfected with pGFP and pGFP APC(1379-2080) were subjected to Duolink PLA using antibodies against GFP (mAb) and β -Catenin (pAb). Counterstaining using GFP (mAb) and subsequent analysis and PLA signal scoring by immunofluorescence microscopy revealed a positive interaction between GFP APC(1379-2080) and β -Catenin relative to GFP control as indicated by the (A) representative images, (B) dot-plot (mean \pm S.D) and (C) table (n, number in sample; * fold change relative to GFP control; IQR, inter-quartile range; SD, standard deviation).



CHAPTER 3

**APC associates with the
Miro/Milton mitochondrial
transport complex**



The dynamic behaviour of mitochondria is essential for many aspects of normal cell function, providing a means for its metabolic roles in ATP generation and calcium buffering, to be conducted in a finely controlled, site-specific manner. Despite the critical nature of mitochondrial motility, the regulatory mechanisms behind this process have yet to be fully elucidated. In this chapter a novel role for the tumour suppressor APC in the regulation of mitochondrial transport is presented. Analysis of U2OS, HDF1314 and NIH 3T3 cell lines by immunofluorescence microscopy revealed that siRNA-mediated silencing of wild-type APC caused the typically branched mitochondrial network, uniformly spread throughout the cytoplasm to completely redistribute to the perinuclear region, in a manner reminiscent of disrupted mitochondrial transport. Treatment of U2OS cells with the microtubule toxin nocodazole, mimicked the mitochondrial redistribution induced by APC, indicating that microtubule based transport of mitochondria may be effected. Distribution of other membrane bound cell organelles following loss of APC was unchanged, as was mitochondrial distribution following loss of EB1, the binding partner through which APC stabilises microtubules, thus indicating that this phenomena was specific to mitochondria, and not a secondary effect of microtubule de-stabilisation. Screening by immunofluorescence microscopy identified potential associations between APC and proteins from the primary mitochondrial transport complex Miro/Milton, which could be confirmed by immunoprecipitation assays in U2OS cells. Finally, Duolink *in situ* PLA was used to finely map the localisation of endogenous APC-Miro/Milton immunocomplexes to the mitochondria in both U2OS and Hela cells in 3-D rendered models, consistent with the localisation of mitochondrial transport complexes. Together, these results indicate a new role for APC in the microtubule-dependent distribution of mitochondria towards the cell periphery through an interaction with the Miro/Milton mitochondrial transport complex.

3.1 Introduction

APC is a large protein with multiple binding domains that facilitate protein-protein interactions integral to its role as a tumour suppressor protein and its capacity to regulate pathways for cell growth and differentiation (Section 1.2.1). The ability of APC to shuttle throughout the cell, to associate with the cytoskeletal microtubule and actin networks, and localise to different cellular compartments (Section 1.2.1.1) is also essential for this multifunctional nature. Previous studies from our group determined for the first time a new subcellular localisation of APC at the mitochondria, wherein it was found to bind and regulate the anti-apoptotic factor Bcl-2 (13). In this study we present a completely new and unexpected function of APC at the mitochondria, defined by its association with the Miro/Milton mitochondrial transport complex to facilitate distribution of mitochondria along microtubules.

Mitochondria are primarily known for playing a pivotal role in providing energy in the form of ATP to the cell through a process known as oxidative phosphorylation. However, mitochondria are also key to a number of other essential cell functions such as apoptosis and calcium buffering (15-17). Critical to these processes is the dynamic, motile nature of mitochondria, which allows for quick redistribution to different regions of the cell in response to cellular signals, for example, movement towards bioenergetically demanding sites, like the cell periphery to provide ATP for cell migration. The importance of regulated mitochondrial transport is discussed further in Section 1.3.2, and Chapters 4 and 5.

Transport of mitochondria is primarily facilitated by kinesin and dynein-dependent movement across the microtubule network towards the plus and minus ends, respectively (271). However, mitochondria have also been reported to associate with a number of myosin motor proteins for short range transport along actin filaments, particularly in neurons (170, 171). For finely regulated transport, mitochondria rely on a number of motor protein adaptor complexes, from which the most well defined is the Miro/Milton complex that drives kinesin dependent anterograde mitochondrial transport along microtubules (for details on other mitochondrial transport mechanisms see Section 1.3.2.2.) This complex was originally identified from genetic screens in *Drosophila* with impaired mitochondrial transport (143, 144), and since then has been

found to be evolutionarily conserved in mammals, with two orthologues identified for each protein, Miro-1/Miro-2 and Milton-1/Milton-2 (145, 146). Miro is a mitochondrial transmembrane protein which through the adaptor Milton, is attached to the KIF5 kinesin motor (148-150).

The close association of APC with both the microtubule and actin networks has been widely reported (see Section 1.2.1.3 for more details). With this in mind, we show for the first time that APC loss specifically disrupts microtubule-based distribution of mitochondria at the cell periphery in epithelial and fibroblastic cell lines. It is proposed that this occurs due to a change in the Miro/Milton/KIF5 mitochondrial transport complex which is shown to interact with APC.

3.2 Methods

3.2.1 Cell culture

U2OS, HeLa, HDF1314 and NIH 3T3 cells were cultured in DMEM under standard conditions as outlined in Section 2.2.3. For mitochondrial distribution and co-localisation experiments, cells were seeded on glass coverslips in 6 well trays, and for Duolink PLA experiments cells were seeded in 8-well chamber slides coated with poly-L-lysine. For experiments using fixed cells, cells were grown to 70-80% confluence prior to fixation. Cells to be subjected to western blotting were seeded in 150cm² flasks for immunoprecipitation assays and 25cm² flasks for siRNA knockdown experiments. The transfection of plasmid DNA for transient expression or siRNAs for gene silencing in cells is described in Section 2.2.3.4.

3.2.2 Cell fixation and staining for immunofluorescence microscopy

Cells were seeded for at least 24 h, fixed with methanol-acetone, probed with relevant antibodies and mounted for immunofluorescence microscopy as outlined in Section 2.2.4. If addition of CMX-Ros or ER-tracker for detection of mitochondria or the endoplasmic reticulum respectively was required this occurred prior to fixation. Concentrations and any further specifications for all antibodies and dyes used in this chapter are outlined in Table 2.2, Table 2.3 and Table 2.4.

3.2.3 Immunofluorescence cell image acquisition and processing

Slides were analysed using the Olympus IX71 DeltaVision Core deconvolution microscope equipped with a CoolSNAP HQ² camera for general image capture (Section 2.2.5). Images collected were further resolved using SoftWorx deconvolution software. For scoring of co-localisation experiments, 200 cells were analysed over 2 independent experiments as outlined in Section 2.2.6. For mitochondrial distribution experiments, 300 cells were scored over 3 independent experiments, with the exception of the nocodazole and latrunculin A experiments (Figure 3.3) where 200 cells were analysed over 2 experiments. Analysis of mitochondrial distribution experiments and Duolink PLA is further described in Section 3.2.4.1 and 3.2.8 respectively.

3.2.4 Quantification of cell organelle distribution

Post-image acquisition, cells treated with control or APCd siRNA and stained with various cell organelle markers were analysed for organelle distribution. Organelle distribution was analysed by marking the nucleus with Hoechst and the cell membrane with IQGAP1, then determining by eye, which of three cellular 'zones', between the nucleus and cell membrane the organelle was able to extend to (see example Figure M3.1). This method was further developed for subsequent experiments looking at mitochondrial distribution.



Figure M3.1: Organelle distribution scoring method

Schematic indicates scoring 'zones' under which organelles are classified. An organelle is classified into a zone depending on how far it extends from the nucleus towards the cell membrane. For example, golgi staining in this U2OS cell indicates that it is localised to the zone 1 cellular region.

3.2.4.1 Quantification of mitochondrial distribution

To quantify mitochondrial distribution, the same principle used to score organelle distribution was implemented and cells were scored into three 'zones' radiating from the nucleus to the cell membrane. These zones constituted 33% (zone 1), 66% (zone 2) and 100% (zone 3) of the cytoplasmic area and mitochondria were scored according to which zone they reached. Figure M3.2 below shows examples of distribution scoring in U2OS cells, however, more detailed scoring parameters, including important features taken into account in the analysis of other cell lines is described in Section 2.2.7.

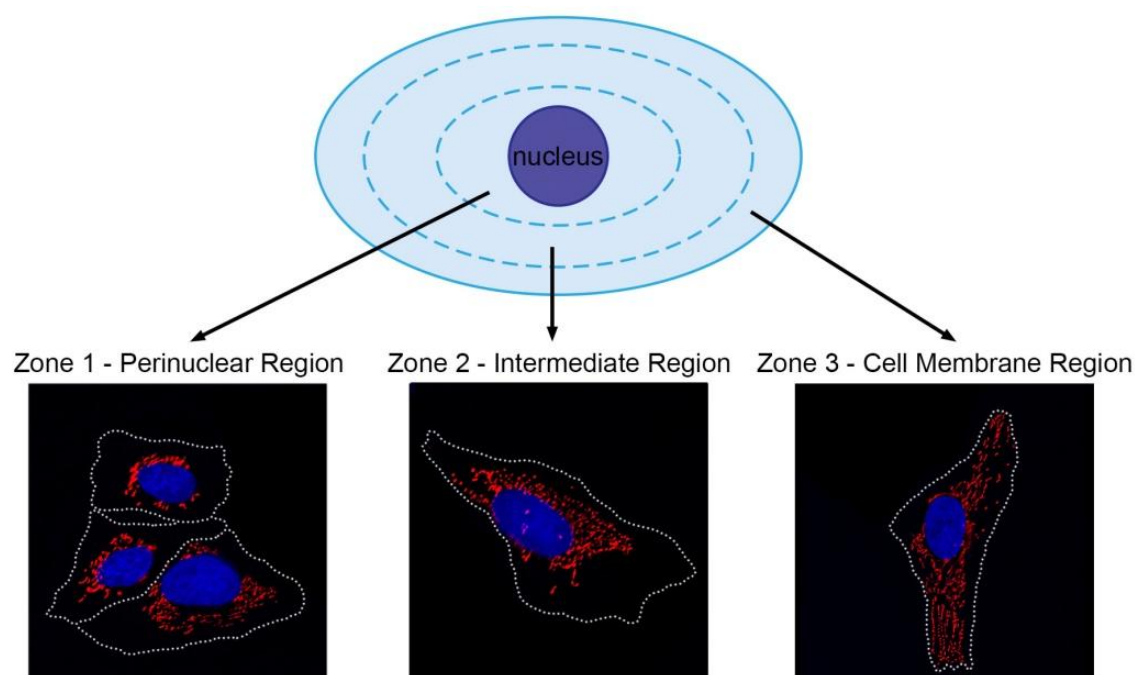


Figure M3.2: Mitochondrial distribution scoring method

Cells were scored into one of three cellular ‘zones’ radiating from the nucleus towards the cell membrane. Classification was dependant on extension from the nucleus.

3.2.5 Drug treatments

Under sterile conditions, sub-confluent cells were treated with nocodazole (33 μ M), latrunculin A (0.5 nM) or DMSO for 1h at 37°C prior to fixation as outlined in Section 2.2.3.5 and Table 2.7.

3.2.6 Immunoprecipitation assays

For immunoprecipitation experiments, cells transfected with pGFP, pGFP Miro-1 and pGFP Milton-2 were collected and lysed with HUNT buffer as outlined in Section 2.2.9.1. Immunoprecipitation was carried out as described in Section 2.2.10, using antibodies against GFP (pAb, Invitrogen), APC (C20, pAb, Santa Cruz) and IgGr (pAb, Sigma-Aldrich) to pull-down target proteins prior to samples being subjected to SDS-PAGE and western blot analysis. Immunoprecipitation experiments were repeated a minimum of 3 times.

3.2.7 Western blot analysis

With the exception of the samples for immunoprecipitation assays described above (Section 3.2.6), cells were collected, lysed using RIPA buffer and processed as described in Section 2.2.9.1. Samples (immunoprecipitates or ~30µg total cell lysate) were separated by SDS-PAGE using 5% (for detection of APC) or 7.5% acrylamide gels, and transferred onto a nitrocellulose membrane (see Sections 2.2.9.3-2.2.9.6). Western blots were probed as described in Section 2.2.9.7, using primary antibodies as per the figure legends. Dilutions for these antibodies and subsequent secondary antibodies are outlined in Table 2.2 and Table 2.3, respectively. Immuno-blots in this chapter were developed on film using ECL (See Section 2.2.9.8).

3.2.8 Duolink Proximity Ligation Assay (PLA)

Duolink PLA (Olink Biosciences) is a relatively new assay designed to detect protein interactions *in situ*. Briefly, as the rationale for this method is described in detail in Section 2.2.8.1, species specific "PLA" probes act as secondary antibodies which are conjugated to short oligonucleotide sequences. The PLA probes attach to primary antibodies of target proteins, and if these proteins are in close proximity (<40nm), the PLA probes ligate and undergo rolling circle amplification, which is then able to attract a complementary fluorophore and generate a quantifiable signal which can be visualised using immunofluorescence microscopy. This is summarised in Figure M3.3.

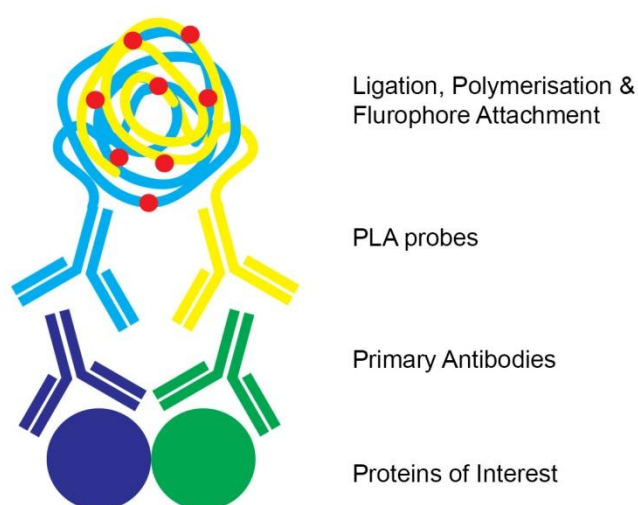


Figure M3.3: Rationale for Duolink PLA

Purple and green circles represent target proteins of interest attached to the respective primary antibody. Blue and yellow symbols represent secondary PLA probes with oligonucleotides attached. Red dots are fluorescent probes

For Duolink PLA experiments in this chapter, primary antibodies against APC (Ab7, mAb, Merck), Miro-1 (pAB, Sigma-Aldrich) and Milton-2 (pAB, Sigma-Aldrich) were used at concentrations outlined in Table 2.2, to visualise APC/Miro-1 and APC/Milton-2 protein interactions by Duolink PLA in cells pre-stained with CMX-Ros. Following image capture, PLA signals were quantified manually, by scoring the number of PLA signals per cell using a DIC channel overlay to determine the boundaries of each cell (see Section 2.2.8.6). Unless stated in the figure legend, Duolink PLA experiments in this chapter obtained data from at least 2 independent experiments per condition. The number of cells scored is outlined in the supplementary figures for each experiment.

U2OS and HeLa cells are very flat, therefore in most cases mitochondria sit on single plane, enabling PLA signals in focus to be scored for mitochondrial localisation from single stack images. Data from PLA/mitochondrial colocalisation studies was collected across 2 independent experiments, with the number of cells scored outlined in the relevant supplementary figures. To further verify mitochondrial localisation in 5-10 cells/sample, z-stack images of cells stained with CMX-Ros were acquired, rendered into 3-D projections and PLA signals scored for mitochondrial localisation. This is described in detail in Section 2.2.8.6.

3.2.9 Graphs and statistics

All graphs and statistics used to display and analyse results in this chapter are outlined in Section 2.2.11.

3.3 Results

3.3.1 Loss of wild-type APC alters the cellular distribution of mitochondria but not of other microtubule-associated organelles

Previous work from our group described the first detection of APC at mitochondria (13). As mitochondria primarily utilise the microtubule network for transport throughout the cytoplasm, and APC is known to bind and stabilise microtubules (28), we next investigated the possibility that APC has a role in regulating the transport of mitochondria and other membrane bound organelles which associate with microtubules including the endoplasmic reticulum, golgi, lysosomes and centrosomes (272). U2OS osteosarcoma cells were treated with control siRNA or APC-specific siRNA to silence APC expression prior to fixing and visualising specific cell organelles (Figure 3.1A,B). Analysis by immunofluorescence microscopy revealed a dramatic redistribution of mitochondria from the cell membrane toward the perinuclear region following silencing of APC. In comparison, loss of APC did not appear to alter the localisation of the endoplasmic reticulum, golgi, lysosomes and centrosomes (for more detail, see Supplementary Figure S3.1), suggesting a specific role for APC in the transport of mitochondria.

3.3.2 Loss of wild-type APC induces a redistribution of mitochondria from the cell membrane to the perinuclear region

To elucidate a potential role for APC in the transport of mitochondria, U2OS cells were again treated with either control or APC (APCd and APC2) siRNAs, stained with the mitochondrial marker CMX-Ros and fixed cells analysed by immunofluorescence microscopy. Mitochondria in control cells were uniformly distributed throughout the cell from the nucleus to the cell membrane, whereas after loss of APC most cells displayed distinct mitochondrial clustering around the nucleus (Figure 3.2A).

To quantify this perinuclear shift, mitochondria were scored according to their position in one of three cellular zones spanning from the perinuclear region (zone 1) to the region bordering the cell membrane (zone 3) (see schematic in Figure 3.2B). Scoring analysis confirmed that loss of full length APC elicited a ~300% increase in the population of cells with mitochondria clustering in the perinuclear region (zone 1) relative to control cells (control= 17%, APCd=52%, APC2= 50%) ($P<0.001$; Figure 3.2C). Conversely, as expected, the population of cells displaying spread out mitochondria (zone 3) significantly decreased following the loss of APC (control= 46%, APCd=13%, APC2= 23%) ($P<0.001$). APC knockdown efficiency was confirmed by microscopy and western blot analysis (Figure 3.2A,D).

To confirm that the perinuclear shift of mitochondria following APC siRNA treatment was not specific to U2OS cells, HDF1314 human fibroblasts and NIH 3T3 mouse fibroblasts were also treated with control or APC (APCd or mAPC1) siRNAs and stained with CMX-Ros and antibodies against APC. Fixed cells were analysed by immunofluorescence microscopy. Loss of APC elicited a dramatic redistribution of mitochondria to the perinuclear region (zone 1) in both HDF1314 cells (control= 8%, APCd=29%) ($P<0.001$) and NIH 3T3 cells (control= 13%, mAPC1=42%) ($P<0.001$) (Figure 3.2E-F), mimicking the results obtained in U2OS cells.

CMX-Ros is an effective mitochondrial dye which accumulates depending on mitochondrial membrane potential. The fluorescence intensity of the CMX-Ros stain was not altered upon treatment with APC siRNA (see mitochondria staining Figure 3.2), indicating that the mitochondrial redistribution observed was not a secondary effect of mitochondrial membrane depolarisation. Importantly, an antibody against mtHSP70 was used as an alternate mitochondrial marker and confirmed the significant redistribution of mitochondria caused by knockdown of APC (Supplementary Figure S3.2).

In addition to inducing mitochondrial perinuclear clustering, loss of APC in U2OS, HDF1314 and NIH 3T3 cells also appeared to cause mitochondria to decrease size, and to become less filamentous and more punctate, suggesting that mitochondrial fission and fusion dynamics may also be affected. Mitochondrial fission/fusion and transport dynamics are intimately linked; they share a number of protein regulators and often if one pathway is disrupted, the other is also affected. In Chapter 7 (Section 7.6), the

appearance of punctate mitochondria following APC knockdown is further examined to determine if this is evidence of APC controlling mitochondrial fission/fusion dynamics, or if it is an indirect consequence of disrupting mitochondrial transport.

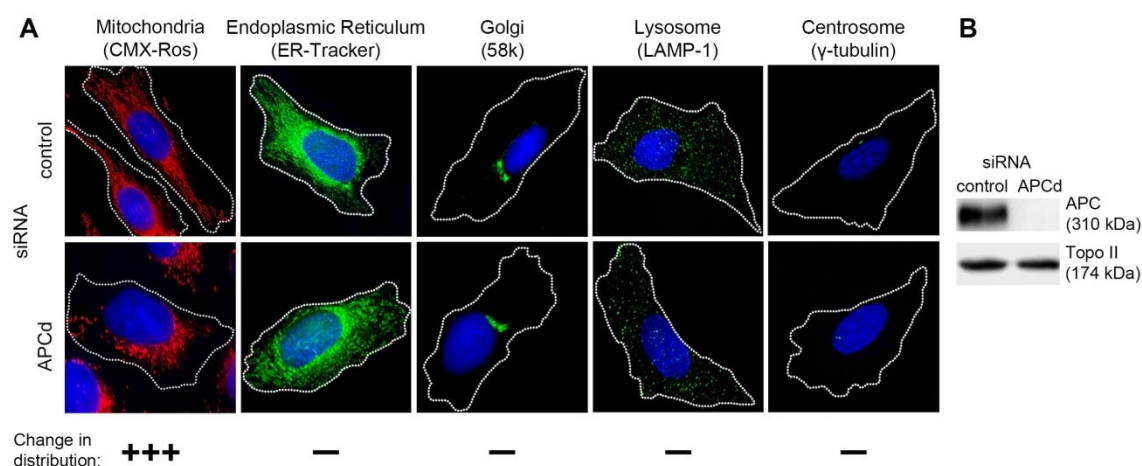


Figure 3.1: Loss of APC alters transport of select microtubule associated organelles.

(A) Sub-confluent U2OS cells were treated with control or APC (APCd) siRNA and stained with dyes CMX-Ros (red) or ER tracker (green), or probed with antibodies against 58k, LAMP-1 or γ -tubulin (green) to detect mitochondria, endoplasmic reticulum, golgi, lysosomes and centrosomes respectively. Cells were co-stained with Hoechst and IQGAP1 (not shown) to indicate the nucleus (blue) and cell membrane (represented by dotted line) respectively and scored for changes in organelle distribution by immunofluorescence microscopy. (B) APC knockdown was confirmed by western blot analysis with Topo II as a loading control.

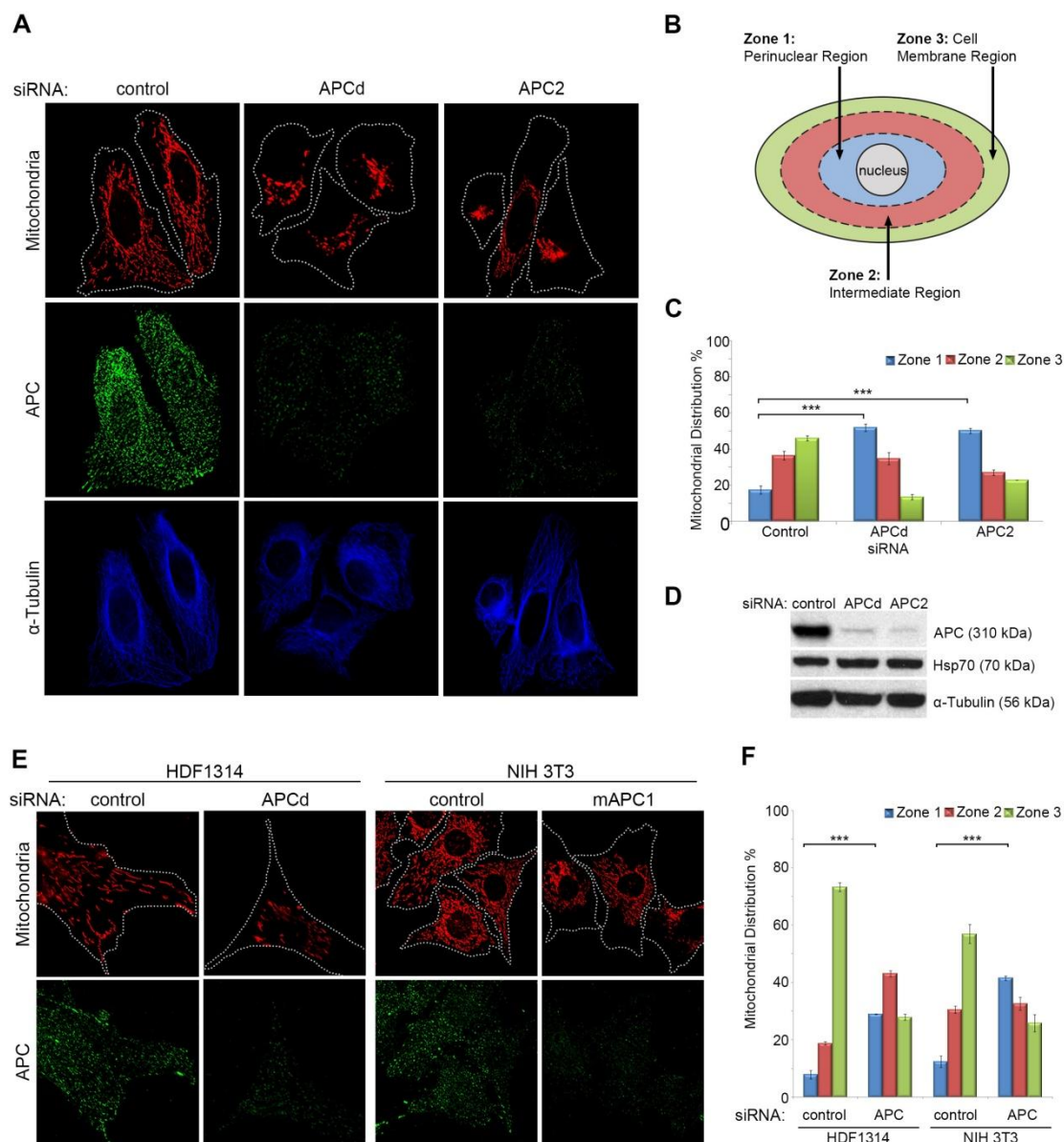


Figure 3.2: Loss of wild-type APC induces a redistribution of mitochondria in U2OS, HDF1314 and NIH 3T3 cells.

(A) APC was silenced in U2OS cells by siRNA (APCd or APC2), and mitochondrial distribution was analysed by immunofluorescence microscopy after staining for mitochondria (CMX-Ros), APC (H290) and microtubules (α -tubulin). The cell membrane is represented by the dotted line. (B) The distribution of mitochondria in different “zones” was scored according to the (C) schematic, revealing a significant redistribution of mitochondria from the cell periphery (zone 3) towards the perinuclear region (zone 1) when APC is knocked down. (D) Loss of APC was confirmed by western blot analysis. (E) HDF1314 and NIH 3T3 cells were treated with APCd siRNA or mouse APC1 (mAPC1) siRNA respectively and mitochondrial distribution analysed by immunofluorescence after staining for mitochondria and APC. (F) Scoring revealed a similar shift in mitochondrial distribution following loss of APC. Significant differences for zone 1 distribution relative to controls, as determined by an unpaired T-test, are indicated (***, $P < 0.001$, % mean \pm S.D).

3.3.3 Destruction of the microtubule network by nocodazole induces a redistribution of mitochondria towards the perinuclear region, similar to that caused by loss of APC.

Mitochondria utilise the microtubule network and, to a lesser extent, actin filaments to move throughout the cell. APC is associated with both these cytoskeletal networks (52-54). Therefore, mitochondrial localisation was assessed following the disruption of the microtubule and actin networks through treatments with nocodazole and latrunculin A, respectively. Treatment with nocodazole induced a redistribution of mitochondria towards the perinuclear region (DMSO= 23%, nocodazole = 43%) ($P < 0.01$), similar to that observed upon loss of APC (Figure 3.3A-B). In comparison, at an identical time point, disruption of the actin network by latrunculin A, at a concentration that disrupted actin filaments but did not impair microtubule integrity, had no effect on mitochondrial distribution (Figure 3.3C-D). However, whilst mitochondrial spread was unaffected in latrunculin A treated cells (zone 1 mitochondria: DMSO = 17%, latrunculin A = 15%) ($P > 0.5$), the mitochondria did appear to be more aggregated and less filamentous. This may be due to alteration in the preferentially short-range movements of mitochondria along actin filaments, as opposed to the long range trafficking that occurs along microtubules (170, 171, 271), or simply a secondary effect resulting from changes in cell shape and structure after actin depolymerisation.

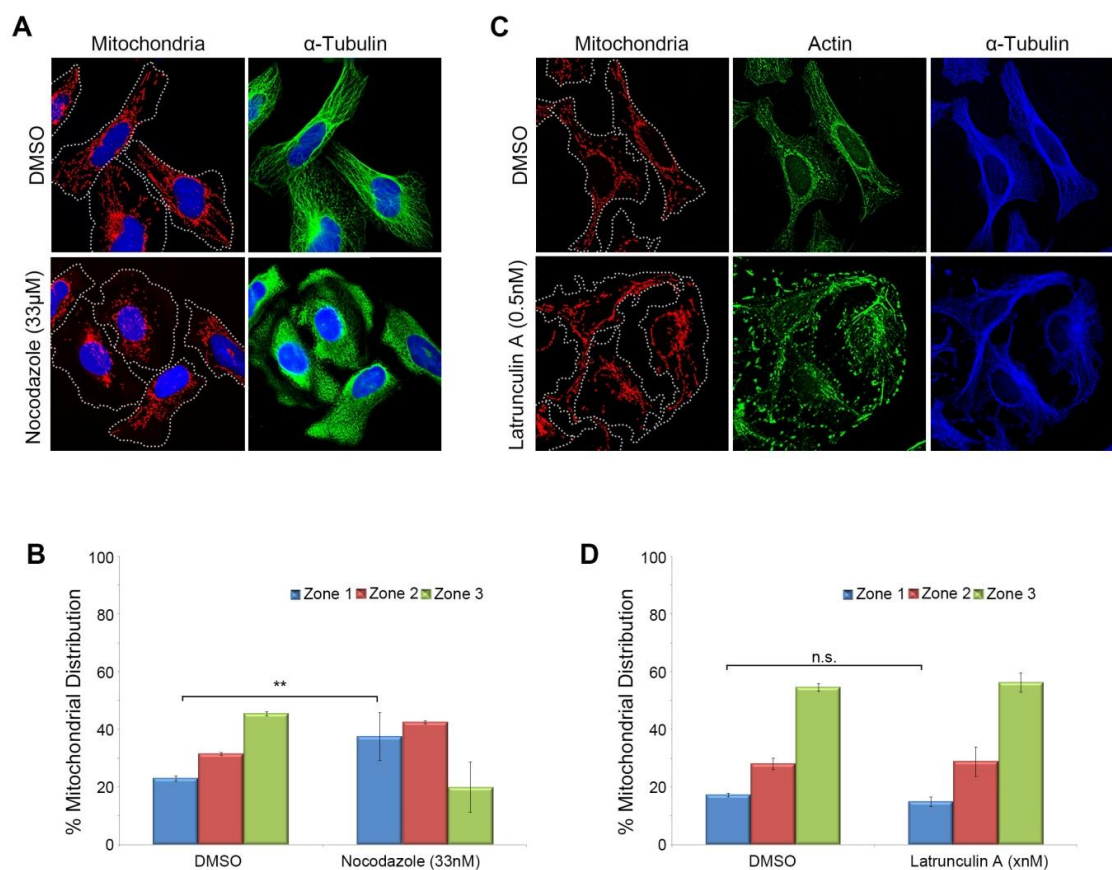


Figure 3.3: Nocodazole but not latrunculin A treatment induces a redistribution of mitochondria in U2OS cells.

(A, C) Sub-confluent cells were treated with DMSO (control), nocodazole or latrunculin A and analysed by immunofluorescence microscopy after staining for mitochondria (CMX-Ros) and microtubules (α -tubulin) or actin (α -actin). (B) Distribution scoring revealed a significant (**, $P < 0.01$) shift of mitochondria towards the zone 1 perinuclear region following destruction of the microtubule network by nocodazole, which was (D) not observed (n.s., not significant) upon disruption of the actin network by latrunculin A (% mean \pm S.D). Statistical significance determined by unpaired T-test.

3.3.4 Mitochondrial redistribution following loss of APC is specific, and not due to microtubule destabilisation

As APC has an important role in microtubule stabilisation (28), it was important to ensure that mitochondrial redistribution following loss of APC was not a secondary effect or consequence of microtubule network disruption. APC is known to interact with EB1 to bind and stabilise the plus-ends of microtubules (67, 70, 71). Therefore, the impact of EB1 knockdown on mitochondria was assessed. Unlike APC siRNA treatment, EB1 knockdown did not alter mitochondrial distribution in HDF1314 cells (Figure 3.4A-C) (zone 1 mitochondria: control = 10%, EB1 = 6%) ($P > 0.5$) despite what looked like a slight disorganisation of the microtubule network when EB1 siRNA treated cells were stained with α -tubulin (Figure 3.4D).

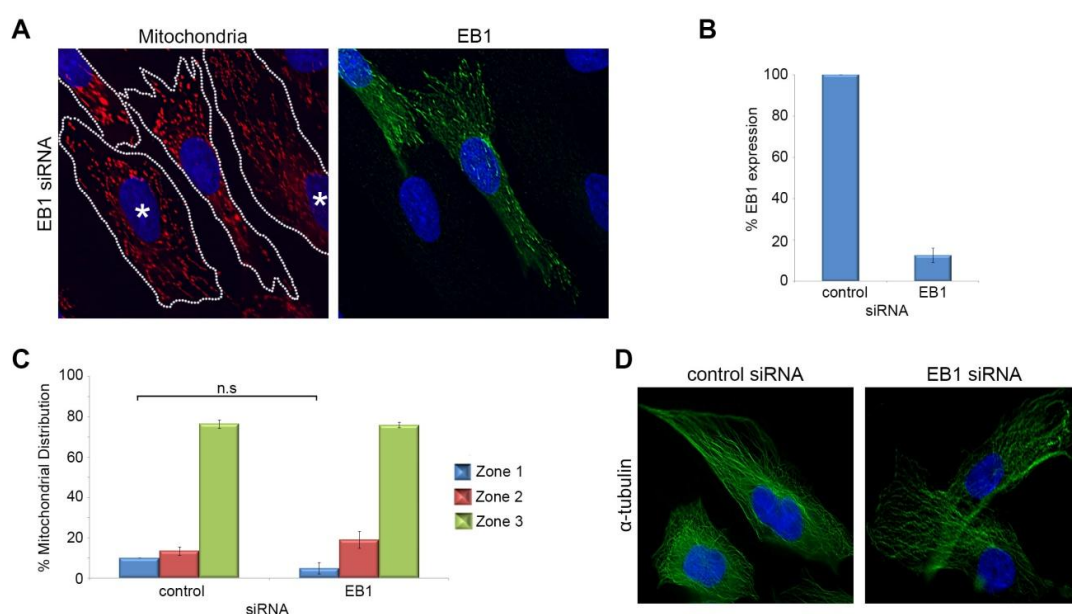


Figure 3.4: Loss of microtubule cap protein EB1 does not induce mitochondrial redistribution in HDF1314 cells.

(A) Sub-confluent cells were treated with control or EB1 siRNA, stained with CMX-Ros (mitochondria, red), Hoechst (blue) and an antibody against EB1 (green) and analysed by immunofluorescence microscopy. Cells displaying EB1 knockdown are indicated by *, and the cell membrane indicated by the dotted line. (B) Efficacy of EB1 siRNA knockdown was confirmed by immunostaining (% mean \pm S.D). (C) Mitochondrial distribution was scored and no significant changes (unpaired T-test) in distribution were observed (n.s., not significant, mean \pm S.D) following loss of EB1 despite the slight microtubule disorganisation observed in the (D) representative images stained with α -tubulin (green) and Hoechst (blue).

Immunostaining of α -tubulin before and after treatment with APC siRNA also revealed only a slight disruption to the microtubule network (Figure 3.2A), especially when compared to the complete obliteration and consequential mitochondrial redistribution seen upon treatment with nocodazole (Figure 3.3A-B). Additionally, transport of other membrane bound organelles which move along microtubules including the endoplasmic reticulum, golgi, lysosomes and centrosomes were unaffected by silencing of full length APC in U2OS cells (Figure 3.1) implying that the microtubule network in general retains organelle transport functionality in the absence of APC.

3.3.5 Mitochondria and APC co-localise with a number of potential co-factors including the Miro/Milton mitochondrial transport complex

To determine if APC may be interacting with known transport complexes to assist mitochondrial movement, a number of co-localisation studies were undertaken. Firstly, mitochondria were assessed for co-localisation with APC and other binding proteins known to traffic along microtubules (Figure 3.5). This data was then compared to co-localisation observed with known mitochondrial transport factors Miro (100%) and Milton (92%) and mediators of mitochondrial fission/fusion Mfn2 (100%), OPA1 (100%), DRP1 (97%) and Fis1 (100%) (Figure 3.5). Mitochondrial co-localisation of KAP3A (13%), a kinesin adaptor protein which connects APC with the KIF3 kinesin complex (26), and β -catenin (6%), were both found to be relatively low in comparison to the proteins known to regulate mitochondrial morphology. In contrast, RanBP2, reported to interact with APC to assist in the regulation of cell polarity (62), showed substantially higher rates of mitochondrial colocalisation (88%). This is unsurprising as RanBP2 has previously been found to have a role in mitochondrial transport (176), however, this is believed to be independent of Miro/Milton transport. In addition, mitochondrial co-localisation of APC was analysed using two different APC-specific antibodies, Ab7 and H290. The strikingly different level of co-localisation between the two antibodies indicates that Ab7 (13%) is not as effective as H290 (45%) in detecting mitochondrial-localised APC, either because it has a lower affinity, or because the epitope is masked when APC is associated with mitochondria.

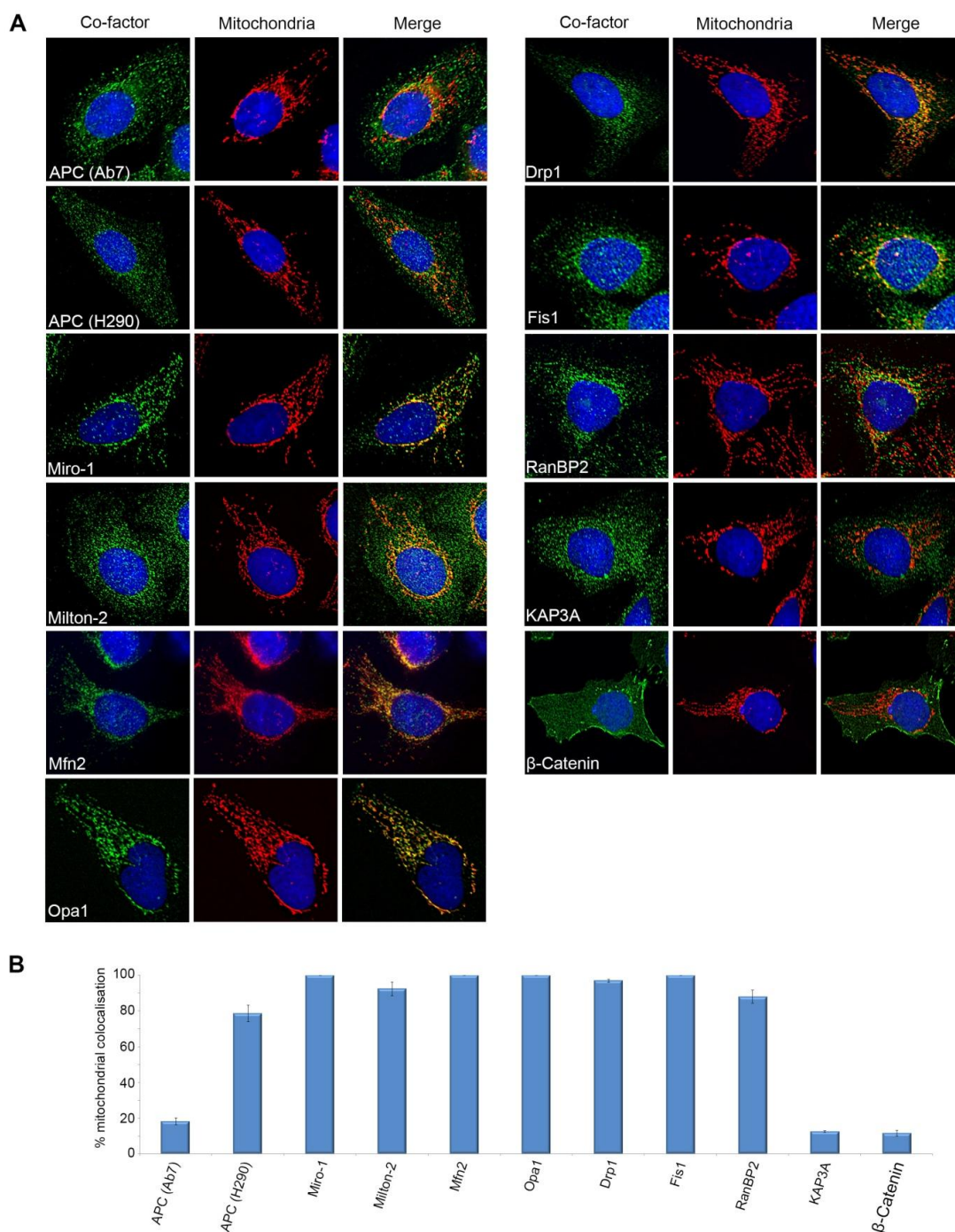


Figure 3.5: Mitochondrial colocalisation with potential co-factors in U2OS cells.

(A) Sub-confluent cells were stained with CMX-Ros (mitochondria) and Hoechst (blue) and probed with antibodies against APC (Ab7 and H290), Miro-1, Milton-2, Mfn2, OPA1, DRP1, Fis1, RanBP2 (pAb), KAP3A and β -Catenin. (B) Cells were scored for co-localisation with mitochondria by immunofluorescence microscopy (% mean \pm S.D).

The endogenous forms of the potential co-factors were then analysed for co-localisation with APC (Figure 3.6) in U2OS cells. As expected, RanBP2, KAP3A and β -catenin all showed a high level of co-localisation with APC (84%, 91% and 94% respectively). More unexpected however, was the equally high level of co-localisation observed between APC and the mitochondrial transport proteins Miro and Milton (89% and 90% respectively), particularly in the perinuclear region and cell membrane protrusions.

Mitochondrial fusion proteins Mfn2 and OPA1 also indicated a high level of co-localisation with APC (83% and 87% respectively), whilst in contrast, DRP1 (23%) and Fis1 (7%) showed little. Given the high level of APC colocalisation with these fusion proteins, and the appearance of punctate mitochondria following the loss of APC (Figure 3.2A), the possibility that APC may modulate mitochondrial morphology through an interaction with these proteins is examined further in Chapter 7. The possibility that APC may regulate mitochondrial transport in association with RanBP2 is also investigated in more detail in Chapter 7.

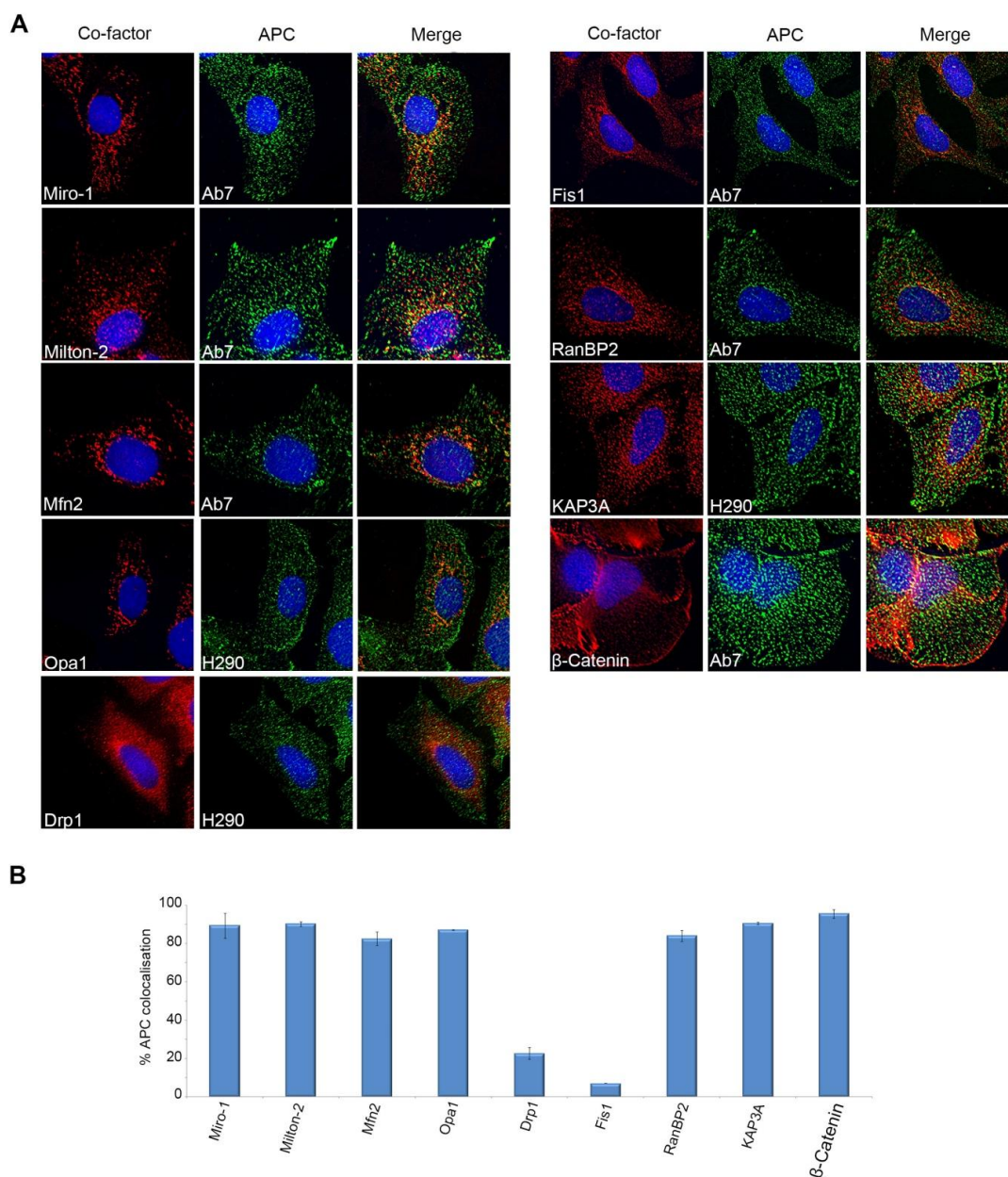


Figure 3.6: APC colocalisation with potential co-factors in U2OS cells.

(A) Sub-confluent cells were probed with antibodies against APC (Ab7 and H290) and either Miro-1, Milton-2, Mfn2, OPA1, DRP1, Fis1, RanBP2 (pAb), KAP3A or β -Catenin. (B) Cells were scored for co-localisation with APC by immunofluorescence microscopy (% mean \pm S.D). Note: use of both monoclonal (Ab7) and polyclonal APC (H290) antibodies were required for co-localisation studies. Despite reduced efficiency in detecting mitochondrial APC with Ab7, this antibody clearly co-stained with Miro-1 and Milton-2.

3.3.6 Specificity of Miro-1 and Milton-2 antibodies

Prior to further investigation, Miro-1 and Milton-2 antibodies were tested for specificity in cell staining experiments. pGFP-tagged Miro-1, Miro-2, Milton-1 or Milton-2 transfected U2OS cells were stained with CMX-Ros and probed with antibodies against GFP and either Miro-1 or Milton-2. Although these were the best commercially available antibodies against Miro-1 and Milton-2, immunofluorescence microscopy suggests that the Miro-1 antibody was not homolog specific and stained GFP-Miro-2 with a higher immunofluorescence intensity than untransfected cells (Supplementary Figure S3.3). The same was true for Milton-2 staining of pGFP-Milton-1 transfected cells relative to those not transfected. For the sake of simplicity, the Miro-1 antibody and detection of proteins Miro-1 and Miro-2 stemming from the use of this antibody will now be referred to as Miro, unless a specific pGFP-tagged ortholog has been transfected and detected using GFP antibodies (not the Miro-1 antibody). The same principle will be applied for the use of the Milton-2 antibody.

3.3.7 APC interacts with the Miro/Milton mitochondrial transport complex

APC co-localisation with Miro and Milton combined with the mitochondrial transport alterations observed upon APC knockdown suggested the possibility of interaction between these proteins. Immunoprecipitation assays in U2OS cells revealed that antibodies against APC were able to pull down GFP-tagged Miro-1 and Milton-2, but not GFP alone (Figure 3.7A, Supplementary Figure S3.4) in transfected cells. Pull-downs in the reverse direction however were less successful. Whilst initial experiments found that GFP antibodies were able to pull down GFP-tagged Miro-1 and endogenous APC in U2OS cells transfected with pGFP Miro-1, the APC pull down could not be repeated (Supplementary Figure S3.4). Furthermore, whilst GFP Milton-2 could also be pulled down by GFP antibodies in cells transfected with pGFP Milton-2, APC could not (Figure 3.7A; Supplementary Figure S3.4). It is possible that the inability of the GFP antibody to pull-down APC in pGFP Miro-1 and Milton-2 transfected samples is due to some steric hindrance/masking of the GFP epitope when Miro/Milton are bound to APC. It could also be due to the difficult nature of APC detection by western blot resulting from the large size of the protein (~310kDa) and the low sensitivity of

antibodies available, such that low levels of APC are difficult to detect. APC antibodies could also pull down GFP Milton-2 and endogenous Miro in HEK 293 APC-inducible cell lines (Supplementary Figure S4.2) discussed further in Chapter 4.

To complement the immunoprecipitation assay data we employed an *in situ* Duolink Proximity Ligation Assay (PLA; for details of the assay see Methods Section 3.2.8), using antibodies targeting endogenous APC and either Miro or Milton to detect potential interactions in U2OS cells. In line with the IP assays, APC/Miro and APC/Milton PLA experiments yielded a positive result, averaging ~25 and ~19 PLA signals per cell, respectively (Figure 3.7B-C). This was significantly higher than control samples that used a single antibody per reaction (PLA signal/cell APC= 0.7, Miro= 0.7, Milton= 0.8) (see Supplementary Figure S3.5 for more details). Similar positive and specific Duolink PLA results between APC/Miro and APC/Milton were observed in repeat experiments in HeLa cells, with PLA signal/cell averaging ~47 and ~18, respectively, which was well above the signal from the single antibody controls (PLA signal/cell APC= 4.4, Miro= 5.1, Milton= 2.5). (Figure 3.7B-C, see Supplementary Figure S3.5 for more details).

Specificity of the APC/Miro interaction by PLA was confirmed by treating U2OS cells with APC siRNA (APCd) prior to performing the assay. The efficiency of APC knockdown was ~60% (Figure 3.6D). As observed in Supplementary Figure S3.6, the PLA signal was significantly reduced by ~45% upon silencing of APC (APC/Miro PLA signal/cell: control siRNA= 21.8, APC siRNA= 12.1).

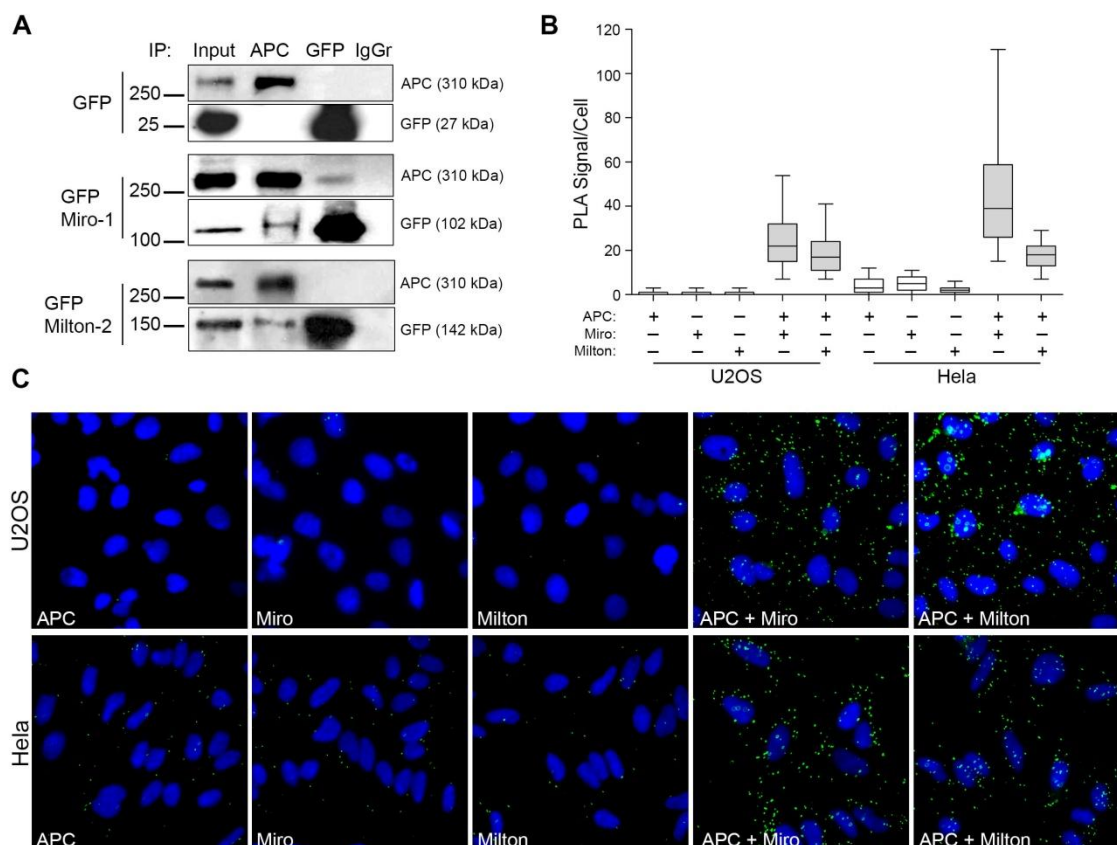


Figure 3.7: APC interacts with the Miro/Milton mitochondrial transport complex in U2OS and HeLa cells

(A) U2OS cells transfected with pGFP, pGFP Miro-1 or pGFP Milton-2 were immunoprecipitated by antibodies against GFP (pAb) and APC (C20, pAb) and analysed by western blot to detect GFP/GFP Miro-1/GFP Milton-2 (GFP, mAb) and APC (Ab1). The APC antibody successfully captured GFP Miro-1 and GFP Milton-2, indicative of a positive interaction between APC and Miro-1/ Milton-2. The GFP antibody also captured APC in cells transfected with pGFP Miro-1, however a similar pull down was not observed in cells transfected with pGFP or pGFP Milton-2. (B-C) Duolink PLA confirmed this interaction *in situ* in U2OS and HeLa cells using antibodies against APC, Miro and Milton. Scoring from analysis by immunofluorescence microscopy, indicate a positive PLA signal between APC/Miro and APC/Milton as observed in the (B) box-and-whisker plot and (C) representative images.

3.3.8 APC/Miro and APC/Milton complexes localise to the mitochondria

After establishing novel interactions between APC with Miro and Milton, we next confirmed that these protein complexes actually localise to the mitochondria. This is critical if they are to be functionally linked to mitochondrial transport. Preliminary immunofluorescence co-localisation studies were employed by staining U2OS cells transfected with pCMV-APC with CMX-Ros and antibodies against APC, Miro or Milton. Microscopic analysis revealed that APC and Miro appeared to co-locate with mitochondria in regions throughout the cell, including cell protrusions (Figure 3.8A). Similar co-localisation between APC and Milton at mitochondria was observed (Figure 3.9A).

Next, to study the position of actual APC/Miro and APC/Milton complexes, more detailed localisation studies were performed in U2OS and Hela cells utilising Duolink PLA assays counterstained for Mitochondria (CMX-Ros) (for *n* cells analysed see Supplementary Figure S3.5B). In U2OS cells ~52% of APC/Miro complexes localised to mitochondria (Figure 3.8C) which was verified by 3D image projections obtained from z-stacks (Figure 3.8B). Co-localisation (46%) of APC/Milton PLA signals was also observed at mitochondria in U2OS cells, and was verified using 3D image projections (Figure 3.9B-C). The similarity in the degree of mitochondrial colocalisation for APC/Miro and APC/Milton PLA signals is consistent with the idea that APC forms a complex with Miro and Milton. Comparable results were also observed in Hela cells which indicated 58% of Miro/APC and 49% of Milton/APC complexes were detected at mitochondria, where localisation could again be confirmed by 3D image projections (Figure 3.8D-E, Figure 3.9D-E).

APC/Miro and APC/Milton PLA signals at mitochondria mostly appeared to be localised to the outer edge of the mitochondria, which is consistent with the formation of the Miro/Milton transport complex on the surface of the outer mitochondrial membrane. To confirm this, electron microscopy would be required. Furthermore, whilst these PLA signals did not appear to preferentially localise to any distinct mitochondrial shape or size, they did seem to localise more frequently to the ends of individual mitochondria, rather than the middle. This was more noticeable when the

mitochondria were rod shaped, rather than punctate. Finally, APC/Miro and APC/Milton PLA signals at mitochondria were observed throughout the entire cell, from the perinuclear region to the tips of cell protrusions, as would be expected for complexes involved in mitochondrial transport.

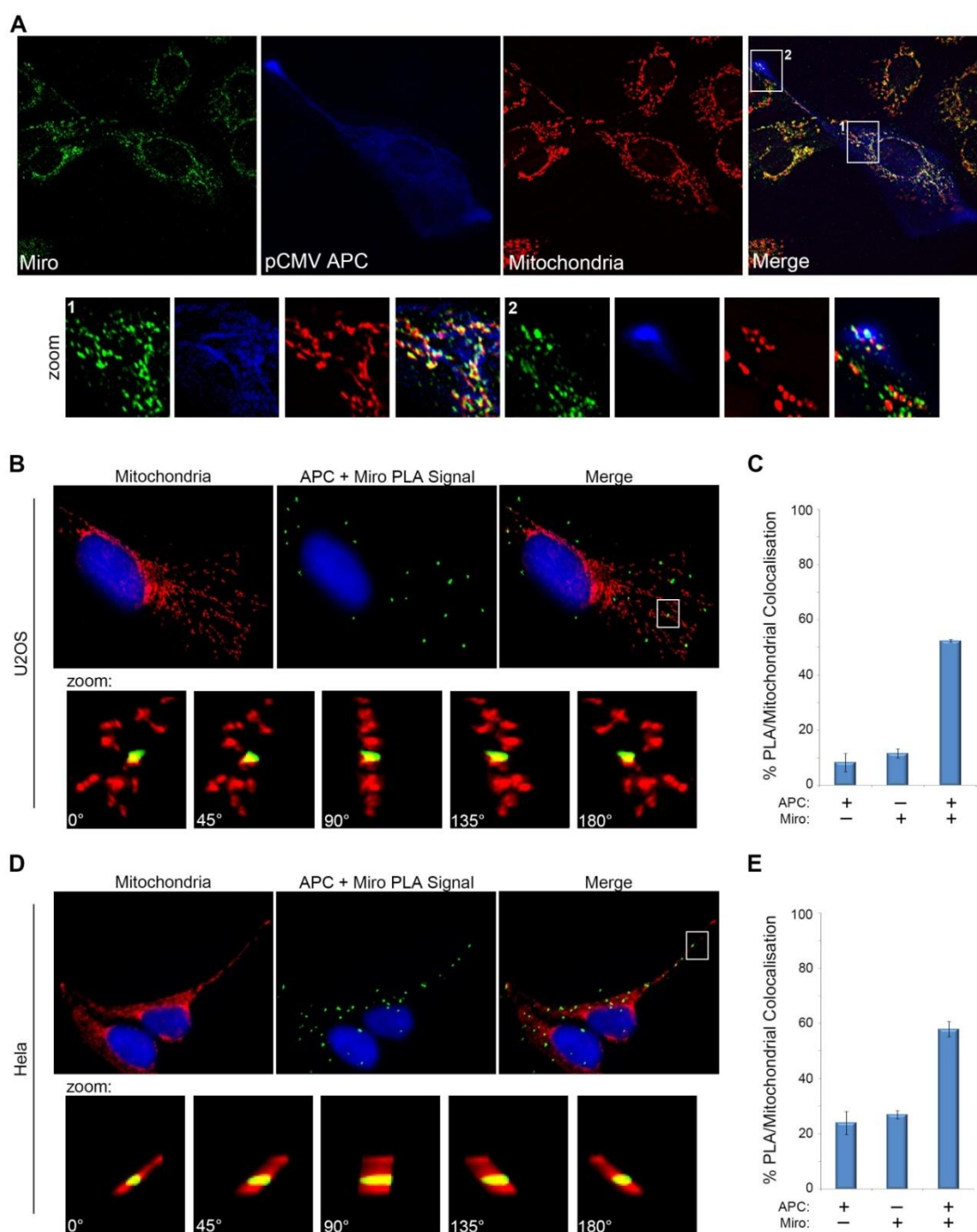


Figure 3.8: APC interacts with Miro at mitochondria in U2OS and HeLa cells

(A) Sub-confluent U2OS cells were transfected with pCMV-APC, stained with CMX-Ros (mitochondria), probed with antibodies against APC (Ab7) and Miro and analysed for colocalisation by immunofluorescence microscopy. pCMV-APC, Miro and mitochondria were observed to co-locate at the perinuclear region (#1) and at cell protrusions (#2). (B-E) Mitochondria were stained using CMX-Ros in U2OS and HeLa cells prior to utilising Duolink PLA to detect interactions between APC and Miro. Scoring (C,E) of immunofluorescence images, revealed APC/Miro PLA signals colocalised with mitochondria in both cells lines (% mean \pm S.D), as observed in the (B,D) representative 3D projections.

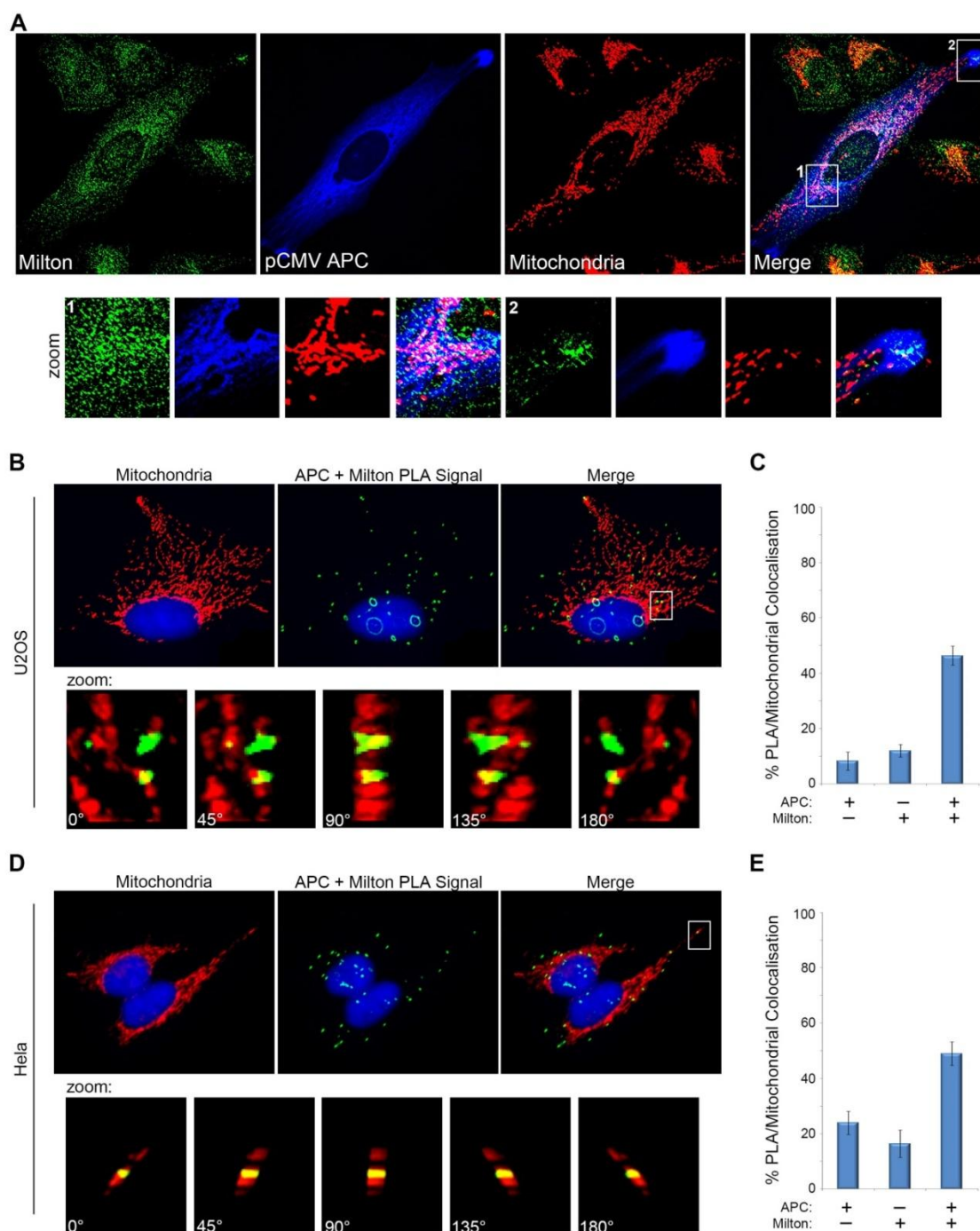


Figure 3.9: APC interacts with Milton at mitochondria in U2OS and HeLa cells

(A) Sub-confluent U2OS cells were transfected with pCMV-APC, stained with CMX-Ros (mitochondria), probed with antibodies against APC (Ab7) and Milton and analysed for colocalisation by immunofluorescence microscopy. pCMV-APC, Milton and mitochondria were observed to co-locate at the perinuclear region (#1) and at cell protrusions (#2). (B-E) Mitochondria were stained using CMX-Ros in U2OS and HeLa cells prior to utilising Duolink PLA to detect interactions between APC and Milton. Scoring (C,E) of immunofluorescence images, revealed APC/Milton PLA signals colocalised with mitochondria in both cell lines (% mean \pm S.D), as observed in the (B,D) representative 3D projections.

3.4 Discussion

APC is a critical regulator of many pathways in normal cell growth and differentiation. Here a new role for APC in the regulation of anterograde mitochondrial transport is described for the first time. The motile nature of mitochondria is essential for swiftly providing energy to cell compartments with high bioenergetic demands, such as membrane protrusions and lamellipodia for cell migration. Loss of APC caused a specific redistribution of mitochondria away from the cell periphery towards the perinuclear region which, upon further investigation, correlated strongly with an interaction between APC and the Miro/Milton transport complex. This protein complex is responsible for transport of mitochondria toward the plus-ends of microtubules at the cell periphery, and a novel regulatory role for APC in this process will be discussed.

3.4.1 APC has a novel and specific role in the subcellular localisation of mitochondria.

APC localises at several cellular compartments, moves along cytoskeletal tracks and has been reported to interact with a number of motor proteins and adaptors involved in vesicle transport (Section 1.2.1). Therefore, it is perhaps not surprising to find that APC has a role in cell organelle transport. The finding that loss of APC disrupts mitochondrial localisation (Figure 3.2) correlates with its previous detection at mitochondria (13). Perturbations in mitochondrial distribution following APC knockdown, presumably through altered transport (this is demonstrated more directly in Chapter 5), were found to be quite specific and other organelles were not affected by the loss of APC (Figure 3.1).

Mitochondrial transport is mediated by a limited number of motor proteins that interact with a wide range of adaptors to ensure that transport of cargo is highly regulated (273, 274). Whilst some kinesins bind directly to their cargo, most organelles bind kinesins indirectly through a unique set of adaptor proteins (273). For example, in addition to mitochondria, KIF5 is also involved in the microtubule-dependent transport of lysosomes and the endoplasmic reticulum (275, 276), both of which associate with a different set of adaptor proteins that they use to attach to KIF5 (277, 278). When APC expression was silenced, there were no observable alterations in the transport of either

of these organelles. This indicates that APC loss is not causing havoc with the general microtubule-transport systems of the cell and, consequently, is likely to be affecting with some specificity the movement of mitochondria through its interaction with the Miro and Milton adaptor proteins.

APC was previously reported to bind to KAP3A, a component of the KIF3 kinesin adaptor complex, by which APC was proposed to be transported in a plus-end directed fashion along microtubules (26). The KIF3/KAP3A complex has been reported to drive the transport of cell organelles, in particular the golgi and lysosomes (279, 280). However, as no changes in distribution for these organelles were observed upon APC knockdown, and as APC has not been reported to localise to these structures, it is unlikely that APC contributes to these processes (other implications of the APC/KAP3A association are discussed in Chapter 7).

In addition to the mitochondria, APC also localises to the centrosome where it has been implicated in centrosome reorientation and cell polarisation (281). In this regard we observed no clear changes in centrosome positioning following the siRNA knockdown of APC in sub-confluent U2OS cells (Figure 3.1), whereas others reported that loss of APC in polarised migrating fibroblasts disrupted centrosome re-orientation and in turn cell polarity in scratch wound assays (75). Whilst these results may point to another role for APC in transporting cell organelles, evidence from the literature suggests that the disruption of centrosome localisation in migrating cells was due more to destabilisation of microtubules, rather than APC association with a motor protein (75).

3.4.2 Evidence for APC transport of mitochondria along microtubules

Mitochondria are highly dynamic in nature and utilise the cytoskeleton for movement throughout the cell. As discussed in Section 1.3.2, kinesin and dynein motors are primarily used to transport mitochondria long distances across microtubules whilst myosin motors typically provide a means for short range transport along actin filaments. APC itself can associate directly and indirectly with both the microtubule and actin networks, and such cytoskeletal interactions are crucial for its role in regulating cellular processes such as co-ordinating cell polarity, stabilising microtubules, promoting F-

actin assembly, and promoting cell adhesion and/or migration (for more information see Section 1.2.1.3). The discovery that APC binds to the microtubule-dependent Miro/Milton complex indicates that APC could stimulate mitochondrial transport via its association with the microtubule system, rather than the actin cytoskeleton.

In this study, loss of APC induced a perinuclear clustering of mitochondria, characteristic of disruption to anterograde microtubule-based transport. This is because unlike actin, which forms a lattice-like network cross-linked in many directions, microtubules form a polarised, radial network, anchored to a central point known as the microtubule organising centre (MTOC) at the centrosome, typically located close to the nucleus. Mitochondria in the cell lines observed thus far (Figure 3.2) typically form branching networks throughout the entire cell. The shift in localisation of mitochondria towards the perinuclear region observed following APC knockdown suggests that their transport along a polarised, radial network emanating from a point close to the nucleus has been disrupted, more consistent with disruption of movement along microtubules rather than along actin filaments which have no central point or polarisation.

To further demonstrate that the influence of APC on mitochondrial distribution was more likely linked to microtubules than actin, cells were exposed to drug treatments to depolymerise microtubules and actin filaments using nocodazole (282) and latrunculin A (283), respectively (Figure 3.3). Treatment with nocodazole caused mitochondria to shift towards the perinuclear region, in a manner similar to, though less severe, than that observed when APC was silenced. On the other hand, treatment with latrunculin A induced no such shift, even though mitochondria looked slightly aggregated and irregular, perhaps due to disruption of short range transport. These results support the notion that APC transport of mitochondria is microtubule based rather than actin based.

The above points when considered together with the binding of APC to the Miro/Milton complex, strongly implicate APC in microtubule based transport of mitochondria. However, one cannot rule out an alternative pathway whereby APC might transport mitochondria along actin. Disrupting plus end-directed long range mitochondrial transport mechanisms, such as Miro/Milton, would mask any additional disruptions to short range actin transport. In this context, it is intriguing to note that unpublished data

from our laboratory suggests that APC interacts with several myosin motors (discussed further in Chapter 7).

3.4.3 APC interacts with the Miro/Milton mitochondrial transport complex to move mitochondria in the anterograde direction

Mitochondrial perinuclear clustering is often observed in cases where anterograde mitochondrial transport has been disrupted. In line with current literature, our results in U2OS, HDF1314 and NIH 3T3 cells (Figure 3.2) are reminiscent of experiments in HeLa cells where siRNA disruption of Miro-1/Miro-2 expression resulted in a dramatic mitochondrial redistribution from the cell periphery to the perinuclear region (165). This phenomena was also observed in mouse cells following disruption of KIF5B gene expression (284). In the study by Tanaka et al. (284), mitochondria in control cells displayed a branching network throughout the cell, whereas in KIF5B disrupted cells the mitochondria were clustered around the nucleus. Therefore the loss of expression of proteins in the Miro/Milton complex result in a very similar perinuclear redistribution of mitochondria to that observed following APC disruption in this study, providing correlative evidence for a functional link between APC and the Miro/Milton complex.

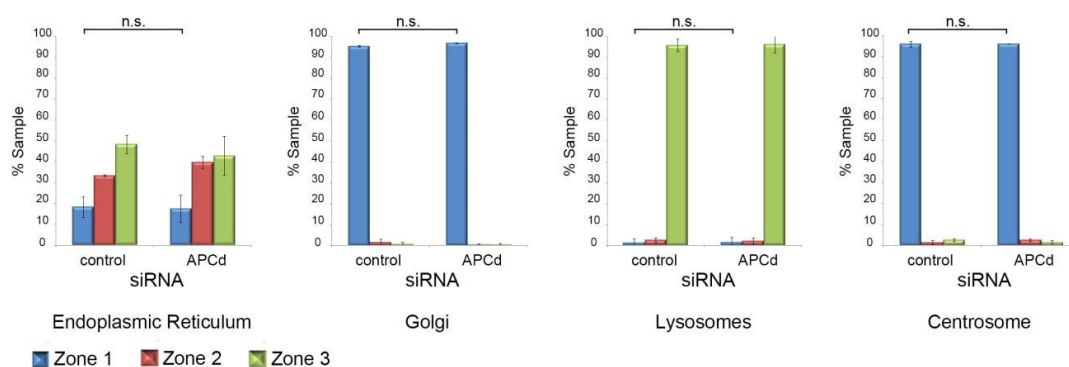
The interaction detected here between APC and the Miro/Milton complex is novel, and now explains an earlier observation showing co-localisation between APC and KIF5 in mouse colon cancer epithelial cells (285). Intriguingly the previous study noted APC/KIF5 co-localisation at cell membrane regions, similar to that observed here between APC and Miro (Figure 3.8A) and APC and Milton (Figure 3.9A). The loss of KIF5 was also reported to reduce APC localisation at the cell periphery (285). Furthermore, APC has been reported to modify KIF5 in *Drosophila* neurons, thereby linking it to vesicle transport (286) in neurons, suggesting a more general and potential functional link between APC and KIF5 in different cell types and species. Unfortunately, due to antibody limitations at the time of the study, an interaction between APC and KIF5 was unable to be confirmed, though it should be noted there is no evidence in the literature to suggest that Miro or Milton associate with any other kinesin proteins. These previous findings, combined with the careful 3-D mapping of APC/Miro and APC/Milton complexes to the outer mitochondrial membrane in this

study, support a role for APC in regulation of Miro/Milton/kinesin transport of mitochondria toward the cell membrane.

3.4.4 Summary

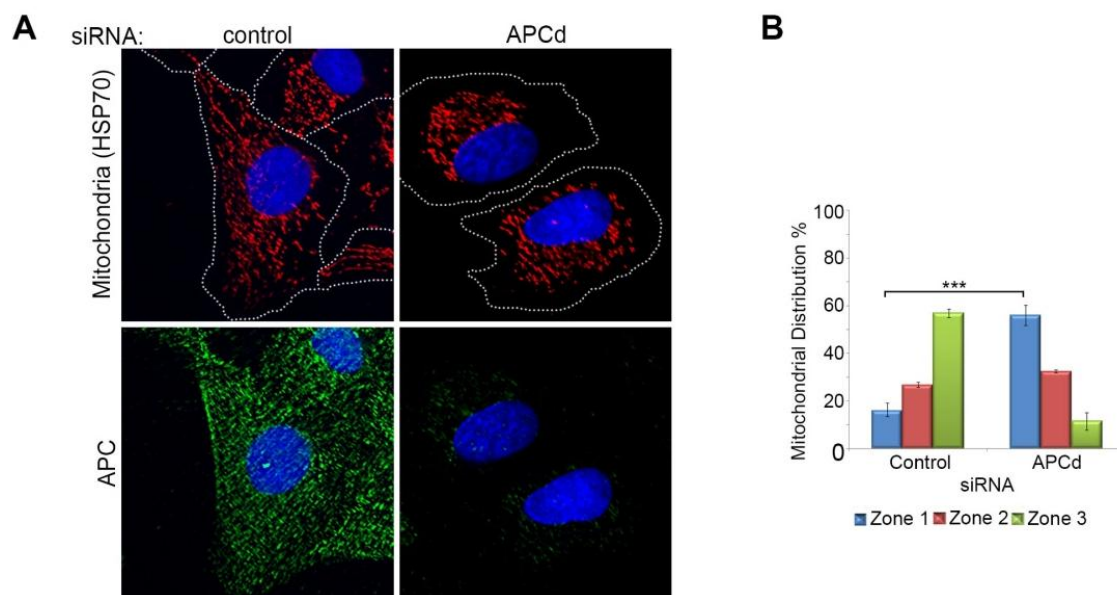
These findings indicate a new role for APC as a regulator of mitochondrial transport. APC binds to the Miro/Milton complex at mitochondria, which in turn facilitates microtubule-based transport in the anterograde direction towards the cell membrane periphery. The truncation of APC, a common feature in ~80% of colorectal cancers, severely disrupts many of its cellular pathways, including its association with microtubules and its regulation of Wnt signalling. How APC truncation impacts on mitochondrial transport, and what physiological effects this has on cellular function is investigated in subsequent chapters (Chapter 4). Other implications for APC-dependent mitochondrial transport will also be discussed, with a particular focus on how localisation of mitochondria at the cell membrane may contribute to the functionality of APC in cell migration (Chapter 5). Furthermore, specifics regarding how APC mediates the Miro/Milton transport complex are examined throughout (Chapters 4-6).

3.5 Supplementary Figures



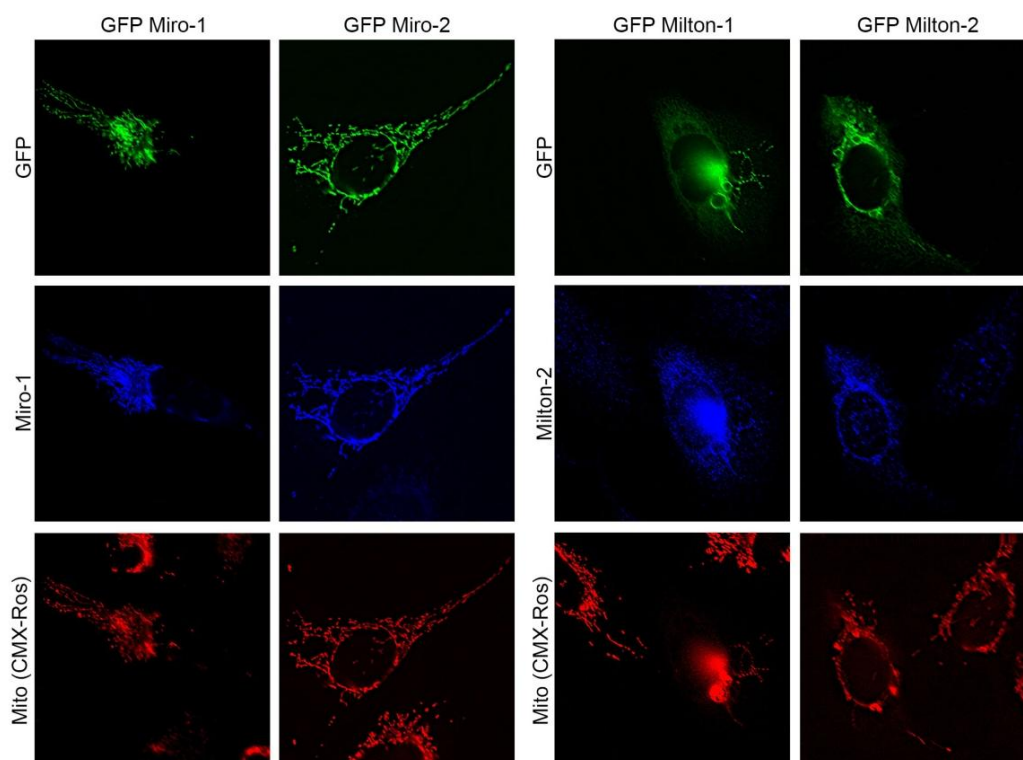
Supplementary Figure S3.1: Loss of APC effects transport of select microtubule associated organelles

Sub-confluent U2OS cells were treated with control or APC (APCd) siRNA and stained with ER tracker or probed with antibodies against 58k, LAMP-1 or γ -tubulin to detect endoplasmic reticulum, golgi, lysosomes and centrosomes respectively, as visualised in Figure 3.1. Cells were scored (% mean \pm S.D) for changes in organelle distribution by immunofluorescence microscopy. Significance was determined using an unpaired T-test (n.s, not significant).



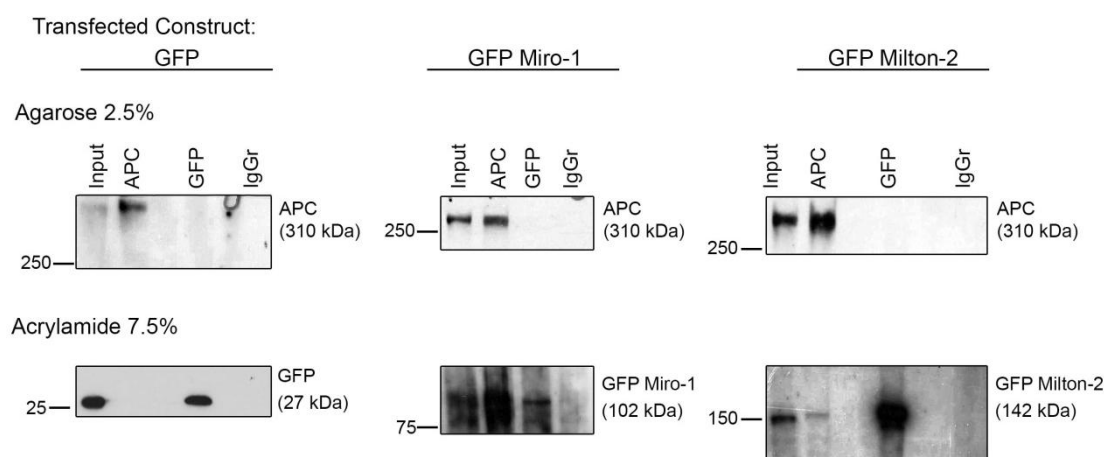
Supplementary Figure S3.2: Loss of wild-type APC induces a redistribution of mitochondria in U2OS stained with HSP70

(A) U2OS cells were treated with APCd siRNA, stained using antibodies against HSP70 (mitochondria) and APC (H290) and analysed by immunofluorescence microscopy. Scoring (B) of mitochondrial distribution (% mean \pm S.D) revealed a significant (***, $P < 0.001$, determined using an unpaired T-test) increase in zone 1 perinuclear clustering following silencing of APC.



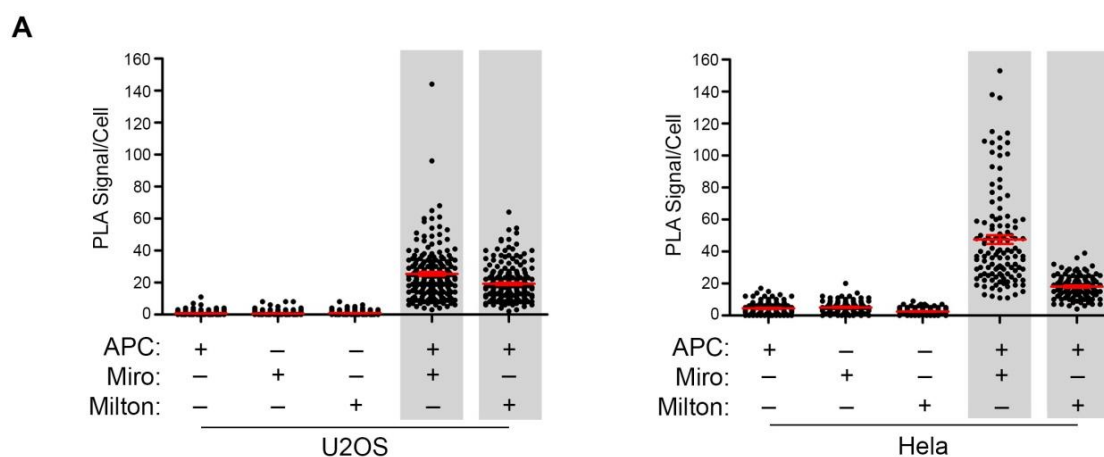
Supplementary Figure S3.3: Miro-1 and Milton-2 antibodies are not homolog specific.

Sub-confluent U2OS cells transfected with pGFP Miro-1, pGFP Miro-2, pGFP Milton-1 or pGFP Milton-2 were stained with CMX-Ros, and probed with antibodies against GFP and either Miro-1 or Milton-2.



Supplementary Figure S3.4: Additional immunoprecipitation blots - GFP Miro-1 and GFP Milton-2 can be immunoprecipitated using an APC antibody

U2OS cells transfected with pGFP, pGFP Miro-1 or pGFP Milton-2 were immunoprecipitated by antibodies against GFP (pAb) and APC (C20, pAb) and analysed by western blot to detect GFP/GFP Miro-1/GFP Milton-2 (GFP, mAb) and APC (Ab1). The APC antibody successfully pulled down GFP Miro-1 and GFP Milton-2, whilst no pull down was observed for the GFP control. APC pull down by GFP was not observed in cells transfected with pGFP, pGFP-Miro-1 or pGFP Milton-2.

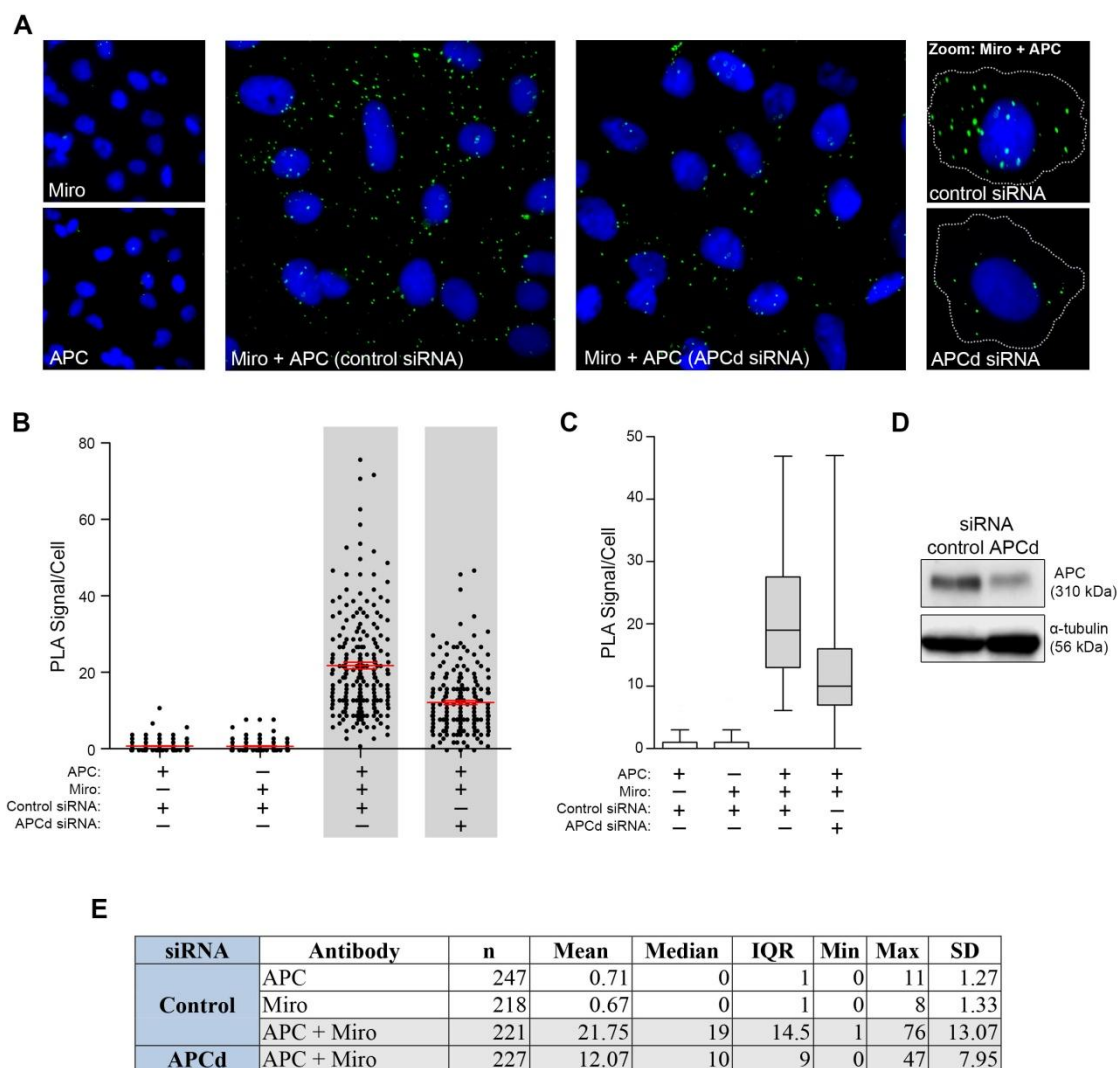


B

Cell Line	Antibody	n	Mean	Median	IQR	Min	Max	SD
U2OS	APC	247	0.71	0	1	0	11	1.27
	Miro	218	0.67	0	1	0	8	1.33
	Milton	213	0.82	0	1	0	8	1.22
	APC + Miro	202	25.46	22	17	3	144	16.16
	APC + Milton	210	19.20	17	13	2	64	10.85
HeLa	APC	120	4.41	3	6	0	17	3.76
	Miro	120	5.07	5	6	0	20	3.59
	Milton	120	2.53	2	2	0	9	1.78
	APC + Miro	120	47.50	39	32.75	11	153	30.05
	APC + Milton	120	18.06	18	9	4	39	6.71

Supplementary Figure S3.5: APC interacts with Miro and Milton in U2OS and HeLa Cells - Expanded Duolink Data

(A-B) Interactions between APC and Miro/Milton were visualised *in situ* using Duolink PLA as described in Figure 3.7. Scoring indicates a positive signal between APC and Miro, and APC and Milton as shown in the (A) dot-plots (mean \pm S.D) and (B) table (n, number in sample; IQR, inter-quartile range; SD, standard deviation).



Supplementary Figure S3.6: Loss of APC decreases the APC/Miro Duolink PLA signal in U2OS cells.

(A-E) Cells were treated with control or APC (APCd) siRNA prior to performing Duolink PLA using antibodies against APC and Miro. (A) Analysis by immunofluorescence microscopy and subsequent scoring visualised in the (B) dot plot (mean \pm S.D) and (C) box-and-whisker plot revealed that the APC/Miro PLA signal was reduced by ~45% upon loss of APC. (D) Knockdown was confirmed by western blot and further details are outlined in the (E) table (n, number in sample; IQR, inter-quartile range; SD, standard deviation).

CHAPTER 4

**Cancer mutations disrupt
binding of APC to
Miro/Milton and impair
mitochondrial transport**

APC is involved in many areas of normal cell growth and differentiation such as Wnt signalling, mitosis, cell migration and cytoskeletal regulation. These processes are mis-regulated by C-terminal truncating APC mutations. In Chapter 3 a novel role for APC in the regulation of mitochondrial transport was proposed, whereby APC binds the Miro/Milton complex to transport mitochondria along microtubules toward the cell periphery in a kinesin-dependent manner. To determine if this function of APC is disrupted by truncating mutations, mitochondrial distribution patterns were interrogated in a number of CRC cell lines harbouring mutant or wild-type APC. In CRC cells expressing mutant APC (SW480 and HT-29), mitochondria were more frequently clustered around the nucleus, indicative of impaired anterograde mitochondrial transport. In comparison, mitochondrial distribution in CRC cell lines expressing wild-type APC (HCT116 and LIM1215) were uniformly distributed throughout the cell extending towards the cell membrane, similar to that observed in epithelial and fibroblastic cells in Chapter 3. Furthermore, in mutant APC cells, siRNA-mediated knockdown of APC did not elicit any mitochondrial redistribution, suggesting that truncated APC was compromised in its ability to transport mitochondria. This idea was supported by recovery of mitochondrial transport to the cell periphery after reconstitution of wild-type APC in mutant HT-29 cells. Immunoprecipitation and Duolink PLA analysis indicated that truncated APC mutants were defective in binding to Miro/Milton, a finding consistent with mapping of the Miro/Milton-binding site to the C-terminal region (2650-2843) of APC. These results suggest that truncation of APC disrupts its capacity to bind Miro/Milton, in turn blocking mitochondrial transport to the cell periphery. This could result in impaired mitochondrial distribution and compromise site-specific functions such as distribution of ATP and calcium buffering, contributing to the carcinogenic process.

4.1 Introduction

APC regulates pathways of cell growth and differentiation including Wnt signalling, spindle formation, chromosome segregation, the DNA repair and damage response, cell polarization and cell migration (Section 1.2.3 and 8, 52, 287, 288). This multifunctional nature makes APC a critical tumour suppressor protein as highlighted by the fact that mutations in the APC gene occur in ~80% of CRCs and are one of the earliest events in the progression of sporadic CRC. APC was first identified as the critical gene mutated in familial adenomatous polyposis (FAP), an autosomal dominant disease carrying a germ line APC mutation and characterised by colorectal polyps and a high risk of early CRC (3-5). A gene mutation in one APC allele can cause FAP, whereas a 'second hit' in the form of a somatic mutation in the remaining allele predisposes patients to increased risk of cancer (7, 8).

The majority of APC mutations localise in a central area known as the mutation cluster region and in general produce a premature stop codon resulting in a truncated APC protein (the most common is a mutation at amino acid 1309), which lacks C-terminal sequences (20). This often results in loss of APC function which is followed by tumour formation. Aberrant β -catenin signalling and in turn continuous transcription of Wnt target proteins is most commonly associated with mutant APC driven tumourigenesis (Section 1.2.3.1 and 3, 5), however a number of other alterations in chromosome stability, cell polarity and cell migration (Sections 1.2.3.2 - 1.2.3.4 and 54, 96, 289) contribute to this process.

The previous chapter presented a new role for APC in the anterograde transport of mitochondria, through an interaction with the Miro/Milton mitochondrial transport complex. Mitochondria are known to be dysfunctional in cancer cells and several aspects of this have been studied including defective metabolism, mitochondrial genome mutations, increased ROS production and alterations in fission/fusion dynamics (Section 1.3.4.2 and 14, 263, 264). Disrupted mitochondrial transport however, has more often been studied in the context of neurological disorders, where, in normal neurons mitochondria are required to travel long distances between the cell body and the axon terminal (Section 1.3.4.1 and 139, 256, 257). The importance of precise regulation of mitochondrial transport and how disruption contributes to carcinogenesis

is only just coming to light. In particular, recent studies in epithelial cells link mitochondrial distribution to cancer cell migration and invasion (18, 19). Other cell signalling pathways known to be disrupted during cell transformation include aberrant gene transcription of growth factors and calcium signalling, which have also been reported to be partially dependent on mitochondrial distribution (see Section 1.3.1.2)

Prior studies in this laboratory have shown that APC mutants display increased mitochondrial localisation (13), which correlated with a protective influence against apoptosis through regulation of Bcl-2, thereby promoting the survival of cancer cells. In this chapter, the truncation of APC in CRC cell lines is shown to disrupt its interaction with the Miro/Milton mitochondrial transport complex through loss of a critical C-terminal binding region, leading to an apparent cessation of mitochondrial anterograde transport which could be restored upon wild-type APC expression. These results, when viewed in the context of current literature indicate a new pathway by which mutant APC loss of function may contribute to CRC carcinogenesis.

4.2 Methods

4.2.1 Cell culture

U2OS osteosarcoma cells, and the colorectal cancer cell lines SW480, HT-29, HCT116 and LIM1215 were cultured in DMEM under standard conditions as outlined in Section 2.2.3. Stable inducible HEK293 cell lines (APC-WT) and (APC-1309) were cultured in DMEM containing 15 g/ml blasticidin and 150 g/ml hygromycin B under standard conditions. APC protein expression was induced by the addition of 2 ng/ml tetracycline 16 h prior to subsequent processing. For mitochondrial distribution and co-localisation experiments, cells were seeded on glass cover slips in 6-well tissue culture plates, and for Duolink PLA experiments, cells were seeded in 8-well chamber slides coated with poly-L-lysine. Cells were grown to 70-80% confluence prior to fixation. For western blotting experiments, cells were seeded into 150 cm² flasks for immunoprecipitation assays and 25 cm² flasks for siRNA knockdown experiments. Further details can be found in Section 2.2.3.1.

The transfection of plasmids and siRNAs for transient expression or gene silencing in cells is described in Section 2.2.3.4. In Duolink PLA assays utilising GFP-tagged constructs, the amount of plasmid transfected was significantly reduced (more details Section 2.2.8.4). For siRNA treatments in CRC cell lines SW480, HT-29, HCT116 and LIM1215, APC siRNAs (APCd and APC2) were pooled to increase efficacy of the knockdown.

4.2.2 Cell fixation and staining for immunofluorescence microscopy

Cells were seeded for at least 24 h, fixed with methanol-acetone, probed with relevant antibodies and mounted for immunofluorescence microscopy as outlined in Section 2.2.4. If detection of mitochondria was required, the addition of the MitoTracker dye, CMX-Ros, occurred prior to fixation. Concentrations and any further specifications for all antibodies and dyes used in this chapter are outlined in Table 2.2, Table 2.3 and Table 2.4.

4.2.3 Immunofluorescence cell image acquisition and processing

Slides were analysed using the Olympus IX71 DeltaVision Core deconvolution microscope equipped with a CoolSNAP HQ² camera for general image capture. The images collected were further resolved using SoftWorx deconvolution software. For mitochondrial distribution experiments, 300 cells were scored over 3 independent experiments with the exception of the HT-29 reconstitution assay (Figure 4.2) where 200 cells were scored over 2 independent experiments. Analysis of mitochondrial distribution experiments and Duolink PLA experiments is further described in Section 4.2.4 and Section 4.2.7, respectively.

4.2.4 Quantification of mitochondrial distribution

Mitochondrial distribution was scored into three ‘zones’ spanning outwards from the nucleus towards the cell membrane as described in Section 2.2.7.2. It should be noted that additional parameters were taken into account when scoring certain cell lines used in this chapter, in particular the smaller colorectal cancer cells. This is outlined in Table 2.9. For analysis of mitochondrial distribution in HT-29 cells expressing GFP, GFP APC-WT and GFP APC-1309 (Figure 4.2), only cells displaying a modest level of transfection were scored, to avoid complications stemming from the microtubule bundling observed when GFP APC-WT is overexpressed.

4.2.5 Immunoprecipitation assays

Immunoprecipitation experiments were performed as described in Section 2.2.10. Cells used for these assays were treated as follows: SW480 cells transfected with plasmids that express GFP, GFP Miro-1 and GFP Milton-2 (Figure 4.3), and HEK293 stable cell lines induced with tetracycline (Supplementary Figure S4.2, pg138), were collected and lysed with HUNT buffer (Appendix 2.1). U2OS cells transfected with plasmids that express GFP and GFP-APC fragments (1-302, 1379-2080 and 2650-2843) (Figure 4.6) were collected and lysed with RIPA buffer. Collection and lysis of cells is described in Section 2.2.9.1. Immunoprecipitation experiments were carried out using antibodies against GFP (pAb, Invitrogen), APC (C20, pAb, Santa Cruz), APC (Ab5, mAb, Merck), Miro-1 (pAb, Sigma-Aldrich), Milton-2 (pAb, Sigma-Aldrich), IgGm (mAb, Sigma-

Aldrich) and IgGr (pAb, Sigma-Aldrich), to pull-down target proteins prior to samples being subjected to SDS-PAGE and western blot analysis. Immunoprecipitation experiments were performed at least twice.

4.2.6 Western blot analysis

Cells were collected, lysed using RIPA buffer and processed as described in Section 2.2.9.1. Samples (immunoprecipitates or ~30 µg total cell lysate) were separated by SDS-PAGE using 5% (for detection of APC), 7.5% or 10% acrylamide gels, and transferred onto a nitrocellulose membrane (see Sections 2.2.9.3-2.2.9.6). Western blots were probed as outlined in Section 2.2.9.7, using primary antibodies as per the figure legends. Dilutions for these antibodies and subsequent secondary antibodies are outlined in Table 2.2 and Table 2.3. Immunoblots in this chapter were developed on film using ECL, with the exception of those in Figure 4.6 and Supplementary Figure S4.1 which were developed using ECL and the BioRad ChemiDoc Imaging System (see Section 2.2.9.8).

4.2.7 Duolink Proximity Ligation Assay (PLA)

Duolink PLA experiments in this chapter employed primary antibodies against APC (Ab7, mAb, Merck), Miro-1 (pAB, Sigma-Aldrich) and Milton-2 (pAB, Sigma-Aldrich) at concentrations outlined in Table 2.2, to visualise protein interactions between APC/Miro and APC/Milton in cells pre-stained with CMX-Ros (more detail in Section 2.2.8). Duolink PLA in cells expressing GFP-APC constructs also used an antibody against GFP (mAb, Roche) to visualise protein interactions between transiently expressed APC sequences and endogenous Miro or Milton (Section 2.2.8.4). Following image capture, PLA signals were quantified manually, by scoring the number of PLA signals per cell using a DIC channel overlay to determine the boundaries of each cell (Section 2.2.8.6). Unless stated in the figure legend, Duolink PLA experiments were performed at least twice for each sample. The number of cells scored is outlined in the supplementary figures for each experiment.

Duolink PLA in cells expressing GFP-tagged APC constructs were compared to control cells expressing GFP alone as a frame of reference for background signal. For these

experiments, only cells expressing a modest level of the transfected plasmid were scored to minimise artefacts caused by overexpression. Low levels of transfection were more readily detected by counterstaining Duolink experiments with GFP (mAb) and the appropriate secondary antibody (as described in 2.2.8.5) following PLA. In exception to the above rule, transfected cells used for the competition Duolink PLA assay (Figure 4.9) were selected for mid-range expression of GFP-tagged construct.

4.2.8 Graphs and statistics

All graphs and statistics used to display and analyse results in this chapter are outlined in Section 2.2.11.

4.3 Results

4.3.1 APC dependent relocalisation of mitochondria is disrupted by truncating APC mutations in colorectal cancer cell lines

Colorectal cancers display a high incidence of APC C-terminal truncating mutations which often lead to disruption of APC function (4, 5, 11). In Chapter 3 it was shown that silencing of full-length APC caused a novel perinuclear redistribution of mitochondria, revealing a role for APC in the normal cellular spread of mitochondria. To investigate whether this activity is altered by truncations of APC typically observed in cancer, mitochondrial distribution was analysed in a number of colorectal cancer cell lines expressing either mutant (SW480(APC 1-1337) and HT-29(APC 1-853/1555)) or wild-type APC (HCT116 and LIM1215) (see schematic Figure 4.1A). Distribution was quantified as previously described in Chapter 3, where mitochondria were scored according to their position in one of three cellular zones radiating from the perinuclear region (zone 1) to the region bordering the cell membrane (zone 3) (see schematic in Figure 4.1B).

Mitochondria in colorectal cancer cell lines retaining wild-type APC (HCT116 and LIM1215) were frequently spread throughout the cell cytoplasm, reaching towards the plasma membrane (zone 3), in a similar manner to that observed in U2OS, HDF1314 and NIH 3T3 cell lines (Figure 3.2). However, this was less often the case for SW480 and HT-29 mutant APC cell lines, where mitochondria were more frequently clustered around the perinuclear region (zone 1), implying that truncation of APC may disrupt its ability to facilitate anterograde transport of mitochondria (Figure 4.1C-D). Furthermore, siRNA-mediated knockdown of wild-type APC induced a significant redistribution of mitochondria away from the cell periphery, towards the perinuclear region in HCT116 cells (zone 1 mitochondria: control=18%, APCd/APC2=28%) ($P>0.01$) and LIM1215 cells (zone 1 mitochondria: control=15%, APCd/APC2=23%) ($P>0.01$). However, no such change in mitochondrial distribution was observed when mutant APC was silenced in SW480 (zone 1 mitochondria: control=37%, APCd/APC2=35%) ($P>0.5$) and HT-29 cell lines (zone 1 mitochondria: control=32%, APCd/APC2=35%) ($P>0.5$), consistent

with the idea that mutant truncated APC is unable to assist in driving mitochondria towards the cell periphery.

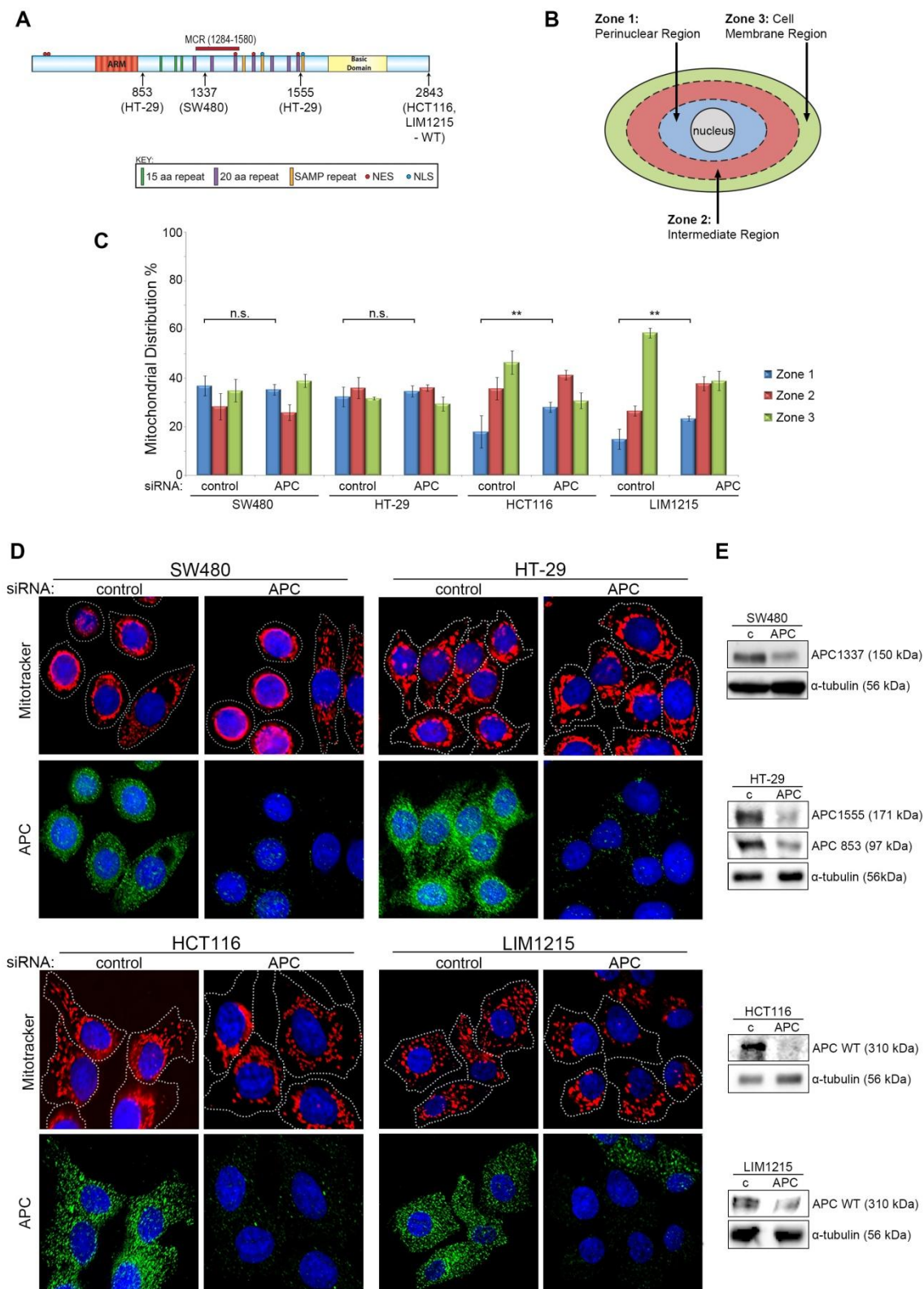


Figure legend over page.

Figure 4.1: Loss of truncated APC in colon cancer cell lines does not induce redistribution of mitochondria

(A) The mutation status of APC in colon cancer cell lines SW480, HT-29, HCT116 and LIM1215 is outlined in the schematic. (B-D) These cell lines were treated with control or APCd/APC2 pooled siRNA for 72 h, stained with CMX-Ros Mitotracker and counterstained with APC antibody (H290) and Hoechst. Mitochondrial distribution was analysed by immunofluorescence microscopy and scored as described in the (B) schematic. (C) Results are indicated on the bar graph with significant differences relative to siRNA control indicated for each cell line (**, $P < 0.01$; n.s., not significant, % mean \pm S.D). Significance determined using unpaired T-test. (D) Representative images are shown (dotted line represents the cell membrane). (E) Knockdown of APC (control (c) and APC siRNAs) was confirmed by western blot analysis with the use of α -tubulin as a loading control.

4.3.2 Mitochondrial localisation towards the plasma membrane is rescued by reconstitution of wild-type APC in mutant APC HT-29 cells

To confirm that disruption of mitochondrial distribution in APC mutant cell lines was due to APC truncation alone, rather than additional defects in the mitochondrial transport complex, GFP-tagged APC wild-type (GFP APC-WT) was transiently expressed in HT-29 cells and analysed by immunofluorescence microscopy to determine if recovery of mitochondrial localisation at the cell periphery was possible (Figure 4.2). The overexpression of APC has been shown to bundle microtubules (28, 60), which could potentially block mitochondrial trafficking, therefore only cells which expressed a modest level of GFP APC-WT were analysed. Mitochondrial scoring of these cells revealed that reconstitution of GFP APC-WT compared to GFP alone significantly stimulated transport of mitochondria away from the perinuclear region (zone 1 mitochondria: GFP=38%, GFP APC-WT=24%)($P < 0.001$) towards the zone 3 cell membrane region (zone 3 mitochondria: GFP=29%, GFP APC-WT=43%)($P < 0.001$), thereby at least partly correcting the mitochondrial transport defect observed in mutant APC cell lines (Figure 4.2).

In parallel, pGFP-tagged APC truncated at amino acid 1309 (GFP APC-1309) was also transfected, and HT-29 cells expressing a modest level of the construct were analysed for mitochondrial distribution (Figure 4.2). As expected, transport of mitochondria to the cell periphery was not recovered, and in fact expression of GFP APC-1309 induced

an increase in zone 1 perinuclear clustering of mitochondria (GFP=38%, GFP APC-1309=25%)($P<0.001$). This could reflect a partial dominant effect, although was not consistently seen in other cell lines.

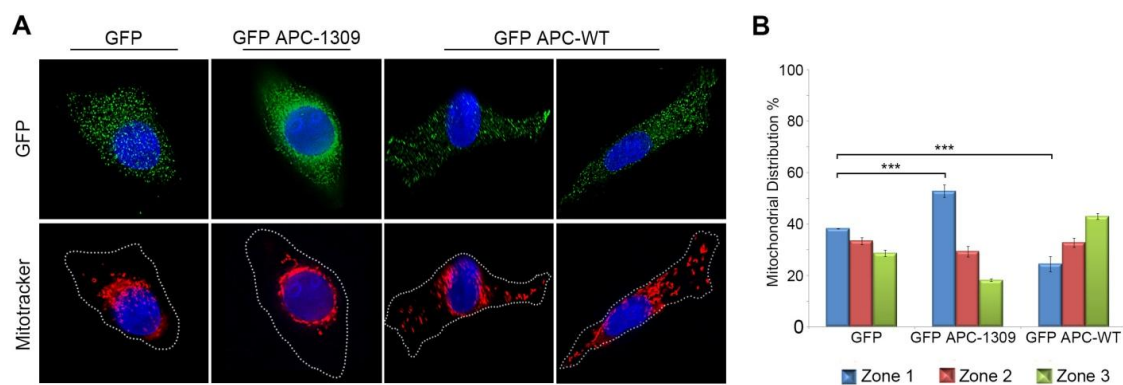


Figure 4.2: Reconstitution of GFP APC-WT expression in HT-29 cells restores mitochondrial distribution to the cell periphery.

(A) Sub-confluent HT-29 cells were transfected with plasmids expressing GFP, GFP APC-1309 or GFP APC-WT for 48 h, stained with CMX-Ros Mitotracker and counterstained with antibodies against GFP (mAb) and Hoechst (blue). Cells were analysed by immunofluorescence microscopy and moderately transfected cells were (B) scored for mitochondrial distribution as previously described. Significant differences relative to control, determined using an unpaired T-test, are indicated (***, $P<0.001$, % mean \pm S.D).

It is interesting to note that Miro, Milton and a number of other proteins involved in regulation of mitochondrial dynamics are readily detected by western blot analysis in SW480 and HT-29 cell lines (mutant APC) at comparable levels to that seen in U2OS, HDF1314 and HCT116 cell lines (wild-type APC) (Supplementary Figure S4.1A). This indicates that the altered steady-state distribution of mitochondria in cells with mutant APC is not caused by defects in expression of Miro/Milton. Furthermore, detection of Miro and Milton by immunofluorescence microscopy in SW480, HT-29 and HCT116 cell lines did not reveal any unusual staining patterns (Supplementary Figure S4.1B).

4.3.3 C-terminal truncating mutations disrupt APC binding to Miro/Milton

The above finding suggests that overexpression of wild-type APC could re-establish normal mitochondrial distribution, and most likely transport, in APC-mutant HT-29 cells. This led to the hypothesis that APC truncation may disrupt its interaction with the Miro/Milton mitochondrial transport complex. To test this, immunoprecipitation assays were performed using lysates from SW480 cells expressing GFP Miro-1 and GFP Milton-2 (Figure 4.3A). While APC antibodies could effectively capture mutant APC, in contrast to experiments in U2OS cells (Figure 3.7), neither GFP Miro-1 nor GFP Milton-2 could be captured. In addition, mutant APC could not be detected when a GFP antibody was used to pull down GFP Miro-1 or GFP Milton-2 (Figure 4.3A).

These results mirror those obtained in induced stable cell lines HEK293 (APC-WT) and HEK293 (APC-1309) transfected with pGFP Milton-2. Both wild-type and mutant APC were successfully pulled down by an APC antibody in these cell lines, however only ectopic full-length APC was able to pull down with GFP Milton-2 and endogenous Miro, despite the fact that HEK293 (APC-1309) cells still contain a baseline of endogenous wild-type APC (see Supplementary Figure S4.2). This result is most likely because the majority of APC pulled down is in the truncated form, therefore any GFP Milton-2 or Miro attached to the wild-type would be an extremely small percentage of the lysate, thus very hard to detect. GFP pull down experiments in both cell lines successfully captured GFP Milton-2, however neither mutant APC-1309 nor wild-type APC-WT could be detected (Supplementary Figure S4.2). This was expected in the case of APC-1309, however in the case of APC-WT, lack of detection may be due to reasons suggested previously in Section 3.3.7, as difficulty was also encountered detecting APC in GFP Milton-2 pull downs in U2OS cells. The capture of GFP Milton-2 from cell extracts also appeared to pull down a higher molecular weight form of endogenous Miro in both HEK293 (APC-1309) and (APC-WT) cell lines which will be discussed further in Chapter 7 (Section 7.1.1).

To confirm this result, Duolink PLA was used to assess interactions between APC and Miro or Milton in CRC cell lines that express mutant APC (SW480 and HT-29) and wild-type APC (LIM1215) (Figure 4.3B-C, expanded in Supplementary Figure S4.3). In

both SW480 and HT-29 cells, no PLA signals above background could be detected between mutant APC and Miro, or mutant APC and Milton. However, in LIM1215 cells which express wild-type APC, a positive PLA signal was observed for both APC/Miro and APC/Milton interactions, presenting on average ~14 and ~6 PLA signals/cell respectively.

In addition to the analysis of endogenous APC-Miro/Milton interactions, Duolink assays were also used to demonstrate that APC truncation reduced the binding of ectopic GFP-tagged APC to the mitochondrial transporters. GFP APC-WT was transiently expressed in SW480 cells, and the Duolink assay identified a positive PLA interaction between GFP-tagged full-length APC and Miro which was ~2.8 fold ($P < 0.001$) above GFP background (Figure 4.4; Supplementary Figure S4.4). In contrast no PLA signal above GFP background was observed in SW480 cells expressing GFP APC-1309 (Figure 4.4; Supplementary Figure S4.4). This result was also verified in U2OS cells where a positive PLA signal, ~1.8 fold above GFP baseline, was observed between GFP and Miro in cells transfected with GFP APC-WT, but not GFP APC-1309 (Supplementary Figure S4.5).

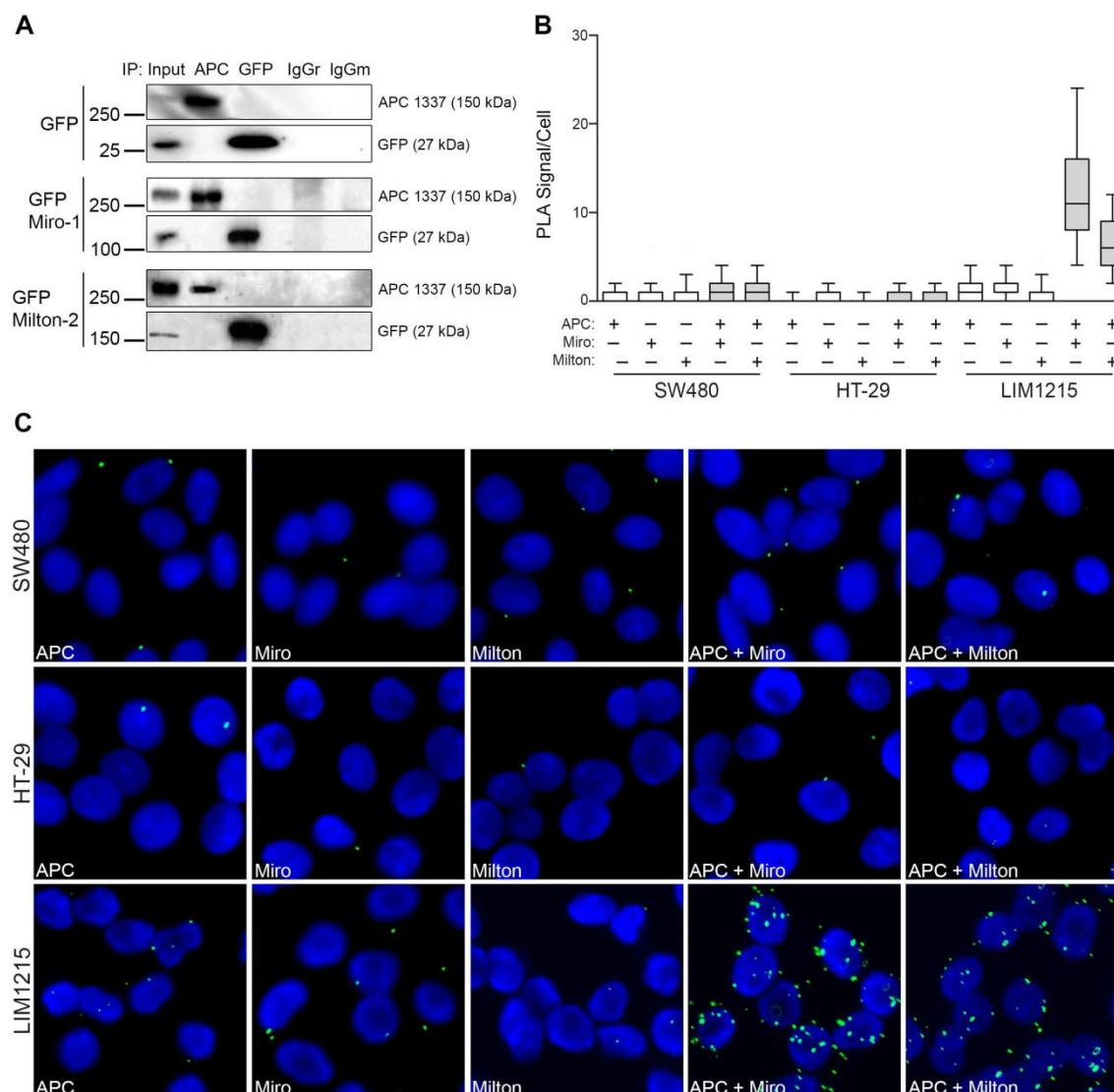


Figure 4.3: Truncated APC does not interact with the Miro/Milton complex in colon cancer cell lines

(A) SW480 (APC 1-1337) cells transfected with plasmids expressing GFP, GFP Miro-1 or GFP Milton-2 were immunoprecipitated by antibodies against GFP (pAb) and APC (Ab5) and analysed by western blot to detect GFP/GFP Miro-1/GFP Milton-2 (GFP, mAb) and APC (Ab1). The APC antibody did not pull down GFP, GFP Miro-1 or GFP Milton-2 and the GFP antibody was unable to pull down APC in any of the transfected samples. (B-C) Duolink PLA was utilised to confirm this result *in situ* in SW480, HT-29 (APC 1-853/1555) and LIM 1215 (APC-WT) cells with antibodies against APC, Miro and Milton. Scoring from analysis by immunofluorescence microscopy confirmed a negative interaction between truncated APC and Miro/Milton in SW480 and HT-29 cells, and a positive interaction between full length APC and Miro/Milton in LIM 1215 cells as observed in the (B) box-and-whisker plot and (C) representative images.

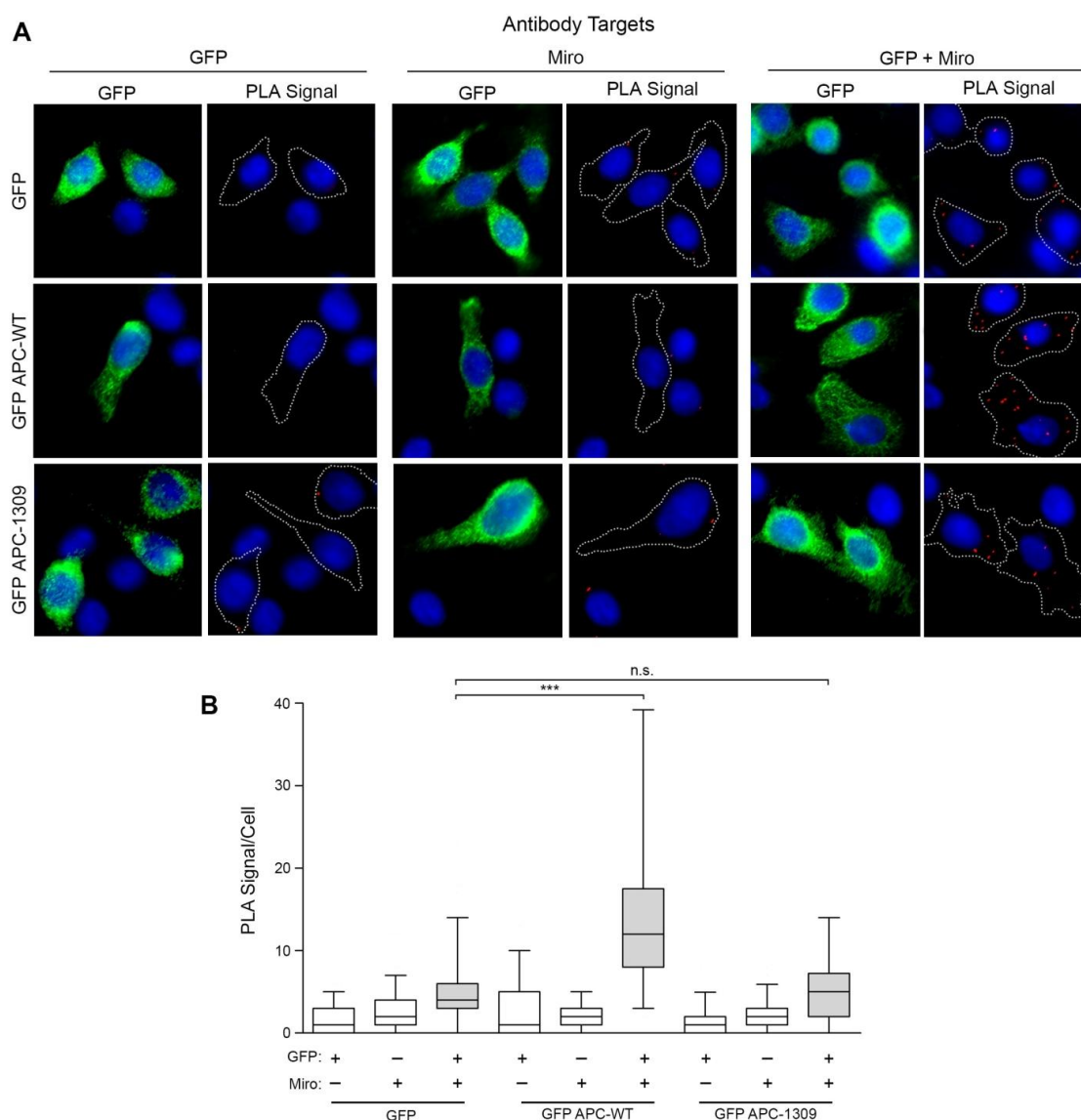


Figure 4.4: Overexpression of GFP APC-WT in SW480 cells restores the APC/Miro interaction as measured by Duolink.

(A-B) pGFP, pGFP APC-WT and pGFP APC-1309 were transfected into SW480 cells 48 h prior to fixation. Duolink PLA was performed using antibodies against GFP (mAb) and Miro. Slides were analysed by (A) immunofluorescence microscopy and modestly transfected cells scored for PLA signals as observed in the (B) box-and-whisker plot. Significant differences relative to GFP control, as determined using the Mann-Whitney U-test, are indicated (***, $P < 0.001$; n.s., not significant).

4.3.4 The Miro-binding region maps to the C-terminal amino acids (2650-2843) of APC

Given that C-terminal truncation of APC disrupted both APC/Miro and APC/Milton interactions, experiments were performed to determine if APC may associate with the complex through its C-terminal sequences. To identify the Miro-binding region of APC, a detailed mapping was performed by Duolink PLA in U2OS cells expressing a range of GFP-tagged APC fragments (1-302, 334-900, 1379-2080, 2226-2644, 2650-2843) as outlined in the schematic in Figure 4.5A and verified by western blot analysis (Figure 4.5B). Using antibodies against Miro and GFP, cells expressing low to moderate levels of each fragment were assessed for *in situ* binding with endogenous Miro (Figure 4.5C,D). Of the five sequences tested, only GFP APC(2650-2843) presented a PLA signal above GFP baseline, where the mean PLA signal/cell increased by ~3.4 fold ($P < 0.001$) compared to GFP alone. The PLA reaction performed on cells using only the individual anti-GFP or anti-Miro antibodies produced no signal. For more details see Supplementary Figure S4.6.

In line with findings above (Figure 4.3), the APC(2650-2843) sequence corresponds with the far C-terminal end of the APC protein, a section which is lost in the vast majority of truncating APC mutations. To confirm this interaction, U2OS cells expressing GFP APC(2650-2843) were immunoprecipitated with an antibody against GFP (Figure 4.6A). In addition to successfully capturing GFP APC(2650-2843), a higher molecular weight form of Miro was detected that was not observed under the same conditions when cells were transfected with pGFP, pGFP APC(1-302) or pGFP APC(1379-2080) (Figure 4.6A). The higher molecular weight form of Miro pulled down suggests that the APC(2650-2843) fragment may bind to a post-translationally modified form of Miro; this will be discussed further in Chapter 7 (Section 7.1.1). Unfortunately, evidence for an interaction was not achievable by reverse immunoprecipitation using the Miro antibody, possibly due to overlap between the antibody epitope and APC binding region. Colocalisation studies also indicate that GFP APC(2650-2843) localises to the mitochondria (Figure 4.6B), further supporting the notion that APC binds to the Miro/Milton complex via its C-terminal sequences, and the finding that truncation of APC disrupts mitochondrial transport.

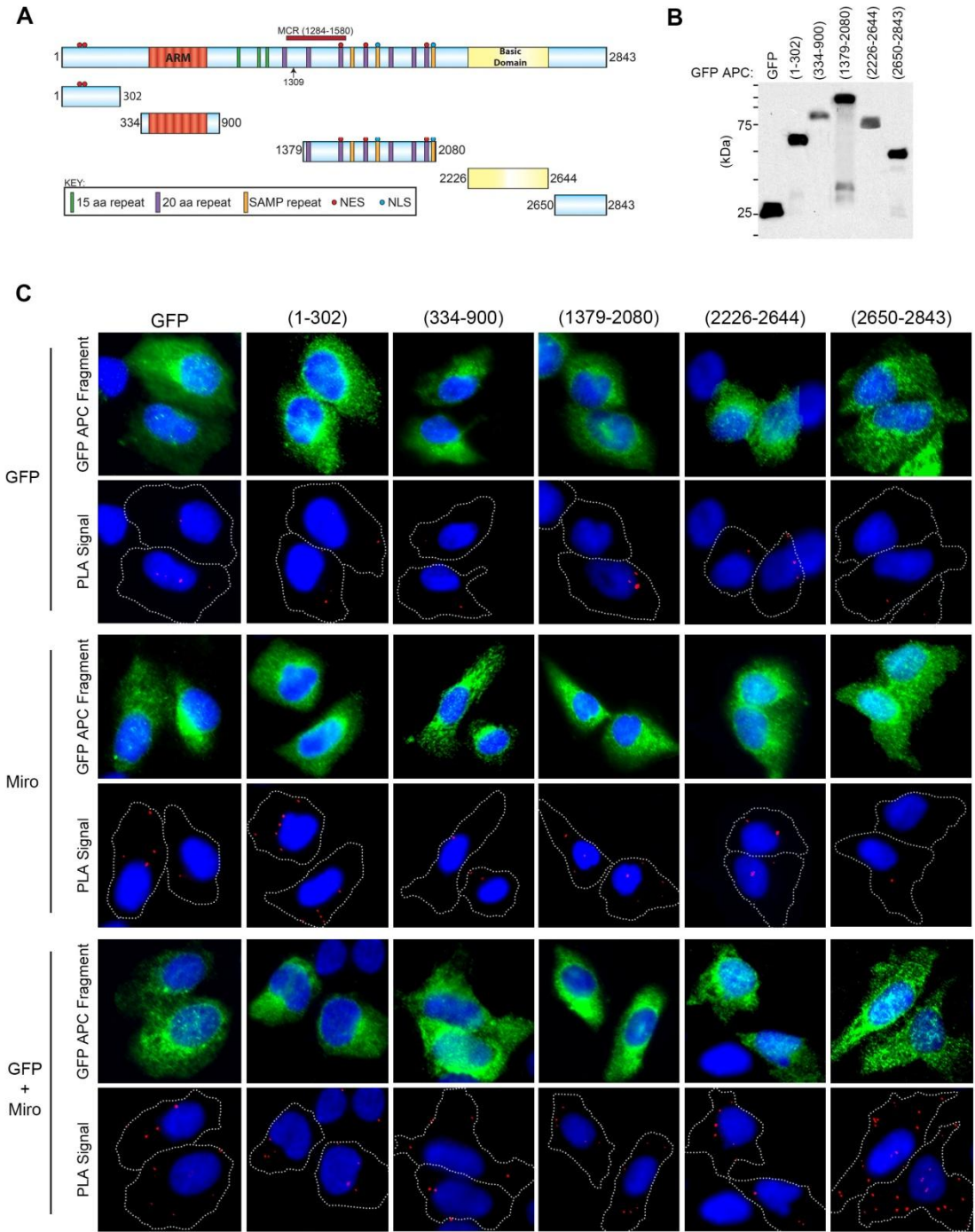


Figure continued over page.

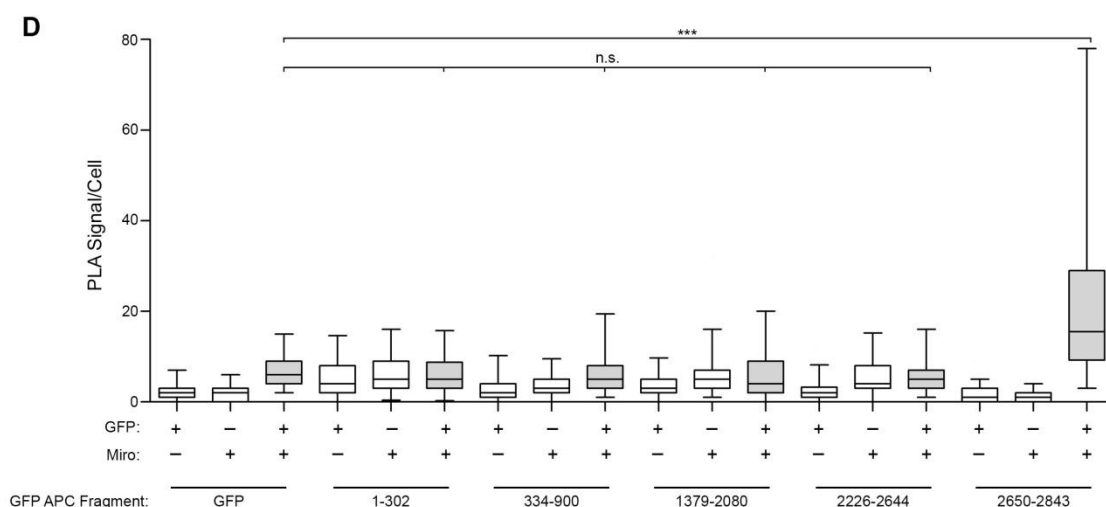


Figure 4.5: The Miro-binding domain of APC maps to the C-terminal sequences by Duolink.

U2OS cells were transfected with pGFP, or the pGFP tagged APC fragments (1-302), (334-900), (1379-2080), (2226-2644) or (2650-2843) described in the (A) schematic which were confirmed by (B) western blot analysis. Duolink PLA was then performed utilising antibodies against GFP (mAb) and Miro, and transfected cells expressing modest levels of GFP proteins were analysed by (C) immunofluorescence microscopy. PLA signals per cell were scored to reveal that only GFP APC(2650-2843) gave a positive interaction by Duolink when compared to the GFP background. This is indicated in the (D) box-and-whisker plot. Significant differences relative to GFP control, as determined using the Mann-Whitney U-test, are indicated (***, $P < 0.001$; n.s., not significant).

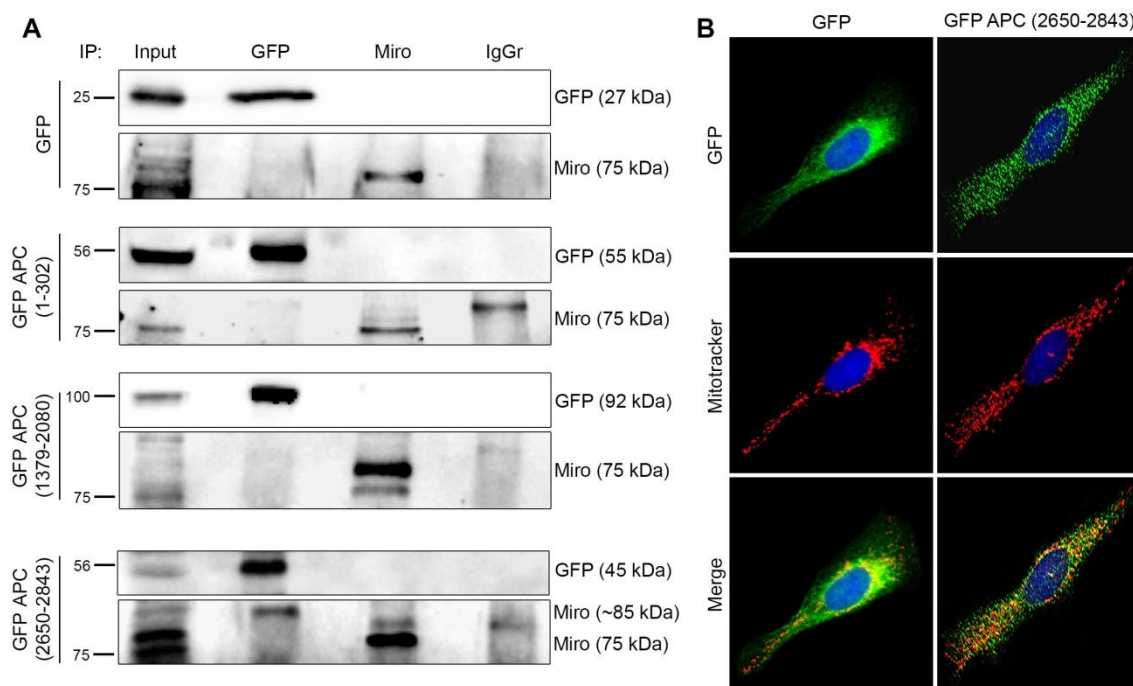


Figure 4.6: The C-terminal sequences of APC are confirmed to interact with Miro by immunoprecipitation and localise to the mitochondria.

(A) U2OS cells transfected with pGFP alone and pGFP-tagged APC fragments (1-302), (1379-2080) and (2650-2843) were immunoprecipitated by antibodies against GFP (pAb) and Miro prior to western blot analysis. Detection by GFP (mAb) revealed that the Miro antibody was unable to pull down any of the GFP-tagged APC fragments. Detection by Miro antibody however revealed that the GFP (pAb) antibody could successfully pull down GFP-APC(2650-2843) and a high molecular weight form of Miro-1 in transfected cell samples. (B) Plasmids encoding GFP and GFP APC(2650-2843) were transfected into U2OS cells for 48 h and stained with CMX-Ros to detect mitochondria prior to fixation. Cells were counterstained with a GFP antibody (mAb) and Hoechst (blue), then analysed for co-localisation by immunofluorescence microscopy.

4.3.5 The APC C-terminal sequence also binds to Milton.

Duolink PLA was used to confirm that GFP APC(2650-2843) also interacts with Milton (Figure 4.7). Scoring of PLA signals between GFP and Milton in U2OS cells transfected with pGFP APC(2650-2843), revealed a positive PLA signal 2.6-fold higher ($P > 0.001$) than those cells transfected with GFP alone (Figure 4.7; Supplementary Figure S4.7), indicating that the C-terminal region of APC does indeed associate with Milton.

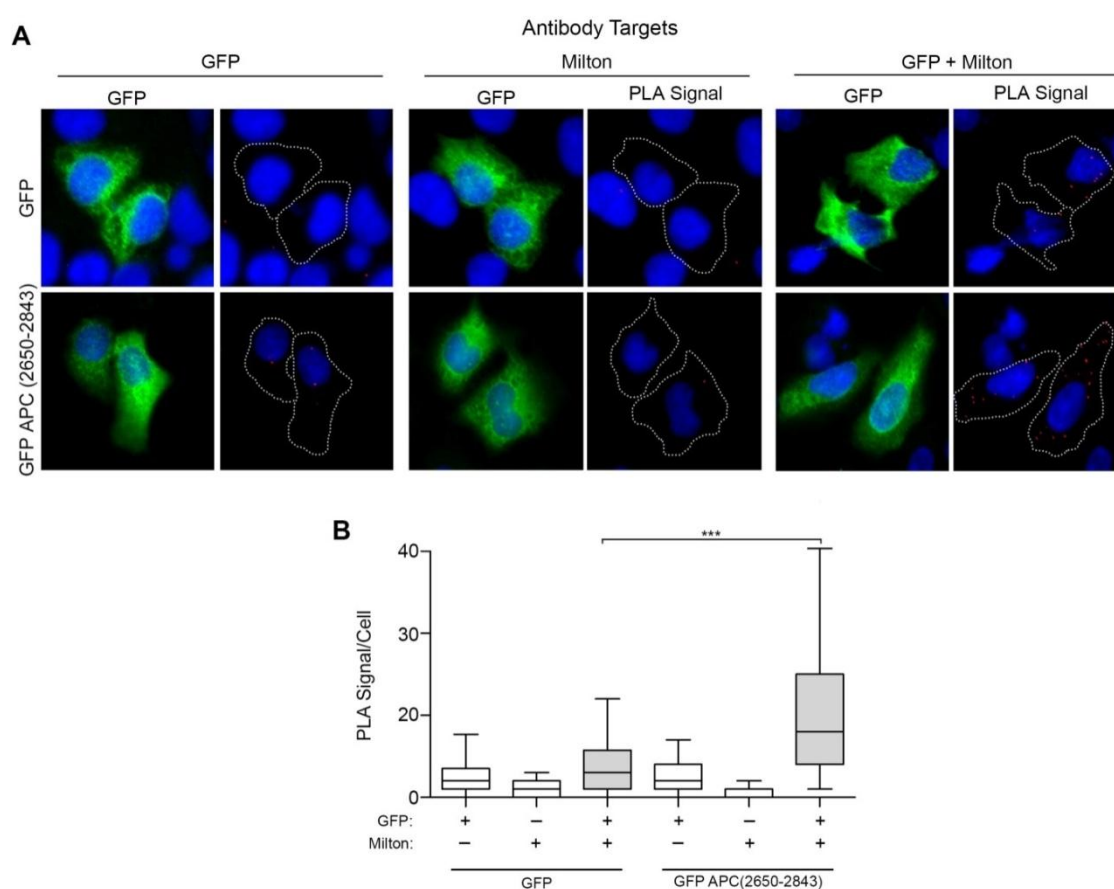


Figure 4.7: The C-terminal sequences of APC also interact with Milton by Duolink PLA.

(A-B) pGFP and pGFP-APC(2650-2843) plasmids were transfected into U2OS cells which were subjected to Duolink PLA using antibodies against GFP (mAb) and Milton. Slides were analysed by immunofluorescence microscopy and (A) representative cell images are shown. (B) Transfected cells were scored for PLA signals and the data quantified and compared here graphically by box-and-whisker plot. Significant differences relative to GFP control, determined using the Mann-Whitney U-test, are indicated (***, $P < 0.001$).

4.3.6 Overexpression of the C-terminal region of APC partially disrupts mitochondrial transport.

Since the C-terminal region of APC was found to interact with the Miro/Milton mitochondrial complex, investigation was undertaken to determine if overexpression of this APC fragment could disrupt mitochondrial transport. Therefore, U2OS cells were transfected with plasmids that expressed GFP or GFP-tagged APC fragments (1-1309), (334-900) and (2650-2843), counterstained with CMX-Ros to detect mitochondria, and scored for mitochondrial distribution by immunofluorescence microscopy. The overexpression of GFP APC(2650-2843) was found to stimulate a small, but significant, shift in mitochondrial distribution towards the perinuclear region when compared to GFP control cells, which was not observed in cells transiently expressing the common colorectal cancer truncation of APC(1-1309) or the Arm domain of APC (334-900) (zone 1 mitochondria: GFP=17%, GFP APC(2650-2843)=23%)($P < 0.05$) (Figure 4.8). This result indicates that the C-terminus has some functional contribution to the APC-dependent regulation of mitochondria.

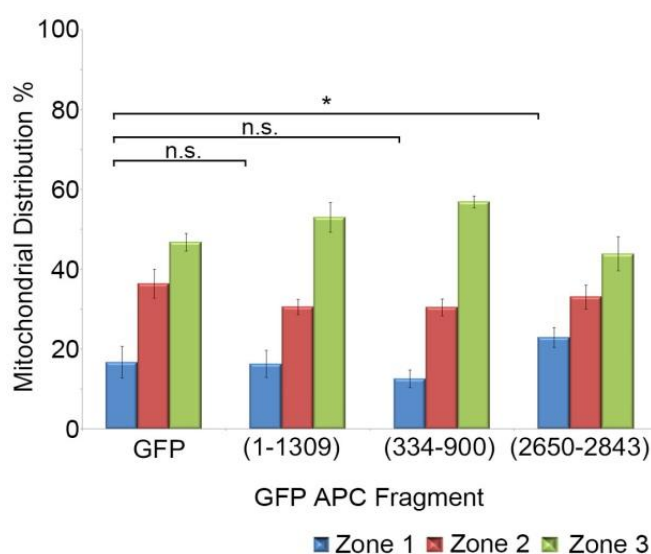


Figure 4.8: The overexpression of APC(2650-2843) partially disrupts mitochondrial distribution.

U2OS cells transfected with pGFP, or pGFP tagged APC fragments (1-1309), (334-900) or (2650-2843) were fixed and stained for mitochondria (CMX-Ros). Transfected cells were scored for mitochondrial distribution by immunofluorescence microscopy. Results are represented in the bar graph (% mean \pm S.D.) where significant differences for zone 1 distribution relative to the GFP control are indicated (*, $P < 0.05$, n.s., not significant). Significance determined using an unpaired T-test.

4.3.7 Overexpression of APC(2650-2843) does not disrupt the interaction between endogenous APC and Miro.

In the above section overexpression of the APC C-terminal region induced a modest perinuclear redistribution of mitochondria. One explanation for why the perinuclear shift was not more substantial could be that overexpression of the C-terminal fragment was not sufficient to completely disrupt the interaction between endogenous APC and Miro/Milton proteins. To test this, U2OS cells expressing GFP APC(2650-2843) were subjected to Duolink PLA using antibodies to detect endogenous APC (Ab7 – detects N-terminal epitope) and Miro. In line with the hypothesis, overexpression of GFP APC(2650-2843) did not significantly ($P > 0.05$) alter the binding of endogenous full-length APC to Miro relative to the GFP control (Figure 4.9; Supplementary Figure S4.8). This suggests that while APC(2650-2843) may contribute, either directly or indirectly, to the binding between the two proteins, it alone is perhaps not sufficient for binding and other APC regions or a particular protein folding may be required.

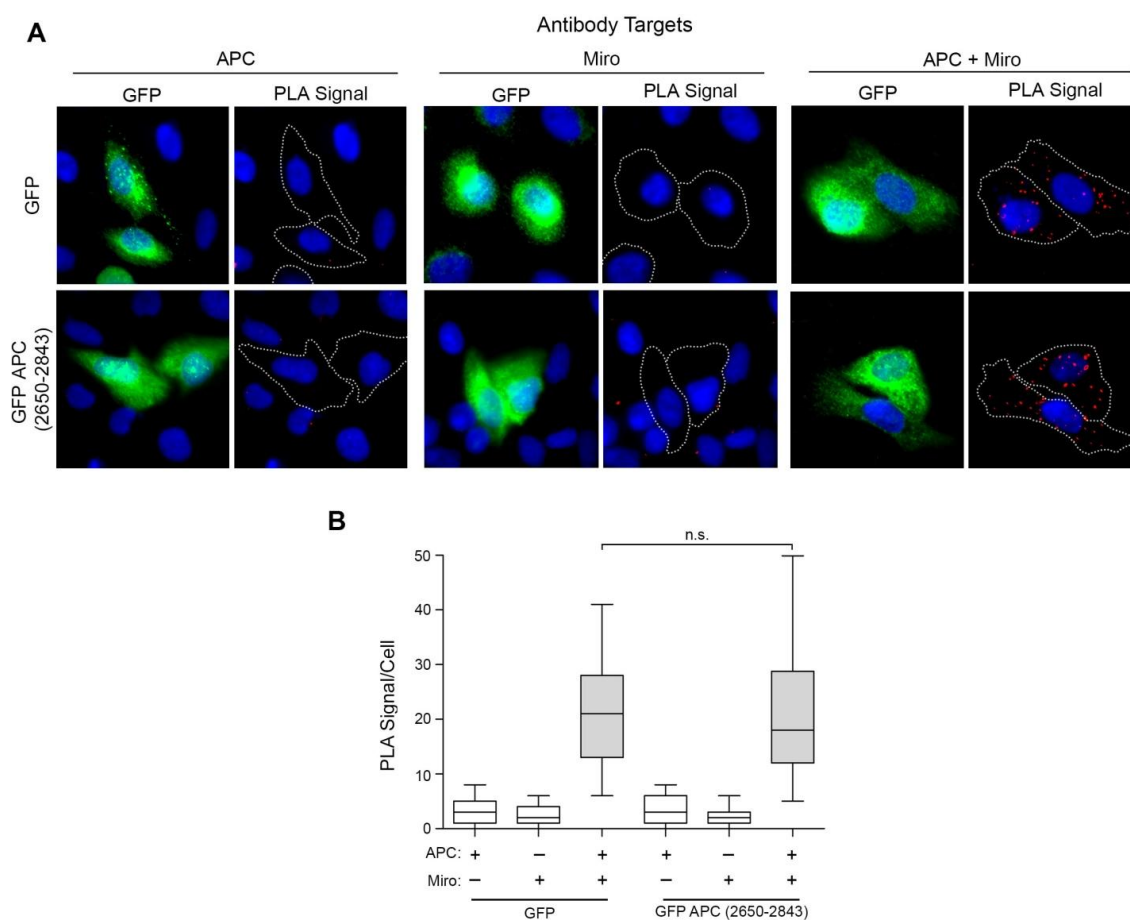


Figure 4.9: Overexpression of APC(2650-2843) does not interrupt the endogenous APC/Miro interaction.

(A-B) U2OS cells transfected with pGFP or pGFP APC(2650-2843) were subject to Duolink PLA using antibodies against APC and Miro. Transfected cells were analysed by (A) immunofluorescence microscopy and scored for PLA signals as observed in the (B) box-and-whisker plot. Significant differences relative to GFP control, determined using the Mann-Whitney U-test, are indicated (n.s., not significant).

4.4 Discussion

In this chapter, the impact of APC truncations on the ability of APC to bind the Miro/Milton transport complex and mediate mitochondrial distribution throughout the cell was assessed in different CRC cell lines. Cancer-associated truncations were found to disrupt APC binding to the Miro/Milton complex, which was mapped to the far C-terminal end (2650-2843) of APC (Figure 4.5, Figure 4.7). In addition, CRC cell lines expressing mutant APC displayed defective mitochondrial localisation patterns indicative of altered anterograde transport, identifying a new consequence of APC mutations. The implications of these observations for APC, mitochondria and cancer biology will be discussed.

4.4.1 Truncating APC mutations disrupt the interaction between APC and the Miro/Milton complex inhibiting mitochondrial transport

Given the disruptions observed in numerous APC functions following CRC-associated truncation of the protein, their effect on the ability of APC to regulate mitochondrial spread within a cell was addressed. This was first assessed for endogenous APC in CRC cell lines that express only truncated APC (SW480 and HT-29, Figure 4.1). In these cell lines, the proportion of cells displaying mitochondria that spread outward to the membrane periphery was much lower than that observed in CRC cell lines expressing wild-type APC (Figure 4.1). Thus, the expression of endogenous APC mutants correlated with disruption of mitochondrial distribution and transport. Colorectal cancers acquire a series of sequential gene mutations during the cell transformation process (3-5), hence in order to test specifically the role of APC gene mutations, ectopic forms of APC were expressed. These experiments revealed that in HT-29 cells the mild overexpression of wild-type APC, but not mutant APC-1309, rescued the defect in mitochondrial distribution (Figure 4.2). These results indicate that truncations in APC contribute to altered mitochondrial localisation, most likely through defects in transport.

Consistent with the inability of mutant APC to drive membrane-directed localisation of mitochondria, the endogenous mutant forms of APC did not associate with Miro or Milton in CRC cell lines (Figure 4.3). Even when overexpressed, the APC-1309 truncated form of APC failed to bind Miro in SW480 cells (Figure 4.4) and U2OS cells

(Supplementary Figure S4.5). In contrast, overexpressed GFP-tagged wild-type APC was found to bind to Miro in both SW480 and U2OS cells. These observations, together with the finding that in APC-mutant CRC cells the endogenous levels of Miro and Milton are not rate-limiting (Supplementary Figure S4.1), provide strong evidence that truncation of APC directly affects its ability to associate with the Miro/Milton complex. This altered association may cause perinuclear accumulation of mitochondria through impairment of the normal Miro/Milton-driven anterograde transport pathway, as proposed in Figure 4.10.

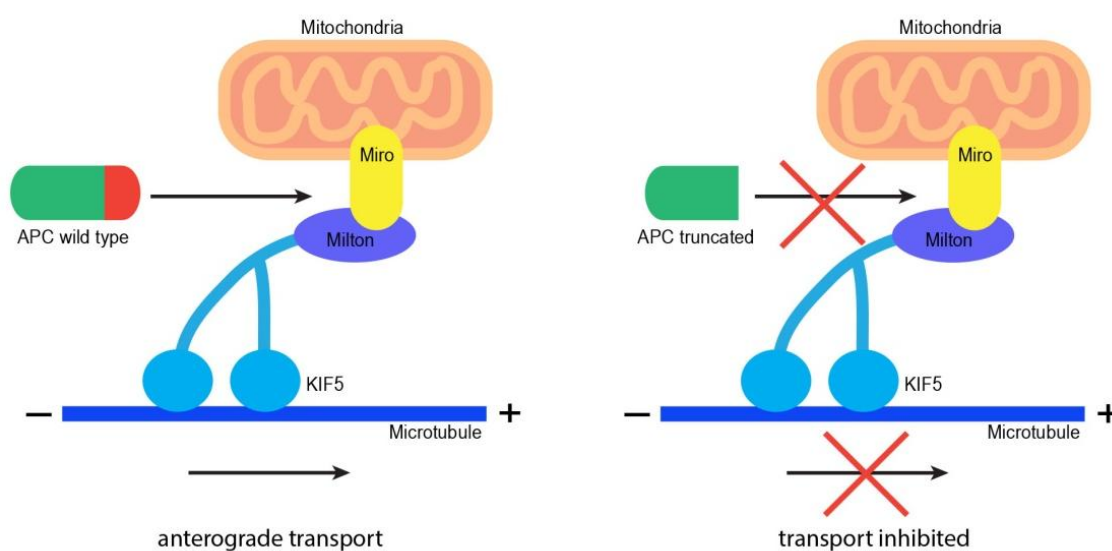


Figure 4.10: Model

Wild-type APC, but not truncated APC, stimulates anterograde transport of mitochondria through a C-terminal association with the Miro/Milton/KIF5 kinesin complex along microtubules.

The distribution of mitochondria is also disrupted by mutations in genes that encode other components of the transport complex. For example, the *Drosophila* homologs for Miro and Milton were originally identified through genetic screenings of *Drosophila* with retinal neurons devoid of axonal and terminal mitochondria (143, 144). Similar observations were also reported in mutant KIF5 *Drosophila* neurons (151). Due to the unique architecture of neuronal cells, disrupted long range transport along the axon have more severe consequences than in other cell types where distances travelled are not as vast. As a result, published studies in other cell types are limited. However, mutation of KIF5 in a murine primary culture from a visceral yolk sack was reported to display

substantial perinuclear clustering of mitochondria compared to control cultures (284), mirroring what was observed in APC mutant colon cancer cell lines in this study.

A sizeable population of SW480 and HT-29 cells still displayed mitochondria in vicinity of the plasma membrane (zone 3). It is possible that in these cells, Miro/Milton complexes remain transport-active even in the absence of bound APC. However, it is more likely that a subset of mitochondria find their way to the cell periphery through the action of alternate kinesin-based motor complexes that facilitate anterograde transport along microtubules such as the RanBP2/KIF5 and KBP/KIF1B α complexes (Section 1.3.2.2 and 176, 180), or potentially Myo10 motor complexes that transport mitochondria along actin filaments (188). For example, in HT-29 cells (APC 1-853/1555), RanBP2 is a potential alternative transporter, as it remains stable due to the reported silencing of the E3 ligase Parkin (which marks RanBP2 for degradation) in this cell system (290, 291). These alternate pathways could remain active or even up-regulated in the sustained absence of wild-type APC, and in turn, a less active Miro/Milton transport complex. The mechanism by which APC mutation disrupts functionality of the Miro/Milton complex is discussed further in Chapters 5 and 6, which look at the role APC plays in complex formation and regulation.

4.4.2 Identification of a C-terminal sequence that mediates binding of APC to Miro/Milton

Duolink PLA identified a Miro-binding site in the C-terminal sequence 2650-2843, located just after the “basic” domain (Figure 4.5). Miro-binding of the 2650-2843 sequence was verified by immunoprecipitation and found to be specific (Figure 4.6; see Section 7.1.1 for discussion about the altered higher molecular weight form of Miro that bound to APC). The identification of the 2650-2843 Miro-binding sequence, which also bound to Milton (Figure 4.7), provides a satisfactory explanation for why APC cancer truncations, almost all of which lose this sequence (4), are unable to bind Miro/Milton. Interestingly, the overexpression of GFP APC(2650-2843) was not sufficient to disrupt the interaction between endogenous APC and Miro (Figure 4.9), indicating that additional sites within APC may contribute to Miro binding. These might be contained in the regions 900-1379 or 2080-2226, for which GFP fragments were not available. It is also possible that optimal binding is context-dependent and interrupted by segregating

APC into fragments, or that overexpression of GFP APC(2650-2843) is insufficient to displace wild type APC. Consistent with the inability of the 2650-2843 fragment to disrupt binding of APC to Miro, only a minor effect on mitochondrial distribution was observed when this sequence was overexpressed (Figure 4.8). This is a stark comparison to the overexpression of a dominant negative form of Miro observed in the literature, where anterograde mitochondrial transport is completely disrupted (148). Overall, these observations suggest that the 2650-2843 sequence is a key binding site for Miro, but may not be the only binding site, and its location at the C-terminus implies that its loss through gene mutation is sufficient to disrupt APC binding to Miro/Milton complexes.

4.4.3 Disruption of mitochondrial transport by APC truncation may contribute to the CRC tumour cell phenotype

The general dysfunction of mitochondria has been widely reported to contribute to many facets of the carcinogenic process including altered energy metabolism, cell viability and replicative stress (14). Whilst the more specific impact of disrupting mitochondrial transport has been studied in other disease phenotypes (139, 256, 257), the impact to the carcinogenic process is only just coming to light. In particular, recent studies link mitochondrial distribution to key aspects of cell function disrupted in carcinogenesis including cell migration (18, 19), calcium signalling (15, 292), and gene transcription (265). Hence, a disturbance of mitochondrial transport could represent another way in which truncated APC exerts its carcinogenic effect on cells.

This study is not the first to link a Wnt target protein to the regulation of mitochondrial transport. The recently discovered protein Alex3 was found to stimulate mitochondrial aggregation and clustering, through an interaction with the Miro/Milton complex (163). Stimulation of the non-canonical Wnt signalling pathway was reported to attenuate the effects of Alex3, in a manner that could not be reproduced by the constitutive activation of β -catenin (161). Therefore it is unlikely that the Alex3 mitochondrial regulatory pathway is disrupted upon the aberrant β -catenin/canonical Wnt signalling observed following APC truncation. The relationship between APC, Alex3 and Wnt signalling in the context of mitochondrial transport is discussed in Chapter 7 (Section 7.2).

4.4.3.1 Mis-regulated ATP targeting by disruption of mitochondrial transport may contribute to CRC carcinogenesis

Aberrant cell migration is a hallmark of cancer (293), and truncation of APC contributes to altered migration through several different pathways including disrupted microtubule stabilisation, actin polymerisation and cell polarity (Section 1.2.3.2 and 52, 54). Recent reports have indicated that mitochondrial localisation at the cell periphery is crucial for supplying ATP reserves required for dynamic membrane movement, and that changes in this process can alter cell migration in several sub-types of cancer (18, 19). It is therefore possible that APC mutations also impact on cell migration indirectly through perturbation of mitochondrial transport (this is addressed in detail in Chapter 5).

ATP is the main energy source for many other cell processes for which the significance of mitochondrial localisation has not yet been described. These include cytoskeletal assembly and disassembly, signalling cascades, and DNA, RNA and protein synthesis. It is assumed that mitochondrial ATP plays a role in these processes under normal cellular conditions, as oxidative phosphorylation is the primary means of ATP synthesis in healthy cells. However, tumour cells, including CRC cells, display vastly increased rates of glycolysis, an alternate method for generating ATP, in the cytosol (the “Warburg effect”, reviewed in 262). Furthermore, pyruvate dehydrogenase kinase (PDK1), an enzyme that promotes aerobic glycolysis through inhibition of the pyruvate dehydrogenase (PDH) complex, and in turn oxidative phosphorylation, was recently identified as a Wnt target gene (294), indicating that truncation of APC may in fact stimulate the glycolytic pathway further through aberrant β -catenin Wnt signalling. Despite this, it is important for bioenergetic structures to achieve a high level of site-specific ATP synthesis through targeting of mitochondria. Unlike energy produced by glycolysis, which must be obtained from non-specific ATP diffusion through the cytoplasm, targeted mitochondria provide a means for consistent site-specific ATP output and fast ADP recycling. Furthermore, it is also metabolically ~18-fold more efficient to produce ATP by oxidative phosphorylation than by glycolysis (295).

The truncation of APC as observed in CRC cells could impact on membrane-directed localisation of mitochondria and ATP reserves, in addition to the supply of energy at other sites yet to be investigated. This is suggested not only by the range of intracellular

shuttling patterns of APC (11, 12) but also the recent finding that APC can bind different myosin motors (Lui and Henderson, unpublished) that may help traffic mitochondria along actin filaments, taking them to parts of the cell different to those targeted by microtubules (discussed further in Section 7.5.3).

4.4.3.2 Disruption of mitochondrial transport may contribute to aberrant calcium signalling in CRC carcinogenesis.

Mitochondria have an essential role in buffering calcium, a key regulator in many facets of cell function, though their ability to take up and release calcium in a site-specific manner (Section 1.3.1.2). Like other metabolites, calcium often accumulates in microdomains, sites within the cell cytoplasm with a localised high calcium ion concentration, usually formed in the vicinity of Ca^{2+} channels (for example at the plasma membrane, golgi and ER). Close proximity of mitochondria to these microdomains can facilitate the rapid uptake of calcium (reviewed in 15), however, the effects of mislocalised mitochondria on calcium buffering are poorly understood. One study does report that mitochondrial contact with the cell periphery is essential for extracellular calcium uptake (190). This is discussed further in the context of cell migration in Chapter 5 (Section 5.4.2).

Impaired calcium signalling is frequently observed in cancer cells where it affects cell migration and proliferation (reviewed in 292, 296). Furthermore, pro-proliferative pathways regulated by calcium signalling are particularly sensitive in colonocytes (297). It is possible that disrupted mitochondrial transport could inhibit effective calcium buffering, in turn contributing to the aberrant calcium signalling observed in cancer cells. The importance of effective mitochondrial transport and distribution in calcium buffering is highlighted by the regulatory EF-hand motifs present in Miro, which when bound to calcium, cause cessation of mitochondrial transport, presumably to facilitate site-specific calcium buffering (153, 158). Intriguingly, Togo and colleagues (298), report that APC attachment to microtubules is calcium regulated. With this in mind, further investigation into if, and how, calcium may regulate APC-dependent mitochondrial transport and what effect APC mutation may have on calcium signalling in carcinogenesis was investigated and will be discussed in Chapter 6.

4.4.3.3 Perinuclear clustering of mitochondria may contribute to aberrant gene transcription in CRC carcinogenesis.

Sustained perinuclear accumulation of mitochondria may also have adverse effects on the cell. Little is known about the physiological role of mitochondrial aggregation in this region, although hypoxia-induced perinuclear clustering of mitochondria in pulmonary artery endothelial cells was reported to create an oxidant rich nuclear domain due to the release of ROS from the mitochondria (265). This increased nuclear ROS can cause oxidative base modifications through a Hypoxia Induced Factor 1 α (HIF-1 α) dependent pathway to facilitate transcription of target genes, such as the growth signal vascular endothelial growth factor (VEGF).

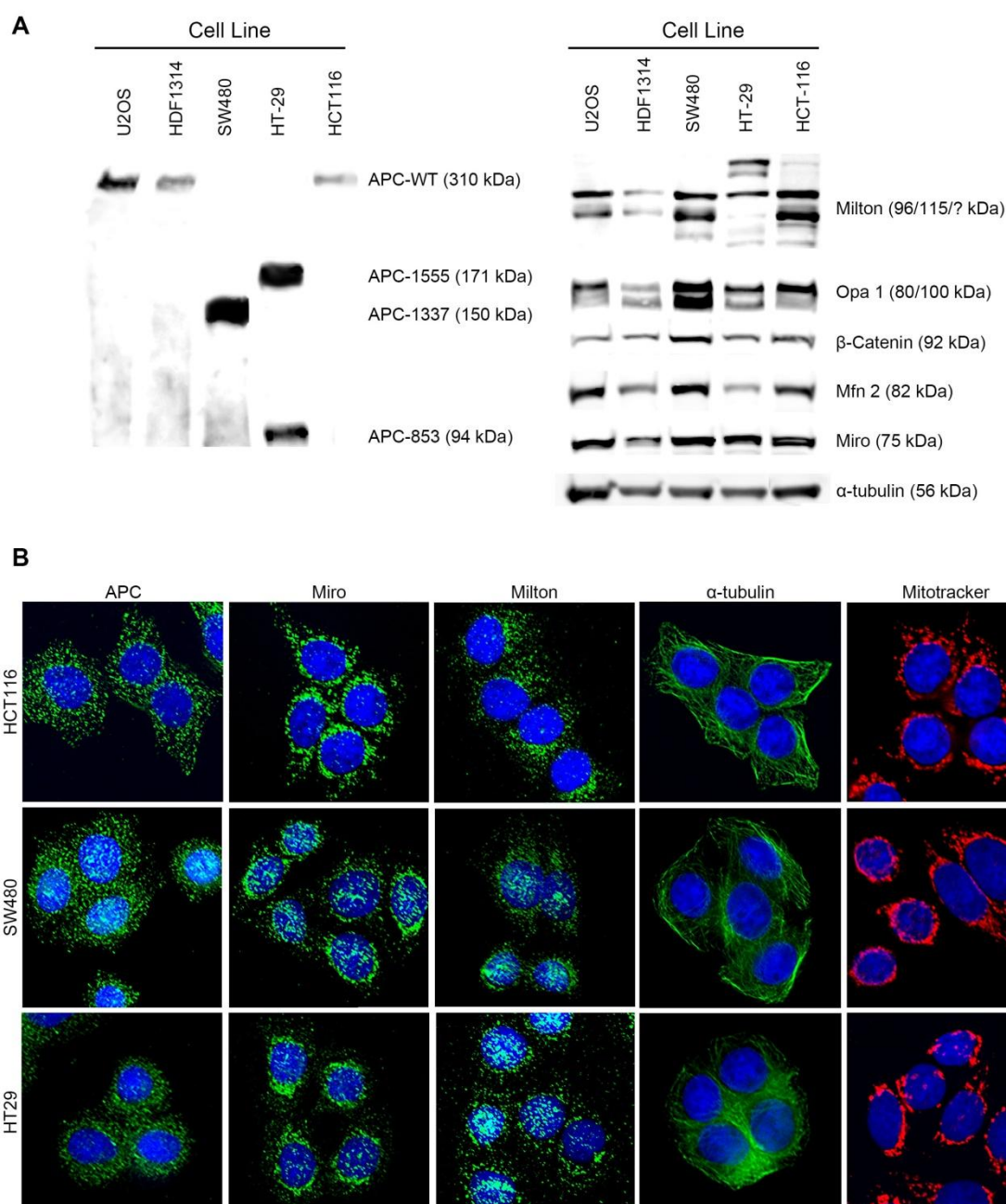
These findings are especially intriguing as high levels of HIF-1 α , the transcriptional master regulator of hypoxia (reviewed in 299), and VEGF have been observed in colon tumour tissues and several colon cancer cell lines (300). Furthermore, APC truncation in the intestinal epithelium was shown to cause an increase in ROS through both a Rac1-dependent pathway (301) and Wnt3a-stimulated mitochondrial biogenesis (302). It is possible that the perinuclear mitochondrial clustering, frequently observed in SW480 and HT-29 mutant APC cell lines (Figure 4.1), assists in formation of an oxidant rich microdomain around the nucleus, even in the absence of hypoxic signals due to the disruption of APC-dependent mitochondrial transport. This could contribute to aberrant transcription of hypoxia-induced genes such as VEGF, NF κ B and a variety of cellular adhesion molecules contributing to carcinogenesis (299). Increased ROS in close proximity to the nucleus could also expose the DNA to carcinogenic promoting mutations, whilst increased ATP from perinuclear mitochondria could provide the nucleus with the energy required for increased DNA transcription.

4.4.4 Summary

These findings indicate that C-terminal deletion of APC prevents its binding to the Miro/Milton complex, in turn disrupting mitochondrial transport in mutant APC CRC cells. Disrupted mitochondrial transport has been implicated in a number of pathways known to be altered in carcinogenesis including cell migration, calcium signalling and gene transcription. This points to a previously unreported mechanism through which

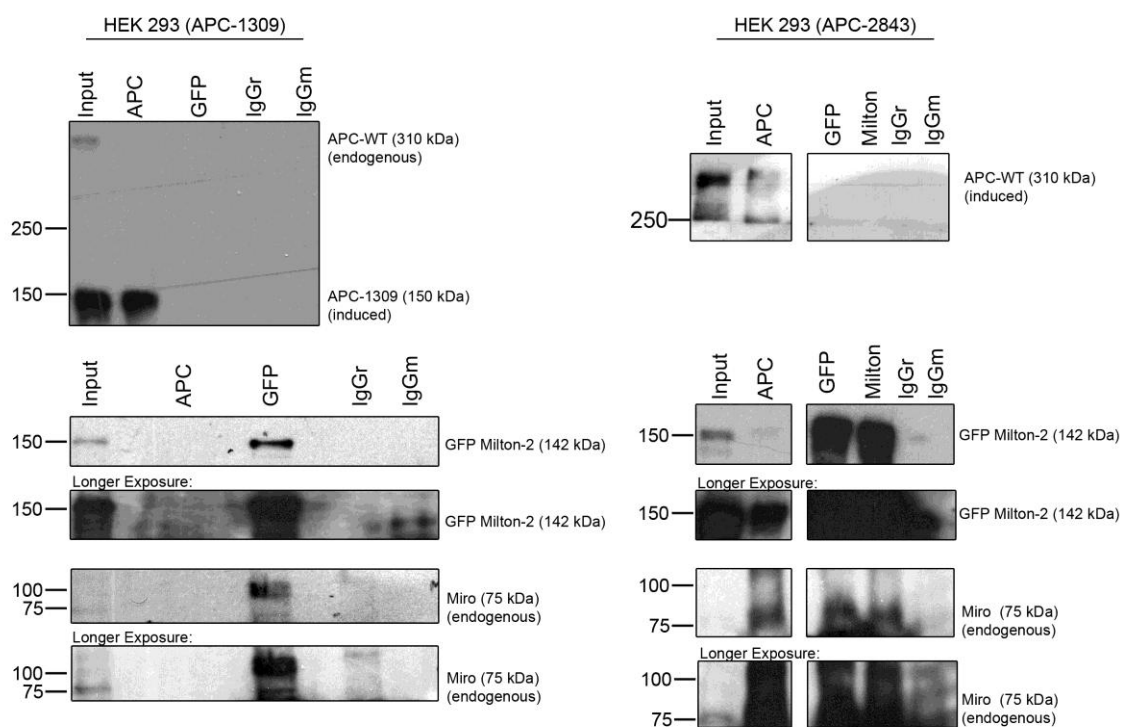
mutation of APC may contribute to tumourigenesis. APC mutation and mitochondrial localisation already have reported roles in cancer cell migration; therefore, potential links between these pathways will be investigated in the following chapters, along with the mechanism by which APC may interact with, and regulate Miro/Milton to drive mitochondrial transport.

4.5 Supplementary Figures



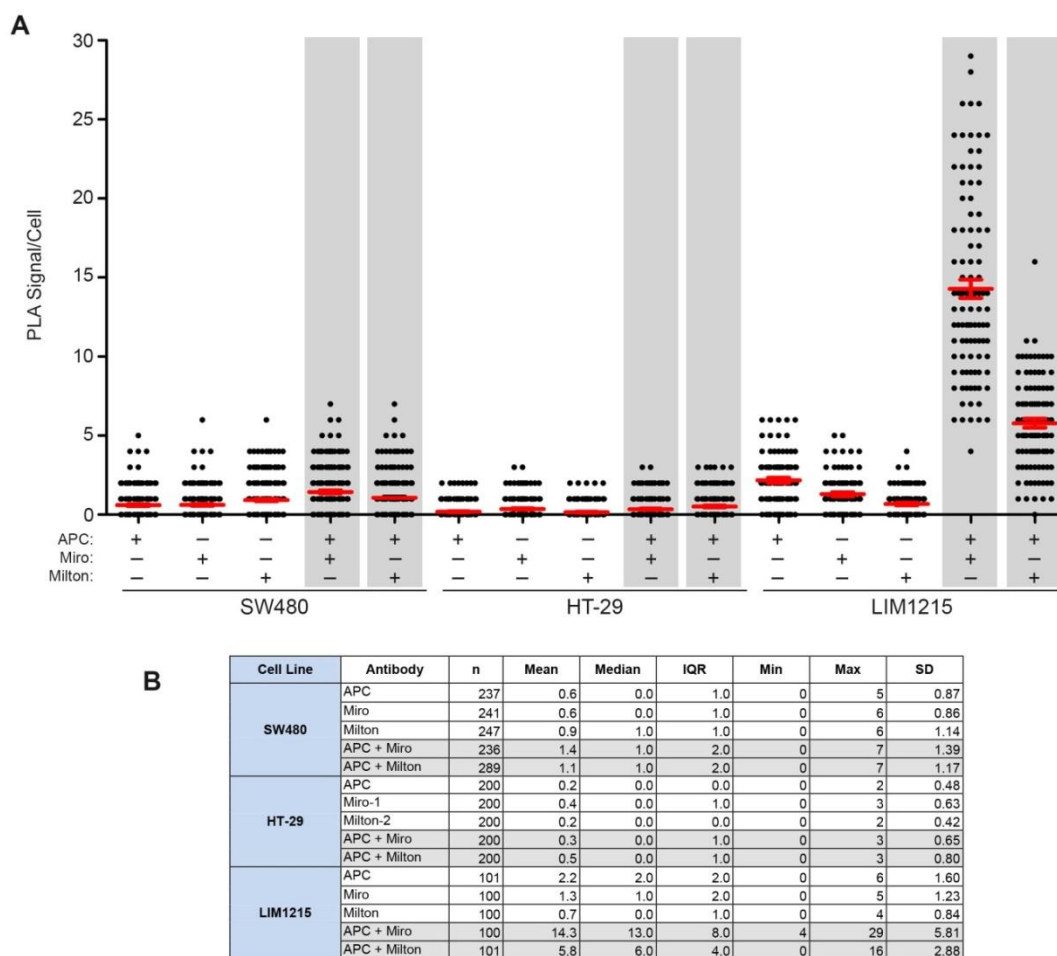
Supplementary Figure S4.1: APC and regulators of mitochondrial dynamics in colon cancer cell lines

(A) U2OS, HDF1314, SW480, HT-29 and HCT116 cells were analysed by western blot. Antibodies against APC (Ab1), Milton, OPA1, β -catenin (mAb), Mfn2, Miro and α -tubulin were used to detect endogenous levels of their respective protein in each of these cell lines. Protein molecular weights (kDa) are indicated in brackets. (B) Sub-confluent HCT116, SW480 and HT-29 cells were fixed and stained with either CMX-Ros Mitotracker (red) or antibodies against APC, Miro, Milton or α -tubulin (green), and analysed by immunofluorescence microscopy.



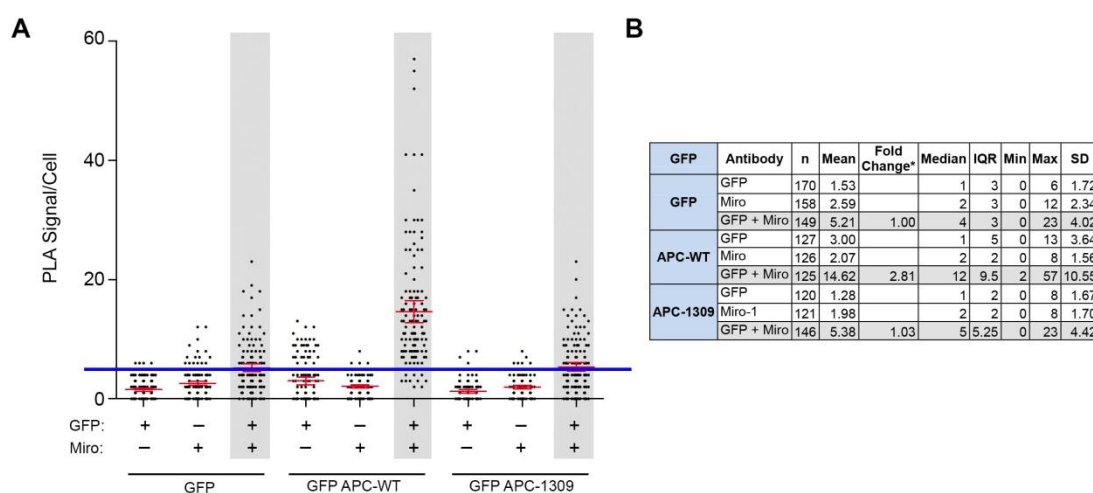
Supplementary Figure S4.2: APC antibodies can immunoprecipitate Miro and Milton in wild-type inducible HEK293 cells, but not mutant inducible HEK293 cells

Inducible HEK293 cell lines transfected with pGFP Milton-2 were treated with tetracycline 16 h prior to immunoprecipitation to induce expression of (APC-1309) or (APC-WT). Cells immunoprecipitated by antibodies against APC (Ab5), GFP (pAb), Milton, IgGr and IgGm, were then analysed by western blot to detect APC (Ab1), GFP Milton-2 (GFP, mAb) and Miro, respectively. The APC antibody was able to pull down endogenous and/or induced APC in both cell lines. Only in cells induced for (APC-WT) could the APC antibody pull down GFP Milton-2 and Miro. The GFP antibody was able to pull down GFP Milton-2 and Miro in both cell lines, but was unable to pull down APC. Protein molecular weights (kDa) are indicated.



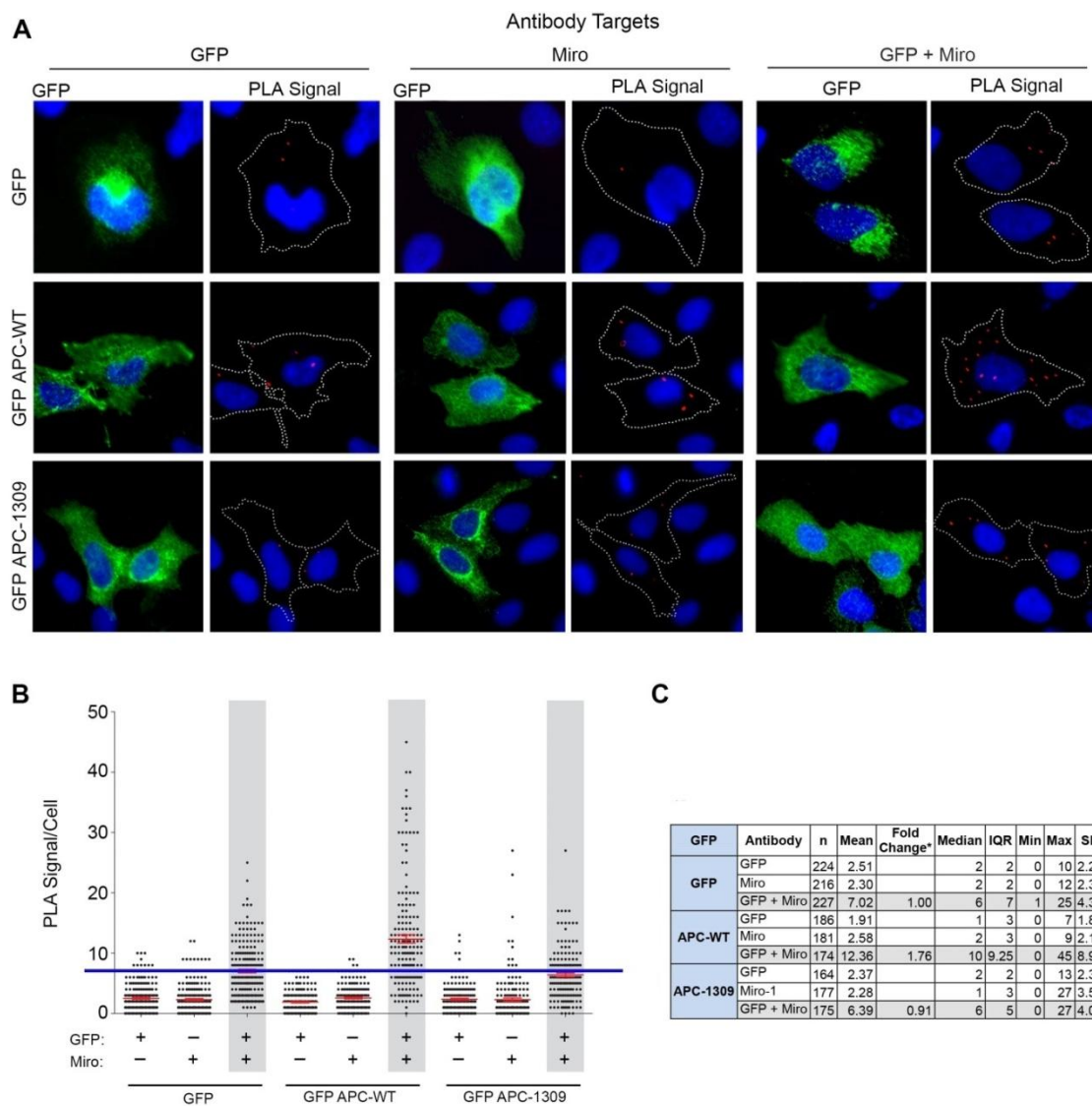
Supplementary Figure S4.3: Truncated APC does not interact with the Miro/Milton complex - Expanded Duolink PLA data

(A-B) Interactions between APC and Miro/Milton were visualised *in situ* by Duolink PLA in SW480, HT-29 and LIM1215 cells as described in Figure 4.3. The PLA signals for APC/Miro and APC/Milton are not above background in SW480 and HT-29 cells, indicating no interaction is present, whilst the PLA signals for APC/Miro and APC/Milton are above background in LIM1215 cells indicating a positive interaction as shown in the (A) dot-plot (mean \pm S.D, shading indicates interactions tested) and (B) table (n, number in sample; IQR, inter-quartile range; SD, standard deviation).



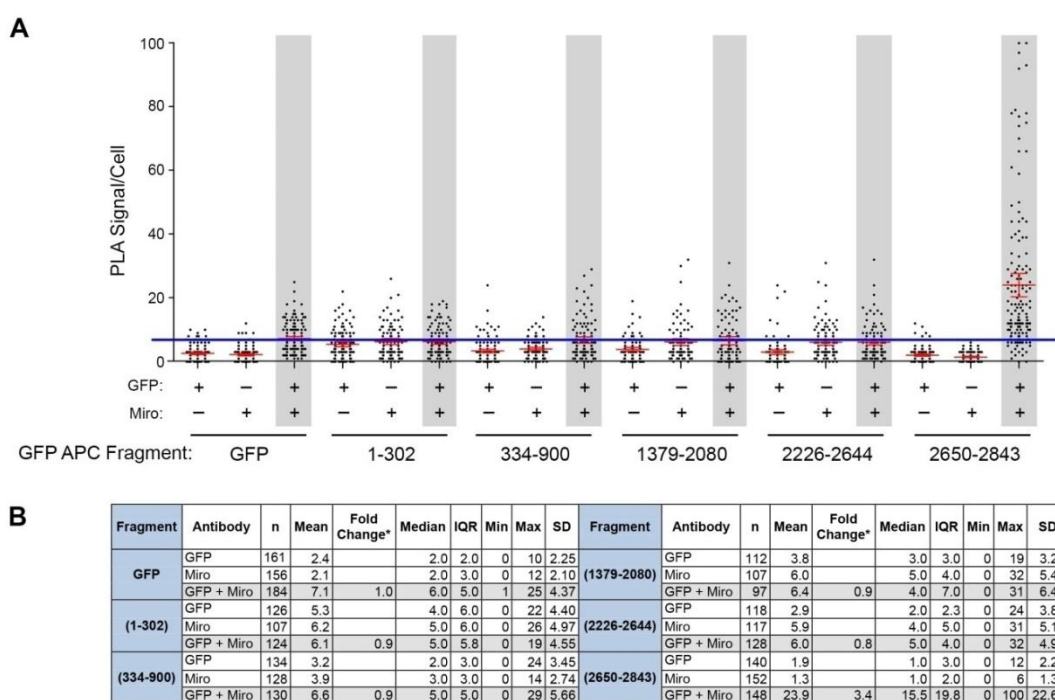
Supplementary Figure S4.4: Reconstitution of GFP APC-WT into SW480 cells restores the APC/Miro interaction by Duolink - Expanded Duolink PLA Data

(A-B) Interactions between GFP and Miro were visualised *in situ* using Duolink PLA in cells transfected with pGFP, pGFP APC-WT and pGFP APC-1309, as described in Figure 4.4. Scoring indicates a positive signal between GFP and Miro in cells transfected with pGFP APC-WT, but not pGFP APC-1309, relative to pGFP control as shown in the (A) dot-plot (mean \pm S.D, shading indicates interactions tested) and (B) table (n, number in sample; * fold change relative to GFP control; IQR, inter-quartile range; SD, standard deviation).



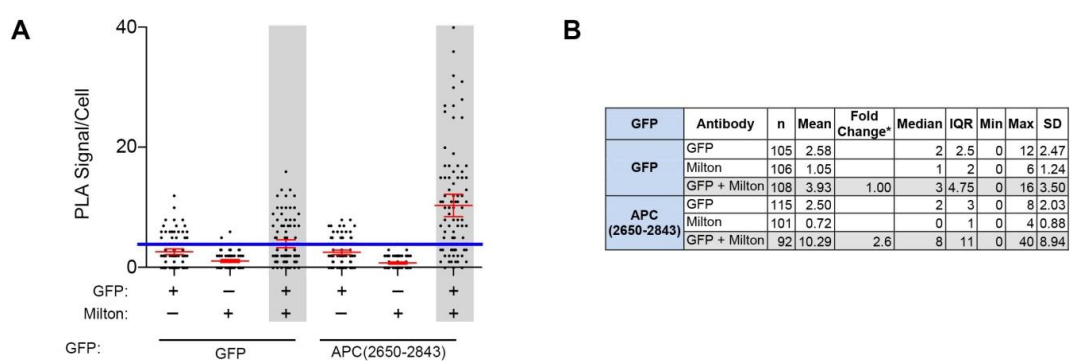
Supplementary Figure S4.5: GFP APC-WT but not GFP APC-1309 interacts with Miro in U2OS cells by Duolink PLA

(A-C) Cells expressing GFP, GFP APC-WT and GFP APC-1309 were subject to Duolink PLA using antibodies against GFP (mAb) and Miro. Scoring analysis by (A) immunofluorescence microscopy indicates a positive signal, above GFP background between GFP APC-WT/Miro but not GFP APC-1309/Miro as indicated by the (B) dot-plot (mean \pm S.D, shading indicates interactions tested) and (C) table (n, number in sample; * fold change relative to GFP control; IQR, inter-quartile range; SD, standard deviation).



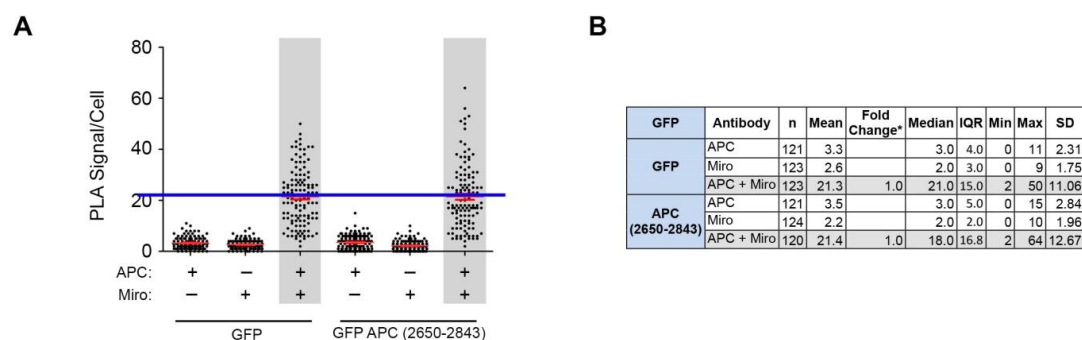
Supplementary Figure S4.6: The C-terminal sequences of APC interact with Miro – Expanded Duolink PLA Data

(A-B) U2OS cells were transfected with pGFP and pGFP-tagged APC fragments (1-302), (334-900), (1379-2080), (2226-2644) and (2650-2843). Duolink PLA was performed using antibodies against GFP (mAb) and Miro as described in Figure 4.5. Scoring of PLA signals indicates that GFP APC(2650-2843) was the only GFP APC fragment to show a positive PLA signal above GFP background as indicated by the (A) dot-plot (mean \pm S.D, shading indicates interactions tested) and (B) table (n, number in sample; * fold change relative to GFP control; IQR, inter-quartile range; SD, standard deviation).



Supplementary Figure S4.7: The C-terminal sequences of APC interact with Milton – Expanded Duolink PLA Data

(A-B) U2OS cells expressing GFP or GFP APC(2650-2843) were subject to Duolink PLA as per Figure 4.7, using antibodies against GFP (mAb) and Milton. Scoring indicates that GFP APC(2650-2843)/Milton shows a positive PLA signal above GFP background as indicated by the (A) dot-plot (mean \pm S.D, shading indicates interactions tested) and (B) table (n, number in sample; * fold change relative to GFP control; IQR, inter-quartile range; SD, standard deviation).



Supplementary Figure S4.8: Overexpression of APC C-terminal sequences does not interrupt the endogenous APC/Miro interaction – Expanded Duolink PLA Data

(A-B) U2OS cells were transfected with pGFP or pGFP APC (2650-2843) and Duolink PLA performed using antibodies against APC and Miro as described in Figure 4.9. Scoring indicates that GFP APC (2650-2843) did not alter the endogenous APC/Miro interaction as shown in the (A) dot-plot (mean \pm S.D, shading indicates interactions tested) and (B) table (n, number in sample; * fold change relative to GFP control; IQR, inter-quartile range; SD, standard deviation).



CHAPTER 5

**APC stimulates the
initiation of mitochondrial
transport to the cell
periphery**



The active transport of mitochondria throughout the cell is integral to its role in a range of key cellular processes, in particular at the cell periphery where accumulation of mitochondria provides ATP for cell migration and modulation of calcium flux. Positioning of mitochondria at the cell membrane requires effective anterograde transport along microtubules, primarily mediated through the Miro/Milton/KIF5 complex. Chapters 3 and 4 established APC as a novel component of this complex, which when silenced or truncated by CRC-associated mutations disrupted mitochondrial transport to the cell membrane. This chapter examines the functional role of APC in regulating mitochondria dynamics in live cells. Wound healing experiments in confluent NIH 3T3 revealed strong colocalisation of APC with mitochondria at cell membrane protrusions associated with active migration. To better understand how loss of APC affects mitochondrial transport, live cell imaging was employed to track real time movement of GFP-labelled mitochondria in NIH 3T3 cells. The most striking observation was that in comparison to control cells, loss of APC significantly reduced mitochondrial motility, specifically by affecting the initiation of anterograde transport. In line with these results, a decrease in the frequency of distinct mitochondrial movements and a decrease in the average mitochondrial displacement and distance travelled were also observed. However, once mitochondrial transport commenced, no alteration in the velocity of transport was recorded between control and APC siRNA treated cells. These results indicate a specific role for APC in stimulating initiation of anterograde mitochondrial transport to the cell periphery, disruption of which may contribute to mislocalisation of ATP and the aberrant cell processes (such as migration) observed in CRC carcinogenesis.

5.1 Introduction

The highly motile nature of mitochondria is essential for supplying targeted energy in the form of ATP to bioenergetically demanding areas of the cell and for optimal regulation of calcium buffering. Mitochondrial transport has traditionally been studied in neurons due to their unique cell architecture which requires long distance transport through the axon from the cell body towards the synaptic terminal (137, 138). Disruptions in this process, which prevent trafficking of mitochondria along the axon, deprives the synaptic terminal of the ATP required for effective synaptic firing, and in turn contributes to a number of neurological conditions (reviewed in 139, 140, 257). More recently, mitochondrial transport has been studied in other cell types including epithelial and lymphocytic cells (18, 19, 142). These studies shed new light on the importance of effective mitochondrial targeting, in particular for cell migration.

At the leading edge of the cell in particular, extensive cytoskeletal remodelling is required for dynamic membrane deformation and the formation of membrane structures, such as actin-dependent lamellipodia or membrane ruffles for cell movement, and microtubule-dependent protrusions for cell polarisation (directionality of movement). Cytoskeletal remodelling requires polymerisation of actin and tubulin monomers into extensive F-actin and microtubule networks, which is an extremely bioenergetically demanding process. Moreover, transportation of membrane-associated proteins and other factors required for cell migration often occurs by kinesin and myosin motors along these cytoskeletal tracks and requires high levels of energy consumption (reviewed in 64). In this context, highly specific positioning of mitochondria at the leading edge has been shown to be essential for providing the ATP required to meet the energy demands to maintain cell migration (18, 19).

APC targeting to the cell periphery is also essential for coordinating persistent and directed cell migration through a multifaceted role in regulating the actin and microtubule networks (see Section 1.2.1.3 and reviews 52, 54). In particular, APC binds to and stabilises the plus-end tips of microtubules by association with EB1, contributing to the maintenance of cell polarity (67, 70). APC also contributes to regulation of the actin network by stimulating actin polymerisation directly and through modulation of substrates such as the GTP exchange factor ASEF and IQGAP1 (57, 58, 72). The

majority of these interactions are mediated through the C-terminal “basic” domain of APC, and as such are lost in truncating mutations in CRC.

Silencing of APC, like blocking the localisation of mitochondria to the cell periphery, has been reported to slow cell migration (65). Results from previous chapters indicate that APC regulates localisation of mitochondria to the cell periphery of sub-confluent cells through the Miro/Milton mitochondrial transport complex. The primary aim of this chapter was to experimentally confirm, for the first time, that APC drives the movement of mitochondria to the outer cell membrane. Here it is shown that APC contributes to the initiation of mitochondrial transport in the anterograde direction, towards the leading edge of actively migrating cells, opening up a new pathway through which APC controls cell migration. It is suggested that APC-dependent mitochondrial localisation at the cell periphery acts synergistically with APC’s cytoskeletal regulatory functions to stimulate cell migration, a process that may be disrupted in CRC carcinogenesis, as reflected by the aberrant migration of colonic epithelial cells in mouse colon crypts (66, 99).

5.2 Methods

5.2.1 Cell culture

NIH 3T3 and HDF1314 fibroblast cells were cultured in DMEM under standard conditions as outlined in Section 2.2.3. For all fixed cell wound healing experiments, cells were seeded on glass cover slips in 6 well trays coated with poly-L-lysine and grown to 100% confluence. For live cell experiments, cells were seeded in 2-well chamber slides coated with poly-L-lysine and grown to 70-80% confluence for sub-confluent experiments and 100% confluence for wound healing experiments. Cells to be subjected to western blotting were seeded in 25 cm² flasks for siRNA knockdown experiments. For more details see Section 2.2.3.1.

Under standard conditions used though out the majority of this thesis, plasmids are transfected for transient expression at ~70% confluence. However, due to pre-treatments and toxicity issues faced in live cell imaging experiments, cells had to be transfected with pGFP2-Mito at ~90% confluence. Following optimisation (Section 5.3.3.2, Table 5.2) using several transfection reagents as described in Section 2.2.3.4, the K2 transfection system was selected. Use of mouse APC siRNAs for gene silencing is also described in Section 2.2.3.4.

5.2.2 Wound Healing

Confluent cells were wounded with a 0.8 mm (PrecisionGlide, BD) needle and washed twice with PBS prior to the addition of new DMEM. Subsequent fixation/immunostaining or live cell imaging was performed 5 h after wounding.

5.2.3 Cell fixation and staining for immunofluorescence microscopy

Cells were seeded for at least 24 h, fixed with methanol-acetone, probed with relevant antibodies and mounted for immunofluorescence microscopy as outlined in Section 2.2.4. Addition of CMX-Ros, where required, for detection of mitochondria occurred prior to fixation. Concentrations and further specifications for antibodies and dyes used in this chapter are outlined in Table 2.2, Table 2.3 and Table 2.4.

5.2.4 Fixed cell immunofluorescence cell image acquisition and processing

Slides were analysed using the Olympus IX71 DeltaVision Core deconvolution microscope equipped with a CoolSNAP HQ² camera for general image capture. Images collected were further resolved using SoftWorx deconvolution software. In wound healing experiments detecting mitochondrial localisation at protrusions (Figure 5.4), 200 cells were scored over 2 independent experiments. Localisation was considered positive if mitochondria reached at least 75% of the protrusion length.

5.2.5 Live cell imaging acquisition and analysis

Live cell imaging was performed using the Olympus IX71 DeltaVision system (above) for image capture at 40x. Whilst imaging, NIH 3T3 cells grown in 2-well chamber slides (Nunc) were maintained at 37°C and 5% CO₂. The following describes optimised conditions for each protocol (for optimisation process see Section 5.3.4). In sub-confluent experiments, cells expressing GFP2-Mito were imaged every 5 s for 5 min. For wound healing experiments (Section 5.2.2), cells transfected with control or mAPC-red siRNA, expressing GFP2-Mito were imaged every 7 s for 5 min. Three z-stack images were acquired in FITC and DIC channels for each time point.

The MTrackJ ImageJ plug-in (303) was used to manually track randomly selected mitochondria in cells at protrusions and the leading edge (Figure M5.1). All mitochondria were tracked in one z-plane, for a minimum of 2 min, and where appropriate, subsequent calculations were normalized to 1 min. Tracking was terminated if mitochondria underwent fission or fusion, or shifted significantly out of focus. The raw data readout assigned co-ordinates for each time-point a single mitochondrion was tracked. This was processed using Microsoft Excel to calculate displacement for each time point, and in turn velocity and other calculations observed in Figure M5.1 and Table 5.3 and Table 5.4. Mitochondria were deemed to be motile if displacement between two consecutive time-points was $>0.1 \mu\text{m/s}$. Anterograde, retrograde and oscillatory transport was assigned to motile mitochondria according to the changes in mitochondrial displacement from the nucleus (ΔDFN) between the first

and final tracking points (Δ DFN $+2.5 \mu\text{m}$ = anterograde, $-2.5 \mu\text{m}$ = retrograde, $-2.5 \mu\text{m}$ - $+2.5 \mu\text{m}$ = oscillating).

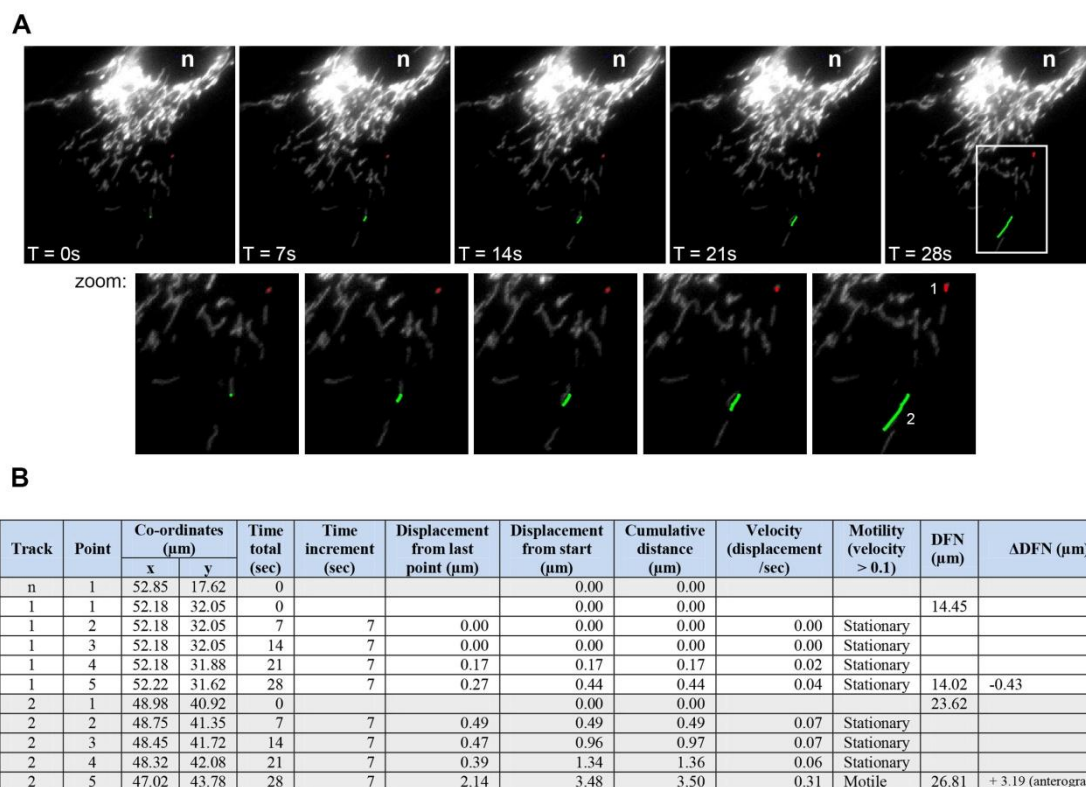


Figure M5.1: Tracking mitochondria using MTrackJ

(A) The nucleus (n) and randomly selected mitochondria were manually tracked in ImageJ using the MTrackJ plug-in. (B) Raw data in the form of (x,y) point co-ordinates from MTrackJ were used to calculate different parameters of mitochondrial movement for each time point in Microsoft Excel (DFN, displacement from nucleus).

Measurements for mitochondria in sub-confluent cells were obtained over two independent experiments (n cells: 10, n mitochondria: 73), whilst measurements for mitochondria in wound healing assays were obtained over three independent experiments (control cells: n [cells] = 18, n [mitochondria] = 202; mAPC-red cells: n [cells] = 18, n [mitochondria] = 189). Cells chosen for imaging in wound healing experiments were healthy, expressed modest GFP2-mito, did not show significant movement over the 5 min time period (visualised in DIC channel) and, for the mAPC-red siRNA treated sample, displayed a clear red fluorescent signal.

5.2.6 Western blot analysis

To confirm APC knockdown, cells were collected, lysed using RIPA buffer and processed as described in Section 2.2.9.1. Total cell lysate samples (~30 µg) were separated by SDS-PAGE using 5% acrylamide gels, and transferred onto a nitrocellulose membrane (see Sections 2.2.9.3-2.2.9.6). Western blots were probed as described in Section 2.2.9.7, using primary antibodies against APC (H290) and α -tubulin. Dilutions for these antibodies, and subsequent secondary antibodies are outlined in Table 2.2 and Table 2.3 respectively. Immunoblots in this chapter were developed by ECL using the ChemiDoc Imaging System (See Section 2.2.9.8).

5.2.7 Graphs and statistics

All graphs and statistics used to display and analyse results in this chapter are outlined in Section 2.2.11.

5.3 Results

5.3.1 Loss of APC slows cell migration

APC plays a well-established and crucial role in cell polarity and migration (see Section 1.2.1.3 and reviews 52, 53, 54) and loss of APC in mouse fibroblasts has previously been implicated in decreased membrane protrusion formation and cell migration (65). To confirm this, NIH 3T3 cells, which are known to display strong APC staining at microtubule-dependent protrusions (27), were treated with control or mouse APC-specific (mAPC) siRNAs and grown to confluence. These cells were then wounded and 5 h later fixed and analysed by immunofluorescence microscopy. In line with the findings by Kroboth and colleagues (65), a significant lag in cell migration was observed for mAPC siRNA treated cells in comparison to control (Figure 5.1), which appeared to correlate with a decrease in the number of cells with microtubule-dependent protrusions at the leading edge, and the presence of mitochondria in this region (described further in Section 5.3.2).

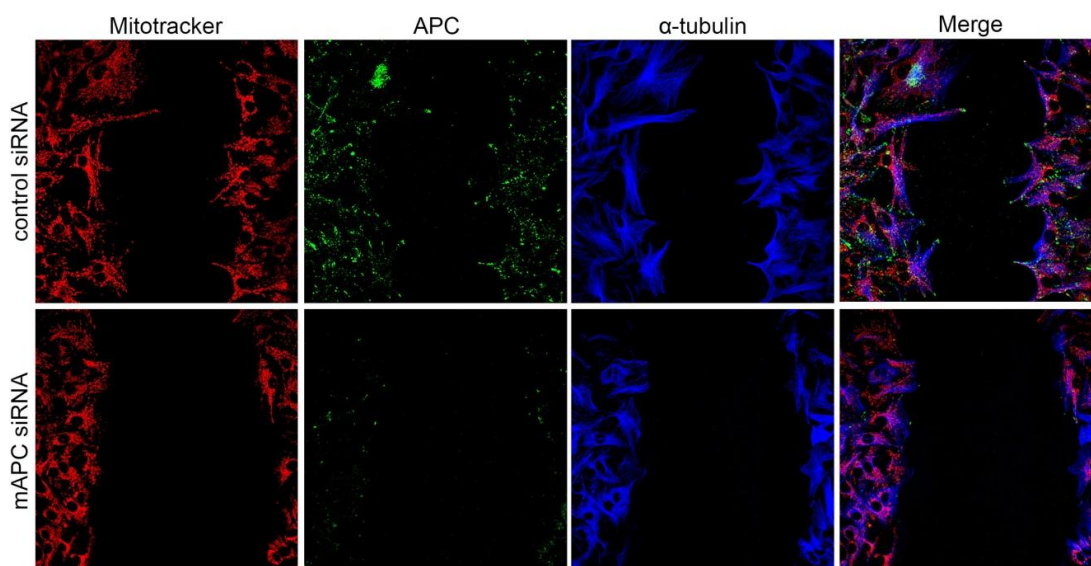


Figure 5.1: Loss of APC slows cell migration in NIH 3T3 cells

Cells treated with control or mAPC siRNA were grown to confluence and wounded. After 5 h of regrowth cells were stained with CMX-Ros Mitotracker, fixed, counter-stained for APC (H290) and α -tubulin and analysed by immunofluorescence microscopy.

5.3.2 Mitochondrial localisation at extended cellular protrusions of actively migrating cells is significantly reduced upon loss of APC.

Whilst APC may be well known to contribute to cell migration through its interactions with other key players like tubulin, actin, IQGAP1 and β -catenin, the importance of mitochondrial dynamics in cell migration is only just coming to light. Recent publications provide experimental evidence to show that regulated mitochondrial distribution is essential for proper migration of T lymphocytes (142), and that accumulation of mitochondria at the leading edge of epithelial breast and prostate cancer cells provides energy to drive cell migration (18, 19). Observations that mitochondrial localisation at the leading edge and cellular protrusions was lost upon knockdown of APC (Figure 5.1) led to further interrogation of mitochondrial staining patterns in this region. Detailed co-staining experiments revealed clearly that mitochondria co-localised with APC and its regulatory cell migration protein partners actin, IQGAP1, α -tubulin (microtubules) and β -catenin (Figure 5.2) at the leading edge of migrating NIH 3T3 cells, including at cell membrane protrusions. Mitochondrial co-localisation at cell migratory regions with cell migration factors was also observed in human HDF1314 cells (Supplementary Figure S5.1)

To further investigate the effect that loss of APC has on mitochondrial localisation in migratory cells at the cell periphery, confluent NIH 3T3 cells were treated with either control or mAPC siRNAs and subjected to a scratch wound assay. The cells were then fixed, stained for mitochondria, APC and α -tubulin and examined 5 h after regrowth (Figure 5.3A). Loss of APC caused a ~20% ($P < 0.01$) reduction in the number cells with microtubule-dependent cellular protrusions at the leading edge of the wound (Figure 5.3B), as well as the number of protrusions per cell (preliminary observations, data not shown), in agreement with previous findings (27). The remaining microtubule-dependent protrusions in mAPC siRNA treated cells appeared to be shorter and less pronounced than their control siRNA treated counterparts and, mitochondrial localisation at the ends of these microtubules was found to decrease by >50% ($P < 0.001$) after APC knockdown (Figure 5.3C). This mirrored prior results obtained in sub-confluent cells (Figure 3.2). This APC-dependent alteration in mitochondrial localisation could potentially decrease the supply of energy to the cell membrane

required for cell migration, contributing to the observed slower rate of migration upon loss of APC (65, and confirmed in Figure 5.1).

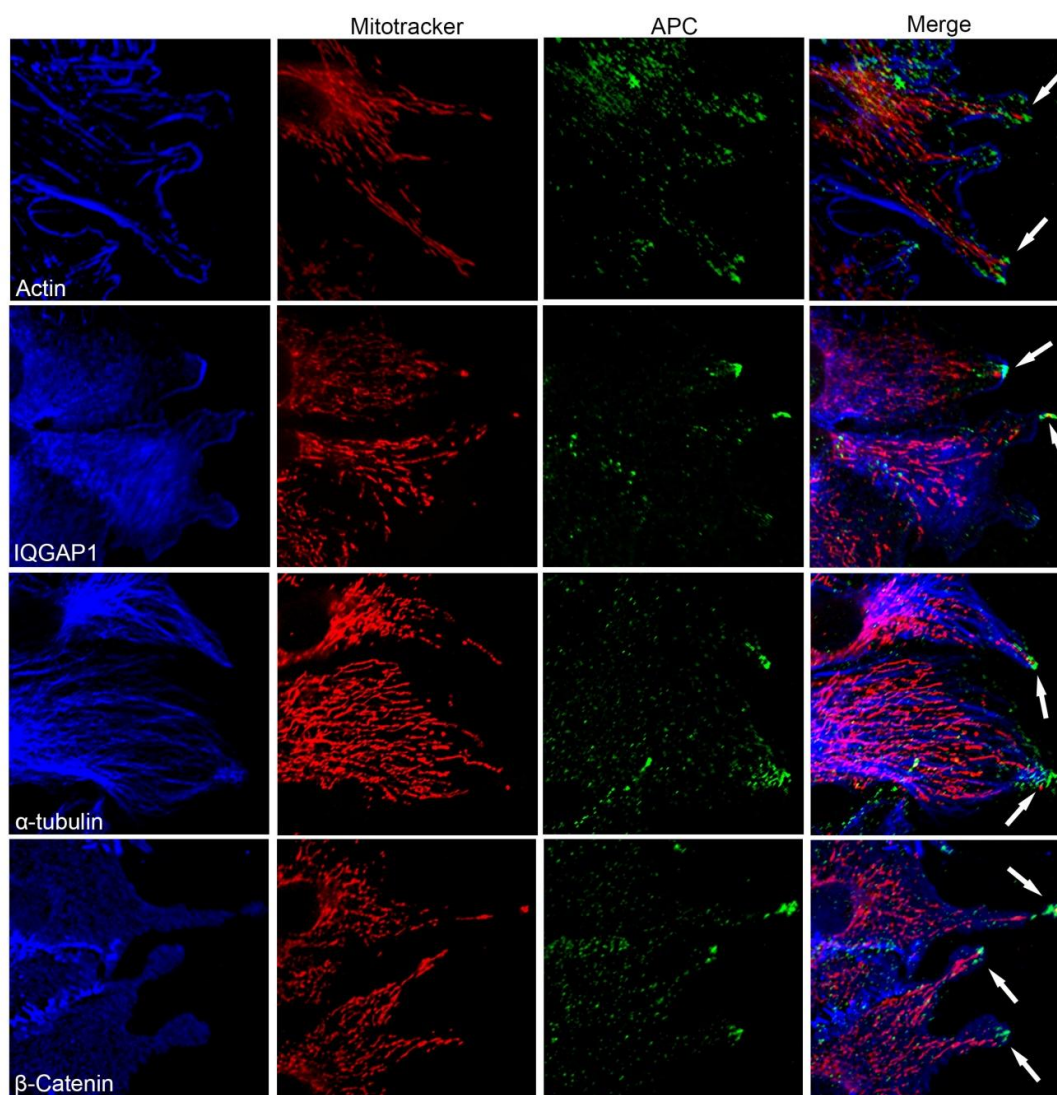


Figure 5.2: APC and mitochondria co-localise with components of the cell cytoskeleton at cell membrane protrusions in NIH 3T3 cells.

Confluent NIH 3T3 cells wounded 5 h prior to fixation and stained with CMX-Ros Mitotracker were counter-stained using antibodies against APC (H290, green) and proteins involved in cell migration (actin, IQGAP1, α -tubulin and β -catenin, blue). Immunofluorescence microscopy of cells at the leading edge of the wound revealed colocalisation between mitochondria, APC and these cell migration factors as indicated by the arrows.

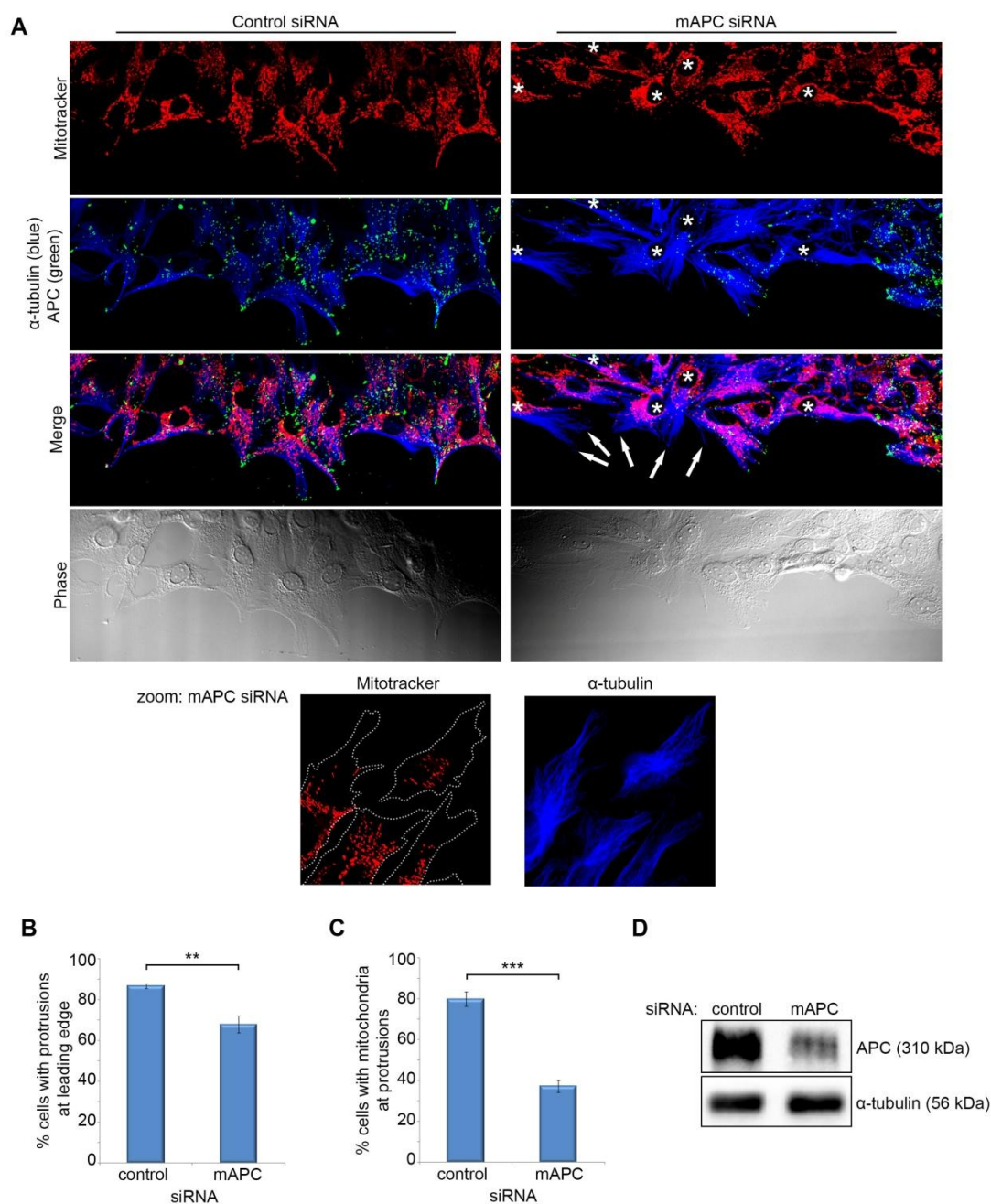


Figure 5.3: Loss of APC reduces mitochondrial localisation at cellular protrusions (A-C) NIH 3T3 cells treated with control or mAPC siRNA were grown to confluence and wounded. After 5h regrowth cells were stained with CMX-Ros Mitotracker, fixed, counter-stained for APC (H290) and α -tubulin and analysed by (A) immunofluorescence microscopy. Cells positive for APC knockdown are indicated by an asterisk (*). (B) Cells displaying cellular protrusions at the leading edge were scored, from which the (C) number of cells presenting mitochondrial localisation at these protrusions was determined. It was revealed that loss of APC significantly reduced the presence of mitochondria at cellular protrusions (indicated by arrows in panel A, and observed in greater detail in the zoom). Significant differences, determined using an unpaired T-test, are indicated (**, $P < 0.01$; ***, $P < 0.001$, % mean \pm S.D). (D) APC knockdown was confirmed by western blot analysis.

5.3.3 Optimisation of imaging mitochondria movement in living cells

The above results in fixed cells and findings in previous chapters support a role for APC/Miro/Milton in microtubule-based mitochondrial transport towards the cell periphery. To investigate more directly whether APC stimulates the actual rate of transport of mitochondria, live cell imaging was employed to determine what impact loss of APC had on real time movement of mitochondria within the cell. Mitochondrial transport has traditionally been studied in neuronal cell lines, in the context of neurological disorders. Research in other cell types is limited and as a result, much of the mitochondrial tracking protocol had to be optimised from the outset. Firstly, as the study was to focus on mitochondrial transport to the leading edge in cell migration it was decided that a fibroblastic cell line would be used as they are ideal for wound healing assays, and because the mitochondria are spread out towards the protrusions allowing for easier tracking. NIH 3T3 cells were chosen because they are less sensitive to toxicity than human HDF1314 cells and as previous experimental data had already been collected in this cell line (Figure 5.1-Figure 5.3). Additionally, a study of mitochondrial transport had already been conducted in sub-confluent NIH 3T3 cells by another group (177), allowing for comparison of methodology and baseline transport results (Figure 5.4). Once optimisation in sub-confluent cells was complete, this method was further optimised for wound healing assays.

5.3.3.1 Visualisation of mitochondria and image capture

The next step was to select a marker for the visualisation of mitochondria in a live cell setting. Several markers, outlined in Table 5.1, were tested prior to GFP2-Mito selection. The interval between each time point was based on the minimum time required for the Olympus IX71 DeltaVision core microscope to undertake image capture. Initial experiments used a 5 s interval, which had to be increased to 7 s following external alterations to the DeltaVision settings.

Table 5.1: Selection of mitochondrial marker for live cell imaging

Sub-confluent NIH 3T3 cells either transfected with 400 ng of pGFP-Mito, pGFP2-Mito or pTomato-Mito plasmid or stained with CMX-Ros Mitotracker (1:10000) or Green Mitotracker (1:5000) were subjected to live cell imaging as described in Section 5.2.5. Mitochondria in 4-5 cells were imaged for each marker.

Marker	Fluorescence Stability	Mitochondrial Visualisation	Toxicity
GFP-Mito	Moderate, most mitochondria visible to at least 5 min, though resolution poor.	Normal at low-moderate transfection levels.	Cells look moderately healthy after image capture.
GFP2-Mito	Good, most mitochondria visible to at least 5 min and resolution ok.	Normal at low-moderate transfection levels.	Cells look moderately healthy after image capture.
Tomato-Mito	Poor, can no longer visualise after 3 minutes.	Bright, covered in fluorescent dots which do not look like mitochondria.	Cells look moderately healthy after image capture.
CMX-Ros Mitotracker	Very good, all mitochondria visible to at least 5 min (if cells do not die) and resolution good.	Normal	Cells often die prior to completion of image capture.
Green Mitotracker	Good, most mitochondria visible to at least 5 min and resolution good.	Normal	Cells do not look healthy after image capture.

5.3.3.2 Optimisation of transfection in cells at 90% confluence

Transfection of pGFP2-Mito for live cell imaging in sub-confluent cells was performed under standard conditions using PEI (Section 2.2.3.4), however difficulty was encountered when transfection of pGFP2-Mito was required for live cell imaging of wounded cells pre-treated with siRNAs. In order to reach confluence, cells needed to be treated with siRNAs at a higher confluence (70-75%) than normal, which meant that transfection occurred when the cells were verging on 90% confluence. Under standard conditions, this resulted in an extremely low rate of transfection. A number of reagents were tested (Section 2.2.3.4), before the K2 transfection system was chosen (Table 5.2).

Table 5.2: Selection of transfection reagent for live cell imaging in wound healing assays

NIH 3T3 cells pre-treated with mAPC-red siRNA were transfected with 400ng pGFP2-Mito using the K2 transfection system. Cells were examined for transfection level of GFP2-Mito and the ability of the cells to reach confluence.

Reagent	Transfection Level	Toxicity
Lipofectamine	No cells transfected.	High, cells could not reach confluence.
Fugene	No cells transfected.	Low.
PEI	5% of cells transfected.	Low-moderate, cells could not reach confluence.
K2	60% of cells transfected	Low.

5.3.4 Measurements of mitochondrial velocity in sub-confluent NIH 3T3 cells are comparable to those in the literature

Mitochondria were visualised in live NIH 3T3 cells following expression of a GFP2-tagged mitochondrial peptide marker (pGFP2-Mito) and the use of time lapse imaging by DeltaVision live cell microscopy to track the mitochondria (Supplementary Figure S5.2). The optimised methodology was as described (Section 5.2.5) and tracking was generally performed over a 5 min period. Analysis of the acquired image data indicated that motile mitochondria moved with an average velocity of 10.06 $\mu\text{m}/\text{min}$. Whilst this is only ~45% of the speed reported in YFP-transfected control cells by Patil and colleagues (Table 5.3), it is still within the same order of magnitude. There are several variations in cell culture and transfection conditions, image acquisition and data analysis that could contribute to this difference in velocity.

Analysis of other parameters (see Table 5.3) revealed that 75.61% of mitochondria were motile; this characteristic is presented as either directed movement (anterograde or retrograde) or oscillatory movement with no net displacement (oscillatory = 38.10%, anterograde = 26.19%, retrograde = 9.52%). The average distance travelled (distance travelled over tracking time), and net displacement (distance between start-point and end-point), of a mitochondrion over 1 min was found to be 3.41 μm and 0.83 μm respectively, the latter of which is comparable to that found by Patil and colleagues (1.11 μm).

Table 5.3: Optimised mitochondrial tracking in sub-confluent NIH 3T3 cells

Mitochondria in sub-confluent 3T3 cells transfected with pGFP2-mito, were tracked using MTrackJ ImageJ plug-in. From the raw tracking data, Microsoft Excel was used to calculate movement parameters of randomly selected mitochondria. Displacement is measured as the net distance between start-point and end-point. Distance refers to total distance travelled during the time period measured. This data was compared to data from control cells in a pre-existing study by Patil et al., 2013 (177).

Overall Mitochondrial Movement		Optimised	Patil 2013
% motile mitochondria		75.61 ± 2.55	
% directionality	Stationary	26.19 ± 2.55	
	Oscillating	38.10 ± 1.85	
	Anterograde	26.19 ± 4.83	
	Retrograde	9.524 ± 9.23	
Average Displacement (µm) (normalised to 1 min)		0.83 ± 0.03	1.11
Average Distance (µm) (normalised to 1 min)		3.41 ± 0.10	
Motile Mitochondria		Optimised	Patil 2013
Average Velocity (µm/min)* *does not include stationary time points	Total	10.06 ± 2.53	22.8
	Anterograde	10.32 ± 3.29	23.4
	Retrograde	9.86 ± 2.85	22.2

5.3.5 Loss of APC decreases initiation of mitochondrial transport

The above methodology was adapted to investigate facets of mitochondrial transport in actively migrating cells. NIH 3T3 fibroblasts treated with control or a red fluorescently tagged mAPC (mAPC-red) siRNA, were transfected with pGFP2-Mito and then grown to confluence and wounded. Following 5 h regrowth, cells were subjected to timelapse imaging by DeltaVision live cell microscopy after which mitochondria at the leading edge were tracked and analysed for several transport parameters over 5 min intervals (see Figure 5.4), as described in Section 5.2.5.

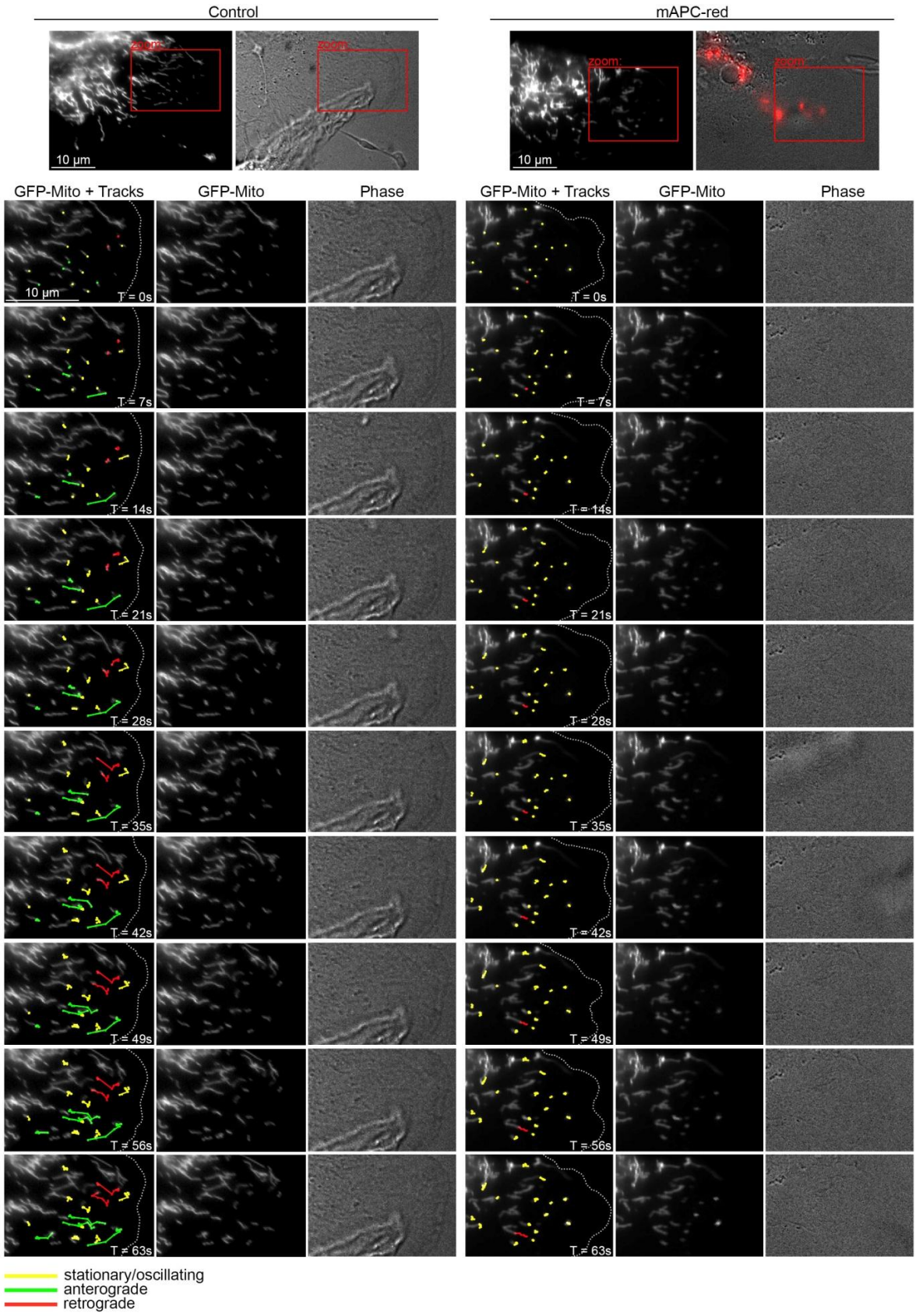


Figure legend over page.

Figure 5.4: Loss of APC reduced the initiation of anterograde mitochondrial transport in NIH 3T3 cells.

NIH 3T3 cells were treated with either control or fluorescently tagged mAPC siRNA (mAPC-red), transfected with a fluorescently tagged mitochondrial marker (pGFP2-Mito) and grown to confluence. Cells were wounded and 5 h later analysed by live cell time lapse imaging, capturing images every 7 s for a total of 5 min. Post image acquisition, mitochondria were selected at random for tracking manually using the ImageJ plug-in MTrackJ. Representative cell images are shown for ~1 min of tracking. Mitochondria are marked for different types of movement: stationary/oscillating (yellow), anterograde (green) and retrograde (red). APC silencing is indicated by red fluorescence.

The most striking observation revealed from analysis of the timelapse images was that loss of APC caused a dramatic decrease (~2.3 fold reduction, $P < 0.01$) in the overall motility of mitochondria (see cell images in Figure 5.4 and graphs in Figure 5.5A). Under control conditions, mitochondria were motile 48.4% of the time, whilst in comparison, only 21.3% of cells transfected with mAPC siRNA were motile. A more detailed analysis revealed that whilst oscillatory movements remained relatively constant following APC knockdown, directed mitochondrial transport was severely diminished. In cells targeted by the mAPC-red siRNA, the frequency of mitochondria displaying anterograde transport dropped significantly from 24.3% to 7.0% ($P < 0.05$, Figure 5.5B). A decrease in mean retrograde transport from 8.7% to 1.7% was also observed, however this was not found to be significant ($P > 0.05$, Figure 5.5B). As expected, the proportion of stationary cells increased after loss of APC from 49.9% to 78.7% ($P < 0.01$, Figure 5.5B).

In line with these results, silencing of APC also significantly decreased the frequency of distinct mitochondrial movements (directional movement without pause) by ~50% in both anterograde and retrograde directions ($P < 0.01$, Figure 5.5C). Furthermore, the average mitochondrial displacement and average distance travelled over the observed time period also significantly decreased ($P < 0.01$, Figure 5.5D-E). These findings suggest that APC has a role in the initiation of long range, directed mitochondrial transport in migrating cells. These results are summarised in Table 5.4 and Figure 5.5, and reflected in the tiled cell images (Figure 5.4) and the time lapse movies (Supplementary Video 5.1 and 5.2) that compare control and mAPC siRNA treated NIH 3T3 cells.

Table 5.4: Effect of APC loss on parameters of mitochondrial transport in migrating NIH 3T3 cells

Mitochondria in migrating NIH 3T3 cells treated with control or mAPC-red and transfected with pGFP2-mito, were tracked using the MTrackJ ImageJ plug-in. From the raw tracking data, Microsoft Excel was used to calculate movement parameters of randomly selected mitochondria. A distinct mitochondrial movement is classified as any directional motion without pause. Significance determined by unpaired T-test (*, $P < 0.05$; **, $P < 0.01$; n.s., not significant).

Overall Mitochondrial Movement		Control	mAPC1	P-Value
% motile mitochondria		48.44 \pm 5.92	21.25 \pm 5.32	**
% directionality	Stationary	49.91 \pm 7.47	78.76 \pm 5.32	**
	Oscillating	17.08 \pm 7.29	12.50 \pm 4.00	n.s.
	Anterograde	24.30 \pm 8.43	7.03 \pm 3.39	*
	Retrograde	8.74 \pm 5.43	1.70 \pm 1.49	n.s.
Average Displacement (μ m) (normalised to 1 min)		1.19 \pm 0.11	0.67 \pm 0.16	**
Average Distance (μ m) (normalised to 1 min)		3.19 \pm 0.14	2.10 \pm 0.20	**
Motile Mitochondria		Control	mAPC1	P-Value
Average Velocity (μ m/min)* *does not include stationary time points	Total	9.27 \pm 0.39	8.82 \pm 0.57	n.s.
	Anterograde	8.98 \pm 0.19	8.99 \pm 0.26	n.s.
	Retrograde	10.13 \pm 0.76	8.75 \pm 0.97	n.s.
Average Distinct Mitochondrial Movements	Anterograde	0.23 \pm 0.03	0.13 \pm 0.07	**
	Retrograde	0.15 \pm 0.04	0.09 \pm 0.03	**
Average Distance of Mitochondrial Movements (μ m)	Anterograde	1.35 \pm 0.20	1.22 \pm 0.16	n.s.
	Retrograde	1.39 \pm 0.18	1.16 \pm 0.25	n.s.

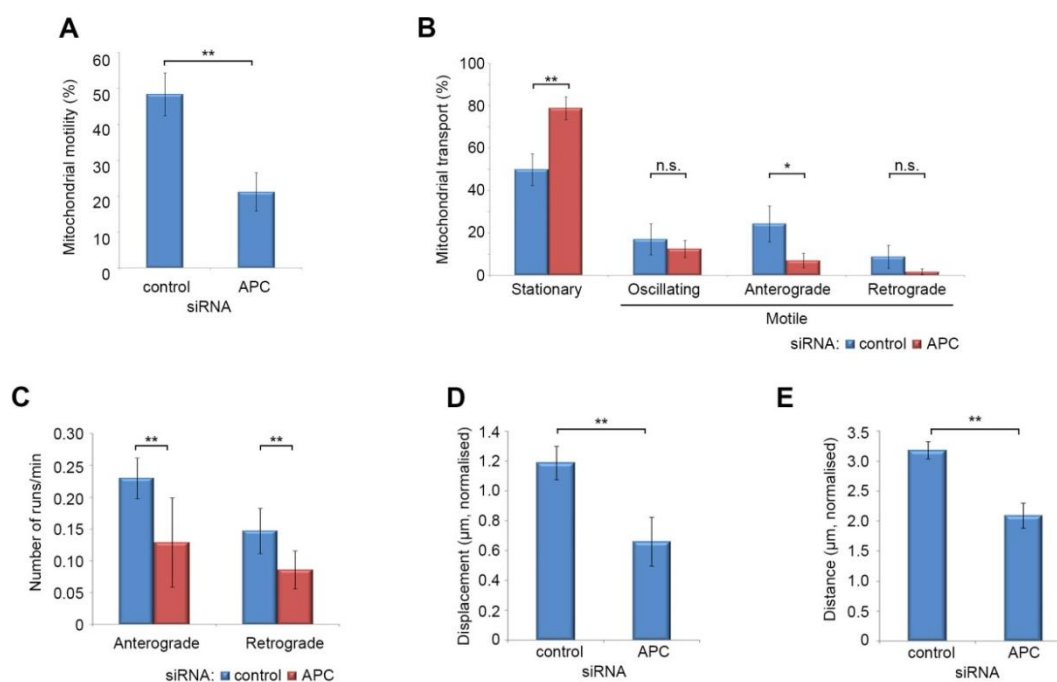


Figure 5.5: Loss of APC disrupts mitochondrial motility

(A-E) Analysis of mitochondrial tracking data from time lapse microscopy performed in wounded NIH 3T3 cells transfected with control or mAPC siRNA (Figure 5.4) was performed in Microsoft Excel from output generated by Image J plug-in MtrackJ. Analysis of mitochondrial motility revealed that loss of APC resulted in (A) decreased mitochondrial transport, particularly in the (B) anterograde direction. This correlated with a decrease in the (C) number of runs (mitochondrial movements without pause or change in direction) mitochondria made per min and a decrease in both (D) the displacement and (E) distance (μm , normalized to 1 min to account for different tracking periods) travelled over the tracking period following loss of APC. Significance, as determined by unpaired T-tests, indicated (*, $P < 0.05$; **, $P < 0.01$; n.s., not significant, % mean \pm S.D).

5.3.6 Loss of APC does not slow the rate of mitochondrial transport

Somewhat surprisingly, analysis of live cell data from the same experiment revealed that loss of APC did not significantly slow the overall rate of mitochondrial transport once movement had been initiated (control siRNA = $9.27 \pm 0.39 \mu\text{m}/\text{min}$, mAPC-red siRNA = $8.82 \pm 0.57 \mu\text{m}/\text{min}$, $P > 0.05$; see Figure 5.6A, and for further details Supplementary Figure S5.3). This lack of difference was also reflected in the average velocities of transport in both anterograde and retrograde directions (Figure 5.6A). Furthermore, the average distance travelled during these distinct mitochondrial

movements (directional motion of mitochondria without pause) was not significantly altered by silencing of APC (Figure 5.6B). These results are summarised in Table 5.4. Collectively, this data suggests a specific role for APC in stimulating the initiation of Miro/Milton driven mitochondrial transport, rather than its ongoing velocity.

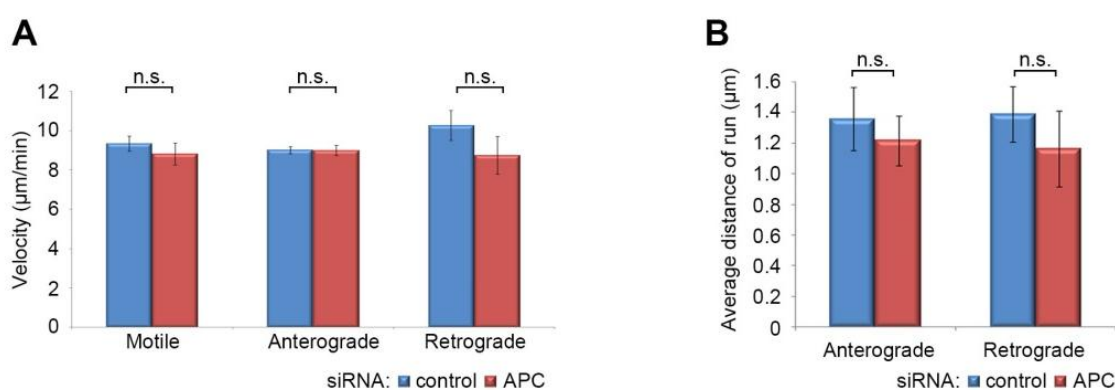


Figure 5.6: Loss of APC has no effect on mitochondrial velocity once transport is initiated

(A-B) Analysis of mitochondrial tracking data from time lapse microscopy performed in wounded NIH 3T3 cells that were transfected with control or mAPC siRNA (Figure 5.4) was performed in Microsoft Excel from output generated by Image J plug-in MtrackJ. Analysis of the rate of mitochondrial movement after transport had been initiated revealed that (A) mitochondrial velocity ($\mu\text{m}/\text{min}$) remained static following APC knockdown, as did the (B) distance (μm) individual mitochondria travelled (runs). Significance relative to control siRNA, determined using an unpaired T-test, is indicated (n.s., not significant, % mean \pm S.D).

5.4 Discussion

The results shown here indicate that APC is required for initiation of anterograde mitochondrial transport, thereby explaining the loss of mitochondrial localisation from cellular protrusions in actively migrating cells following APC silencing. These findings also explain the previously observed net shift in mitochondria away from the cell periphery in APC siRNA treated sub-confluent cells, which was shown to correlate with interaction between APC and the Miro/Milton mitochondrial transport complex.

Recent studies that link mitochondrial localisation to cell migration suggest a new role for APC in regulating mitochondrial transport and subsequently supplying ATP to the cell membrane. This hypothesis could, in part, explain the decrease in protrusion formation and cell migration observed here and elsewhere when APC is silenced (27, 65). C-terminal truncating APC mutations were previously (Chapter 4) shown to disrupt APC binding to Miro/Milton, and in turn mitochondrial transport. The potential impact of this on anterograde transport initiation and in turn cell migration and polarity will be discussed.

5.4.1 APC appears to stimulate the initiation, rather than the velocity, of anterograde mitochondrial transport

Live cell imaging data suggests a specific role for APC in the initiation of mitochondrial transport, rather than modulation of the rate of kinesin motor-driven translocation. Support for this notion primarily comes from the finding that siRNA silencing of APC in actively migrating NIH 3T3 cells decreased the total pool of motile mitochondria from 48.4% to 21.3%, whilst the velocity of the motile pool remained stable. Furthermore, decreased mitochondrial movement following loss of APC correlated directly with a drop in the incidence of distinct mitochondrial movements, and a decrease in mitochondrial net displacement and distance travelled over the tracking time period. Treatment with mAPC siRNA elicited no change in the distance travelled by mitochondria after transport had commenced, further indicating a very specific role for APC in initiation of mitochondrial transport. These results are summarised in Figure 5.5, Figure 5.6 and Table 5.4.

A role for APC in “kick-starting” mitochondrial movement makes sense in the context of what is currently known about the mechanism of Miro/Milton-driven transport. In fact, there is evidence that Miro/Milton complexes function in the same way by stimulating mitochondrial transport initiation rather than velocity. For instance, when investigating Milton-1 in the axons of hippocampal pyramidal neurons, Brickley and Stephenson (154) observed that knockdown of Milton-1 gene expression diminished the pool of motile mitochondria from 36% to 16%, whilst the velocity of motile mitochondria remained unaltered. Moreover, silencing of Alex3, a newly discovered regulator of the Miro/Milton complex, also reduced mitochondrial motility but had no effect on velocity (163), a phenomenon likewise observed upon disruption of Miro (152, 153). In these cases, as observed here for APC, the loss of Milton, Miro or Alex3 each caused a decrease in anterograde transport of mitochondria, supporting the view that APC is a positive regulator of the Miro/Milton/KIF5 complex.

The mitochondrial motility pool most affected by mAPC siRNA treatment was that of anterograde transport, where mitochondrial movement decreased from 24.3% to 7.0%. Whilst the data from live cell analysis also indicated that the pool of mitochondria moving in a retrograde direction was diminished following loss of APC, this was not found to be statistically significant. Interestingly, both Miro (167, 168) and Milton (169) have been implicated in retrograde mitochondrial transport through interactions with the dynein motor, an association which may occur separately from APC. The mild alteration in retrograde transport may be due to disruption of bidirectional transport which has been reported to interfere with crosstalk between different motor protein complexes (304). Oscillatory transport movements remained static after APC silencing, suggesting an alternate mechanism of transport to the microtubule-dependent Miro/Milton system, perhaps one which is actin-based. This is in agreement with the notion that short-range mitochondrial transport is typically mediated by actin-motors (170, 171).

5.4.2 APC stimulates transport of mitochondria to cell membrane protrusions and the leading edge: Implications for cell migration.

APC is known to regulate cell migration and polarity through specific processes such as promotion of F-actin assembly, centrosome re-orientation and microtubule stabilisation and anchoring (Section 1.2.1.3 and reviews 52, 54). These are primarily facilitated through APC at the cellular periphery, in particular at membrane protrusions. Recently, mitochondrial localisation to membrane structures such as protrusions in epithelial cell lines has also been found to contribute to cell migration and polarity. In this study, image analysis of migrating NIH 3T3 cells revealed colocalisation between APC and mitochondria at these membrane protrusions (Figure 5.2), suggesting a link between the two pathways and a potential novel mechanism through which APC may contribute to cell migration and polarity.

In agreement with prior studies (27), loss of APC in migrating cells caused a ~20% reduction in the number of cells displaying protrusions (Figure 5.3B). Of those remaining protrusions which appeared noticeably smaller in size, a >50% depletion in mitochondrial co-localisation was observed (Figure 5.3C) indicating disrupted mitochondrial transport to the cell periphery, agreeing with previous results in sub-confluent cells (Figure 3.2) and findings that APC loss impairs anterograde transport (Figure 5.5B). Previously, Desai and colleagues (18) showed that siRNA silencing of Miro-1 reduced mitochondria at the leading edge in MDA-MB-231 breast cancer epithelial cells correlating with a ~3-fold decrease in speed and directional persistence of cells. In the same cell line, Zhao and colleagues (19) found that blocking mitochondrial distribution to the leading edge reduced the size of lamellipodia in cells by 60%, in turn significantly slowing cell migration. This phenomenon is not limited to epithelial cell lines, as Campello and colleagues (142) showed that by blocking mitochondrial transport to the uropod, the primary migratory structure in T-cell lymphocytes, cell polarisation was disrupted and cell migration was reduced by >80%.

Regulated cell migration requires movement at the membrane primarily mediated through remodelling of the actin network, and also direction (polarity) which is largely dependent on the microtubule network. This cytoskeletal remodelling is a bioenergetically demanding process, and studies by Campello, Desai and Zhao (18, 19,

142) indicate that mitochondria are targeted to cell migratory regions to provide the ATP necessary to fulfil these energy requirements (discussed further in Section 5.4.2.1).

Mitochondrial contact with the cell periphery is also essential for extracellular calcium uptake (190), where increased $[Ca^{2+}]_i$ has been shown to contribute to cell migration through a number of Ca^{2+} signalling pathways, contributing to focal adhesion turnover, actin assembly and migration directionality (reviewed in 292). In a similar manner to the targeted release of ATP from mitochondria, liberation of Ca^{2+} from mitochondrial stores, and conversely intracellular Ca^{2+} uptake, may also alter $[Ca^{2+}]_i$ at the leading edge. Hence, APC may stimulate the membrane-directed provision of ATP and calcium through regulation of mitochondrial localisation.

5.4.2.1 APC may target mitochondrial ATP to cellular protrusions and the leading edge to supply energy for cell migration

The cytoskeletal remodelling that occurs in cell migration is a bioenergetically demanding process which is highly dependent on a constant supply of ATP (64). Like other metabolites, ATP is known to accrue in microcompartments with its substrates in numerous areas of the cell, including the cytoskeleton where the actin and microtubule networks, along with numerous scaffolding proteins, create mechanical barriers to prevent diffusion of ATP away from target sites (reviewed in 305, 306). This function is facilitated by targeted localisation of mitochondria to directly supply ATP to the microcompartment, rather than non-specific ATP diffusion through the cytoplasm. A localised concentration of mitochondria allows for faster generation of ATP after hydrolysis through recycling of ADP back into the mitochondria for oxidative phosphorylation, thereby providing a continuous supply of ATP. There it is likely to represent a primary energy source for actin and microtubule polymerisation during cell migration.

The polymerisation of actin subunits into F-actin mechanically pushes the cell membrane forward, causing it to expand in a process catalysed by ATP hydrolysis. Indications that the ATP required is mitochondrial in origin come from several studies. In particular, uncoupling of ATP synthesis by CCCP (Carbonyl cyanide *m*-chlorophenyl hydrazone) treatment was shown to decrease F-actin polymerisation, and as a result

reduced lamellipodia formation in MDA-MB-231 breast cancer cells, correlating with a slowing of cell migration (19). This mirrors results described in T-cell lymphocytes, where uncoupling of ATP synthesis also reduced the rate of cell migration (142), however, in that study impaired migration was not attributed to altered actin polymerisation, but rather to an inability to activate the ATPase activity of myosin II, which is required for the contraction of the actin network. Thus mitochondrial ATP is required to catalyse a range of processes that drive cell migration.

Evidence that mitochondrial ATP is required for microtubule polymerisation in the formation of cellular protrusions is less well defined. Findings in this chapter show that APC-siRNA dependent loss of mitochondria from the cell membrane correlated with a decrease in the number and size of protrusions (Figure 5.3). This data, combined with the known efficiency of mitochondrial ATP microcompartment formation suggest that APC may contribute to protrusion formation not only through its ability to stabilize microtubule bundles (70) but perhaps also via delivery of mitochondrial ATP. As previously described (Section 1.2.1.3), APC localises to and regulates the microtubule and actin networks. This raises the possibility that once APC delivers mitochondria to the cell periphery, it may also act as an anchor to tether mitochondria to these energy-demanding sites, assisting in the formation of ATP microdomains. These mitochondria could work in synergy with APC's other roles and act like a battery to provide a highly specific localised source of ATP.

5.4.3 APC mutation may contribute to aberrant cell migration in CRC through disruption of mitochondrial transport

The loss of mitochondria at the leading edge of actively migrating cells, as described in Section 5.4.2, deprives this region of metabolites required for effective membrane dynamics and motility. In Chapter 4 it was shown that APC interaction with the Miro/Milton mitochondrial complex was diminished in APC-mutant CRC cell lines, resulting in a perinuclear mitochondrial clustering similar to that observed when wild-type APC is silenced. Given that the binding domains for Miro/Milton and numerous cytoskeletal binding domains are lost upon APC mutation, it makes sense that APC truncation affects mitochondrial targeting to the membrane. The impact of APC mutations on migration may not, however, always mimic that observed by complete loss

of APC. For instance, Kawasaki and colleagues (73) reported that C-terminal truncated APC mutants exhibit a gain of function to constitutively activate the Rac1 exchange factor ASEF in colon cancer cell lines, leading to modest stimulation of cell migration through regulation of actin. More recent studies (96) however, indicate that APC truncations most often cause erratic cell movement due to loss of polarity and directionality, and this is thought to be due to reduced APC-dependent formation of membrane protrusions, and may also be affected by loss of targeted mitochondria.

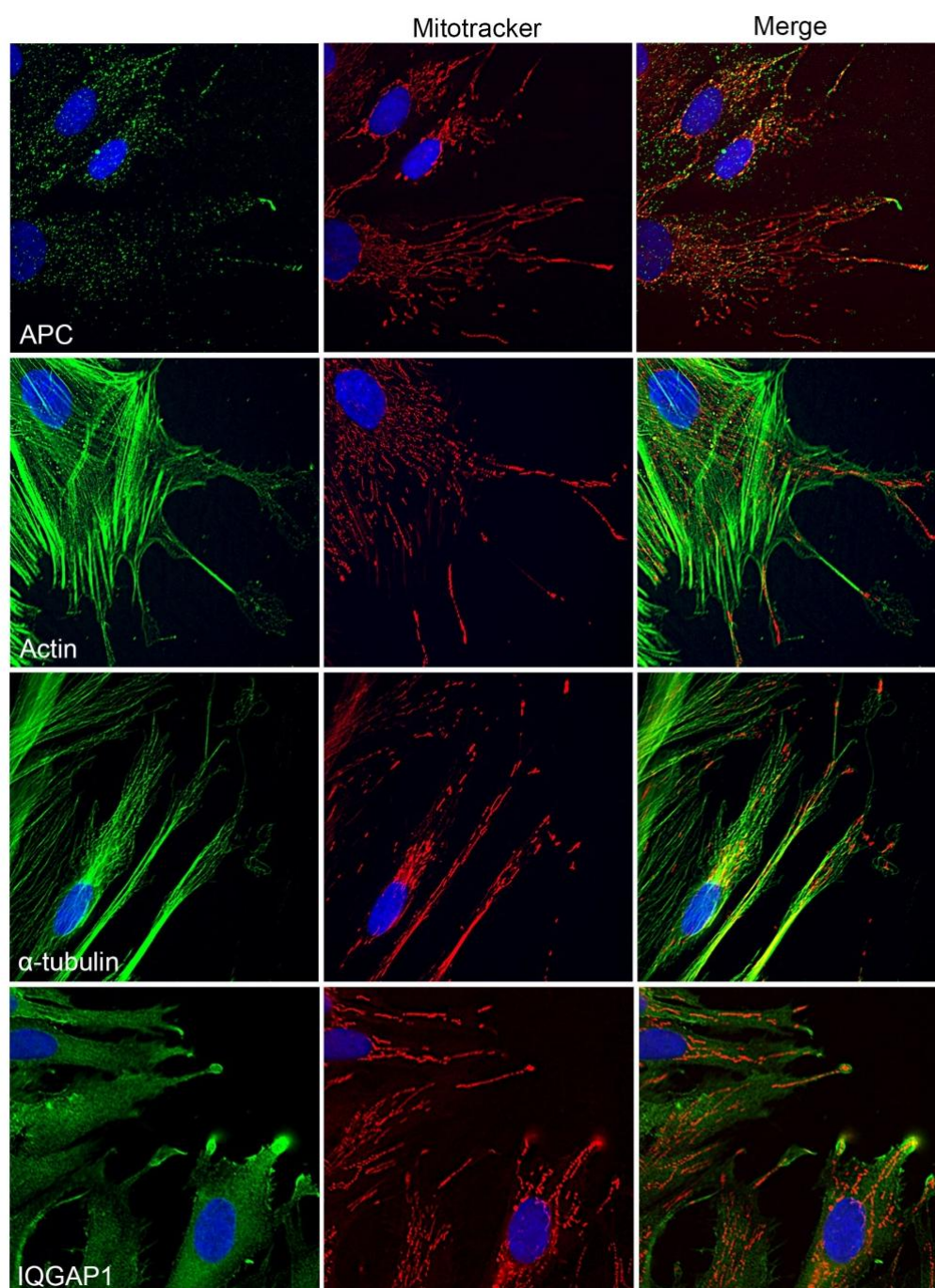
Perturbations in mitochondrial transport are linked to aberrant cell migration in carcinogenesis (18, 19). These studies indicate that mitochondria in invasive breast and prostate cancer cell lines preferentially cluster at the leading edge, contributing to increased migration speed and invasion. Disruption of anterograde mitochondrial transport (described in Section 5.4.2), attenuated these invasive properties and slowed cell migration, and similar principles are likely to apply to a range of other cell types and tissues. Cells in the gut are highly proliferative and over the course of 3-5 days, following generation at the base of the colon crypt, they migrate upwards undergoing several phases of differentiation before they are shed or undergo apoptosis.

Whilst little is known about the mechanisms of colon crypt migration, experiments in APC (Min/+) mice (99) and inducible APC knockout mice (66), demonstrated a slowing of cell migration along the crypt-villus axis. In addition, Nelson and colleagues (96) reported that expression of truncated APC caused a loss in directional cell migration towards the tip of colon crypt villi. These effects were attributed to a loss of APC cytoskeletal regulation, however, results from this thesis support an additional contribution through loss of APC-dependent mitochondrial targeting. Retention of cells in the lower zone of colon crypts is observed and favourable in CRC as this region is highly proliferative. Retention also increases the opportunity to acquire further selective advantages, particularly given the toxic, DNA-damaging environment of the gut.

In APC-mutant CRC cells, some of the metabolic demands at the periphery could still be met by mitochondria reaching the membrane through the action of other mitochondrial transport pathways (Section 1.3.2.2), however as outlined in Section 5.4.2.1, the localisation and interaction of APC with elements of the cytoskeleton is likely to specifically anchor mitochondria to these regions. Similarly, energy provided

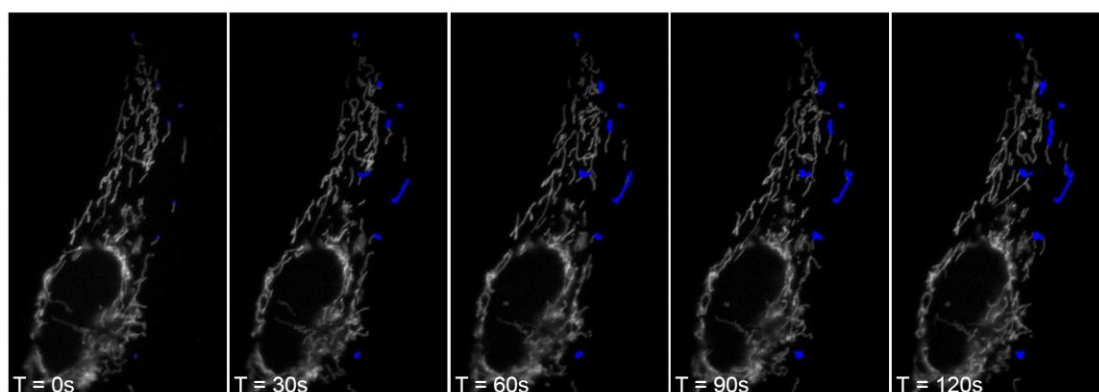
by glycolysis in the cytoplasm, known to be substantially heightened in mutant APC CRC cells (14), would not be an effective energy source.

5.5 Supplementary Figures



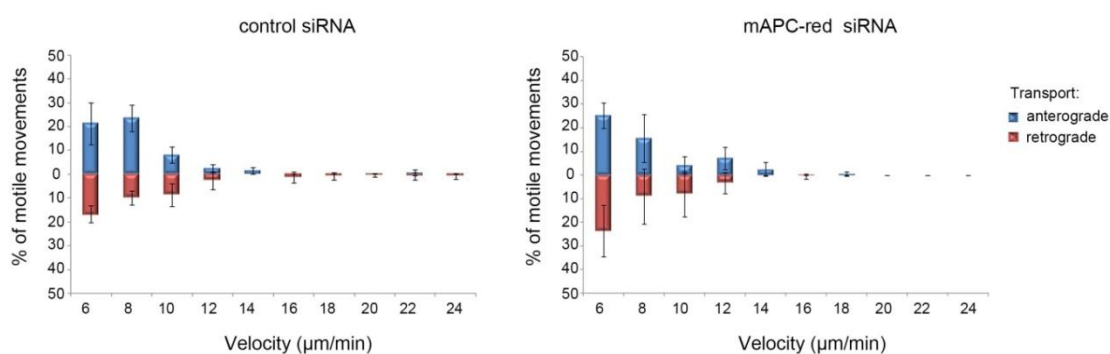
Supplementary Figure S5.1: Mitochondria co-localise with components of the cell cytoskeleton at cell membrane protrusions in HDF1314 cells

Confluent HDF1314 cells were wounded 5 h prior to fixation and counterstained with CMX-Ros Mitotracker, Hoechst and antibodies against proteins involved in cell migration (APC, actin, α -tubulin and IQGAP1). Analysis by immunofluorescence microscopy of cells at the leading edge of the wound indicated colocalisation between mitochondria and the cell migration factors.



Supplementary Figure S5.2: Mitochondrial tracking in sub-confluent NIH 3T3 cells

Sub-confluent cells expressing GFP2-Mito were subject to live cell, time lapse imaging every 5 s for a total of 5 min. Post acquisition, randomly selected mitochondria were manually tracked using ImageJ plug-in MTrackJ. Representative images from ~2 min of mitochondrial tracking are shown (mitochondrial tracks indicated in blue).



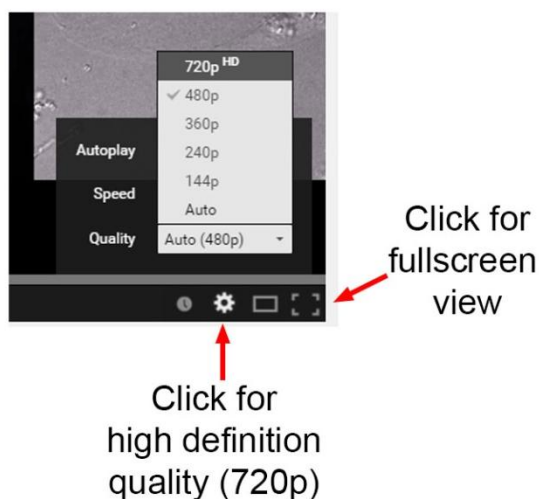
Supplementary Figure S5.3: Loss of APC does not alter mitochondrial transport velocity in 3T3 cells

No difference in transport velocity was observed for cells transfected with either control siRNA or mAPC1-red siRNA when GFP2-labelled mitochondria were tracked using MTrackJ.

5.6 Supplementary Videos

Note for videos

These videos are best viewed full screen, in high definition. The diagram below indicates how to alter these parameters.



Supplementary Video 5.1: NIH 3T3 cell transfected with pGFP2-Mito and control siRNA

Please view Supplementary Video 5.1 by following this link:

<http://tinyurl.com/KateMillsVideo5-1>

NIH 3T3 cells were treated with control siRNA and transfected with a fluorescently tagged mitochondrial marker (pGFP2-Mito) whilst being grown to confluence. Cells were wounded and 5 h later analysed by live cell time lapse imaging, capturing images every 7 s for a total of 5 min, utilising the FITC and DIC channels over 3 focal planes (z-stack) . Post image acquisition, mitochondria were selected at random for tracking manually using the ImageJ plug-in MTrackJ. The middle plane from the z-stack acquired was compressed into an AVI file using ImageJ at a rate of 5 frames per second. The video shows GFP2-mito (FITC) with and without MTrackJ tracking data on the left and middle respectively, as well as the cell periphery and nucleus imaged using white light (DIC) on the right.

Supplementary Video 5.2: NIH 3T3 cell transfected with pGFP2-Mito and mAPC-red siRNA

Please view Supplementary Video 5.2 by following this link:

<http://tinyurl.com/KateMillsVideo5-2>

NIH 3T3 cells were treated with mAPC-red (here labelled mAPC1-555) siRNA and transfected with a fluorescently tagged mitochondrial marker (pGFP2-Mito) whilst being grown to confluence. Cells were wounded and 5 h later analysed by live cell time lapse imaging, capturing images every 7 s for a total of 5 min, utilising the FITC and DIC channels over 3 focal planes (z-stack) . Post image acquisition, mitochondria were selected at random for tracking manually using the ImageJ plug-in MTrackJ. The middle plane from the z-stack acquired was compressed into an AVI file using ImageJ at a rate of 5 frames per second. The video shows GFP2-mito (FITC) with and without MTrackJ tracking data on the left and middle respectively, as well as the cell periphery and nucleus imaged using white light (DIC) on the right.

CHAPTER 6

**APC promotes the
formation of the
mitochondrial transport
complex by stabilising
Miro/Milton**

Previous chapters established a novel role for APC in the initiation of anterograde mitochondrial transport facilitated through its association with the Miro/Milton transport complex (Chapters 3 and 5). APC binds Miro/Milton via its far C-terminal end, supporting the impaired mitochondrial transport observed in CRC cell lines expressing mutant truncated APC (Chapter 4). In this chapter, the mechanism through which APC interacts with the Miro/Milton complex to regulate transport is investigated in more detail. A series of binding studies to investigate interactions between proteins in the mitochondrial transport complex were conducted in U2OS (wild-type APC) and SW480 (APC 1-1337) cell lines. Analysis found that the knockdown of wild-type APC in U2OS cells, or expression of mutant APC in SW480 cells, compromised the binding between Miro and Milton. In comparison, the interaction between Milton and KIF5 remained intact. These results suggest that APC mediates the association between Miro and Milton, potentially acting as a scaffold, whilst C-terminal deletion of APC inhibits complex formation and as a result disrupts mitochondrial transport. Additional experiments indicate that the involvement of APC in mitochondrial transport is independent of calcium modulation.

6.1 Introduction

The anterograde shuttling of mitochondria by the Miro/Milton transport complex is a dynamic pathway essential to maintain the morphology, number and distribution of mitochondria. As previously described (Section 1.3.2.1 and Figure 1.5), the transport complex consists of Miro, a mitochondrial transmembrane protein which attaches the mitochondria to the KIF5 kinesin motor protein through an adaptor protein, Milton (148-150). The roles of mitochondria in ATP production and calcium buffering are very site-specific (see Section 1.3.2.3). As such, fine regulation of mitochondrial distribution is required to respond to the constantly changing conditions within the cell, as reflected by the growing number of signalling pathways shown to directly affect and modify components of the Miro/Milton complex (Section 1.3.2.1). Many of these signalling pathways have yet to be fully elucidated, therefore defining the regulatory role of the novel Miro/Milton partner APC, a known protein scaffold (9, 12) which has a vast array of binding partners, may provide a stepping stone for further investigation.

Post-translational modification is one mode through which the Miro/Milton complex is regulated. For example, following localised increases in glucose concentration, rapid ATP production is induced and mitochondrial transport is reported to be suspended through the O-GlcNAcylation of Milton by the metabolic sensor O-linked N-acetylglucosamine transferase (OGT) (156). Miro is also susceptible to post-translational modification via PINK1/Parkin dependent pathways which inhibit mitochondrial transport by promoting the phosphorylation (152, 157) and subsequent poly-ubiquitination of Miro, which in turn leaves it susceptible to proteasomal degradation (165, 166) (for further details on post translational modifications see Section 1.3.2.1).

A number of well-known signalling pathways and molecules also regulate mitochondrial transport. In particular, intracellular calcium concentrations modulate stability of the Miro/Milton complex, reflecting a role for mitochondria in calcium buffering (see Section 1.3.1.2). When intracellular calcium levels are elevated, calcium binds to a pair of EF-hand motifs located in the middle region of Miro, arresting mitochondrial transport. Whilst the exact mechanism by which this occurs is controversial (Section 1.3.2.1), calcium binding appears to cause a conformational

change in the complex, resulting in dissociation of the mitochondria from microtubules (153, 159). Additionally, hypoxia and the non-canonical Wnt signalling pathways have also been implicated in the regulation of mitochondrial transport through the HUMMR (304) and Alex3 (161, 163) proteins, respectively.

This chapter investigates the mechanism through which APC stimulates anterograde mitochondrial transport, and supports a role for APC as a scaffold in assembly of the Miro/Milton mitochondrial transport complex. It is also shown that despite existing reports in the literature indicating that the association of APC with microtubules is calcium dependent (298), modulation of calcium did not alter the localisation of APC at mitochondria, or its interaction with calcium-sensitive Miro, in the experimental settings used here.

6.2 Methods

6.2.1 Cell culture

U2OS osteosarcoma and SW480 adenocarcinoma cells were cultured in DMEM under standard conditions as outlined in Section 2.2.3. For co-localisation experiments, cells were seeded on glass cover slips in 6 well trays, and for Duolink PLA experiments, cells were seeded in 8-well chamber slides coated with poly-L-lysine. Cells were grown to 70-80% confluence prior to fixation. For live cell experiments, cells were seeded in 2-well chamber slides coated with poly-L-lysine and grown to 70-80% confluence. For western blotting experiments, cells were seeded into 150 cm² flasks for immunoprecipitation assays and 25 cm² flasks for siRNA knockdown experiments. For more details see Section 2.2.3.1. The transfection of plasmids and siRNAs for transient expression or gene silencing in cells is described in Section 2.2.3.4. In Duolink PLA assays utilising GFP-tagged constructs, the amount of plasmid transfected was significantly reduced (for more details see 2.2.8.4).

6.2.2 Drug Treatments

Under sterile conditions, sub-confluent cells were treated with calcimycin (the calcium ionophore A23187, used to increase intracellular calcium) (20 µM) or DMSO (vehicle) for 5 min at 37°C prior to subsequent experimentation as outlined in Section 2.2.3.5 and Table 2.7.

6.2.3 Cell fixation and staining for immunofluorescence microscopy

Cells were seeded for at least 24 h, fixed with methanol-acetone, probed with relevant antibodies and mounted for immunofluorescence microscopy as outlined in Section 2.2.4. If addition of CMX-Ros for detection of mitochondria was required this occurred prior to fixation. Concentrations and any further specifications for all antibodies and dyes used in this chapter are outlined in Table 2.2, Table 2.3 and Table 2.4.

6.2.4 Immunofluorescence cell image acquisition and processing

Slides were analysed using the Olympus IX71 DeltaVision Core deconvolution microscope equipped with a CoolSNAP HQ² camera for general image capture. Images collected were further resolved using SoftWorx deconvolution software. For co-localisation experiments 200 cells were scored over 2 independent experiments. Analysis of Duolink PLA experiments is further described in Section 6.2.8.

6.2.5 Live cell imaging acquisition and analysis

Live cell imaging was performed using the Olympus IX71 DeltaVision system (above) for image capture at 40x. During imaging, U2OS cells stained with Mitotracker CMX-Ros (1:10000, 15 min), treated with either calcimycin or DMSO were maintained at 37°C and 5% CO₂. Cells were imaged every 5 s for 2 min. Confirmation that calcimycin treatment decreased mitochondrial transport was obtained from observation of two independent experiments (n cells: 5-8 per condition). Cell data was obtained between 5 and 15 min post calcimycin or DMSO treatment.

6.2.6 Immunoprecipitation assays

U2OS cells treated with control or APCd siRNA and untreated SW480 cells were collected and lysed with RIPA buffer as described in Section 2.2.9.1. Immunoprecipitation was carried out using Miro-1 (pAb, Sigma-Aldrich), Milton-2 (pAb, Sigma-Aldrich) and IgGr (pAb, Sigma-Aldrich) antibodies to pull-down target proteins prior to samples being subjected to SDS-PAGE and western blot analysis as described in Section 2.2.10. Immunoprecipitation experiments in U2OS cells were performed twice, whilst experiments in SW480 cells were performed once.

6.2.7 Western blot analysis

Cells were collected, lysed using RIPA buffer and processed as described in Section 2.2.9.1. Samples (immunoprecipitates or ~30µg total cell lysate) were separated by SDS-PAGE using 5% (for detection of APC) or 7.5% acrylamide gels, and transferred onto a nitrocellulose membrane (see Sections 2.2.9.3-2.2.9.6). Western blots were

probed as outlined in Section 2.2.9.7, using primary antibodies as per the figure legends. Dilutions for these antibodies and subsequent secondary antibodies are outlined in Table 2.2 and Table 2.3, respectively. Immunoblots in this chapter were developed using the BioRad ChemiDoc Imaging System and ECL (see Section 2.2.9.8).

6.2.8 Duolink Proximity Ligation Assay (PLA)

Duolink PLA experiments in this chapter employed primary antibodies against KIF5 (mAb, Millipore), GFP (mAb, Roche), Miro-1 (pAb, Sigma-Aldrich), Milton-2 (pAb, Sigma-Aldrich) and APC (mAb, Merck) at concentrations outlined in Table 2.2 to visualise interactions between KIF5/Milton, APC/Miro and GFP-tagged constructs/Miro. Following image capture, PLA signals were quantified manually, by scoring the number of PLA signals per cell using a DIC channel overlay to determine the boundaries of each cell (Section 2.2.8.6). Duolink PLA experiments were performed twice and the number of cells scored is outlined in the supplementary figures for each experiment.

Duolink PLA in cells expressing GFP Miro-1 constructs were compared to control cells expressing GFP alone as a frame of reference for background signal. For these experiments, only cells expressing a modest level of the transfected plasmid were scored to minimise artefacts caused by overexpression (Section 2.2.8.4). Low levels of transfection were more readily detected by counterstaining Duolink experiments with GFP (mAb) and the appropriate secondary antibody (as described in Section 2.2.8.5) following PLA.

6.2.9 Graphs and statistics

All graphs and statistics used to display and analyse results in this chapter are outlined in Section 2.2.11.

6.3 Results

APC has been reported to act as a scaffold in numerous protein complexes throughout the cell (12), including the well-known multi-protein β -catenin destruction complex (9). Previous chapters indicate that APC regulates anterograde mitochondrial transport through an interaction with the Miro/Milton complex, which is lost upon CRC-associated APC mutations. Whilst it was shown that APC associates with the Miro/Milton complex through its C-terminal sequence, the part of the complex through which APC exerts its effects is unknown. To determine whether APC has a role in stabilising components of the Miro/Milton mitochondrial transport complex, two simple models were tested: (1) APC links Milton to the kinesin KIF5 (Figure 6.1A), and (2) APC stabilises binding of Milton to Miro (Figure 6.2A).

6.3.1 Full-length APC is not required for the ability of Milton to interact with KIF5

To assess the first model, which proposes that the APC C-terminus links Milton to KIF5 to facilitate mitochondrial transport (Figure 6.1A), Duolink PLA was used to assess the Milton/KIF5 interaction in U2OS (wild-type APC) and SW480 (APC 1-1337) cell lines. In both cell lines, a positive PLA signal above background level was observed for Milton/KIF5 (PLA signal/cell: U2OS = 10.7, SW480 = 7.1) (Figure 6.1B,C, Figure S6.1), indicating that binding was retained between the two proteins when APC C-terminal sequences were lost. In both cell lines, Milton/KIF complexes locate correctly at the mitochondria as shown by Duolink PLA and counterstained for mitochondria (U2OS = 41%, SW480 = 37%) (Figure 6.1D,E). Thus, the ability of Milton/KIF5 complexes to form at mitochondria does not depend on expression of full-length APC. These findings do not support the model proposed in Figure 6.1A, and suggest that CRC-related APC mutations have no bearing on the KIF5/Miro interaction.

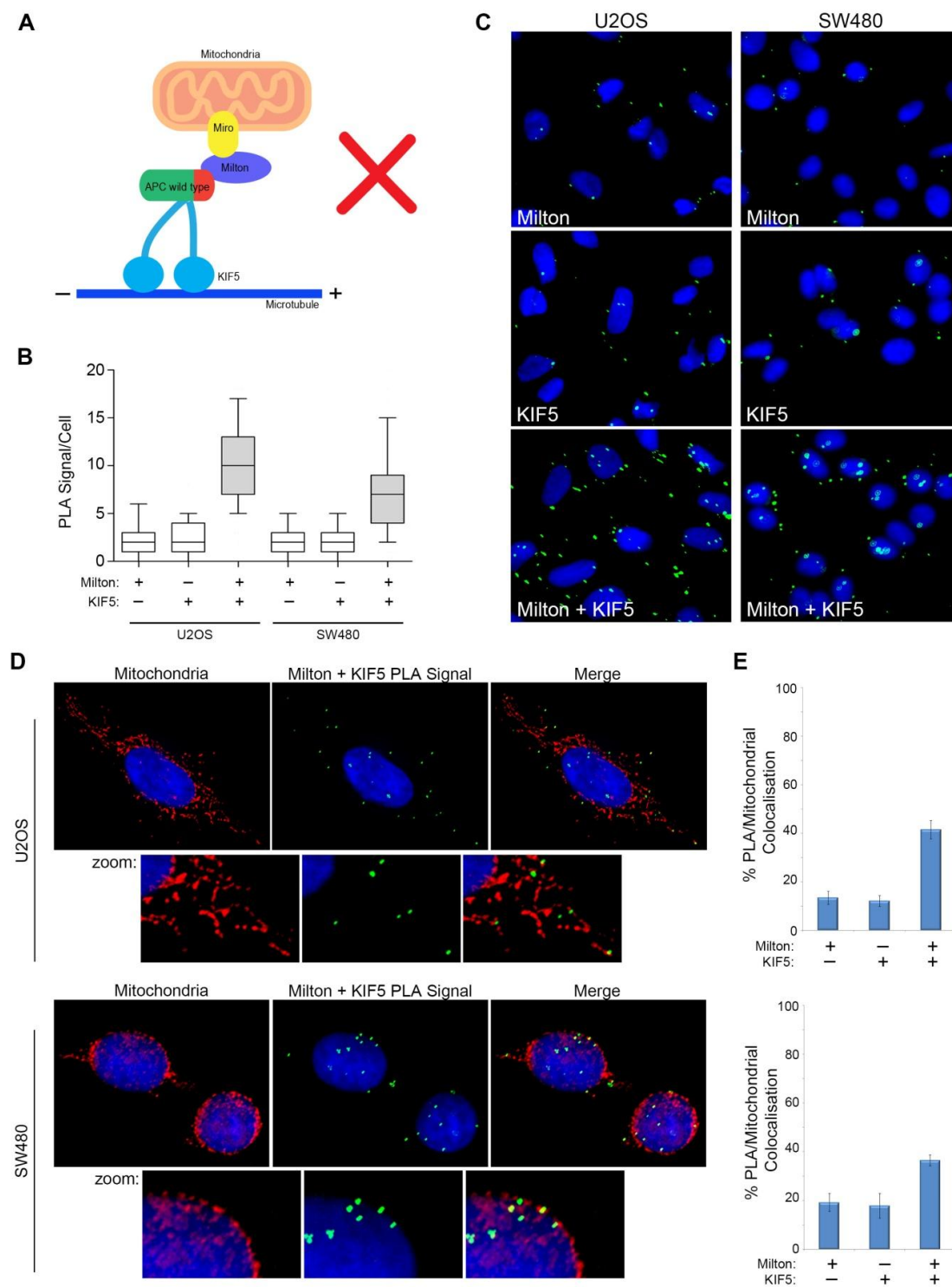


Figure legend over page.

Figure 6.1: Evidence that APC is not required for the ability of Milton to interact with KIF5

(A) Schematic detailing the model to be tested, wherein the APC C-terminus is required for optimal interaction between Milton and KIF5. (B-C) Duolink PLA was utilised to detect interactions between KIF5 and Milton in U2OS and SW480 cell lines. Scoring analysis of cells by immunofluorescence microscopy revealed a positive interaction between KIF5 and Milton in both cell lines as observed in the (B) box-and-whisker plot and (C) representative images. (D-E) KIF5/Milton PLA signals were analysed by immunofluorescence microscopy for mitochondrial colocalisation in cells counterstained with Mitotracker CMX-Ros, as observed in the (D) representative images and (E) scored in the bar graphs (% mean \pm S.D). Milton/KIF5 PLA signals localised well at mitochondria in U2OS and SW480 cells. This data argues against the proposed model and reveals that Milton binding to KIF5 does not require full-length APC.

6.3.2 Loss of APC diminishes the GFP Miro-1/Milton interaction

The next model tested (Figure 6.2A), proposes that APC facilitates the association of Milton and Miro. Duolink PLA was performed in U2OS cells expressing low to moderate levels of GFP or GFP Miro-1, treated with either control siRNA or APC siRNA (Figure 6.2B-D, and Supplementary Figure S6.3 for validation of APC knockdown). Antibodies against GFP and Milton were used to analyse cells expressing GFP Miro-1 for *in situ* binding with endogenous Milton. As expected, in control cells the mean number of GFP-Miro / Milton PLA signals per cell was ~3.1 fold higher than cells expressing GFP alone. More intriguing however, was the finding that when treated with APC siRNA, the number of GFP-Miro / Milton PLA signals per cell was only ~1.3 fold higher than GFP control (Figure 6.2B, Supplementary Figure S6.3). When samples were normalised and background subtracted, the data indicated that loss of APC reduced the number of detectable Miro/Milton complexes by ~84% (Figure 6.2C). Thus APC may have a role in mediating the interaction between Miro and Milton. These Duolink results were confirmed by immunoprecipitation assays in U2OS cells, where the reciprocal pull down of Miro and Milton by their respective antibodies was diminished in cells treated with APC siRNA (Supplementary Figure S6.4). These results provide supporting evidence for the model outlined in Figure 6.2A, which suggests that APC stabilises the interaction between Miro and Milton, possibly by acting as a scaffold, or by post-translational modification of Miro or Milton.

During immunoprecipitation experiments it was also noted that in control cells, the 96 kDa isoform of Milton was preferentially pulled down by the Miro antibody, indicating that this is the form which most often interacts with Miro. Furthermore, the higher molecular weight form of Miro, previously observed to interact with APC (Figures S3.4 and S4.2) and speculated to be post-translationally modified was preferentially pulled down by the Milton antibody, suggesting that this form also binds Milton. This is discussed further in Chapter 7 (Section 7.1.1).

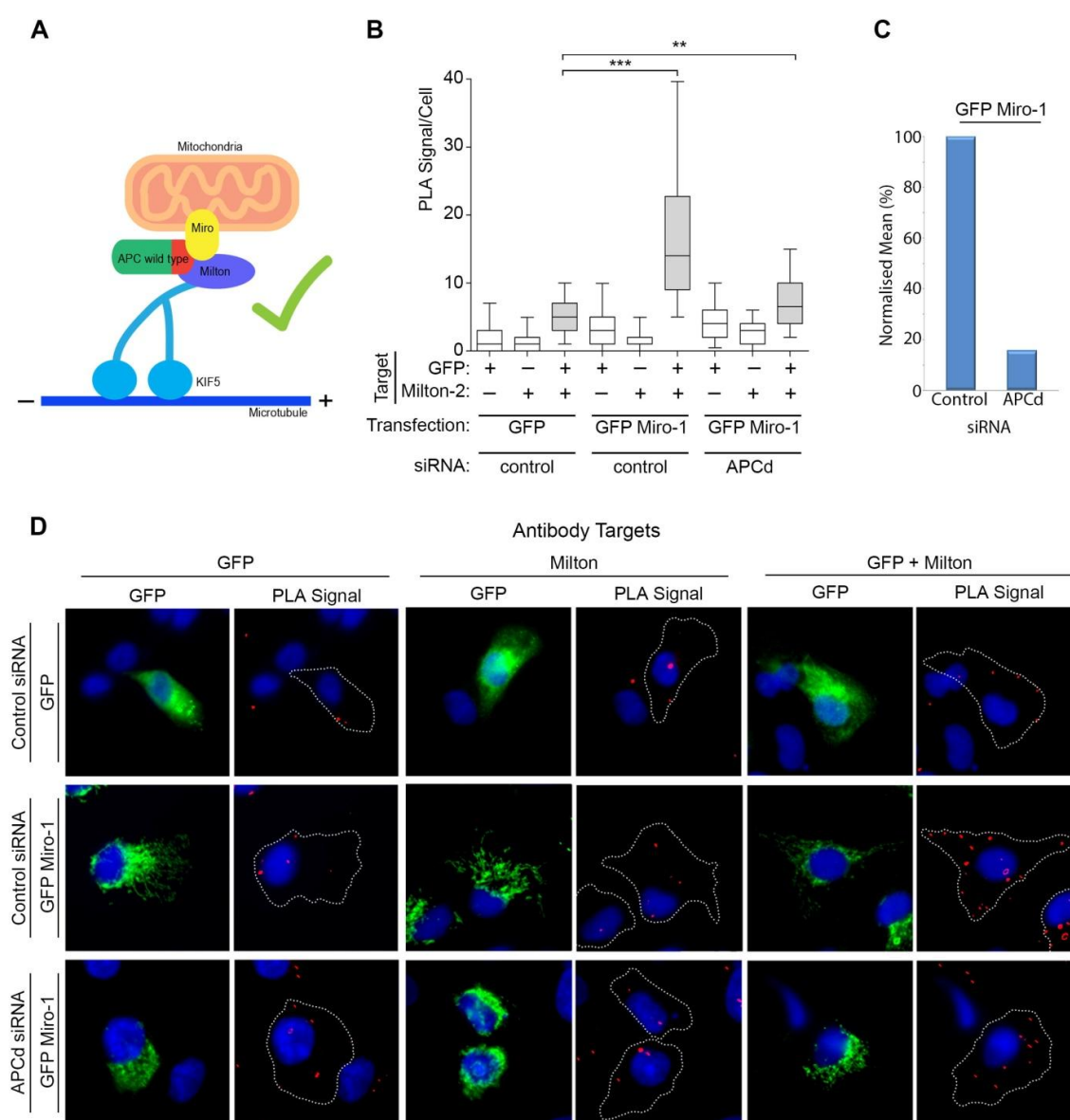


Figure legend over page.

Figure 6.2: Loss of APC disrupts the interaction between GFP Miro-1 and Milton in U2OS cells by Duolink

(A) Schematic detailing the model to be tested wherein APC acts as a scaffold between Miro and Milton via a C-terminal interaction. (B-D) U2OS cells treated with either control or APC siRNAs (APCd), and transfected with pGFP or pGFP Miro-1 were subjected to Duolink PLA using antibodies against GFP (mAb) and Milton. Moderately transfected cells were selected for analysis by immunofluorescence microscopy, where scoring of PLA signals revealed a positive interaction between GFP Miro-1 and Milton, which as shown by the (B) box-and-whisker plot was significantly reduced upon APC knockdown. Significant differences relative to GFP control, as determined using the Mann-Whitney U-test, are indicated (**, $P < 0.01$; ***, $P < 0.001$). (C) This reduction is highlighted in the bar graph where the PLA/Signal per cell for GFP Miro-1/Milton interactions was subtracted from GFP/Milton background and normalised. This supports the proposed model. (D) Representative images are shown.

6.3.3 APC truncation correlates with loss of the Miro/Milton interaction

As loss of APC was shown to disrupt the interaction between Miro and Milton, investigation was undertaken to see if deletion of the Miro/Milton binding region of APC, by C-terminal truncation, had a similar effect (see Figure 6.3A). Duolink PLA assays were performed in SW480 (APC 1-1337) cells expressing low to moderate levels of GFP or GFP Miro-1. Analysis of GFP/Milton interactions in GFP Miro-1 expressing cells revealed no PLA signal above GFP background (Figure 6.3C-D, Supplementary Figure S6.4), indicating that ectopic Miro did not interact with endogenous Milton.

This negative interaction between ectopic Miro and endogenous Milton was also verified with endogenous Miro in SW480 cells by immunoprecipitation assays. The Miro antibody was unable to pull down Milton, and the Milton antibody was unable to pull down Miro, even following long exposure times (Supplementary Figure S6.5), despite successful pull-down of their respective proteins (Figure 6.3B). These results suggest that APC truncation disrupts the Miro/Milton interaction, which could explain the disrupted mitochondrial transport observed in SW480 and other mutant APC cell lines. This supports the notion that the APC C-terminal region is required for APC to mediate an interaction between Miro and Milton.

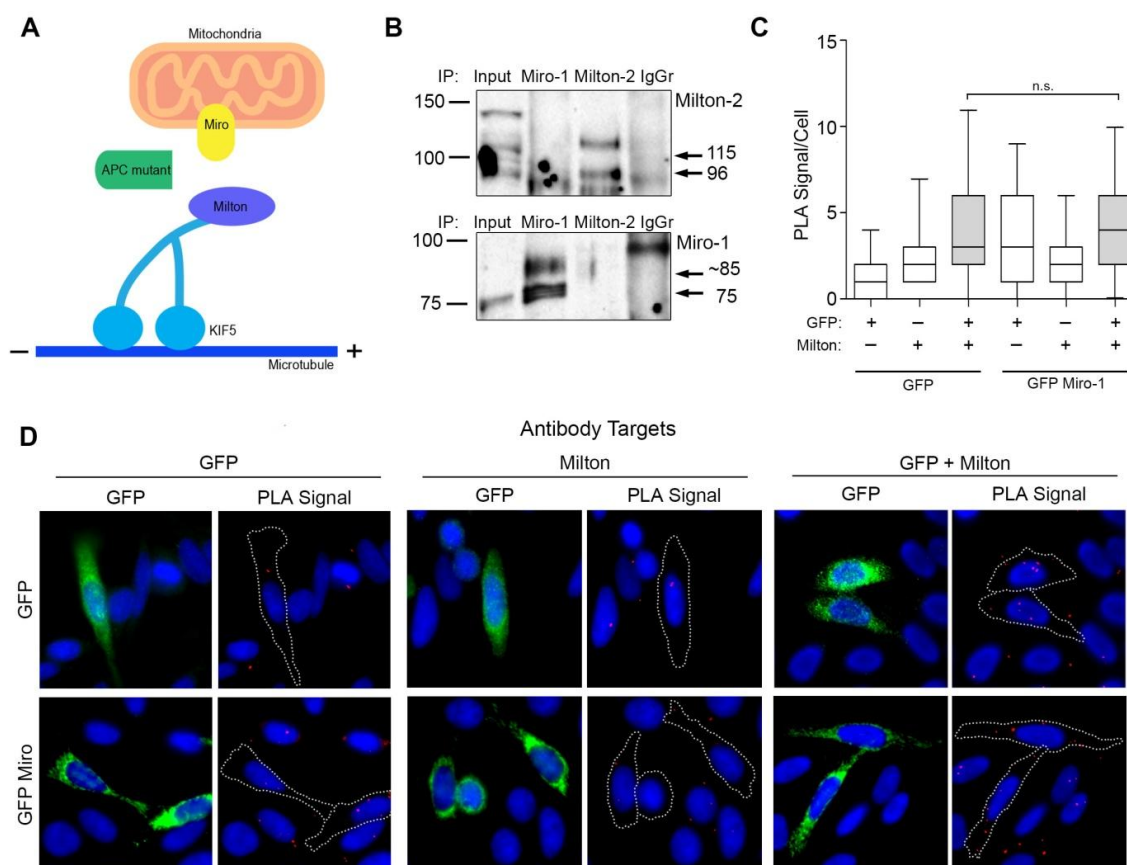


Figure 6.3: Miro does not interact with Milton in SW480 mutant APC cells

(A) Schematic detailing the model to be tested, wherein C-terminal APC truncation disrupts the interaction between Miro and Milton. (B) SW480 cells were immunoprecipitated by antibodies against Miro and Milton and analysed by western blot. Detection using the Miro and Milton antibodies revealed that Miro was unable to pull down Milton, and Milton was unable to pull down Miro. (C-D) Cells transfected with pGFP or pGFP Miro-1 were subjected to Duolink PLA using antibodies against GFP (mAb) and Milton. Moderately transfected cells were selected for analysis by immunofluorescence microscopy, where scoring of PLA signal revealed that the interaction between GFP Miro-1 and Milton did not produce a signal above GFP background level. This is observed in the (C) box-and-whisker plot and (D) representative images and supports the proposed model. Significant differences, determined using Mann-Whitney U-test, relative to GFP control are indicated (n.s., not significant).

6.3.4 Loss of APC does not alter the expression or mitochondrial localisation of Miro or Milton

The current proposed model (Figure 6.2A) supported by preliminary data (Sections 6.3.2 and 6.3.3) suggests that APC facilitates the interaction between Miro and Milton, which is lost when APC is silenced. Of course the Miro/Milton complex might also be diminished by loss of APC if APC regulates the expression of Miro or Milton, possibly by protecting the complex from their reported ubiquitination and degradation via the PINK1/Parkin pathway (165, 166). To exclude this possibility, western blot analysis of total cell extracts was performed, however the experiment revealed no changes in overall protein expression of Miro/Milton following the loss of APC (Figure 6.4A). This was confirmed by immunofluorescence microscopy, where the intensity of Miro and Milton staining appeared unaltered after APC siRNA treatment. Furthermore, the mitochondrial localisation of both proteins also remained unchanged after APC knockdown (Figure 6.4B-D), indicating that disruption of the Miro/Milton complex was not simply due to an APC-dependent relocalisation of these proteins away from mitochondria.

6.3.5 Calcimycin treatment inhibits mitochondrial transport without altering the localisation of Miro, Milton and APC at the mitochondria

Increased intracellular calcium has been widely reported to contribute to the cessation of mitochondrial transport by binding the EF-hands of Miro and, in turn, altering the structure of the Miro/Milton mitochondrial transport complex (153, 159). As studies in the literature are conflicting regarding how these structural changes affect transport, calcium regulation of APC in the context of the Miro/Milton transport complex was investigated.

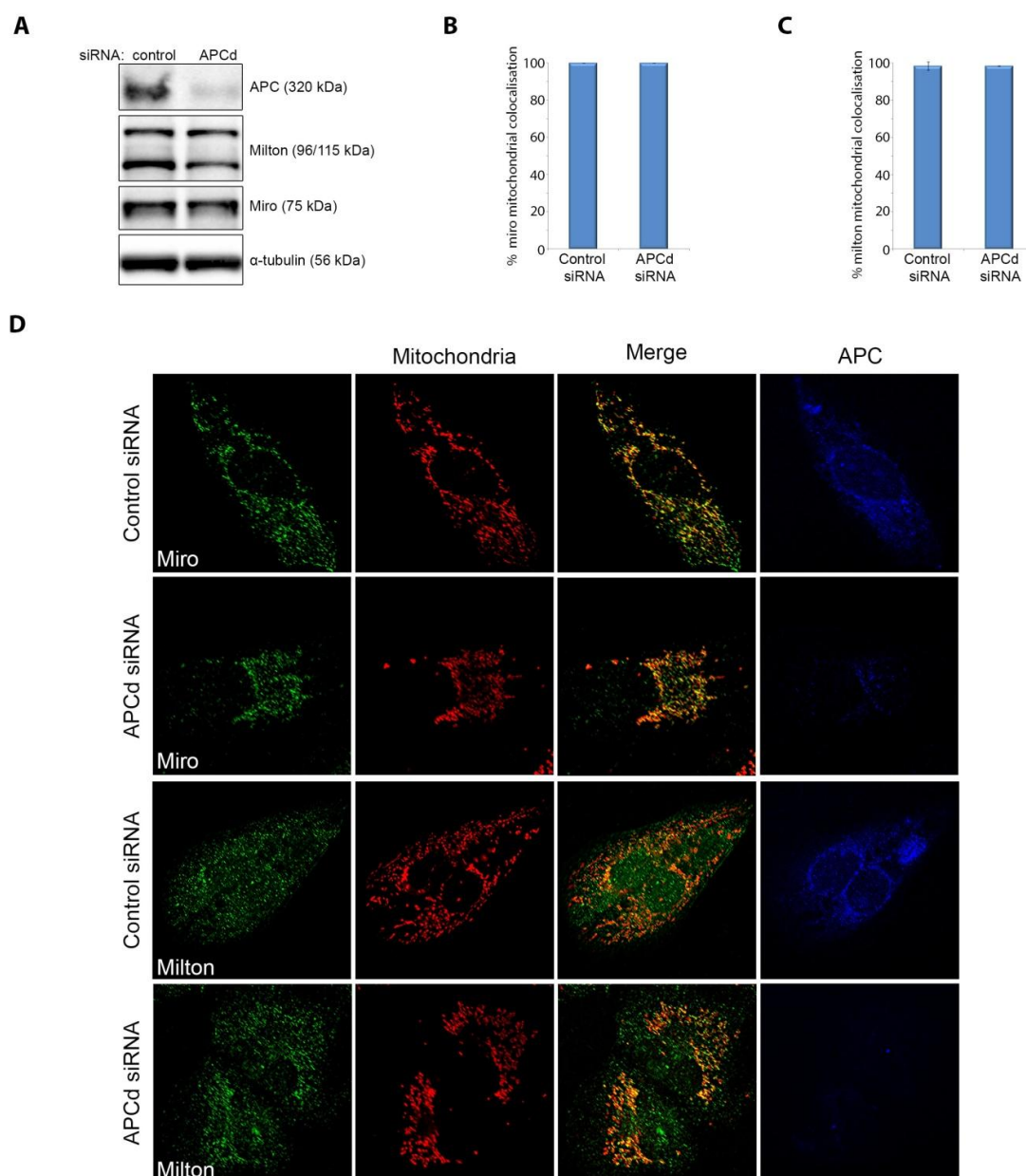


Figure 6.4: Loss of APC does not alter mitochondrial localisation or expression of Miro or Milton in U2OS cells

(A) Cells treated with control or APC (APCd) siRNA were subjected to western blot analysis, APC knockdown was confirmed and further detection of Milton and Miro revealed no changes in their expression levels following loss of APC. α -tubulin was used as a loading control. (B-D) Sub-confluent cells treated with control or APC (APCd) siRNA were stained with CMX-Ros (mitochondria) and APC (Ab7) and probed with antibodies against Miro or Milton. Cells were analysed by immunofluorescence microscopy where scoring revealed no changes in (B) Miro or (C) Milton mitochondrial localisation following loss of APC (% mean \pm S.D). (D) Representative images are shown.

The calcium-dependent arrest of mitochondrial transport has previously been observed *in vitro* following treatment with the calcium ionophore calcimycin (153), which acts to increase intracellular calcium. To confirm this observation under conditions utilised in this thesis, sub-confluent U2OS cells stained with Mitotracker CMX-Ros were treated for 5 minutes with calcimycin before being subjected to timelapse imaging by DeltaVision live cell microscopy over a 2 minute period. Treatment with 20 μM calcimycin was observed to be sufficient to stall mitochondrial transport (Figure 6.5) without disrupting the microtubule network, indicating that this cessation of mitochondrial transport was not a secondary effect of microtubule depolymerisation (see fixed cells Figure 6.7A).

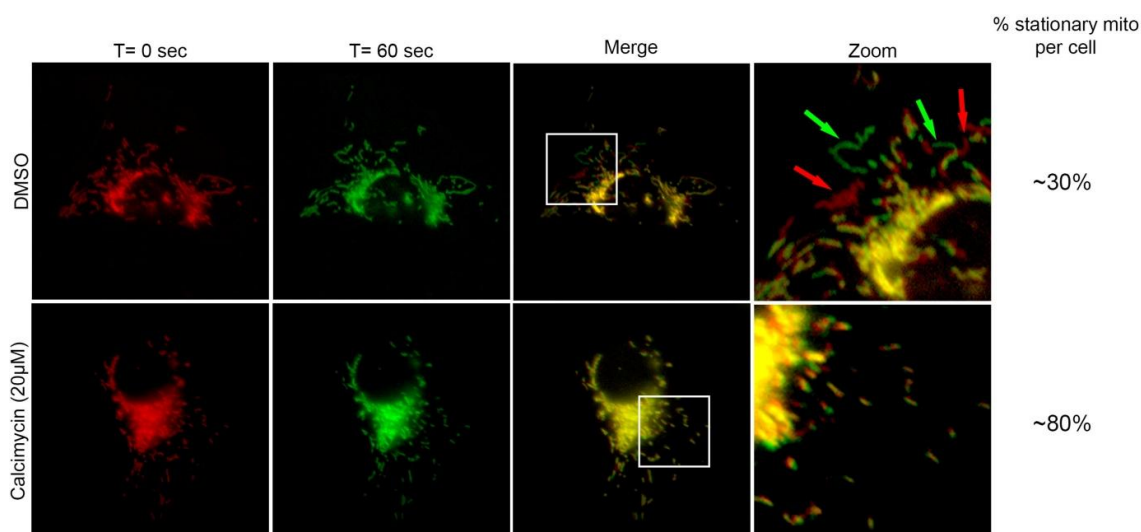


Figure 6.5: Treatment with calcimycin (20 μM) inhibits mitochondrial transport.

U2OS cells stained with Mitotracker CMX-Ros were treated with DMSO or calcimycin (20 μM) for 5 min prior to live cell timelapse imaging. Images were captured every 5 s for a total of 2 min. For each treatment, representative cell images show mitochondria at two time points 1 min apart. Mitochondria that remained stationary over this time point appear yellow in the merged images. Arrows in DMSO zoom panel indicate examples of motile mitochondria from T=0 s (red) to T=60 s (green).

In line with current literature, the mitochondrial localisation of Miro and Milton remained unchanged following treatment with calcimycin (Figure 6.6A-C) (153). Mitochondrial localisation of APC also remained unchanged (Figure 6.6A,D) indicating that relocalisation of these transport proteins away from the mitochondria is not responsible for inhibition of mitochondrial transport.

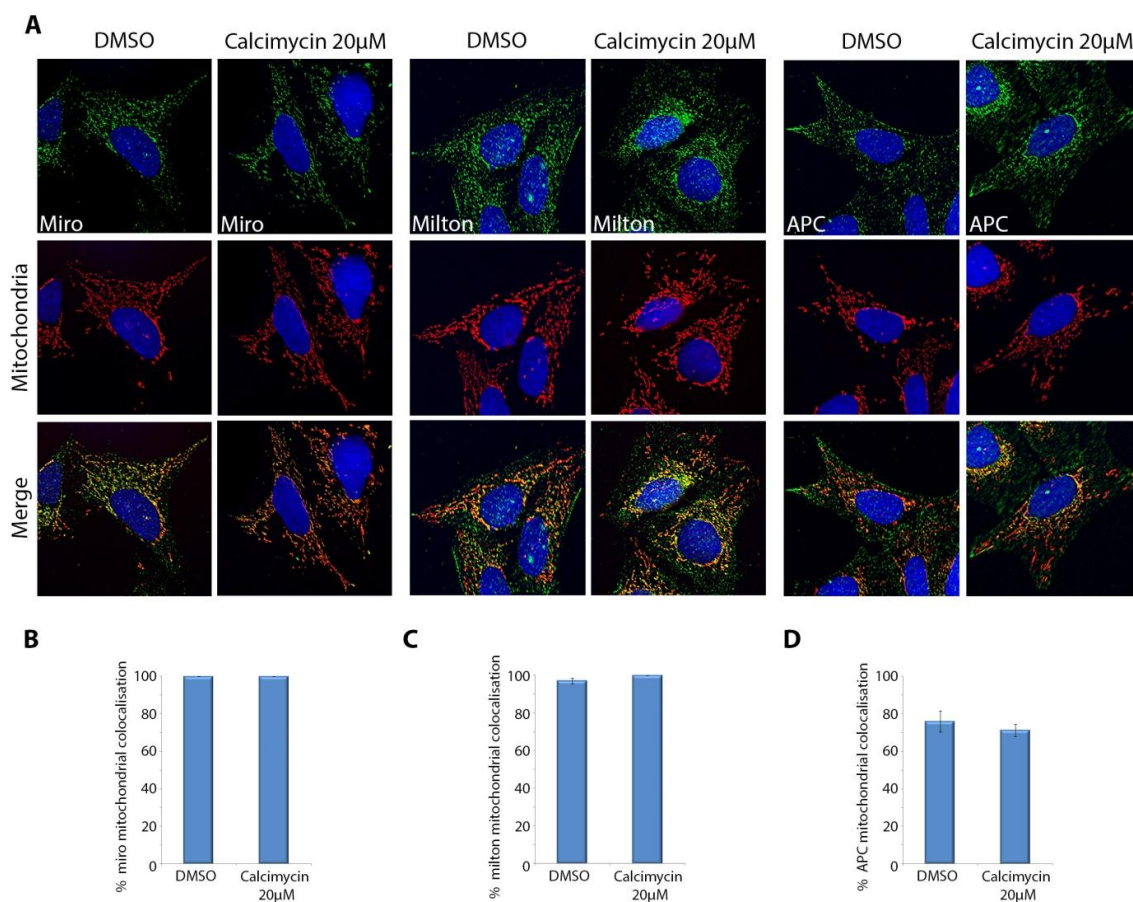


Figure 6.6: Calcimycin treatment does not alter mitochondrial localisation or expression of Miro, Milton or APC in U2OS cells

(A-D) Sub-confluent cells treated with DMSO or calcimycin (20 μ M) were stained with CMX-Ros (mitochondria) and Hoechst (blue) and probed with antibodies against Miro, Milton or APC (H290). Analysis by (A) immunofluorescence microscopy revealed no changes in (B) Miro, (C) Milton or (D) APC mitochondrial localisation following calcimycin treatment (% mean \pm S.D).

6.3.6 Calcimycin treatment does not alter APC localisation at microtubule clusters

Given the calcium-sensitivity of the Miro/Milton transport complex, it is intriguing that APC has also been reported to be calcium regulated. A previous report (298) suggested that under increased intracellular calcium concentrations induced by ionomycin (1 μ M) treatment, APC dissociates from microtubule clusters. This is interesting as it is possible that this detachment of APC from microtubules could offer a mechanism by which mitochondrial transport is stalled when intracellular calcium concentrations rise,

particularly if APC attachment to microtubules is required for transport. In U2OS cells however, calcium dependent APC dissociation from microtubule clusters could not be verified following treatment with calcimycin at concentrations sufficient to disrupt mitochondrial transport (20 μ M, Figure 6.5). It is possible that the calcium dependent APC re-localisation observed by Togo (298) is cell type specific, or that the intracellular levels of calcium induced by treatment with 20 μ M calcimycin is not sufficient to match those induced by ionomycin treatment. This result does however show that APC dissociation from microtubules is not a contributing factor to calcium regulated cessation of mitochondrial transport.

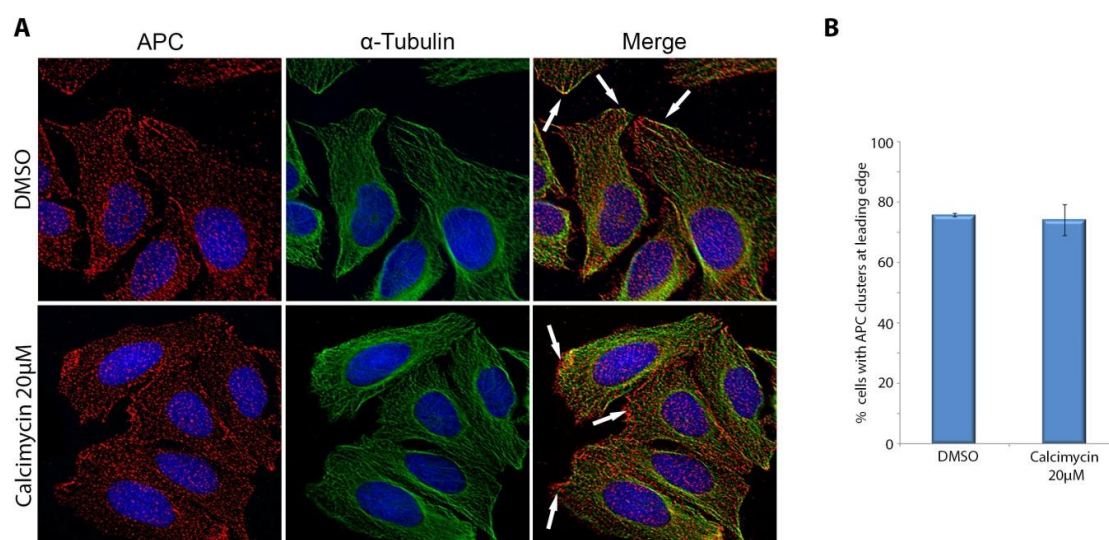


Figure 6.7: Calcimycin treatment does not alter APC localisation at microtubule clusters in U2OS cells

(A-B) Sub-confluent cells treated with DMSO or calcimycin (20 μ M) were probed with antibodies against α -tubulin and APC (H290) and stained with Hoechst. Analysis by immunofluorescence microscopy revealed no changes in APC localisation at microtubule clusters following calcimycin treatment as indicated by the arrows in the (A) representative images, and the (B) scoring data (% mean \pm S.D).

6.3.7 Calcimycin treatment does not alter the APC-Miro interaction

Although findings in this chapter indicate that the localisation of APC at microtubules and mitochondria is not calcium dependent (Figure 6.6 and Figure 6.7), this does not exclude the possibility that the interaction between APC and the calcium sensitive Miro is altered following spikes in intracellular calcium. In fact, the recently discovered Wnt

signalling protein Alex3, which also interacts with the mitochondrial transport complex, was reported to dissociate from Miro following increased intracellular calcium levels (161, 163).

To determine if APC binding to Miro was regulated in a similar calcium-dependent manner as reported for Alex3, Duolink PLA was used to assess interactions between APC and Miro in U2OS cells treated with DMSO or calcimycin (Figure 6.8; Figure S6.6). The APC/Miro interaction produced positive PLA signals, which were almost identical in cells treated with DMSO or calcimycin. This finding indicates that unlike Alex3, the APC/Miro interaction is not calcium-dependent, and therefore it is unlikely to be involved in the structural alterations observed following the calcium-induced stalling of mitochondrial transport.

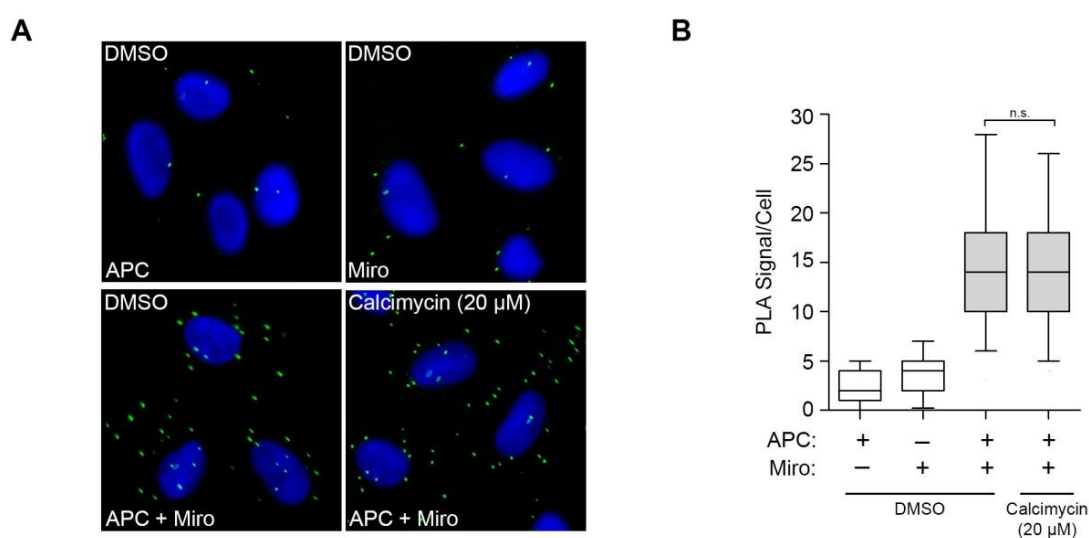


Figure 6.8: Calcimycin treatment does not alter the APC-Miro interaction by Duolink

(A-B) U2OS cells treated with DMSO or calcimycin (20μM) were subject to Duolink PLA using antibodies against APC (Ab7) and Miro. Scoring by immunofluorescence microscopy revealed that calcimycin treatment did not significantly alter the interaction between APC and Miro as shown in the (A) representative images and the (B) box-and-whisker plot. Significant differences relative to DMSO control, as determined using the Mann-Whitney U-test, are indicated (n.s., not significant).

6.4 Discussion

Data from the previous chapters describes a novel role for APC in anterograde mitochondrial transport through a C-terminal interaction with the Miro/Milton mitochondrial transport complex, which is lost in APC mutant CRC cell lines and proposed to lead to disrupted mitochondrial distribution. Whilst it was determined that APC was essential in the initiation of mitochondrial transport, the mechanism behind this process was previously unclear. Preliminary findings in this chapter indicate a role for APC in mediating or stabilising the interaction between Miro and Milton (6.4.1), and suggest that the influence APC has on the mitochondrial complex is independent of calcium regulation (6.4.2).

6.4.1 Evidence to support a role for APC in regulating the interaction between Miro and Milton

Preliminary assessments in this chapter on the influence of APC on components of the Miro/Milton complex, and their association with mitochondria and each other, suggest that APC may somehow mediate the interaction between Miro and Milton. The primary evidence for this hypothesis is the finding that both APC knockdown in U2OS cells and APC truncation in SW480 cells disrupt the association between Miro and Milton, as shown by both Duolink PLA and immunoprecipitation assays (Figure 6.2, Figure 6.3, Supplementary Figure S6.3). In contrast, APC truncation did not alter the association between Milton and KIF5 by Duolink in SW480 cells (Figure 6.1), suggesting that unlike Miro/Milton this interaction complex is independent of APC. Furthermore, the Milton/KIF5 PLA signal retained mitochondrial localisation (Figure 6.1D,E) in SW480 cells, a finding that is somewhat surprising, given that Miro is thought to be the primary mitochondrial anchor in the Miro/Milton complex. Milton has previously been reported to localise to mitochondria independent of Miro (149), so it is possible that the Milton/KIF5 complexes localise to the mitochondria, even without transport functionality. This is supported by the finding that mitochondrial localisation of Milton is also retained following the loss of APC in U2OS cells (Figure 6.4C-D).

The Miro/Milton interaction has been evolutionarily conserved from *Drosophila* to humans, and the binding sites have been mapped to the N-terminal regions for both

proteins (149, 150, see Figure 6.9A). It is less clear from the literature if these two proteins interact directly and without the assistance of other co-factors. Findings from this chapter identify APC as one potential co-factor important for promoting the Miro/Milton interaction by acting as a scaffold to tether the complex together and assist in its assembly (Figure 6.9B). This is not unreasonable given the known roles of APC as a scaffold in numerous other cellular pathways including the formation of the β -catenin destruction complex (9, 12). Given that there is no published evidence of direct binding between Miro and Milton it is possible that APC performs an adaptor role, acting as a bridge to link the two proteins (Figure 6.9C). Scaffold proteins have also been known to recruit partner proteins to specific regions of the cell. Whilst, the mitochondrial localisation of Miro and Milton following loss of APC remains unchanged, it remains possible that APC recruits additional co-factors yet to be identified to assist in complex formation.

APC could also mediate the Miro/Milton interaction by recruiting an enzyme that post-translationally modifies Miro or Milton to influence their association (Figure 6.9D). It was shown in previous chapters that APC binds to a higher molecular weight form of Miro, speculated to be post-translationally modified (discussed in Section 7.1.1). Although findings in this chapter indicate that Milton also preferentially binds a higher molecular weight form of Miro (Supplementary Figure S6.4), immunoprecipitation assays show a strong pull down of this same band by the Miro antibody in SW480 mutant APC cells (Figure 6.3B), suggesting that this particular potential modification of Miro may not be APC mediated. These findings do not exclude the possibility that APC mediates other post-translational modifications by regulating previously defined modification enzymes like PINK1/Parkin and OGT (for more details see Section 6.4.1.1), or through an entirely new pathway made possible given APC's huge range of binding partners like GSK-3 β . Future biochemical experiments are required to delineate the specific forms of Miro that bind Milton and APC.

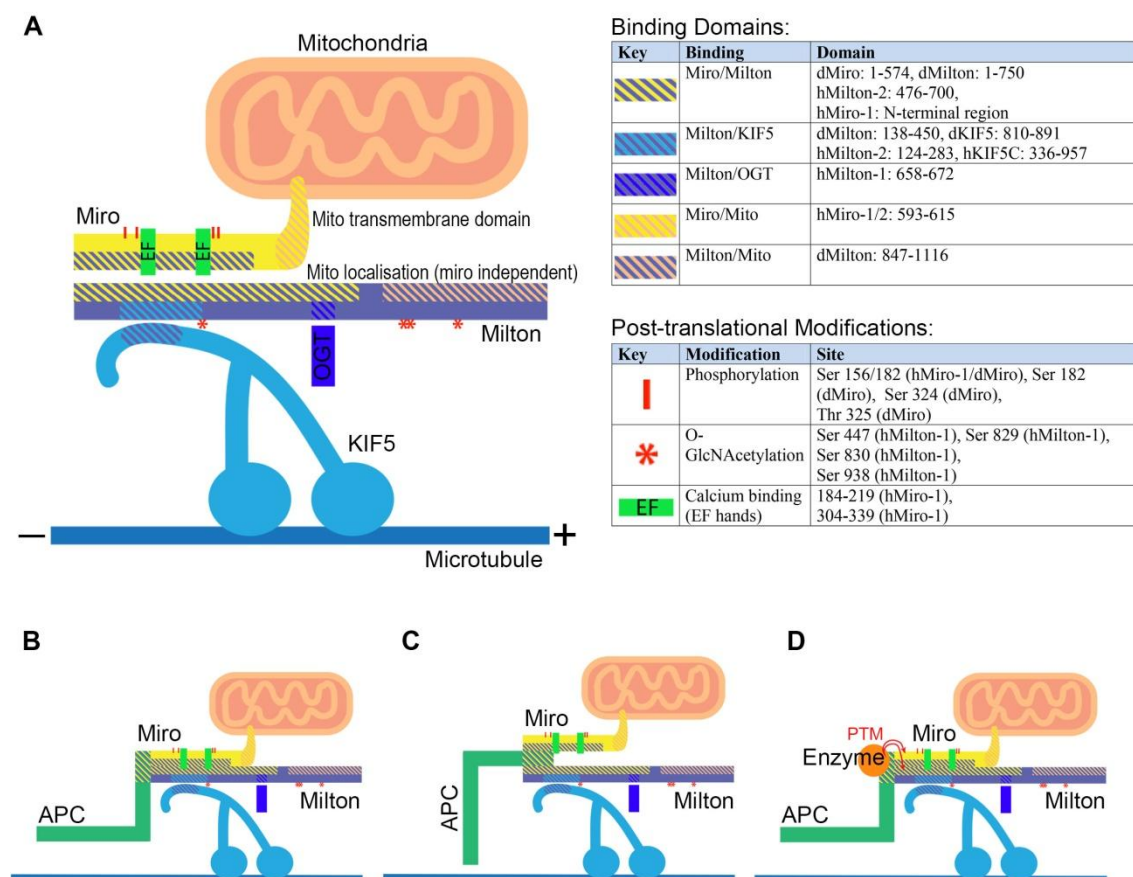


Figure 6.9: The Miro/Milton mitochondrial transport complex

(A) A schematic that outlines sites of protein interaction and post-translational modification in the Miro/Milton complex, as currently defined in the literature (see Figure 1.5A for reference details). (B-D) Evidence from this chapter suggests that APC is required to facilitate the Miro/Milton interaction, possibly by acting as a scaffold (B) or adaptor (C), or by recruiting an enzyme to post-translationally modify the complex (D). APC may also act by recruiting additional co-factors like bridging molecules, or enzymes for post-translational modification (PTM) yet to be identified.

This investigation into the role of APC in the Miro/Milton complex is only in its preliminary stage, and further experimentation is needed to elucidate, which, if any, of the mechanisms presented (and outlined in Figure 6.9B-D) match APC's functionality. This could include determining in greater detail the binding of APC, Miro and Milton by using a purified protein system to determine if the APC/Milton, APC/Miro and Miro/Milton interactions are direct, or indirect. In mutant APC SW480 cells where Miro/Milton binding is defective, full-length ectopic APC could be overexpressed to determine if, as predicted, the Miro/Milton association could be re-established. In addition, to determine if APC could mediate any post-translational modifications, mass

spectrometry could be performed on Miro/Milton and compared between cell lines with full length and mutant APC.

6.4.1.1 Possible involvement of APC in Miro/Milton post-translational modification pathways

As described previously (Section 1.3.2.1), numerous studies in the literature indicate that the mitochondrial transport complex is subject to post translational modification though the PINK1/Parkin mediated phosphorylation and ubiquitination of Miro (152, 157, 165) and the OGT regulated O-GlcNAcylation of Milton (156). APC regulation of Miro through the PINK1/Parkin pathway is unlikely despite reports that both PINK1 and Parkin are abnormally expressed in colon cancer cell lines (307), as these modifications modulate mitochondrial transport by marking Miro for proteosomal degradation. As shown in Figure 6.4, protein expression levels of Miro are unaltered following loss of APC by western blot analysis and immunofluorescence microscopy.

Like PINK1 and Parkin, it was also proposed that increased rates of O-GlcNAcylation and OGT expression are markers for carcinogenesis (reviewed in 308), particularly colon cancer (309), a finding attributed to the O-GlcNAc modification of a number of oncogenic factors including p56, MYC, NF κ B, and β -catenin. Interestingly, targeting OGA (O-GlcNAcase), the enzyme responsible for de-O-GlcNAcylation which is also reported to be upregulated in CRC, has been shown to attenuate carcinogenesis in APC (Min/+) mice in a mechanism independent of Wnt signalling (310). It is unclear if these findings impact on the reported inhibition of mitochondrial transport following the O-GlcNAcylation of Milton in the presence of increased intracellular glucose (156), particularly given the highly glycolytic nature of CRC cells. This challenge is further compounded since the pathways of O-GlcNAcylation and OGT/OGA in cancer are a relatively new field, and thus poorly understood. Further investigation is required to determine if APC has any role in regulating O-GlcNAcylation, or recruiting/inhibiting OGT/OGA to Milton.

6.4.2 APC regulation of the Miro/Milton mitochondrial transport complex is not calcium dependent.

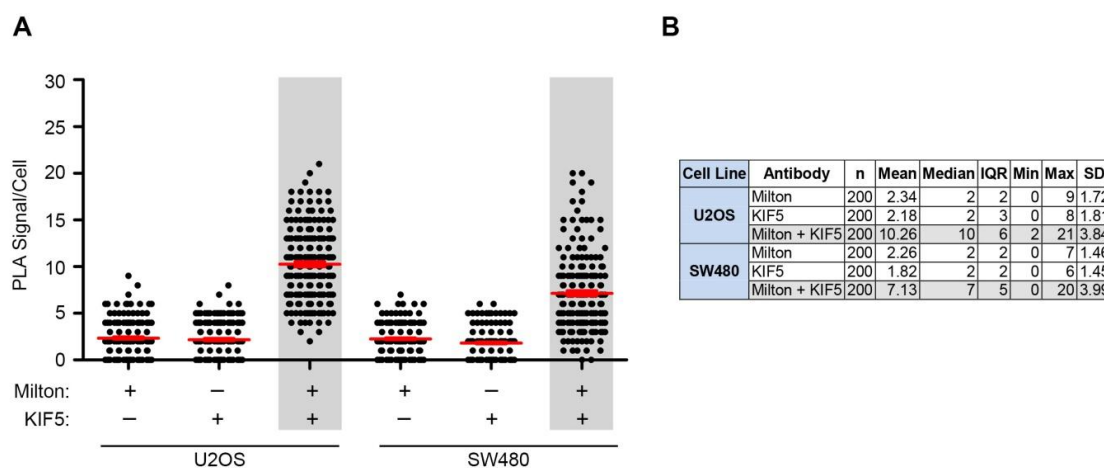
The cessation of mitochondrial transport through calcium regulation of the Miro/Milton transport complex is reflective of the role of mitochondria in calcium buffering, where proximity to regions of high intracellular calcium is essential for effective uptake (311). The literature clearly supports the modification of Miro, wherein the Miro EF-hand motifs bind to calcium, as a mechanism behind the disruption to mitochondrial transport, however, the changes in protein-protein interactions that cause dissociation of the Miro/Milton complex from microtubules following calcium binding is unclear (see Section 1.3.2.1 and 153, 159). Prior studies by Togo and colleagues (298), indicating that APC dissociates from microtubules in the presence of increased calcium, suggested that APC may contribute to this calcium regulation of mitochondria. However, preliminary investigations in this chapter do not support this hypothesis.

When calcimycin was used to boost intracellular calcium to levels sufficient to disrupt mitochondrial transport (Figure 6.5), APC localisation to both the mitochondria and microtubules remained unchanged (Figure 6.6A,D, Figure 6.7). This was consistent with earlier reports that other components of the transport complex, Miro and Milton, remain attached to mitochondria following calcium-induced disruption of mitochondrial transport (153, 159, and confirmed in Figure 6.6A-C). However, indications that the pool of APC localised to microtubules remained unchanged following increased intracellular calcium, was somewhat surprising given the findings reported by Togo and colleagues (298).

It is possible that the intracellular calcium levels required to displace APC from microtubules is higher than that required to inhibit mitochondrial transport. Previous studies into the differences between calcimycin, and ionomycin, used in the study by (298), indicate that ionomycin has a higher specificity for calcium ion uptake (312) and therefore might be more effective than the calcimycin used here. It is also possible that the calcium regulation of APC and mitochondrial components vary between different cell types and under different experimental conditions.

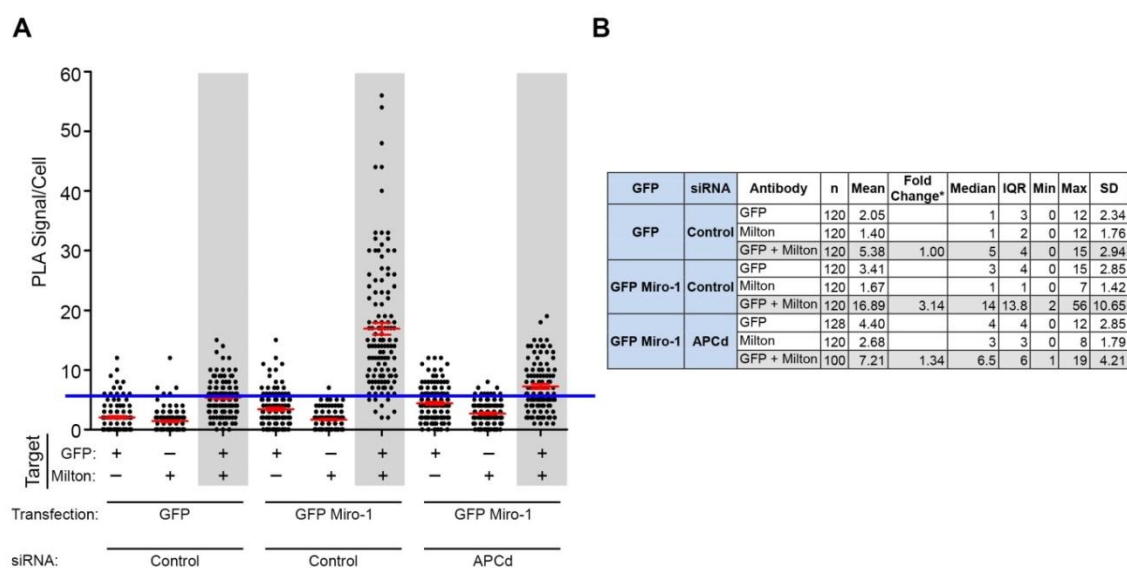
Duolink PLA experiments of calcimycin-treated U2OS cells suggest that the conformational change in the mitochondrial transport complex induced by calcium binding does not affect the Miro/APC interaction (Figure 6.8). This contrasts with the calcium-dependent binding observed between Miro and the newly discovered Wnt protein Alex3 (163) and further supports the notion that the role of APC in the mitochondrial transport complex is calcium-independent. These findings are still in their preliminary stages and further experiments are required to confirm this data. For example, intracellular calcium levels induced by treatment with calcimycin need to be monitored and Miro calcium binding needs to be confirmed at the calcimycin concentrations used to arrest mitochondrial transport. Experiments could also be confirmed using another calcium ionophore such as ionomycin, and repeated with the inclusion of a calcium chelator such as BAPTA-AM to determine whether the absence of calcium alters the activity of Miro, Milton or APC.

6.5 Supplementary Figures



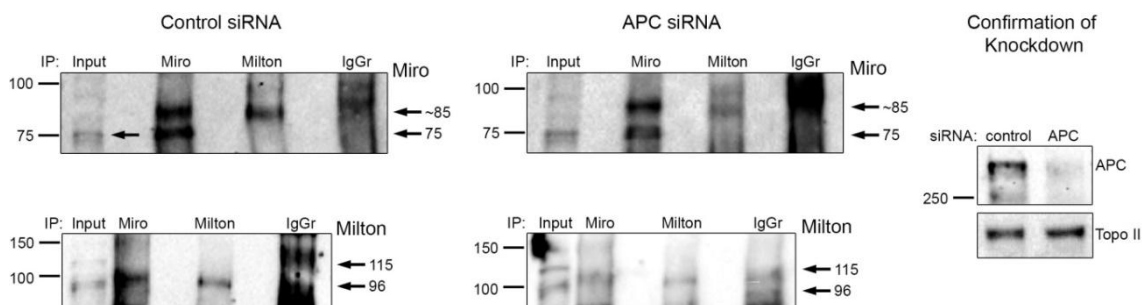
Supplementary Figure S6.1: Milton interacts with KIF5 in APC wild-type and mutant cell lines by Duolink– expanded Duolink data

(A-B) Interactions between Milton and KIF5 were visualised *in situ* in U2OS and SW480 cell lines using Duolink PLA as described in Figure 6.1. Scoring indicates a positive signal between Milton and KIF5 in both cell lines as shown in the (A) dot-plots (mean \pm S.D) and (B) table (n, number in sample; IQR, inter-quartile range; SD, standard deviation).



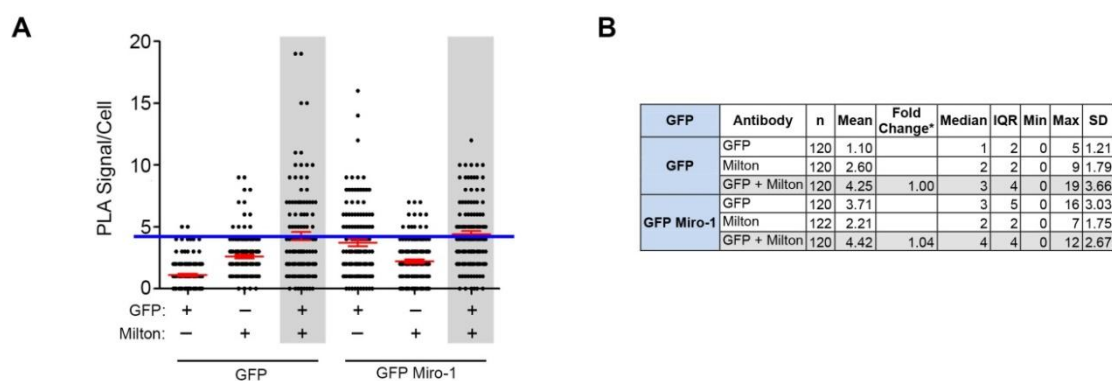
Supplementary Figure S6.2: Loss of APC disrupts the interaction between GFP Miro-1 and Milton in U2OS cells – expanded Duolink data

(A-B) U2OS cells were treated with control or APC (APCd) siRNA, transfected with pGFP or pGFP Miro-1 and Duolink PLA performed using antibodies against GFP and Milton as described in Figure 6.2. Scoring indicates that treatment with APC siRNA disrupted the interaction between GFP Miro-1 and Milton as shown in the (A) dot-plot (mean \pm S.D) and (B) table (n, number in sample; * fold change relative to GFP control; IQR, inter-quartile range; SD, standard deviation).



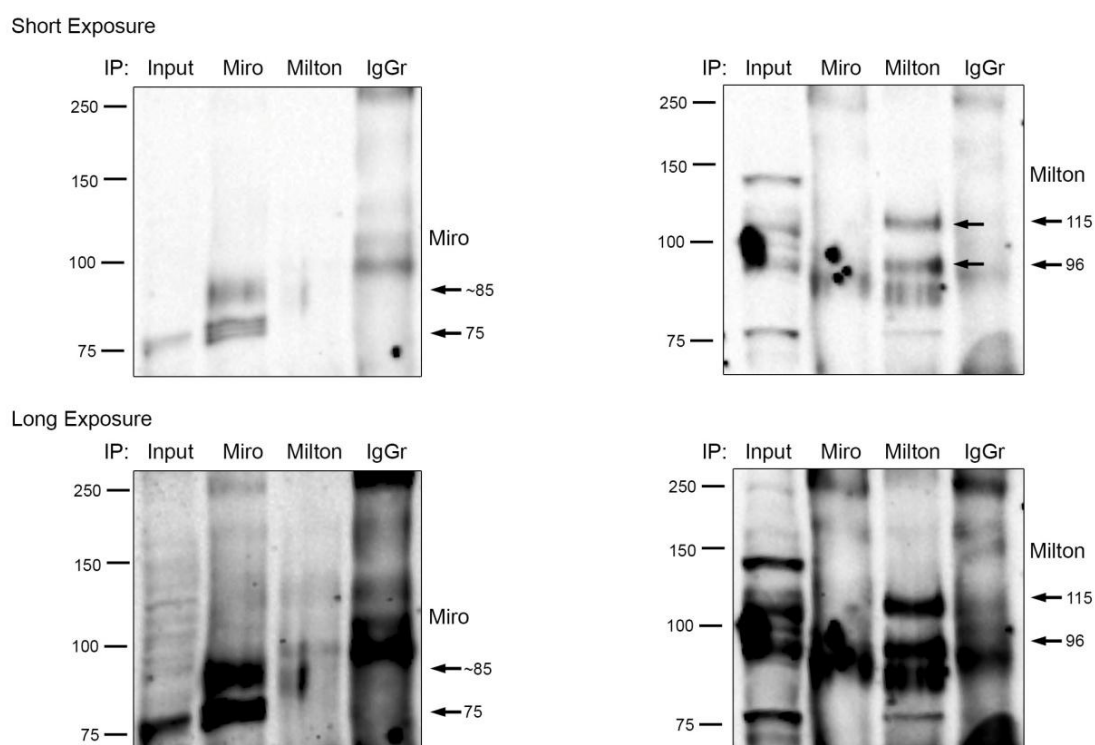
Supplementary Figure S6.3: Immunoprecipitation assays suggest that loss of APC in U2OS cells may disrupt the interaction between Miro and Milton

Cells treated with control or APC (APC_d) siRNA were immunoprecipitated by antibodies against Miro and Milton and analysed by western blot. The Miro antibody successfully pulled down both Miro and the 96 kDa form of Milton in cells treated with control siRNA, however in cells treated with APC siRNA amount of Milton pulled down appeared to be diminished. The Milton antibody successfully pulled down the 96 kDa form of Milton and Miro in cells treated with control siRNA, however in cells treated with APC siRNA the amount of Miro pulled down also appeared to be diminished. The blots shown are from the same experiment, however the extract was run on separate gels to avoid overlapping Miro and Milton bands.



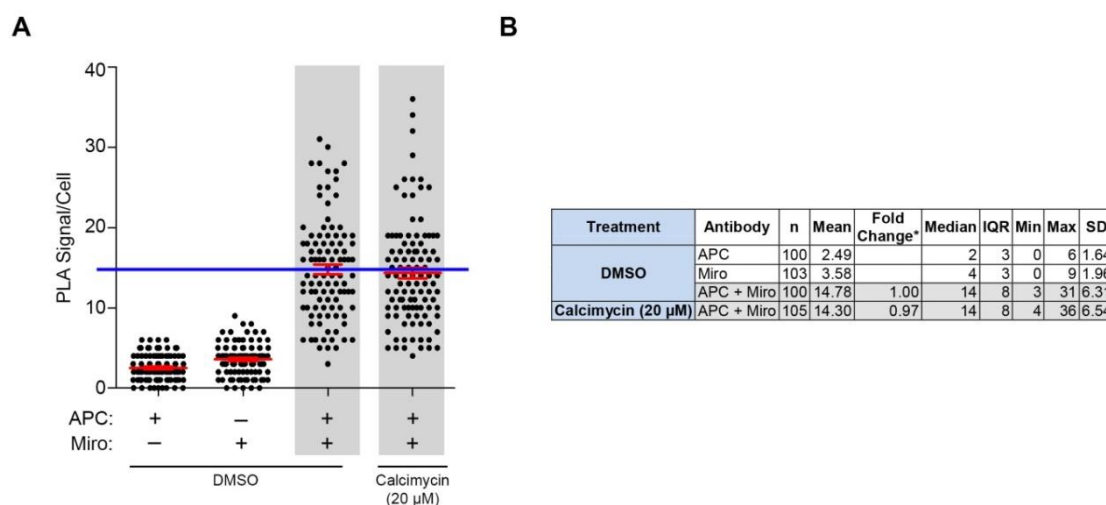
Supplementary Figure S6.4: GFP Miro-1 does not interact with Milton in SW480 mutant APC cells – expanded Duolink data

(A-B) SW480 cells were transfected with pGFP or pGFP Miro-1 and Duolink PLA performed using antibodies against GFP and Milton as described in Figure 6.3. Scoring indicates that GFP Miro-1 and Milton did not produce a signal above GFP background level as shown in the (A) dot-plot (mean \pm S.D) and (B) table (n, number in sample; * fold change relative to GFP control; IQR, inter-quartile range; SD, standard deviation).



Supplementary Figure S6.5: Miro does not interact with Milton in SW480 mutant APC cells by IP – longer time points

SW480 cells were immunoprecipitated using antibodies against Miro and Milton and analysed by western blot. Whilst pull-down of their respective proteins by the Miro and Milton antibodies was successful, the Miro antibody was unable to pull down Milton and vice versa.



Supplementary Figure S6.6: Calcimycin treatment does not alter the APC-Miro interaction – Expanded Duolink Data

(A-B) U2OS cells treated with DMSO or calcimycin (20 μ M) were subject to Duolink PLA using antibodies against APC (Ab7) and Miro as described in Figure 6.8. Scoring indicates that calcimycin treatment did not alter the interaction between APC and Miro as shown in the (A) dot-plot (mean \pm S.D) and (B) table (n, number in sample; * fold change relative to DMSO control; IQR, inter-quartile range; SD, standard deviation).

CHAPTER 7

General Overview and Discussion

This thesis has presented the first evidence to indicate a role for APC in the anterograde microtubule-dependent transport of mitochondria, facilitated by the Miro/Milton/KIF5 complex. In particular, APC was shown to stimulate the initiation of mitochondrial transport by stabilising the association between the mitochondrial anchor Miro and the kinesin adaptor Milton. APC truncation of the C-terminal end, as often observed in CRC, results in loss of the ‘Miro-binding domain’ and reduced both formation of the transport complex and mitochondrial movement towards the cell periphery. This new pathway of APC action, and its disruption by mutation, may explain some of the aberrant cell properties, such as altered polarity of migration, displayed by CRC cell lines and colonic crypt epithelial cells that express mutant APC.

7.1 APC is a novel regulator of the Miro/Milton mitochondrial pathway

Cells expressing wild-type APC were found to display mitochondria distributed throughout the cell in a uniformly spread manner, whereas the loss of APC shifted mitochondria towards the perinuclear region (Chapter 3), analogous to that observed when other components of the transport complex were disrupted (165, 284). The finding that APC associated with Miro and Milton, key proteins from the primary transport complex at mitochondria, consolidated this analysis. Truncation of the C-terminal ‘Miro binding domain’ of APC by CRC mutation inhibited APC binding to the Miro/Milton complex (Chapter 4), and correlated with reduced mitochondrial transport (discussed further in 7.2). This deficit was rescued in mutant-expressing CRC cells by reconstitution of wild-type APC, thus linking APC to trafficking of mitochondria to the cell periphery (Chapter 4). Results from live cell imaging showed that APC was involved specifically in the initiation of anterograde mitochondrial transport, rather than negatively regulating retrograde transport or altering transport velocity (Chapter 5). When APC expression was silenced, a larger proportion of the mitochondria became stationary, and this correlated with a decrease in anterograde movement, similar to that seen previously after loss of Miro or Milton (152-154, 163). Preliminary binding studies (Chapter 6) suggest that this may be due to the ability of APC to stabilise the interaction between Miro and Milton, the binding of which was impaired when APC was lost

through siRNA treatment or C-terminal truncation (summarised in Figure 7.1, ‘zoom’ panels). This idea is in line with APC’s scaffolding role in numerous other protein complexes (9, 12). The mechanism by which APC stabilises the Miro/Milton complex, and which of these proteins bind one another directly, are yet to be defined (see Section 7.7 for future directions). There is also some evidence that APC binds to a post-translationally modified form of Miro (Section 7.1.1).

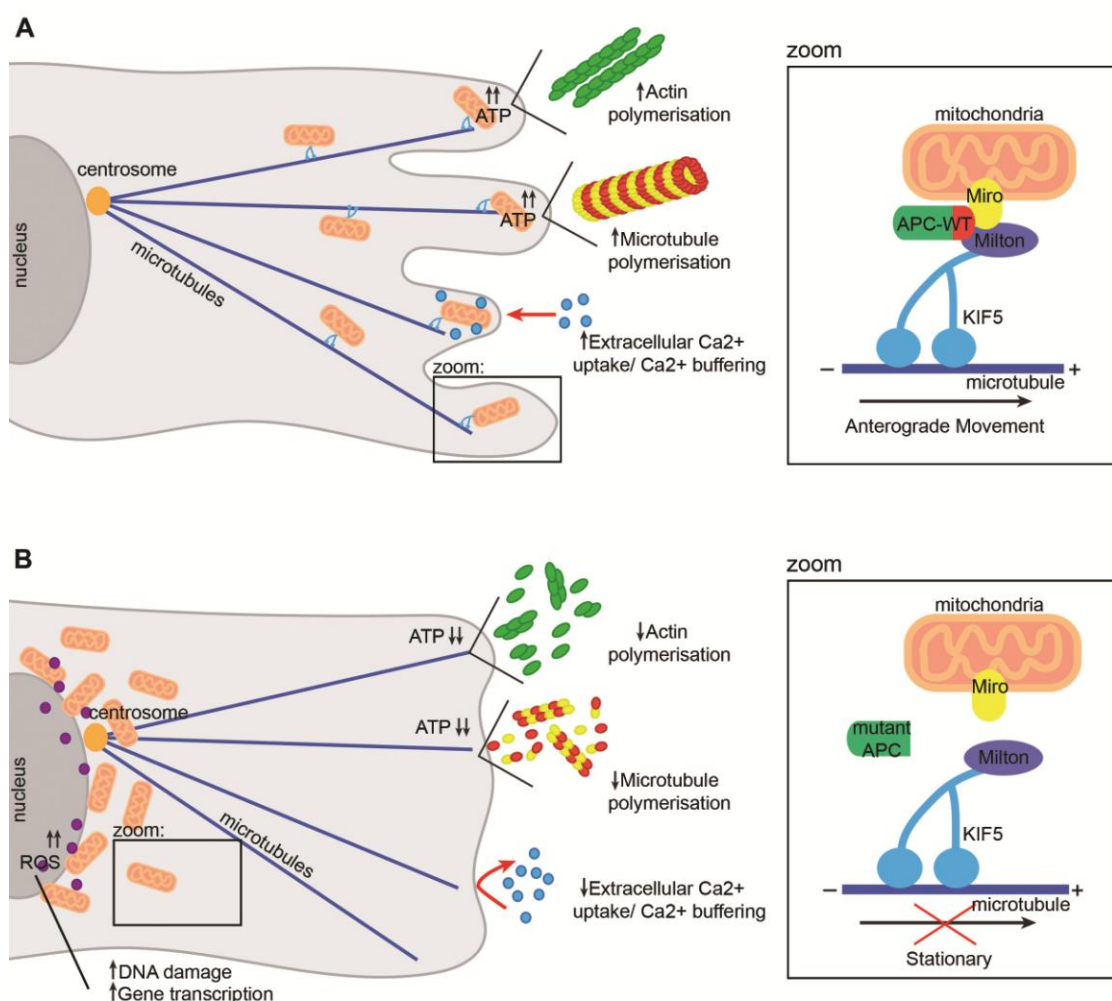


Figure 7.1: APC truncation impairs formation of the Miro/Milton/KIF5 motor complex, preventing anterograde transport of mitochondria.

(A) Findings from this study implicate APC as a key regulator of membrane-directed mitochondrial transport. (B) Such transport is compromised when APC is mutated in CRC. This model speculates on how APC-dependent mitochondrial transport may contribute to normal cell function, and how APC gene mutations could contribute to CRC carcinogenesis through misregulation of these pathways.

7.1.1 APC may interact with a post-translationally modified form of Miro.

APC may bind to a post-translationally modified form of Miro as suggested by immunoprecipitation of GFP-APC(2650-2843) with endogenous Miro in U2OS cells (Supplementary Figure S7.1). The band detected was higher (~85 kDa) than that of the predicted size for Miro (~75 kDa), both of which were visible in the input lane. Higher molecular weight bands of ectopic GFP-Miro were also observed in U2OS lysates, upon immunoprecipitation by wild-type endogenous APC (Supplementary Figure S7.1B). Furthermore an ~85 kDa endogenous form of Miro was observed in HEK293 cell lysates with induced expression of wild-type APC, and transfected with pGFP Milton-2, where antibodies against both APC and Milton appeared to preferentially capture this ~85 kDa Miro isoform (Supplementary Figure S7.1C). Endogenous Milton also appeared to preferentially capture this ~85kDa Miro in U2OS cells (Supplementary Figure S7.1D).

It is possible, that even though Miro-1 and Miro-2 are the same size and have the same predicted molecular weight (146), because the Miro antibody used for detection is not homolog specific (Supplementary Figure S3.3), the higher form detected simply results from the two homologs separating differently along the gel. However, as two bands are also clearly observed in Supplementary Figure S7.1B for ectopic GFP Miro-1 pulled down by APC and detected using anti-GFP, it is more likely that Miro has undergone some form of post-translational modification to which APC and Milton bind.

APC can act as scaffold to mediate phosphorylation of β -catenin by GSK3 β (reviewed in 9). Whilst Miro is not known to be modified by GSK3 β , it can undergo post-translational modification through the PINK1/Parkin pathway which orchestrates mitochondria quality control, mitophagy, and transport. PINK1 was reported to phosphorylate Miro, correlating with a cessation of mitochondrial transport in *Drosophila* neurons (152, 157) . Parkin on the other hand, can poly-ubiquitinate Miro upon membrane depolarisation, targeting it to the proteasome for degradation (165, 166). At this stage, it is unclear whether APC or Milton actually promote modification of Miro or whether they selectively bind an existing post-translationally modified sub-pool of Miro. If the modification is poly- ubiquitination, there was no evidence that

APC altered the stability of this form of Miro (Chapter 6), however it is worth further study as the preferential binding of the larger Miro isoform to APC and Milton suggests that it contributes to mitochondrial transport.

7.2 APC truncation disrupts mitochondrial transport

The initiation and progression of CRC primarily occurs through truncation of the C-terminus of APC, a region known to bind to numerous other regulatory partners involved in normal cell function whose loss might contribute to carcinogenesis (see Section 1.2.3). APC truncation disrupted its association with the Miro/Milton complex, a finding supported by mapping of the ‘Miro-binding domain’ to APC (2650-2843). The effects of C-terminal deletion were reflected by the impaired mitochondrial distribution in mutant APC cell lines, wherein mitochondria accumulated more around the nucleus and less at the plasma membrane region. Reconstitution of wild-type APC recovered APC binding to the Miro/Milton complex, and partly restored mitochondrial transport to the cell periphery (Chapter 4). The results indicate that C-terminal truncation decreases mitochondrial transport to the cell periphery (Figure 7.1B), which may contribute to CRC tumorigenesis (discussed further in Section 7.3).

It is possible that APC mutations contribute to alterations in mitochondrial transport through other pathways. For example, MacLeod and colleagues (313) indicated that in HT-29 CRC cells the truncated APC, but not ectopic wild-type APC, stimulates Wnt5a secretion in the presence of calcium. Separately, Wnt5a stimulation of the non-canonical Wnt signalling pathway is reported to target Alex3 (a positive regulator of mitochondrial transport) for degradation in a concentration dependent manner, which could in turn inhibit mitochondrial transport (161). It is hard to reconcile these results given that elsewhere Wnt5a has been reported to be silenced in most CRC cell lines (including HT-29) by promoter methylation, whilst expressing well in normal cell types (314). More direct alternatives through which wild-type and mutant APC could regulate mitochondrial transport are discussed in Section 7.5.

7.3 Disruption of mitochondrial transport may contribute to CRC

APC truncation mutations contribute to CRC carcinogenesis by disrupting a range of key tumour suppressor activities such as β -catenin turnover (leading to aberrant Wnt signalling, see reviews 3, 5), mitosis chromosome segregation, cell polarity and cell migration (see Section 1.2.3 and reviews 52, 54, 289). As shown in this study (Chapters 4 and 6), C-terminal truncation of APC also appears to disrupt assembly of the Miro/Milton transport complex, and in turn affects mitochondrial movement towards the cell periphery. It is possible that this impairment contributes to carcinogenesis (Figure 7.1).

One mechanism by which impaired mitochondrial transport may contribute to CRC is through irregular targeting of mitochondrial ATP. In particular, recent studies have indicated that localisation of mitochondria at the cell periphery is essential for effective cell migration and, that disruption to this, slows the rate by cutting off the ATP supply essential for F-actin and microtubule polymerisation (18, 19). Data from Chapter 5 show that siRNA mediated loss of APC decreased the rate of cell migration, correlating with a loss of mitochondria at the cell periphery and microtubule-dependent protrusions. C-terminal deletion of APC also impaired mitochondrial movement to the cell periphery, suggesting that it may likewise perturb directed cell migration. This hypothesis is in line with studies that report a decrease in the rate of cell migration along the crypt-villi axis in APC (Min/+) and APC knockout mice (66, 99). Furthermore, disruption to microtubule polymerisation, required for maintenance of cell polarity may also account for the loss of directed cell migration observed in APC (Min/+) mice (96). Retention of cells at the base of colonic crypts may be favourable for cancer cell expansion and survival as this region is highly proliferative. Disruptions in the targeting of mitochondrial ATP reserves may further impact the numerous other regulatory pathways for which it supplies energy. This area requires further investigation.

The disruption of mitochondrial transport may also affect calcium buffering, through the loss of site-specific uptake, and release of calcium by mitochondria (15) and disruption of mitochondrial membrane positioning for extracellular calcium uptake (190). This

may contribute to the aberrant calcium signalling frequently observed in cancer cells which disturbs regulation of cell proliferative and migratory pathways (292, 296). Furthermore, the perinuclear clustering, resulting from disruption of outward, anterograde mitochondrial movement may assist in the creation of an oxidant-rich nuclear domain due to the continuous release of mitochondrial ROS in a confined environment (265). Highly concentrated ROS in close proximity to the nucleus could stimulate transcription of hypoxia-induced genes such as VEGF and NF κ B, and expose the DNA to oxidative damage, promoting carcinogenesis (299). These mechanisms through which disruption to mitochondrial transport can promote carcinogenesis may act synergistically with aberrant pathways arising from APC truncation.

7.4 Other Implications for APC in mitochondrial transport

Disruption to APC-dependent mitochondrial ATP supply to the cell periphery may have implications not only relevant to CRC, but also to other cell and tissue processes such as wound healing, embryonic development and the immune response. Alternative outcomes are briefly outlined below.

7.4.1 Regulation of CNS structure and function.

APC is expressed highly in the brain, particularly in neurons (315, 316), and contributes to the proliferation, differentiation and process formation of various cell types in the CNS (317-320), through both its Wnt and cytoskeletal regulatory pathways. A previous study implicated APC in the modification of KIF5-mediated vesicle transport in neurons (286), suggesting that mitochondrial dynamics may also contribute to the regulation of some of these pathways. For instance, APC is enriched at the tips of growth regions in hippocampal neurons and retinal ganglion cells where it is involved in outgrowth and elongation (321, 322). It is assumed that ATP is required for this process, and in line with this notion mitochondrial dynamics and positioning have been shown to be essential for the growth rate of retinal ganglion cells (323). The ability of APC to localise to these areas of growth, where it regulates cytoskeletal function, may act in

synergy with its capacity for mitochondrial transport, to supply the energy required in neuronal outgrowth. Furthermore, as outlined in Section 1.3.4.1 and reviewed in (139-141), mitochondrial transport defects are associated with numerous neurological diseases such as Alzheimer's, Parkinson's and Huntington's diseases. Canonical Wnt signalling is reported to have neuroprotective effects in Alzheimer's disease by preventing the permeabilisation of the mitochondrial membrane induced by β -amyloids (324), however APC dysfunction has not yet been reported.

7.4.2 Regulation of development

Mitochondrial distribution changes during embryonic development to meet specific demands including mediating nuclear-mitochondrial signalling, energy supply and segregation for proper mitochondrial inheritance. Moreover, alterations to mitochondrial dynamics and morphology impair embryonic development in different organisms (325). This is highlighted by studies demonstrating that complete loss of functional DRP1, OPA1 or Mfn1/2, required to mediate mitochondrial morphology were embryonically lethal in mice (326-328). Loss of APC in KO mice is also embryonically lethal (329, 330), however due to its multifaceted nature, this is not surprising. APC's role as a suppressor of Wnt signalling is a crucial in the regulation of development, however results from this study raise the possibility that it may also contribute to this process through regulated transport of mitochondria.

7.5 APC as a potential regulator of other mitochondrial transport pathways

7.5.1 APC and RanBP2

Ran-binding protein-2 (RanBP2) was originally identified as a mobile nucleoporin involved in nucleocytoplasmic transport of proteins (331, 332). Since then numerous roles have emerged for RanBP2 in normal cell function. In particular, RanBP2 has been reported to stimulate anterograde mitochondrial movement through the direct association, and activation, of the KIF5B/C motor domain (176, 177). These studies

showed that overexpression of a dominant-negative form of RanBP2 in NIH 3T3 cells resulted in perinuclear clustering of mitochondria (176), similar to that observed following APC wild-type knockdown across numerous cell lines, including NIH 3T3 (Figure 3.1). An unrelated study identified the formation of RanBP2/APC complexes in the maintenance of cell polarity (62), and preliminary studies confirming that RanBP2 co-located well at mitochondria and with APC (Figure 3.5, Figure 3.6) suggested that further investigation is warranted to examine if this RanBP2/APC association also influenced mitochondrial transport.

To confirm these findings, and to examine if the mutational status of APC had any bearing on RanBP2-mediated mitochondrial transport, U2OS (APC-WT) and SW480 (APC 1-1377) cell lines were treated with control or RanBP2 siRNAs, and analysed by immunofluorescence microscopy. In U2OS cells, loss of RanBP2 induced redistribution of mitochondria toward the perinuclear region, as described by Cho and colleagues (176), although to a lesser extent (31%) than that observed after APC knockdown (52%) (Supplementary Figure S7.2). The loss of RanBP2 also elicited a small increase in perinuclear mitochondrial clustering in SW480 cells expressing mutant APC 1-1337 (Supplementary Figure S7.2). These results suggest that if APC/RanBP2 immunocomplexes are involved in mitochondrial transport, they operate through a pathway alternate to the APC/Miro/Milton complex. This notion was confirmed by Duolink PLA, where attempts to produce PLA-positive signals between RanBP2 and Miro in U2OS cells were unsuccessful (Supplementary Figure S7.3).

To confirm the association between APC and RanBP2 proposed in previous studies (62), Duolink PLA was employed using antibodies targeting endogenous APC and RanBP2 to detect potential interactions. In agreement, PLA experiments showed a positive interaction between APC and RanBP2, with U2OS and SW480 cells yielding ~18 and ~13 PLA signals/cell respectively (Figure Supplementary Figure S7.4A-B). This was confirmed by immunoprecipitation in U2OS lysates (Supplementary Figure S7.4C). Murawala and colleagues (62) mapped the RanBP2 binding domain to the middle section of APC (residues 1211-1859), however, the detection of APC/RanBP2 complexes in SW480 (APC 1-1337) cells, suggests that this domain could be further isolated to the 1211-1337 region. APC/RanBP2 PLA signals did not locate at mitochondria (Supplementary Figure S7.4D,E) suggesting that APC and RanBP2s

mitochondrial transport functionality are independent of one another, or that they influence mitochondria transport indirectly.

7.5.2 APC and other kinesin pathways

APC is also reported to associate with a number of kinesin motor proteins which have yet to be assessed for mitochondrial transport capabilities. These include KIF17 which has a role in microtubule stabilisation (68), and KIF3A/B. The APC/KIF3 association is mediated by an APC ARM domain interaction with adaptor protein KAP3A, and was shown to be necessary for APC localisation at membrane clusters (26). KAP3A was assessed in the preliminary stages of this study as a candidate through which APC may mediate mitochondrial transport, however weak mitochondrial co-localisation (Figure 3.3), and the finding that loss of mutant APC (retains KAP3A binding) did not affect mitochondrial distribution (Figure 4.1), makes it less likely that APC/KAP3A/KIF3 is a transport pathway for mitochondria.

7.5.3 Myosin

In addition to microtubule-dependent transport of mitochondria highlighted in this study, the actin network also facilitates mitochondrial trafficking through the use of myosin motor proteins (summarised in Section 1.3.2.2). In particular, myosin motors, Myosin V, Myosin VI (187) and Myosin XIX (188) have been implicated in actin-dependent transport of mitochondria in mammalian cell lines. Whilst there are no existing reports in the literature suggesting APC interacts with myosin motors, unpublished mass spectrometry data (Lui and Henderson) identified several myosin isoforms as putative binding partners for APC. These findings, coupled with the close association APC with the actin network (Section 1.2.1.3), open up the possibility of an alternate actin-dependent mitochondrial transport pathway for APC. Due to the short-range nature of actin-dependent mitochondrial movement (170, 171), it is likely that any loss of transport across the actin network by APC knockdown would be masked by disruption to its long-range microtubule-dependent actions. Further investigation is required to determine if APC/actin-dependent mitochondrial transport is a viable pathway.

7.6 APC in mitochondrial morphology

Preliminary observations in Chapter 3, indicated that the mitochondrial network in U2OS, HDF1314 and NIH 3T3 cells became more fragmented when treated with APC siRNA (Figure 3.2), suggesting that loss of APC may also contribute to mitochondrial fission and fusion dynamics. The ability of mitochondria to fuse and divide is another key facet to their dynamic nature, enabling them to form large interconnected networks or discrete fragments/puncta in response to various cell signals (Section 1.3.3). Mitochondrial transport and fission/fusion dynamics are intimately linked. On a mechanistic level, functional transport is required to bring mitochondria into contact to facilitate fusion, and move mitochondria apart to facilitate fission. Furthermore, several regulatory proteins overlap in both mitochondrial transport and morphology pathways. PINK1/Parkin for example, known to post-translationally modify Miro/Milton (see Section 7.1.1), also ubiquitinates the fission/fusion regulatory proteins Mfn1/2, DRP1 and Fis1, targeting them to the proteasome for degradation (229, 246). Mfn2 has also been implicated in axonal mitochondrial transport (162), whilst overexpression of Milton has been shown to induce morphological defects in mitochondria (270). This interconnectivity also presents itself in disease pathology, where mutations in a number of key fission/fusion proteins contribute to the same neurodegenerative diseases observed following defects in mitochondrial transport. These include Charcot Marie Tooth, autosomal dominant optic atrophy, Alzheimer's disease and Parkinson's disease (reviewed in 139, 140, 192).

7.6.1 APC knockdown causes changes in mitochondrial morphology

To confirm the fragmentation of mitochondria observed in Figure 3.2 following loss of APC, and to determine if C-terminal truncation had any impact, wild-type APC was silenced in U2OS and LIM1215 cell lines, whilst mutant APC was silenced in SW480 and HT-29 cell lines. These cells were stained with CMX-Ros to detect mitochondria and analysed by microscopy. Individual mitochondria were scored as either a puncta ($\sim < 2 \mu\text{m}$) or a rod ($\sim \geq 2 \mu\text{m}$) according to their length, and from this cells were assigned as either punctate ($>66\%$ puncta), mixed ($<66\%$ puncta and $<66\%$ rods) or rods ($>66\%$ rods). This is explained in detail in Section 2.2.7.3.

Scoring analysis (Supplementary Figure S7.5) revealed that U2OS cells present a primarily mixed morphology. LIM1215 CRC cells showed a preference for punctate mitochondria, however this was not as pronounced as the punctate pattern observed in the mutant APC CRC cell lines. Silencing of wild-type APC increased the population of cells displaying punctate mitochondria relative to control (Supplementary Figure S7.5). However, loss of mutant APC did not alter the already large proportion of cells with a punctate mitochondrial morphology (Supplementary Figure S7.5). These results suggest that if APC influences mitochondrial morphology independently from transport, this is mediated by sequences in the C-terminal region.

7.6.2 Binding studies

A number of fission/fusion regulatory proteins (Mfn2, OPA1, DRP1 and Fis1) were assessed for their ability to bind APC. An initial screen of these proteins for colocalisation with APC (Figure 3.6) revealed that both fusion proteins, Mfn2 and OPA1 showed a high level of colocalisation (83% and 87% respectively), while in contrast, DRP1 (23%) and Fis1 (7%) showed little. The use of Duolink PLA detected no specific PLA signal between APC and these regulators of mitochondrial morphology (Supplementary Figure S7.6), underscoring the specific nature of its interaction with Miro/Milton.

7.7 Future direction, clinical implications and conclusion

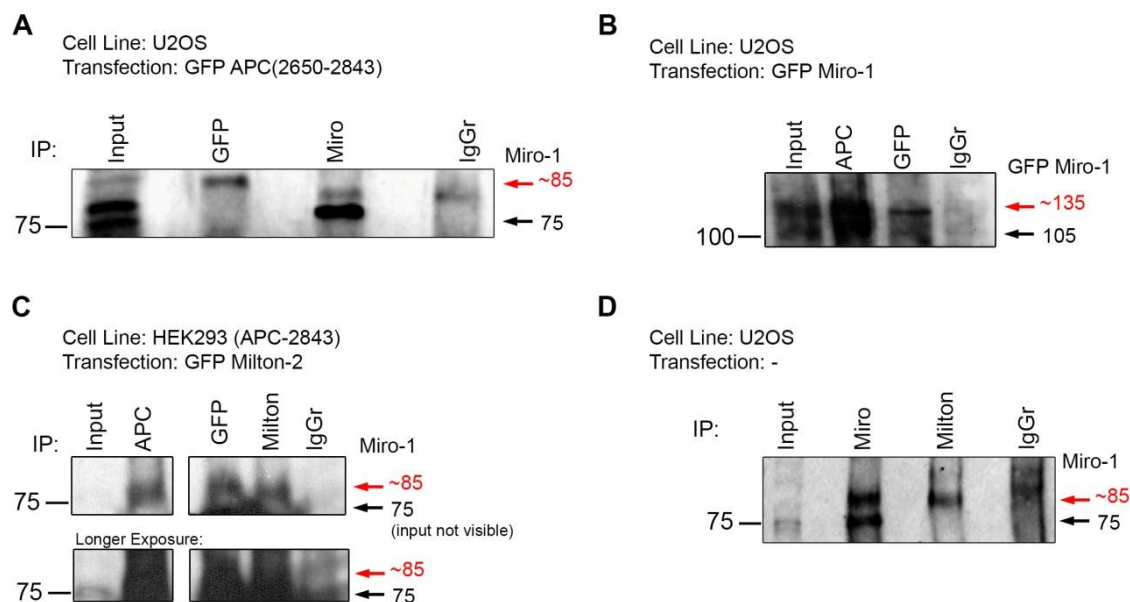
To further define how APC alters mitochondrial transport, the structural biology of the complex needs to be further investigated. This could involve determining which components of the transport complex bind directly to one another, through the use of purified protein binding assays. A proteomic approach could be used to identify any other co-factors involved in the formation of the complex and mass spectrometry used to investigate possible Miro post-translational modifications that may facilitate APC-binding. Moreover, the impact of APC on Miro/Milton association, and on mitochondrial transport, should be further analysed over a broad range of cell types, and

in mouse models such as the APC (Min/+) mouse. Tissue samples could also be interrogated in a similar manner.

To determine the broader impacts of this newly defined mitochondrial transport pathway, ATP production could be analysed in more detail to verify that loss or truncation of APC does slow cell migration by impairing energy supply at the cell periphery. One approach to this could be through immunofluorescence detection and analysis of an ATP substrate in actively migrating cells following APC knockdown. Mitochondrial localisation, and how this correlates with the distribution of cells in CRC organoids, or the colon crypts of normal and APC (Min/+) mice could also be examined.

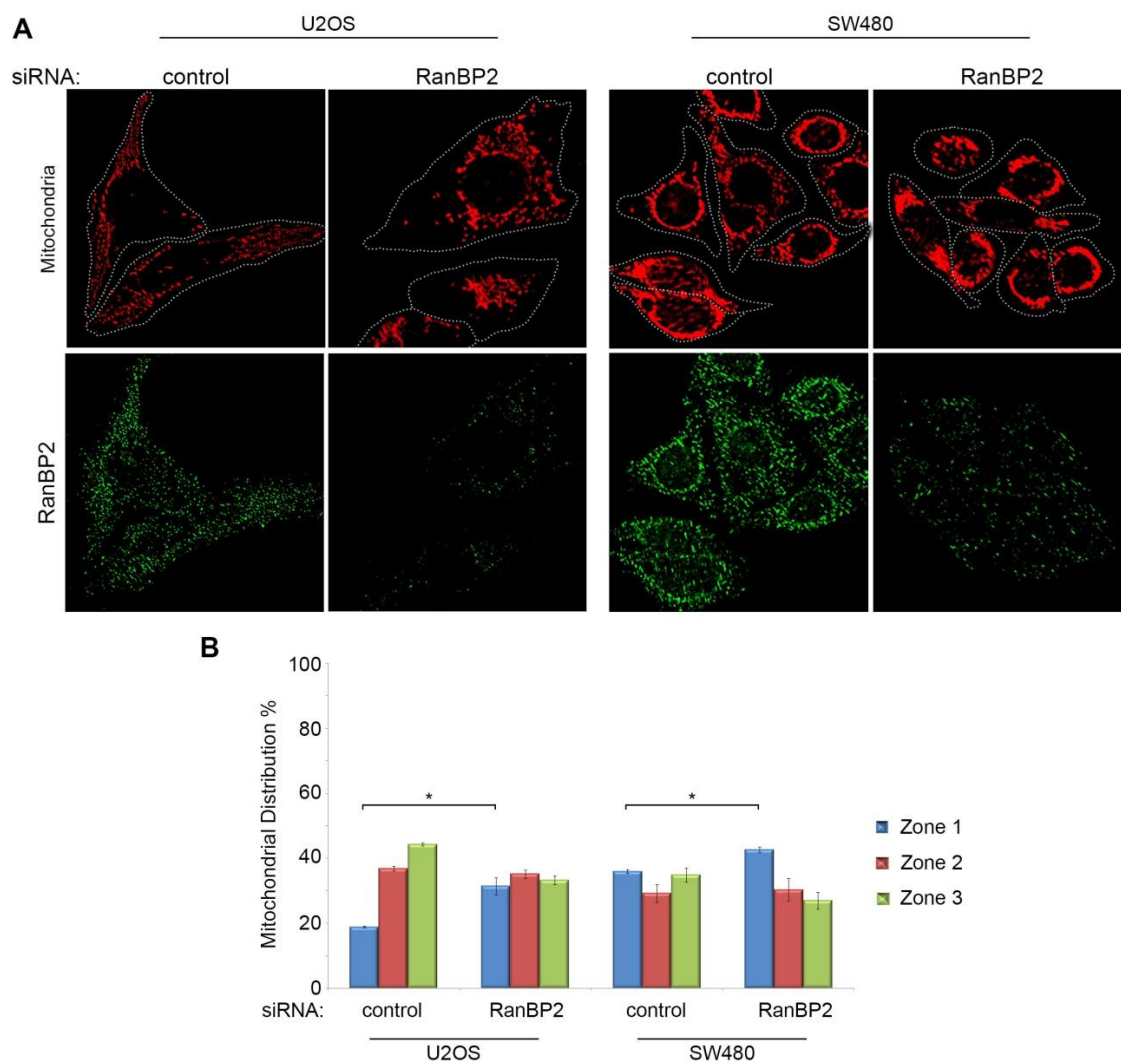
The recent development of chemotherapeutic drugs that target mitochondrial function, highlight the importance of understanding all pathways in carcinogenesis for the discovery of new drug targets. Drugs indirectly targeting mitochondrial dynamics have already been developed. For example, the CT20 peptide promotes mitochondrial aggregation and membrane hyperpolarization leading to the detachment and death of metastatic breast cancer cells through disruption of membrane protrusions and F-actin polymerisation (333). Mitochondrial ATP production has also been targeted to inhibit migration and invasion of cancer cells by treatment with graphene (334). Findings in this thesis which implicate APC in mitochondrial transport open up a new pathway through which APC mutation may perturb normal cell function and drive carcinogenesis, and in turn present a range of new protein partners which could be targeted for therapeutic use.

7.8 Supplementary Figures



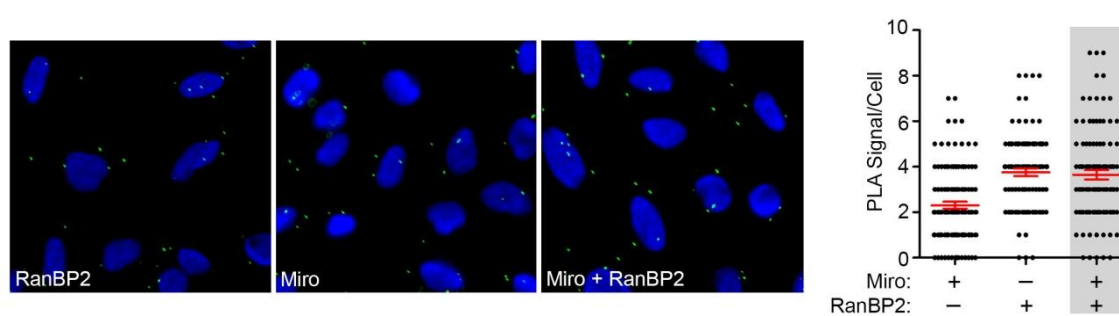
Supplementary Figure S7.1: APC and Milton may bind to a post-translationally modified form of Miro.

Potential post-translationally modified Miro bands are indicated by arrows in red. (A) U2OS cells transfected with pGFP tagged APC (2650-2843) were immunoprecipitated by antibodies against GFP (pAb) and Miro prior to western blot analysis. Detection by Miro antibody revealed that the GFP antibody could successfully pull down a high molecular weight form of Miro-1 in transfected cell samples (Supplementary Figure S4.6A). (B) U2OS cells transfected with pGFP Miro-1 were immunoprecipitated by antibodies against APC (C20, pAb) and GFP (pAb). Detection by GFP revealed that the APC antibody successfully pulled down GFP Miro-1 (Figure S3.4). (C) Inducible HEK 293 cell lines transfected with pGFP Milton-2 were treated with tetracycline 16 h prior to immunoprecipitation to induce expression of (APC-WT). Cells were immunoprecipitated by antibodies against APC (Ab5), GFP (pAb) and Milton, then analysed by western blot to detect Miro. The APC and GFP antibodies were able to pull down a higher size band for Miro (Figure S4.4). (D) U2OS cells were immunoprecipitated by antibodies against Miro and Milton and analysed by western blot. The Milton antibody successfully pulled down a higher weight form of Miro (Supplementary Figure S6.4).

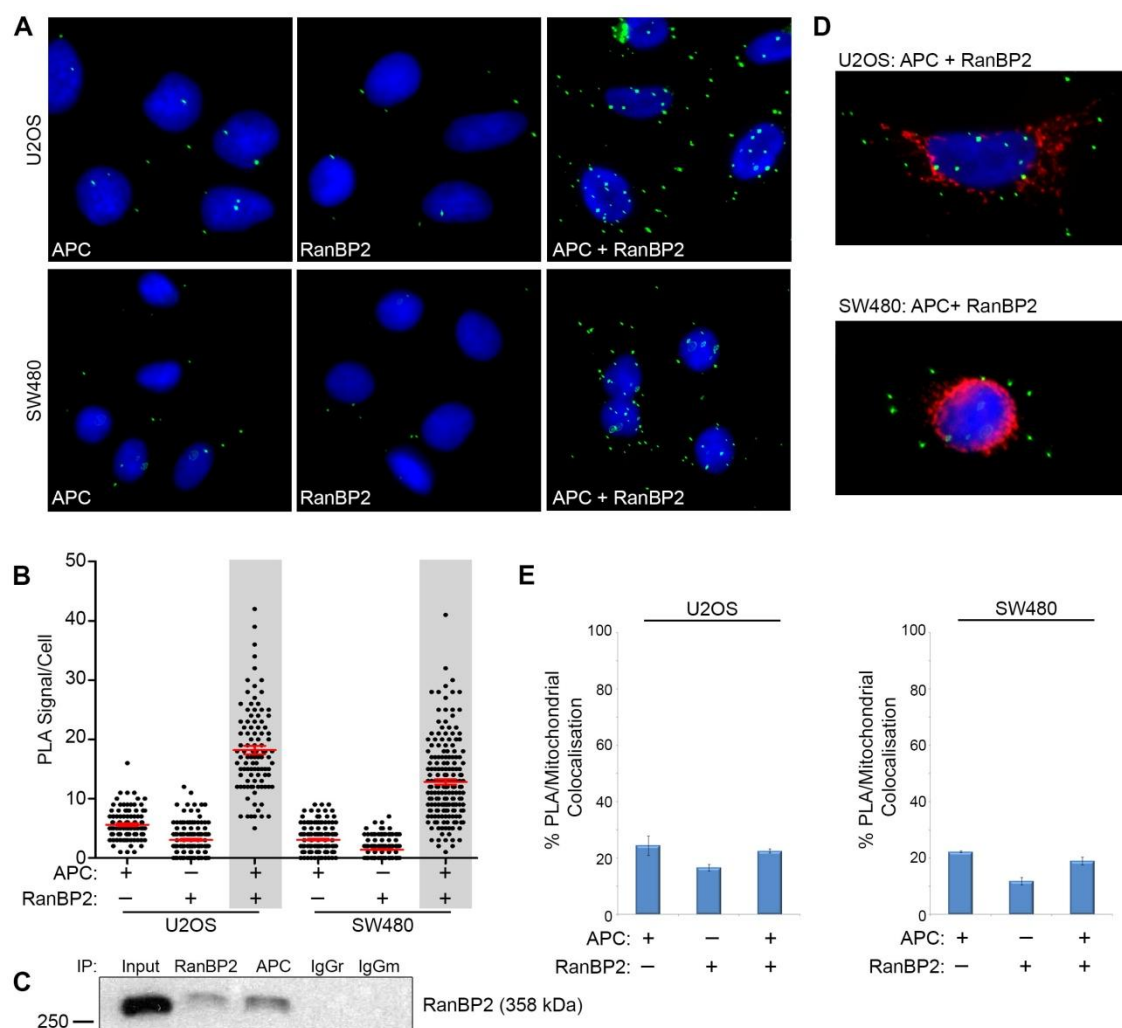


Supplementary Figure S7.2: Loss of RanBP2 induces redistribution of mitochondria in U2OS and SW480 cells

(A) U2OS and SW480 cells were treated by RanBP2 siRNA, and mitochondrial distribution analysed by immunofluorescence microscopy after staining for mitochondria (CMX-Ros) and RanBP2 (pAb). The cell membrane is represented by the dotted line. (B) Mitochondrial distribution was scored revealing a significant redistribution of mitochondria from the cell periphery (zone 3) towards the perinuclear region (zone 1) when RanBP2 was lost. Significant differences for zone 1 distribution relative to controls, determined by an unpaired T-test, are indicated (*, $P < 0.05$, % mean \pm S.D).

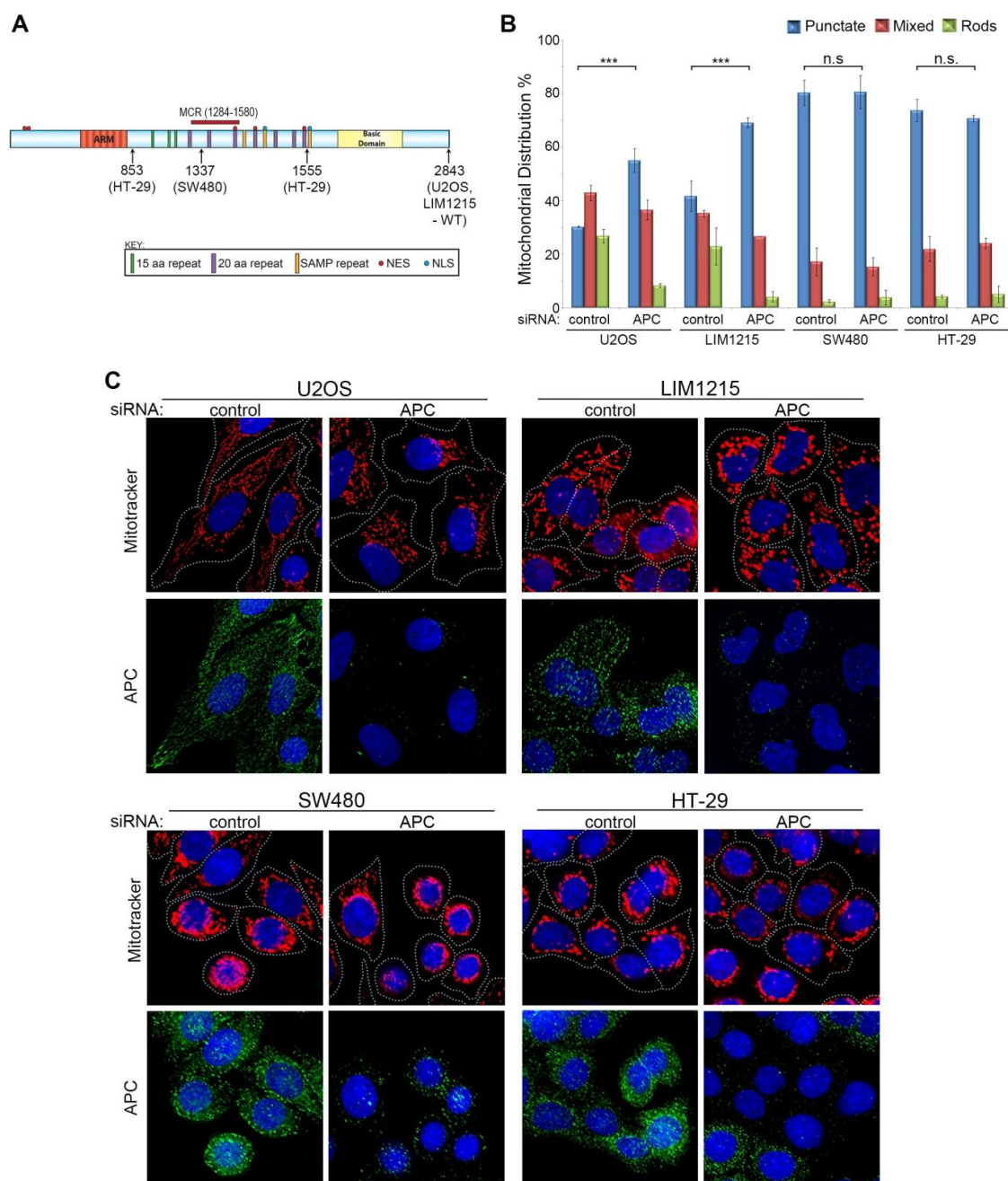


Supplementary Figure S7.3: RanBP2 does not interact with Miro by Duolink PLA. U2OS cells were subject to Duolink PLA using antibodies against RanBP2 (mAb) and Miro (pAb). Representative images are shown and scoring quantification, as seen in the dot-plots (mean \pm S.D), revealed no PLA signal/cell above background level.



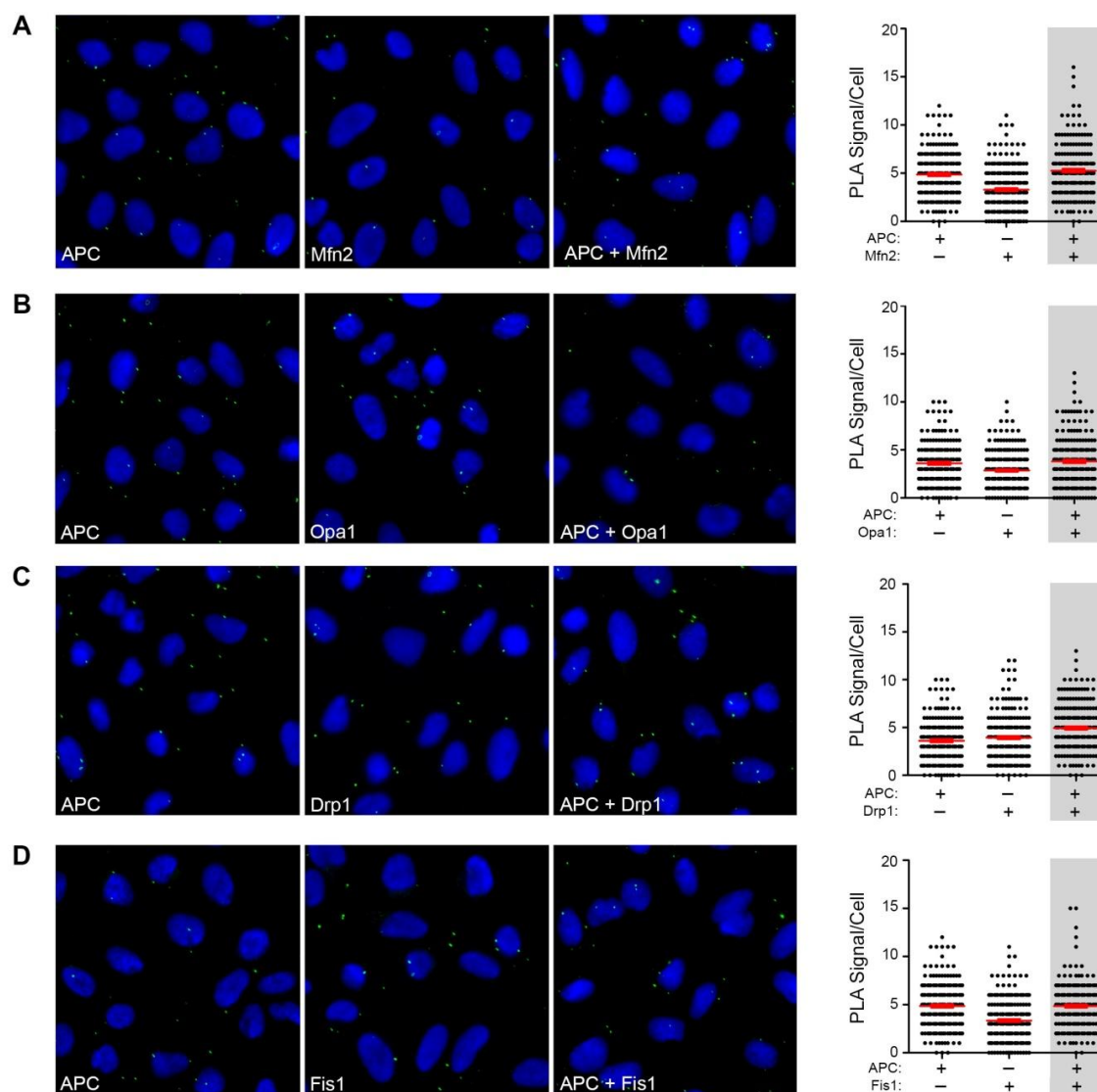
Supplementary Figure S7.4: APC/RanBP2 immunocomplexes do not localise to mitochondria.

(A-B) U2OS and SW480 cell lines were subject to Duolink PLA using antibodies against APC (H290) and RanBP2 (mAb). Scoring from analysis by immunofluorescence microscopy, showed a positive PLA signal, between APC and RanBP2, above background level in both cell lines, as observed in the (A) representative images and (B) dot plot (mean \pm S.D). (C) This interaction was confirmed by immunoprecipitation in lysates of U2OS cells whereby an APC antibody (C20) successfully captured endogenous RanBP2. (D-E) Analysis of mitochondrial localisation for APC/RanBP2 PLA signals in U2OS and SW480 cells pre-stained with CMX-Ros, indicated poor localisation for APC/RanBP2 immunocomplexes as observed in the (D) representative images and (E) scored in the graph.



Supplementary Figure S7.5: Loss of wild-type, but not truncated APC induces fragmentation of mitochondria.

(A) The mutation status of APC in U2OS, LIM1215, SW480 and HT-29 is outlined the schematic. (B-C) These cell lines were treated with control, APCd (U2OS) or APCd/APC2 pooled siRNA (LIM1215, SW480, HT-29) for 72h, stained with CMX-Ros Mitotracker and counterstained with APC antibody (H290) and Hoechst. Mitochondrial morphology was analysed by immunofluorescence microscopy and scored as described Section 2.2.7.3. (B) Results are indicated on the bar graph with significant differences for punctate mitochondria relative to siRNA control, as determined by an unpaired T-test, shown for each cell line (***, $P < 0.001$; n.s., not significant, % mean \pm S.D). (C) Representative images are shown (dotted line represents the cell membrane).



Supplementary Figure S7.6: APC does not interact with key regulators of mitochondrial fission and fusion by Duolink PLA.

(A-D) Duolink PLA was utilised to detect interactions between APC and mediators of mitochondrial morphology using antibodies against APC (Ab1 or H290), and (A) Mfn2, (B) OPA1, (C) DRP1 or (D) Fis1. No PLA signal above background was detected for any interaction investigated as visualised in the representative images and dot-plots (mean \pm S.D).



References



1. AIHW. Cancer in Australia: in brief 2014. In: Welfare AIOHa, editor. Canberra2014.
2. WHO. World Cancer Report 2014: World Health Organization; 2014.
3. Fodde R, Smits R, Clevers H. APC, signal transduction and genetic instability in colorectal cancer. *Nat Rev Cancer*. 2001 Oct;1(1):55-67.
4. Senda T, Iizuka-Kogo A, Onouchi T, Shimomura A. Adenomatous polyposis coli (APC) plays multiple roles in the intestinal and colorectal epithelia. *Med Mol Morphol*. 2007 Jun;40(2):68-81.
5. Polakis P. The many ways of Wnt in cancer. *Curr Opin Genet Dev*. 2007 Feb;17(1):45-51.
6. Kinzler KW, Vogelstein B. Lessons from hereditary colorectal cancer. *Cell*. 1996 Oct 18;87(2):159-70.
7. Galiatsatos P, Foulkes WD. Familial adenomatous polyposis. *The American journal of gastroenterology*. 2006 Feb;101(2):385-98.
8. Fearnhead NS, Britton MP, Bodmer WF. The ABC of APC. *Hum Mol Genet*. 2001 Apr;10(7):721-33.
9. Stamos JL, Weis WI. The beta-catenin destruction complex. *Cold Spring Harb Perspect Biol*. 2013 Jan;5(1):a007898.
10. Burgess AW, Faux MC, Layton MJ, Ramsay RG. Wnt signaling and colon tumorigenesis--a view from the periphery. *Experimental cell research*. 2011 Nov 15;317(19):2748-58.
11. Brocardo M, Henderson BR. APC shuttling to the membrane, nucleus and beyond. *Trends Cell Biol*. 2008 Dec;18(12):587-96.
12. Lui C, Mills K, Brocardo MG, Sharma M, Henderson BR. APC as a mobile scaffold: regulation and function at the nucleus, centrosomes, and mitochondria. *IUBMB life*. 2012 Mar;64(3):209-14.
13. Brocardo M, Lei Y, Tighe A, Taylor SS, Mok MT, Henderson BR. Mitochondrial targeting of adenomatous polyposis coli protein is stimulated by truncating cancer mutations: regulation of Bcl-2 and implications for cell survival. *J Biol Chem*. 2008 Feb 29;283(9):5950-9.
14. Boland ML, Chourasia AH, Macleod KF. Mitochondrial dysfunction in cancer. *Front Oncol*. 2013;3:292.
15. Contreras L, Drago I, Zampese E, Pozzan T. Mitochondria: the calcium connection. *Biochim Biophys Acta*. 2010 Jun-Jul;1797(6-7):607-18.
16. Tait SW, Green DR. Mitochondria and cell signalling. *J Cell Sci*. 2012 Feb 15;125(Pt 4):807-15.

17. McBride HM, Neuspiel M, Wasiak S. Mitochondria: more than just a powerhouse. *Curr Biol*. 2006 Jul 25;16(14):R551-60.
18. Desai SP, Bhatia SN, Toner M, Irimia D. Mitochondrial localization and the persistent migration of epithelial cancer cells. *Biophys J*. 2013 May 7;104(9):2077-88.
19. Zhao J, Zhang J, Yu M, Xie Y, Huang Y, Wolff DW, et al. Mitochondrial dynamics regulates migration and invasion of breast cancer cells. *Oncogene*. 2013 Oct;32(40):4814-24.
20. Miyoshi Y, Nagase H, Ando H, Horii A, Ichii S, Nakatsuru S, et al. Somatic mutations of the APC gene in colorectal tumors: mutation cluster region in the APC gene. *Human molecular genetics*. 1992 Jul;1(4):229-33.
21. Lal G, Gallinger S. Familial adenomatous polyposis. *Seminars in surgical oncology*. 2000 Jun;18(4):314-23.
22. Neufeld KL, Zhang F, Cullen BR, White RL. APC-mediated downregulation of beta-catenin activity involves nuclear sequestration and nuclear export. *EMBO reports*. 2000 Dec;1(6):519-23.
23. Henderson BR, Fagotto F. The ins and outs of APC and beta-catenin nuclear transport. *EMBO Rep*. 2002 Sep;3(9):834-9.
24. Zhang F, White RL, Neufeld KL. Phosphorylation near nuclear localization signal regulates nuclear import of adenomatous polyposis coli protein. *Proc Natl Acad Sci U S A*. 2000 Nov 7;97(23):12577-82.
25. Galea MA, Eleftheriou A, Henderson BR. ARM domain-dependent nuclear import of adenomatous polyposis coli protein is stimulated by the B56 alpha subunit of protein phosphatase 2A. *J Biol Chem*. 2001 Dec 7;276(49):45833-9.
26. Jimbo T, Kawasaki Y, Koyama R, Sato R, Takada S, Haraguchi K, et al. Identification of a link between the tumour suppressor APC and the kinesin superfamily. *Nat Cell Biol*. 2002 Apr;4(4):323-7.
27. Sharma M, Leung L, Brocardo M, Henderson J, Flegg C, Henderson BR. Membrane localization of adenomatous polyposis coli protein at cellular protrusions: targeting sequences and regulation by beta-catenin. *J Biol Chem*. 2006 Jun 23;281(25):17140-9.
28. Zumbunn J, Kinoshita K, Hyman AA, Nathke IS. Binding of the adenomatous polyposis coli protein to microtubules increases microtubule stability and is regulated by GSK3 beta phosphorylation. *Curr Biol*. 2001 Jan 9;11(1):44-9.
29. Mimori-Kiyosue Y, Shiina N, Tsukita S. Adenomatous polyposis coli (APC) protein moves along microtubules and concentrates at their growing ends in epithelial cells. *The Journal of cell biology*. 2000 Feb 7;148(3):505-18.
30. Breitman M, Zilberberg A, Caspi M, Rosin-Arbesfeld R. The armadillo repeat domain of the APC tumor suppressor protein interacts with Striatin family members. *Biochim Biophys Acta*. 2008 Oct;1783(10):1792-802.

31. Brocardo M, Nathke IS, Henderson BR. Redefining the subcellular location and transport of APC: new insights using a panel of antibodies. *EMBO Rep.* 2005 Feb;6(2):184-90.
32. Cadigan KM, Peifer M. Wnt signaling from development to disease: insights from model systems. *Cold Spring Harb Perspect Biol.* 2009 Aug;1(2):a002881.
33. Clevers H. Wnt/beta-catenin signaling in development and disease. *Cell.* 2006 Nov 3;127(3):469-80.
34. Cong F, Schweizer L, Varmus H. Wnt signals across the plasma membrane to activate the beta-catenin pathway by forming oligomers containing its receptors, Frizzled and LRP. *Development.* 2004 Oct;131(20):5103-15.
35. Niehrs C. The complex world of WNT receptor signalling. *Nature reviews Molecular cell biology.* 2012 Dec;13(12):767-79.
36. Seeling JM, Miller JR, Gil R, Moon RT, White R, Virshup DM. Regulation of beta-catenin signaling by the B56 subunit of protein phosphatase 2A. *Science.* 1999 Mar 26;283(5410):2089-91.
37. Rubinfeld B, Albert I, Porfiri E, Fiol C, Munemitsu S, Polakis P. Binding of GSK3beta to the APC-beta-catenin complex and regulation of complex assembly. *Science.* 1996 May 17;272(5264):1023-6.
38. Liu J, Xing Y, Hinds TR, Zheng J, Xu W. The third 20 amino acid repeat is the tightest binding site of APC for beta-catenin. *Journal of molecular biology.* 2006 Jun 30;360(1):133-44.
39. Eklof Spink K, Fridman SG, Weis WI. Molecular mechanisms of beta-catenin recognition by adenomatous polyposis coli revealed by the structure of an APC-beta-catenin complex. *EMBO J.* 2001 Nov 15;20(22):6203-12.
40. Behrens J, Jerchow BA, Wurtele M, Grimm J, Asbrand C, Wirtz R, et al. Functional interaction of an axin homolog, conductin, with beta-catenin, APC, and GSK3beta. *Science.* 1998 Apr 24;280(5363):596-9.
41. Spink KE, Polakis P, Weis WI. Structural basis of the Axin-adenomatous polyposis coli interaction. *EMBO J.* 2000 May 15;19(10):2270-9.
42. Schneikert J, Ruppert JG, Behrens J, Wenzel EM. different Roles for the axin interactions with the SAMP versus the second twenty amino acid repeat of adenomatous polyposis coli. *PLoS One.* 2014;9(4):e94413.
43. Xing Y, Clements WK, Kimelman D, Xu W. Crystal structure of a beta-catenin/axin complex suggests a mechanism for the beta-catenin destruction complex. *Genes Dev.* 2003 Nov 15;17(22):2753-64.
44. Ha NC, Tonzuka T, Stamos JL, Choi HJ, Weis WI. Mechanism of phosphorylation-dependent binding of APC to beta-catenin and its role in beta-catenin degradation. *Molecular cell.* 2004 Aug 27;15(4):511-21.

45. Su Y, Fu C, Ishikawa S, Stella A, Kojima M, Shitoh K, et al. APC is essential for targeting phosphorylated beta-catenin to the SCFbeta-TrCP ubiquitin ligase. *Molecular cell*. 2008 Dec 5;32(5):652-61.
46. Yang J, Zhang W, Evans PM, Chen X, He X, Liu C. Adenomatous polyposis coli (APC) differentially regulates beta-catenin phosphorylation and ubiquitination in colon cancer cells. *The Journal of biological chemistry*. 2006 Jun 30;281(26):17751-7.
47. Mendoza-Topaz C, Mieszczanek J, Bienz M. The Adenomatous polyposis coli tumour suppressor is essential for Axin complex assembly and function and opposes Axin's interaction with Dishevelled. *Open biology*. 2011 Nov;1(3):110013.
48. Henderson BR. Nuclear-cytoplasmic shuttling of APC regulates beta-catenin subcellular localization and turnover. *Nat Cell Biol*. 2000 Sep;2(9):653-60.
49. Rosin-Arbesfeld R, Townsley F, Bienz M. The APC tumour suppressor has a nuclear export function. *Nature*. 2000 Aug 31;406(6799):1009-12.
50. Hamada F, Bienz M. The APC tumor suppressor binds to C-terminal binding protein to divert nuclear beta-catenin from TCF. *Dev Cell*. 2004 Nov;7(5):677-85.
51. Sierra J, Yoshida T, Joazeiro CA, Jones KA. The APC tumor suppressor counteracts beta-catenin activation and H3K4 methylation at Wnt target genes. *Genes Dev*. 2006 Mar 1;20(5):586-600.
52. Etienne-Manneville S. APC in cell migration. *Adv Exp Med Biol*. 2009;656:30-40.
53. Akiyama T, Kawasaki Y. Wnt signalling and the actin cytoskeleton. *Oncogene*. 2006 Dec 4;25(57):7538-44.
54. Nathke I. Cytoskeleton out of the cupboard: colon cancer and cytoskeletal changes induced by loss of APC. *Nat Rev Cancer*. 2006 Dec;6(12):967-74.
55. Sakamoto Y, Boeda B, Etienne-Manneville S. APC binds intermediate filaments and is required for their reorganization during cell migration. *The Journal of cell biology*. 2013 Feb 4;200(3):249-58.
56. Okada K, Bartolini F, Deaconescu AM, Moseley JB, Dogic Z, Grigorieff N, et al. Adenomatous polyposis coli protein nucleates actin assembly and synergizes with the formin mDia1. *J Cell Biol*. 2010 Jun 28;189(7):1087-96.
57. Kawasaki Y, Senda T, Ishidate T, Koyama R, Morishita T, Iwayama Y, et al. Asef, a link between the tumor suppressor APC and G-protein signaling. *Science*. 2000 Aug 18;289(5482):1194-7.
58. Watanabe T, Wang S, Noritake J, Sato K, Fukata M, Takefuji M, et al. Interaction with IQGAP1 links APC to Rac1, Cdc42, and actin filaments during cell polarization and migration. *Dev Cell*. 2004 Dec;7(6):871-83.

59. Matsumine A, Ogai A, Senda T, Okumura N, Satoh K, Baeg GH, et al. Binding of APC to the human homolog of the Drosophila discs large tumor suppressor protein. *Science*. 1996 May 17;272(5264):1020-3.
60. Munemitsu S, Souza B, Muller O, Albert I, Rubinfeld B, Polakis P. The APC gene product associates with microtubules in vivo and promotes their assembly in vitro. *Cancer Res*. 1994 Jul 15;54(14):3676-81.
61. Su LK, Burrell M, Hill DE, Gyuris J, Brent R, Wiltshire R, et al. APC binds to the novel protein EB1. *Cancer Res*. 1995 Jul 15;55(14):2972-7.
62. Murawala P, Tripathi MM, Vyas P, Salunke A, Joseph J. Nup358 interacts with APC and plays a role in cell polarization. *J Cell Sci*. 2009 Sep 1;122(Pt 17):3113-22.
63. Kita K, Wittmann T, Nathke IS, Waterman-Storer CM. Adenomatous polyposis coli on microtubule plus ends in cell extensions can promote microtubule net growth with or without EB1. *Mol Biol Cell*. 2006 May;17(5):2331-45.
64. Vicente-Manzanares M, Horwitz AR. Cell migration: an overview. *Methods in molecular biology*. 2011;769:1-24.
65. Kroboth K, Newton IP, Kita K, Dikovskaya D, Zumbunn J, Waterman-Storer CM, et al. Lack of adenomatous polyposis coli protein correlates with a decrease in cell migration and overall changes in microtubule stability. *Mol Biol Cell*. 2007 Mar;18(3):910-8.
66. Sansom OJ, Reed KR, Hayes AJ, Ireland H, Brinkmann H, Newton IP, et al. Loss of Apc in vivo immediately perturbs Wnt signaling, differentiation, and migration. *Genes Dev*. 2004 Jun 15;18(12):1385-90.
67. Askham JM, Moncur P, Markham AF, Morrison EE. Regulation and function of the interaction between the APC tumour suppressor protein and EB1. *Oncogene*. 2000 Apr 6;19(15):1950-8.
68. Jaulin F, Kreitzer G. KIF17 stabilizes microtubules and contributes to epithelial morphogenesis by acting at MT plus ends with EB1 and APC. *The Journal of cell biology*. 2010 Aug 9;190(3):443-60.
69. Pfister AS, Hadjihannas MV, Rohrig W, Schambony A, Behrens J. Amer2 protein interacts with EB1 protein and adenomatous polyposis coli (APC) and controls microtubule stability and cell migration. *The Journal of biological chemistry*. 2012 Oct 12;287(42):35333-40.
70. Wen Y, Eng CH, Schmoranzler J, Cabrera-Poch N, Morris EJ, Chen M, et al. EB1 and APC bind to mDia to stabilize microtubules downstream of Rho and promote cell migration. *Nat Cell Biol*. 2004 Sep;6(9):820-30.
71. Nakamura M, Zhou XZ, Lu KP. Critical role for the EB1 and APC interaction in the regulation of microtubule polymerization. *Curr Biol*. 2001 Jul 10;11(13):1062-7.

72. Moseley JB, Bartolini F, Okada K, Wen Y, Gundersen GG, Goode BL. Regulated binding of adenomatous polyposis coli protein to actin. *The Journal of biological chemistry*. 2007 Apr 27;282(17):12661-8.
73. Kawasaki Y, Sato R, Akiyama T. Mutated APC and Asef are involved in the migration of colorectal tumour cells. *Nature cell biology*. 2003 Mar;5(3):211-5.
74. Reilein A, Nelson WJ. APC is a component of an organizing template for cortical microtubule networks. *Nature cell biology*. 2005 May;7(5):463-73.
75. Etienne-Manneville S, Manneville JB, Nicholls S, Ferenczi MA, Hall A. Cdc42 and Par6-PKCzeta regulate the spatially localized association of Dlg1 and APC to control cell polarization. *The Journal of cell biology*. 2005 Sep 12;170(6):895-901.
76. Manneville JB, Jehanno M, Etienne-Manneville S. Dlg1 binds GKAP to control dynein association with microtubules, centrosome positioning, and cell polarity. *The Journal of cell biology*. 2010 Nov 1;191(3):585-98.
77. Collin L, Schlessinger K, Hall A. APC nuclear membrane association and microtubule polarity. *Biol Cell*. 2008 Apr;100(4):243-52.
78. Rusan NM, Peifer M. Original CIN: reviewing roles for APC in chromosome instability. *The Journal of cell biology*. 2008 Jun 2;181(5):719-26.
79. Kaplan KB, Burds AA, Swedlow JR, Bekir SS, Sorger PK, Nathke IS. A role for the Adenomatous Polyposis Coli protein in chromosome segregation. *Nat Cell Biol*. 2001 Apr;3(4):429-32.
80. Green RA, Kaplan KB. Chromosome instability in colorectal tumor cells is associated with defects in microtubule plus-end attachments caused by a dominant mutation in APC. *J Cell Biol*. 2003 Dec 8;163(5):949-61.
81. Deka J, Herter P, Sprenger-Haussels M, Koosch S, Franz D, Muller KM, et al. The APC protein binds to A/T rich DNA sequences. *Oncogene*. 1999 Oct 7;18(41):5654-61.
82. Brocardo MG, Borowiec JA, Henderson BR. Adenomatous polyposis coli protein regulates the cellular response to DNA replication stress. *Int J Biochem Cell Biol*. 2011 Sep;43(9):1354-64.
83. Schneikert J, Behrens J. Truncated APC is required for cell proliferation and DNA replication. *Int J Cancer*. 2006 Jul 1;119(1):74-9.
84. Jaiswal AS, Narayan S. A novel function of adenomatous polyposis coli (APC) in regulating DNA repair. *Cancer Lett*. 2008 Nov 28;271(2):272-80.
85. Benchabane H, Ahmed Y. The adenomatous polyposis coli tumor suppressor and Wnt signaling in the regulation of apoptosis. *Adv Exp Med Biol*. 2009;656:75-84.
86. Chen T, Yang I, Irby R, Shain KH, Wang HG, Quackenbush J, et al. Regulation of caspase expression and apoptosis by adenomatous polyposis coli. *Cancer Res*. 2003 Aug 1;63(15):4368-74.

87. Qian J, Perchiniak EM, Sun K, Groden J. The mitochondrial protein hTID-1 partners with the caspase-cleaved adenomatous polyposis cell tumor suppressor to facilitate apoptosis. *Gastroenterology*. 2010 Apr;138(4):1418-28.
88. Su LK, Johnson KA, Smith KJ, Hill DE, Vogelstein B, Kinzler KW. Association between wild type and mutant APC gene products. *Cancer Res*. 1993 Jun 15;53(12):2728-31.
89. Joslyn G, Richardson DS, White R, Alber T. Dimer formation by an N-terminal coiled coil in the APC protein. *Proc Natl Acad Sci U S A*. 1993 Dec 1;90(23):11109-13.
90. Korinek V, Barker N, Morin PJ, van Wichen D, de Weger R, Kinzler KW, et al. Constitutive transcriptional activation by a beta-catenin-Tcf complex in APC^{-/-} colon carcinoma. *Science*. 1997 Mar 21;275(5307):1784-7.
91. Morin PJ, Sparks AB, Korinek V, Barker N, Clevers H, Vogelstein B, et al. Activation of beta-catenin-Tcf signaling in colon cancer by mutations in beta-catenin or APC. *Science*. 1997 Mar 21;275(5307):1787-90.
92. Chiurillo MA. Role of the Wnt/beta-catenin pathway in gastric cancer: An in-depth literature review. *World journal of experimental medicine*. 2015 May 20;5(2):84-102.
93. Song L, Li Y, He B, Gong Y. Development of Small Molecules Targeting the Wnt Signaling Pathway in Cancer Stem Cells for the Treatment of Colorectal Cancer. *Clinical colorectal cancer*. 2015 Feb 17.
94. Rosin-Arbesfeld R, Ihrke G, Bienz M. Actin-dependent membrane association of the APC tumour suppressor in polarized mammalian epithelial cells. *EMBO J*. 2001 Nov 1;20(21):5929-39.
95. Lesko AC, Goss KH, Yang FF, Schwertner A, Hultur I, Onel K, et al. The APC tumor suppressor is required for epithelial cell polarization and three-dimensional morphogenesis. *Biochim Biophys Acta*. 2015 Mar;1854(3):711-23.
96. Nelson SA, Li Z, Newton IP, Fraser D, Milne RE, Martin DM, et al. Tumorigenic fragments of APC cause dominant defects in directional cell migration in multiple model systems. *Disease models & mechanisms*. 2012 Nov;5(6):940-7.
97. Lamprecht SA, Lipkin M. Migrating colonic crypt epithelial cells: primary targets for transformation. *Carcinogenesis*. 2002 Nov;23(11):1777-80.
98. Moss SF, Liu TC, Petrotos A, Hsu TM, Gold LI, Holt PR. Inward growth of colonic adenomatous polyps. *Gastroenterology*. 1996 Dec;111(6):1425-32.
99. Mahmoud NN, Boolbol SK, Bilinski RT, Martucci C, Chadburn A, Bertagnolli MM. Apc gene mutation is associated with a dominant-negative effect upon intestinal cell migration. *Cancer Res*. 1997 Nov 15;57(22):5045-50.
100. Kawasaki Y, Tsuji S, Muroya K, Furukawa S, Shibata Y, Okuno M, et al. The adenomatous polyposis coli-associated exchange factors Asef and Asef2 are required for adenoma formation in Apc(Min/+)⁺mice. *EMBO reports*. 2009 Dec;10(12):1355-62.

101. Faux MC, Ross JL, Meeker C, Johns T, Ji H, Simpson RJ, et al. Restoration of full-length adenomatous polyposis coli (APC) protein in a colon cancer cell line enhances cell adhesion. *Journal of cell science*. 2004 Jan 26;117(Pt 3):427-39.
102. Thompson SL, Compton DA. Examining the link between chromosomal instability and aneuploidy in human cells. *The Journal of cell biology*. 2008 Feb 25;180(4):665-72.
103. Draviam VM, Xie S, Sorger PK. Chromosome segregation and genomic stability. *Current opinion in genetics & development*. 2004 Apr;14(2):120-5.
104. Fodde R, Kuipers J, Rosenberg C, Smits R, Kielman M, Gaspar C, et al. Mutations in the APC tumour suppressor gene cause chromosomal instability. *Nat Cell Biol*. 2001 Apr;3(4):433-8.
105. Green RA, Wollman R, Kaplan KB. APC and EB1 function together in mitosis to regulate spindle dynamics and chromosome alignment. *Mol Biol Cell*. 2005 Oct;16(10):4609-22.
106. Martino-Echarri E, Henderson BR, Brocardo MG. Targeting the DNA replication checkpoint by pharmacologic inhibition of Chk1 kinase: a strategy to sensitize APC mutant colon cancer cells to 5-fluorouracil chemotherapy. *Oncotarget*. 2014 Oct 30;5(20):9889-900.
107. Huang X, Guo B. Adenomatous polyposis coli determines sensitivity to histone deacetylase inhibitor-induced apoptosis in colon cancer cells. *Cancer Res*. 2006 Sep 15;66(18):9245-51.
108. Dihlmann S, Kloor M, Fallsehr C, von Knebel Doeberitz M. Regulation of AKT1 expression by beta-catenin/Tcf/Lef signaling in colorectal cancer cells. *Carcinogenesis*. 2005 Sep;26(9):1503-12.
109. Mezhybovska M, Wikstrom K, Ohd JF, Sjolander A. The inflammatory mediator leukotriene D4 induces beta-catenin signaling and its association with antiapoptotic Bcl-2 in intestinal epithelial cells. *The Journal of biological chemistry*. 2006 Mar 10;281(10):6776-84.
110. Mezhybovska M, Yudina Y, Abhyankar A, Sjolander A. Beta-catenin is involved in alterations in mitochondrial activity in non-transformed intestinal epithelial and colon cancer cells. *British journal of cancer*. 2009 Nov 3;101(9):1596-605.
111. Johannsen DL, Ravussin E. The role of mitochondria in health and disease. *Current Opinion in Pharmacology*. [doi: DOI: 10.1016/j.coph.2009.09.002]. 2009;9(6):780-6.
112. Chen C, Paw BH. Cellular and mitochondrial iron homeostasis in vertebrates. *Biochim Biophys Acta*. 2012 Sep;1823(9):1459-67.
113. Mena NP, Urrutia PJ, Lourido F, Carrasco CM, Nunez MT. Mitochondrial iron homeostasis and its dysfunctions in neurodegenerative disorders. *Mitochondrion*. 2015 Mar;21:92-105.

114. Scheffler IE. *Mitochondria*: Wiley; 2011.
115. Desideri E, Vegliante R, Ciriolo MR. Mitochondrial dysfunctions in cancer: genetic defects and oncogenic signaling impinging on TCA cycle activity. *Cancer letters*. 2015 Jan 28;356(2 Pt A):217-23.
116. Serra D, Mera P, Malandrino MI, Mir JF, Herrero L. Mitochondrial fatty acid oxidation in obesity. *Antioxidants & redox signaling*. 2013 Jul 20;19(3):269-84.
117. Huttemann M, Lee I, Samavati L, Yu H, Doan JW. Regulation of mitochondrial oxidative phosphorylation through cell signaling. *Biochim Biophys Acta*. 2007 Dec;1773(12):1701-20.
118. Smeitink J, van den Heuvel L, DiMauro S. The genetics and pathology of oxidative phosphorylation. *Nature reviews Genetics*. 2001 May;2(5):342-52.
119. Chaban Y, Boekema EJ, Dudkina NV. Structures of mitochondrial oxidative phosphorylation supercomplexes and mechanisms for their stabilisation. *Biochim Biophys Acta*. 2014 Apr;1837(4):418-26.
120. Papa S, Martino P, Capitanio G, Gaballo A, De Rasmio D, Signorile A, et al. The Oxidative Phosphorylation System in Mammalian Mitochondria. In: Scatena R, Bottoni P, Giardina B, editors. *Advances in Mitochondrial Medicine*: Springer Netherlands; 2012. p. 3-37.
121. Walsh C, Barrow S, Voronina S, Chvanov M, Petersen OH, Tepikin A. Modulation of calcium signalling by mitochondria. *Biochim Biophys Acta*. 2009 Nov;1787(11):1374-82.
122. Graier WF, Frieden M, Malli R. Mitochondria and Ca(2+) signaling: old guests, new functions. *Pflügers Archiv : European journal of physiology*. 2007 Dec;455(3):375-96.
123. Hajnoczky G, Csordas G, Das S, Garcia-Perez C, Saotome M, Sinha Roy S, et al. Mitochondrial calcium signalling and cell death: approaches for assessing the role of mitochondrial Ca²⁺ uptake in apoptosis. *Cell calcium*. 2006 Nov-Dec;40(5-6):553-60.
124. Gincel D, Zaid H, Shoshan-Barmatz V. Calcium binding and translocation by the voltage-dependent anion channel: a possible regulatory mechanism in mitochondrial function. *Biochem J*. 2001 Aug 15;358(Pt 1):147-55.
125. Rapizzi E, Pinton P, Szabadkai G, Wieckowski MR, Vandecasteele G, Baird G, et al. Recombinant expression of the voltage-dependent anion channel enhances the transfer of Ca²⁺ microdomains to mitochondria. *The Journal of cell biology*. 2002 Nov 25;159(4):613-24.
126. Kirichok Y, Krapivinsky G, Clapham DE. The mitochondrial calcium uniporter is a highly selective ion channel. *Nature*. 2004 Jan 22;427(6972):360-4.
127. Alonso MT, Villalobos C, Chamero P, Alvarez J, Garcia-Sancho J. Calcium microdomains in mitochondria and nucleus. *Cell calcium*. 2006 Nov-Dec;40(5-6):513-25.

128. Gunter TE, Pfeiffer DR. Mechanisms by which mitochondria transport calcium. *The American journal of physiology*. 1990 May;258(5 Pt 1):C755-86.
129. Scorziello A, Savoia C, Sisalli MJ, Adornetto A, Secondo A, Boscia F, et al. NCX3 regulates mitochondrial Ca(2+) handling through the AKAP121-anchored signaling complex and prevents hypoxia-induced neuronal death. *Journal of cell science*. 2013 Dec 15;126(Pt 24):5566-77.
130. Li MX, Dewson G. Mitochondria and apoptosis: emerging concepts. *F1000prime reports*. 2015;7:42.
131. Lopez J, Tait SW. Mitochondrial apoptosis: killing cancer using the enemy within. *British journal of cancer*. 2015 Mar 17;112(6):957-62.
132. Gillies LA, Kuwana T. Apoptosis regulation at the mitochondrial outer membrane. *Journal of cellular biochemistry*. 2014 Apr;115(4):632-40.
133. Willis SN, Adams JM. Life in the balance: how BH3-only proteins induce apoptosis. *Current opinion in cell biology*. 2005 Dec;17(6):617-25.
134. Reubold TF, Eschenburg S. A molecular view on signal transduction by the apoptosome. *Cellular signalling*. 2012 Jul;24(7):1420-5.
135. Tait SW, Ichim G, Green DR. Die another way--non-apoptotic mechanisms of cell death. *Journal of cell science*. 2014 May 15;127(Pt 10):2135-44.
136. Lartigue L, Kushnareva Y, Seong Y, Lin H, Faustin B, Newmeyer DD. Caspase-independent mitochondrial cell death results from loss of respiration, not cytotoxic protein release. *Mol Biol Cell*. 2009 Dec;20(23):4871-84.
137. Lin MY, Sheng ZH. Regulation of mitochondrial transport in neurons. *Experimental cell research*. 2015 May 15;334(1):35-44.
138. Sheng ZH. Mitochondrial trafficking and anchoring in neurons: New insight and implications. *J Cell Biol*. 2014 Mar 31;204(7):1087-98.
139. Chaturvedi RK, Flint Beal M. Mitochondrial diseases of the brain. *Free Radic Biol Med*. 2013 Oct;63:1-29.
140. Corrado M, Scorrano L, Campello S. Mitochondrial dynamics in cancer and neurodegenerative and neuroinflammatory diseases. *International journal of cell biology*. 2012;2012:729290.
141. Sheng ZH, Cai Q. Mitochondrial transport in neurons: impact on synaptic homeostasis and neurodegeneration. *Nature reviews Neuroscience*. 2012 Feb;13(2):77-93.
142. Campello S, Lacalle RA, Bettella M, Manes S, Scorrano L, Viola A. Orchestration of lymphocyte chemotaxis by mitochondrial dynamics. *J Exp Med*. 2006 Dec 25;203(13):2879-86.

143. Guo X, Macleod GT, Wellington A, Hu F, Panchumarthi S, Schoenfield M, et al. The GTPase dMiro is required for axonal transport of mitochondria to Drosophila synapses. *Neuron*. 2005 Aug 4;47(3):379-93.
144. Stowers RS, Megeath LJ, Gorska-Andrzejak J, Meinertzhagen IA, Schwarz TL. Axonal transport of mitochondria to synapses depends on milton, a novel Drosophila protein. *Neuron*. 2002 Dec 19;36(6):1063-77.
145. Brickley K, Smith MJ, Beck M, Stephenson FA. GRIF-1 and OIP106, members of a novel gene family of coiled-coil domain proteins: association in vivo and in vitro with kinesin. *J Biol Chem*. 2005 Apr 15;280(15):14723-32.
146. Fransson A, Ruusala A, Aspenstrom P. Atypical Rho GTPases have roles in mitochondrial homeostasis and apoptosis. *J Biol Chem*. 2003 Feb 21;278(8):6495-502.
147. Cox RT, Spradling AC. Milton controls the early acquisition of mitochondria by Drosophila oocytes. *Development*. 2006 Sep;133(17):3371-7.
148. Fransson S, Ruusala A, Aspenstrom P. The atypical Rho GTPases Miro-1 and Miro-2 have essential roles in mitochondrial trafficking. *Biochem Biophys Res Commun*. 2006 Jun 2;344(2):500-10.
149. Glater EE, Megeath LJ, Stowers RS, Schwarz TL. Axonal transport of mitochondria requires milton to recruit kinesin heavy chain and is light chain independent. *J Cell Biol*. 2006 May 22;173(4):545-57.
150. MacAskill AF, Brickley K, Stephenson FA, Kittler JT. GTPase dependent recruitment of Grif-1 by Miro1 regulates mitochondrial trafficking in hippocampal neurons. *Mol Cell Neurosci*. 2009 Mar;40(3):301-12.
151. Hurd DD, Saxton WM. Kinesin mutations cause motor neuron disease phenotypes by disrupting fast axonal transport in Drosophila. *Genetics*. 1996 Nov;144(3):1075-85.
152. Wang X, Winter D, Ashrafi G, Schlehe J, Wong YL, Selkoe D, et al. PINK1 and Parkin Target Miro for Phosphorylation and Degradation to Arrest Mitochondrial Motility. *Cell*. 2011 Nov 11;147(4):893-906.
153. Wang X, Schwarz TL. The mechanism of Ca²⁺ -dependent regulation of kinesin-mediated mitochondrial motility. *Cell*. 2009 Jan 9;136(1):163-74.
154. Brickley K, Stephenson FA. Trafficking kinesin protein (TRAK)-mediated transport of mitochondria in axons of hippocampal neurons. *J Biol Chem*. 2011 May 20;286(20):18079-92.
155. Smith MJ, Pozo K, Brickley K, Stephenson FA. Mapping the GRIF-1 binding domain of the kinesin, KIF5C, substantiates a role for GRIF-1 as an adaptor protein in the anterograde trafficking of cargoes. *J Biol Chem*. 2006 Sep 15;281(37):27216-28.
156. Pekkurnaz G, Trinidad JC, Wang X, Kong D, Schwarz TL. Glucose regulates mitochondrial motility via Milton modification by O-GlcNAc transferase. *Cell*. 2014 Jul 3;158(1):54-68.

157. Tsai PI, Course MM, Lovas JR, Hsieh CH, Babic M, Zinsmaier KE, et al. PINK1-mediated phosphorylation of Miro inhibits synaptic growth and protects dopaminergic neurons in *Drosophila*. *Scientific reports*. 2014;4:6962.
158. Saotome M, Safiulina D, Szabadkai G, Das S, Fransson A, Aspenstrom P, et al. Bidirectional Ca²⁺-dependent control of mitochondrial dynamics by the Miro GTPase. *Proc Natl Acad Sci U S A*. 2008 Dec 30;105(52):20728-33.
159. Macaskill AF, Rinholm JE, Twelvetrees AE, Arancibia-Carcamo IL, Muir J, Fransson A, et al. Miro1 is a calcium sensor for glutamate receptor-dependent localization of mitochondria at synapses. *Neuron*. 2009 Feb 26;61(4):541-55.
160. Li Y, Lim S, Hoffman D, Aspenstrom P, Federoff HJ, Rempe DA. HUMMR, a hypoxia- and HIF-1 α -inducible protein, alters mitochondrial distribution and transport. *J Cell Biol*. 2009 Jun 15;185(6):1065-81.
161. Serrat R, Lopez-Domenech G, Mirra S, Quevedo M, Garcia-Fernandez J, Ulloa F, et al. The non-canonical Wnt/PKC pathway regulates mitochondrial dynamics through degradation of the arm-like domain-containing protein Alex3. *PLoS One*. 2013;8(7):e67773.
162. Misko A, Jiang S, Wegorzewska I, Milbrandt J, Baloh RH. Mitofusin 2 is necessary for transport of axonal mitochondria and interacts with the Miro/Milton complex. *J Neurosci*. 2010 Mar 24;30(12):4232-40.
163. Lopez-Domenech G, Serrat R, Mirra S, D'Aniello S, Somorjai I, Abad A, et al. The Eutherian *Armcx* genes regulate mitochondrial trafficking in neurons and interact with Miro and Trak2. *Nat Commun*. 2012;3:814.
164. Yi M, Weaver D, Hajnoczky G. Control of mitochondrial motility and distribution by the calcium signal: a homeostatic circuit. *The Journal of cell biology*. 2004 Nov 22;167(4):661-72.
165. Liu S, Sawada T, Lee S, Yu W, Silverio G, Alapatt P, et al. Parkinson's disease-associated kinase PINK1 regulates Miro protein level and axonal transport of mitochondria. *PLoS genetics*. 2012;8(3):e1002537.
166. Birsa N, Norkett R, Wauer T, Mevissen TE, Wu HC, Foltynie T, et al. Lysine 27 ubiquitination of the mitochondrial transport protein Miro is dependent on serine 65 of the Parkin ubiquitin ligase. *J Biol Chem*. 2014 May 23;289(21):14569-82.
167. Morlino G, Barreiro O, Baixauli F, Robles-Valero J, Gonzalez-Granado JM, Villa-Bellosta R, et al. Miro-1 links mitochondria and microtubule Dynein motors to control lymphocyte migration and polarity. *Mol Cell Biol*. 2014 Apr;34(8):1412-26.
168. Russo GJ, Louie K, Wellington A, Macleod GT, Hu F, Panchumarthi S, et al. *Drosophila* Miro is required for both anterograde and retrograde axonal mitochondrial transport. *J Neurosci*. 2009 Apr 29;29(17):5443-55.
169. van Spronsen M, Mikhaylova M, Lipka J, Schlager MA, van den Heuvel DJ, Kuijpers M, et al. TRAK/Milton motor-adaptor proteins steer mitochondrial trafficking to axons and dendrites. *Neuron*. 2013 Feb 6;77(3):485-502.

170. Ligon LA, Steward O. Role of microtubules and actin filaments in the movement of mitochondria in the axons and dendrites of cultured hippocampal neurons. *The Journal of comparative neurology*. 2000 Nov 20;427(3):351-61.
171. Morris RL, Hollenbeck PJ. Axonal transport of mitochondria along microtubules and F-actin in living vertebrate neurons. *The Journal of cell biology*. 1995 Dec;131(5):1315-26.
172. Langford GM. Actin- and microtubule-dependent organelle motors: interrelationships between the two motility systems. *Current opinion in cell biology*. 1995 Feb;7(1):82-8.
173. Perez-Olle R, Lopez-Toledano MA, Goryunov D, Cabrera-Poch N, Stefanis L, Brown K, et al. Mutations in the neurofilament light gene linked to Charcot-Marie-Tooth disease cause defects in transport. *Journal of neurochemistry*. 2005 May;93(4):861-74.
174. Uttam J, Hutton E, Coulombe PA, Anton-Lamprecht I, Yu QC, Gedde-Dahl T, Jr., et al. The genetic basis of epidermolysis bullosa simplex with mottled pigmentation. *Proc Natl Acad Sci U S A*. 1996 Aug 20;93(17):9079-84.
175. Winter L, Abrahamsberg C, Wiche G. Plectin isoform 1b mediates mitochondrion-intermediate filament network linkage and controls organelle shape. *The Journal of cell biology*. 2008 Jun 16;181(6):903-11.
176. Cho KI, Cai Y, Yi H, Yeh A, Aslanukov A, Ferreira PA. Association of the kinesin-binding domain of RanBP2 to KIF5B and KIF5C determines mitochondria localization and function. *Traffic*. 2007 Dec;8(12):1722-35.
177. Patil H, Cho KI, Lee J, Yang Y, Orry A, Ferreira PA. Kinesin-1 and mitochondrial motility control by discrimination of structurally equivalent but distinct subdomains in Ran-GTP-binding domains of Ran-binding protein 2. *Open Biol*. 2013 Mar;3(3):120183.
178. Cai Q, Gerwin C, Sheng ZH. Syntabulin-mediated anterograde transport of mitochondria along neuronal processes. *J Cell Biol*. 2005 Sep 12;170(6):959-69.
179. Nangaku M, Sato-Yoshitake R, Okada Y, Noda Y, Takemura R, Yamazaki H, et al. KIF1B, a novel microtubule plus end-directed monomeric motor protein for transport of mitochondria. *Cell*. 1994 Dec 30;79(7):1209-20.
180. Wozniak MJ, Melzer M, Dorner C, Haring HU, Lammers R. The novel protein KBP regulates mitochondria localization by interaction with a kinesin-like protein. *BMC Cell Biol*. 2005;6:35.
181. Tanaka K, Sugiura Y, Ichishita R, Mihara K, Oka T. KLP6: a newly identified kinesin that regulates the morphology and transport of mitochondria in neuronal cells. *J Cell Sci*. 2011 Jul 15;124(Pt 14):2457-65.
182. Pilling AD, Horiuchi D, Lively CM, Saxton WM. Kinesin-1 and Dynein are the primary motors for fast transport of mitochondria in *Drosophila* motor axons. *Mol Biol Cell*. 2006 Apr;17(4):2057-68.

183. Jimenez-Mateos EM, Gonzalez-Billault C, Dawson HN, Vitek MP, Avila J. Role of MAP1B in axonal retrograde transport of mitochondria. *Biochem J*. 2006 Jul 1;397(1):53-9.
184. Trinczek B, Ebner A, Mandelkow EM, Mandelkow E. Tau regulates the attachment/detachment but not the speed of motors in microtubule-dependent transport of single vesicles and organelles. *Journal of cell science*. 1999 Jul;112 (Pt 14):2355-67.
185. Chen Y, Sheng ZH. Kinesin-1-syntrophin coupling mediates activity-dependent regulation of axonal mitochondrial transport. *The Journal of cell biology*. 2013 Jul 22;202(2):351-64.
186. Kang JS, Tian JH, Pan PY, Zald P, Li C, Deng C, et al. Docking of axonal mitochondria by syntrophin controls their mobility and affects short-term facilitation. *Cell*. 2008 Jan 11;132(1):137-48.
187. Pathak D, Sepp KJ, Hollenbeck PJ. Evidence that myosin activity opposes microtubule-based axonal transport of mitochondria. *J Neurosci*. 2010 Jun 30;30(26):8984-92.
188. Quintero OA, DiVito MM, Adikes RC, Kortan MB, Case LB, Lier AJ, et al. Human Myo19 is a novel myosin that associates with mitochondria. *Curr Biol*. 2009 Dec 15;19(23):2008-13.
189. Attwell D, Laughlin SB. An energy budget for signaling in the grey matter of the brain. *Journal of cerebral blood flow and metabolism : official journal of the International Society of Cerebral Blood Flow and Metabolism*. 2001 Oct;21(10):1133-45.
190. Varadi A, Cirulli V, Rutter GA. Mitochondrial localization as a determinant of capacitative Ca²⁺ entry in HeLa cells. *Cell calcium*. 2004 Dec;36(6):499-508.
191. Escobar-Henriques M, Anton F. Mechanistic perspective of mitochondrial fusion: tubulation vs. fragmentation. *Biochim Biophys Acta*. 2013 Jan;1833(1):162-75.
192. Chan DC. Fusion and fission: interlinked processes critical for mitochondrial health. *Annual review of genetics*. 2012;46:265-87.
193. Chan DC. Mitochondrial fusion and fission in mammals. *Annual review of cell and developmental biology*. 2006;22:79-99.
194. Hall AR, Burke N, Dongworth RK, Hausenloy DJ. Mitochondrial fusion and fission proteins: novel therapeutic targets for combating cardiovascular disease. *British journal of pharmacology*. 2014 Apr;171(8):1890-906.
195. da Silva AF, Mariotti FR, Maximo V, Campello S. Mitochondria dynamism: of shape, transport and cell migration. *Cell Mol Life Sci*. 2014 Jun;71(12):2313-24.
196. Song Z, Ghochani M, McCaffery JM, Frey TG, Chan DC. Mitofusins and OPA1 mediate sequential steps in mitochondrial membrane fusion. *Mol Biol Cell*. 2009 Aug;20(15):3525-32.

197. Rojo M, Legros F, Chateau D, Lombes A. Membrane topology and mitochondrial targeting of mitofusins, ubiquitous mammalian homologs of the transmembrane GTPase Fzo. *Journal of cell science*. 2002 Apr 15;115(Pt 8):1663-74.
198. Legros F, Lombes A, Frachon P, Rojo M. Mitochondrial fusion in human cells is efficient, requires the inner membrane potential, and is mediated by mitofusins. *Mol Biol Cell*. 2002 Dec;13(12):4343-54.
199. Zorzano A, Liesa M, Sebastian D, Segales J, Palacin M. Mitochondrial fusion proteins: dual regulators of morphology and metabolism. *Seminars in cell & developmental biology*. 2010 Aug;21(6):566-74.
200. de Brito OM, Scorrano L. Mitofusin 2 tethers endoplasmic reticulum to mitochondria. *Nature*. 2008 Dec 4;456(7222):605-10.
201. Cipolat S, Rudka T, Hartmann D, Costa V, Serneels L, Craessaerts K, et al. Mitochondrial rhomboid PARL regulates cytochrome c release during apoptosis via OPA1-dependent cristae remodeling. *Cell*. 2006 Jul 14;126(1):163-75.
202. Delettre C, Lenaers G, Griffoin JM, Gigarel N, Lorenzo C, Belenguer P, et al. Nuclear gene OPA1, encoding a mitochondrial dynamin-related protein, is mutated in dominant optic atrophy. *Nature genetics*. 2000 Oct;26(2):207-10.
203. Ishihara N, Fujita Y, Oka T, Mihara K. Regulation of mitochondrial morphology through proteolytic cleavage of OPA1. *Embo j*. 2006 Jul 12;25(13):2966-77.
204. Delettre C, Griffoin JM, Kaplan J, Dollfus H, Lorenz B, Faivre L, et al. Mutation spectrum and splicing variants in the OPA1 gene. *Human genetics*. 2001 Dec;109(6):584-91.
205. Akepati VR, Muller EC, Otto A, Strauss HM, Portwich M, Alexander C. Characterization of OPA1 isoforms isolated from mouse tissues. *Journal of neurochemistry*. 2008 Jul;106(1):372-83.
206. Smirnova E, Griparic L, Shurland DL, van der Blik AM. Dynamin-related protein Drp1 is required for mitochondrial division in mammalian cells. *Mol Biol Cell*. 2001 Aug;12(8):2245-56.
207. Mears JA, Lackner LL, Fang S, Ingerman E, Nunnari J, Hinshaw JE. Conformational changes in Dnm1 support a contractile mechanism for mitochondrial fission. *Nature structural & molecular biology*. 2011 Jan;18(1):20-6.
208. Friedman JR, Lackner LL, West M, DiBenedetto JR, Nunnari J, Voeltz GK. ER tubules mark sites of mitochondrial division. *Science*. 2011 Oct 21;334(6054):358-62.
209. Pedrola L, Espert A, Wu X, Claramunt R, Shy ME, Palau F. GDAP1, the protein causing Charcot-Marie-Tooth disease type 4A, is expressed in neurons and is associated with mitochondria. *Human molecular genetics*. 2005 Apr 15;14(8):1087-94.
210. Tondera D, Czauderna F, Paulick K, Schwarzer R, Kaufmann J, Santel A. The mitochondrial protein MTP18 contributes to mitochondrial fission in mammalian cells. *Journal of cell science*. 2005 Jul 15;118(Pt 14):3049-59.

211. Karbowski M, Jeong SY, Youle RJ. Endophilin B1 is required for the maintenance of mitochondrial morphology. *The Journal of cell biology*. 2004 Sep 27;166(7):1027-39.
212. Lokireddy S, Wijesoma Isuru W, Teng S, Bonala S, Gluckman Peter D, McFarlane C, et al. The Ubiquitin Ligase Mul1 Induces Mitophagy in Skeletal Muscle in Response to Muscle-Wasting Stimuli. *Cell metabolism*. 2012 11/7;16(5):613-24.
213. Yun J, Puri R, Yang H, Lizzio MA, Wu C, Sheng ZH, et al. MUL1 acts in parallel to the PINK1/parkin pathway in regulating mitofusin and compensates for loss of PINK1/parkin. *eLife*. 2014;3:e01958.
214. Ziviani E, Tao RN, Whitworth AJ. *Drosophila* parkin requires PINK1 for mitochondrial translocation and ubiquitinates mitofusin. *Proc Natl Acad Sci U S A*. 2010 Mar 16;107(11):5018-23.
215. Eura Y, Ishihara N, Oka T, Mihara K. Identification of a novel protein that regulates mitochondrial fusion by modulating mitofusin (Mfn) protein function. *Journal of cell science*. 2006 Dec 1;119(Pt 23):4913-25.
216. Hoppins S, Edlich F, Cleland MM, Banerjee S, McCaffery JM, Youle RJ, et al. The soluble form of Bax regulates mitochondrial fusion via MFN2 homotypic complexes. *Molecular cell*. 2011 Jan 21;41(2):150-60.
217. Choi SY, Huang P, Jenkins GM, Chan DC, Schiller J, Frohman MA. A common lipid links Mfn-mediated mitochondrial fusion and SNARE-regulated exocytosis. *Nature cell biology*. 2006 Nov;8(11):1255-62.
218. Head B, Griparic L, Amiri M, Gandre-Babbe S, van der Blik AM. Inducible proteolytic inactivation of OPA1 mediated by the OMA1 protease in mammalian cells. *The Journal of cell biology*. 2009 Dec 28;187(7):959-66.
219. Song Z, Chen H, Fiket M, Alexander C, Chan DC. OPA1 processing controls mitochondrial fusion and is regulated by mRNA splicing, membrane potential, and Yme1L. *The Journal of cell biology*. 2007 Aug 27;178(5):749-55.
220. Merkwirth C, Dargazanli S, Tatsuta T, Geimer S, Lower B, Wunderlich FT, et al. Prohibitins control cell proliferation and apoptosis by regulating OPA1-dependent cristae morphogenesis in mitochondria. *Genes Dev*. 2008 Feb 15;22(4):476-88.
221. An HJ, Cho G, Lee JO, Paik SG, Kim YS, Lee H. Higd-1a interacts with Opa1 and is required for the morphological and functional integrity of mitochondria. *Proc Natl Acad Sci U S A*. 2013 Aug 6;110(32):13014-9.
222. Yoon Y, Krueger EW, Oswald BJ, McNiven MA. The mitochondrial protein hFis1 regulates mitochondrial fission in mammalian cells through an interaction with the dynamin-like protein DLP1. *Mol Cell Biol*. 2003 Aug;23(15):5409-20.
223. Zhao J, Liu T, Jin S, Wang X, Qu M, Uhlen P, et al. Human MIEF1 recruits Drp1 to mitochondrial outer membranes and promotes mitochondrial fusion rather than fission. *Embo j*. 2011 Jul 20;30(14):2762-78.

224. Otera H, Wang C, Cleland MM, Setoguchi K, Yokota S, Youle RJ, et al. Mff is an essential factor for mitochondrial recruitment of Drp1 during mitochondrial fission in mammalian cells. *The Journal of cell biology*. 2010 Dec 13;191(6):1141-58.
225. Liu T, Yu R, Jin SB, Han L, Lendahl U, Zhao J, et al. The mitochondrial elongation factors MIEF1 and MIEF2 exert partially distinct functions in mitochondrial dynamics. *Experimental cell research*. 2013 Nov 1;319(18):2893-904.
226. Palmer CS, Osellame LD, Laine D, Koutsopoulos OS, Frazier AE, Ryan MT. MiD49 and MiD51, new components of the mitochondrial fission machinery. *EMBO reports*. 2011 Jun;12(6):565-73.
227. Fang L, Hemion C, Goldblum D, Meyer P, Orgul S, Frank S, et al. Inactivation of MARCH5 prevents mitochondrial fragmentation and interferes with cell death in a neuronal cell model. *PLoS One*. 2012;7(12):e52637.
228. Karbowski M, Neutzner A, Youle RJ. The mitochondrial E3 ubiquitin ligase MARCH5 is required for Drp1 dependent mitochondrial division. *The Journal of cell biology*. 2007 Jul 2;178(1):71-84.
229. Wang H, Song P, Du L, Tian W, Yue W, Liu M, et al. Parkin ubiquitinates Drp1 for proteasome-dependent degradation: implication of dysregulated mitochondrial dynamics in Parkinson disease. *The Journal of biological chemistry*. 2011 Apr 1;286(13):11649-58.
230. Cribbs JT, Strack S. Reversible phosphorylation of Drp1 by cyclic AMP-dependent protein kinase and calcineurin regulates mitochondrial fission and cell death. *EMBO reports*. 2007 Oct;8(10):939-44.
231. Chang CR, Blackstone C. Cyclic AMP-dependent protein kinase phosphorylation of Drp1 regulates its GTPase activity and mitochondrial morphology. *The Journal of biological chemistry*. 2007 Jul 27;282(30):21583-7.
232. Cereghetti GM, Stangherlin A, Martins de Brito O, Chang CR, Blackstone C, Bernardi P, et al. Dephosphorylation by calcineurin regulates translocation of Drp1 to mitochondria. *Proc Natl Acad Sci U S A*. 2008 Oct 14;105(41):15803-8.
233. Wasiak S, Zunino R, McBride HM. Bax/Bak promote sumoylation of DRP1 and its stable association with mitochondria during apoptotic cell death. *The Journal of cell biology*. 2007 May 7;177(3):439-50.
234. Braschi E, Zunino R, McBride HM. MAPL is a new mitochondrial SUMO E3 ligase that regulates mitochondrial fission. *EMBO reports*. 2009 Jul;10(7):748-54.
235. Zunino R, Schauss A, Rippstein P, Andrade-Navarro M, McBride HM. The SUMO protease SENP5 is required to maintain mitochondrial morphology and function. *Journal of cell science*. 2007 Apr 1;120(Pt 7):1178-88.
236. Tondera D, Grandemange S, Jourdain A, Karbowski M, Mattenberger Y, Herzig S, et al. SLP-2 is required for stress-induced mitochondrial hyperfusion. *Embo j*. 2009 Jun 3;28(11):1589-600.

237. Babbar M, Sheikh MS. Metabolic Stress and Disorders Related to Alterations in Mitochondrial Fission or Fusion. *Molecular and cellular pharmacology*. 2013;5(3):109-33.
238. Mishra P, Chan DC. Mitochondrial dynamics and inheritance during cell division, development and disease. *Nature reviews Molecular cell biology*. 2014 Oct;15(10):634-46.
239. Chen H, Vermulst M, Wang YE, Chomyn A, Prolla TA, McCaffery JM, et al. Mitochondrial fusion is required for mtDNA stability in skeletal muscle and tolerance of mtDNA mutations. *Cell*. 2010 Apr 16;141(2):280-9.
240. Chen H, Chomyn A, Chan DC. Disruption of fusion results in mitochondrial heterogeneity and dysfunction. *The Journal of biological chemistry*. 2005 Jul 15;280(28):26185-92.
241. Rossignol R, Faustin B, Rocher C, Malgat M, Mazat JP, Letellier T. Mitochondrial threshold effects. *Biochem J*. 2003 Mar 15;370(Pt 3):751-62.
242. Taylor RW, Turnbull DM. Mitochondrial DNA mutations in human disease. *Nature reviews Genetics*. 2005 May;6(5):389-402.
243. Kim I, Rodriguez-Enriquez S, Lemasters JJ. Selective degradation of mitochondria by mitophagy. *Archives of biochemistry and biophysics*. 2007 Jun 15;462(2):245-53.
244. Narendra D, Tanaka A, Suen DF, Youle RJ. Parkin is recruited selectively to impaired mitochondria and promotes their autophagy. *The Journal of cell biology*. 2008 Dec 1;183(5):795-803.
245. Narendra DP, Jin SM, Tanaka A, Suen DF, Gautier CA, Shen J, et al. PINK1 is selectively stabilized on impaired mitochondria to activate Parkin. *PLoS biology*. 2010 Jan;8(1):e1000298.
246. Chan NC, Salazar AM, Pham AH, Sweredoski MJ, Kolawa NJ, Graham RL, et al. Broad activation of the ubiquitin-proteasome system by Parkin is critical for mitophagy. *Human molecular genetics*. 2011 May 1;20(9):1726-37.
247. Tanaka A, Cleland MM, Xu S, Narendra DP, Suen DF, Karbowski M, et al. Proteasome and p97 mediate mitophagy and degradation of mitofusins induced by Parkin. *The Journal of cell biology*. 2010 Dec 27;191(7):1367-80.
248. Gomes LC, Di Benedetto G, Scorrano L. During autophagy mitochondria elongate, are spared from degradation and sustain cell viability. *Nat Cell Biol*. 2011 May;13(5):589-98.
249. Frank S, Gaume B, Bergmann-Leitner ES, Leitner WW, Robert EG, Catez F, et al. The role of dynamin-related protein 1, a mediator of mitochondrial fission, in apoptosis. *Dev Cell*. 2001 Oct;1(4):515-25.
250. Breckenridge DG, Stojanovic M, Marcellus RC, Shore GC. Caspase cleavage product of BAP31 induces mitochondrial fission through endoplasmic reticulum

- calcium signals, enhancing cytochrome c release to the cytosol. *The Journal of cell biology*. 2003 Mar 31;160(7):1115-27.
251. Suen DF, Norris KL, Youle RJ. Mitochondrial dynamics and apoptosis. *Genes Dev*. 2008 Jun 15;22(12):1577-90.
252. Germain M, Mathai JP, McBride HM, Shore GC. Endoplasmic reticulum BIK initiates DRP1-regulated remodelling of mitochondrial cristae during apoptosis. *Embo j*. 2005 Apr 20;24(8):1546-56.
253. Cassidy-Stone A, Chipuk JE, Ingeman E, Song C, Yoo C, Kuwana T, et al. Chemical inhibition of the mitochondrial division dynamin reveals its role in Bax/Bak-dependent mitochondrial outer membrane permeabilization. *Dev Cell*. 2008 Feb;14(2):193-204.
254. Scorrano L. Keeping mitochondria in shape: a matter of life and death. *European journal of clinical investigation*. 2013 Aug;43(8):886-93.
255. Turnbull DM, Rustin P. Genetic and biochemical intricacy shapes mitochondrial cytopathies. *Neurobiology of disease*. 2015 Feb 12.
256. Katsetos CD, Koutzaki S, Melvin JJ. Mitochondrial dysfunction in neuromuscular disorders. *Seminars in pediatric neurology*. 2013 Sep;20(3):202-15.
257. Chen L, Winger AJ, Knowlton AA. Mitochondrial dynamic changes in health and genetic diseases. *Molecular biology reports*. 2014 Nov;41(11):7053-62.
258. Saxton WM, Hollenbeck PJ. The axonal transport of mitochondria. *Journal of cell science*. 2012 May 1;125(Pt 9):2095-104.
259. Cartoni R, Martinou JC. Role of mitofusin 2 mutations in the physiopathology of Charcot-Marie-Tooth disease type 2A. *Experimental neurology*. 2009 Aug;218(2):268-73.
260. Votruba M. Molecular genetic basis of primary inherited optic neuropathies. *Eye (London, England)*. 2004 Nov;18(11):1126-32.
261. Yan MH, Wang X, Zhu X. Mitochondrial defects and oxidative stress in Alzheimer disease and Parkinson disease. *Free radical biology & medicine*. 2013 Sep;62:90-101.
262. Koppenol WH, Bounds PL, Dang CV. Otto Warburg's contributions to current concepts of cancer metabolism. *Nat Rev Cancer*. 2011 May;11(5):325-37.
263. Cantor JR, Sabatini DM. Cancer cell metabolism: one hallmark, many faces. *Cancer discovery*. 2012 Oct;2(10):881-98.
264. DeBerardinis RJ, Lum JJ, Hatzivassiliou G, Thompson CB. The biology of cancer: metabolic reprogramming fuels cell growth and proliferation. *Cell metabolism*. 2008 Jan;7(1):11-20.

265. Al-Mehdi AB, Pastukh VM, Swiger BM, Reed DJ, Patel MR, Bardwell GC, et al. Perinuclear mitochondrial clustering creates an oxidant-rich nuclear domain required for hypoxia-induced transcription. *Science signaling*. 2012 Jul 3;5(231):ra47.
266. Lennon FE, Salgia R. Mitochondrial dynamics: biology and therapy in lung cancer. *Expert opinion on investigational drugs*. 2014 May;23(5):675-92.
267. Chiche J, Rouleau M, Gounon P, Brahimi-Horn MC, Pouyssegur J, Mazure NM. Hypoxic enlarged mitochondria protect cancer cells from apoptotic stimuli. *Journal of cellular physiology*. 2010 Mar;222(3):648-57.
268. Tighe A, Johnson VL, Taylor SS. Truncating APC mutations have dominant effects on proliferation, spindle checkpoint control, survival and chromosome stability. *J Cell Sci*. 2004 Dec 15;117(Pt 26):6339-53.
269. Barth AI, Siemers KA, Nelson WJ. Dissecting interactions between EB1, microtubules and APC in cortical clusters at the plasma membrane. *J Cell Sci*. 2002 Apr 15;115(Pt 8):1583-90.
270. Koutsopoulos OS, Laine D, Osellame L, Chudakov DM, Parton RG, Frazier AE, et al. Human Mitons associate with mitochondria and induce microtubule-dependent remodeling of mitochondrial networks. *Biochim Biophys Acta*. 2010 May;1803(5):564-74.
271. Frederick RL, Shaw JM. Moving mitochondria: establishing distribution of an essential organelle. *Traffic*. 2007 Dec;8(12):1668-75.
272. Hirokawa N, Noda Y, Tanaka Y, Niwa S. Kinesin superfamily motor proteins and intracellular transport. *Nat Rev Mol Cell Biol*. 2009 Oct;10(10):682-96.
273. Hirokawa N, Noda Y. Intracellular transport and kinesin superfamily proteins, KIFs: structure, function, and dynamics. *Physiol Rev*. 2008 Jul;88(3):1089-118.
274. Klopfenstein DR, Vale RD, Rogers SL. Motor protein receptors: moonlighting on other jobs. *Cell*. 2000 Nov 10;103(4):537-40.
275. Wozniak MJ, Bola B, Brownhill K, Yang YC, Levakova V, Allan VJ. Role of kinesin-1 and cytoplasmic dynein in endoplasmic reticulum movement in VERO cells. *J Cell Sci*. 2009 Jun 15;122(Pt 12):1979-89.
276. Nakata T, Hirokawa N. Point mutation of adenosine triphosphate-binding motif generated rigor kinesin that selectively blocks anterograde lysosome membrane transport. *J Cell Biol*. 1995 Nov;131(4):1039-53.
277. Rosa-Ferreira C, Munro S. Arl8 and SKIP act together to link lysosomes to kinesin-1. *Dev Cell*. 2011 Dec 13;21(6):1171-8.
278. Chang J, Lee S, Blackstone C. Protrudin binds atlastins and endoplasmic reticulum-shaping proteins and regulates network formation. *Proc Natl Acad Sci U S A*. 2013 Sep 10;110(37):14954-9.

279. Stauber T, Simpson JC, Pepperkok R, Vernos I. A role for kinesin-2 in COPI-dependent recycling between the ER and the Golgi complex. *Curr Biol*. 2006 Nov 21;16(22):2245-51.
280. Brown CL, Maier KC, Stauber T, Ginkel LM, Wordeman L, Vernos I, et al. Kinesin-2 is a motor for late endosomes and lysosomes. *Traffic*. 2005 Dec;6(12):1114-24.
281. Etienne-Manneville S, Hall A. Cdc42 regulates GSK-3beta and adenomatous polyposis coli to control cell polarity. *Nature*. 2003 Feb 13;421(6924):753-6.
282. Jordan MA, Thrower D, Wilson L. Effects of vinblastine, podophyllotoxin and nocodazole on mitotic spindles. Implications for the role of microtubule dynamics in mitosis. *Journal of cell science*. 1992 Jul;102 (Pt 3):401-16.
283. Coue M, Brenner SL, Spector I, Korn ED. Inhibition of actin polymerization by latrunculin A. *FEBS letters*. 1987 Mar 23;213(2):316-8.
284. Tanaka Y, Kanai Y, Okada Y, Nonaka S, Takeda S, Harada A, et al. Targeted disruption of mouse conventional kinesin heavy chain, kif5B, results in abnormal perinuclear clustering of mitochondria. *Cell*. 1998 Jun 26;93(7):1147-58.
285. Cui H, Dong M, Sadhu DN, Rosenberg DW. Suppression of kinesin expression disrupts adenomatous polyposis coli (APC) localization and affects beta-catenin turnover in young adult mouse colon (YAMC) epithelial cells. *Experimental cell research*. 2002 Oct 15;280(1):12-23.
286. Henthorn KS, Roux MS, Herrera C, Goldstein LS. A role for kinesin heavy chain in controlling vesicle transport into dendrites in *Drosophila*. *Mol Biol Cell*. 2011 Nov;22(21):4038-46.
287. Aoki K, Taketo MM. Adenomatous polyposis coli (APC): a multi-functional tumor suppressor gene. *J Cell Sci*. 2007 Oct 1;120(Pt 19):3327-35.
288. Hanson CA, Miller JR. Non-traditional roles for the Adenomatous Polyposis Coli (APC) tumor suppressor protein. *Gene*. 2005 Nov 21;361:1-12.
289. Caldwell CM, Green RA, Kaplan KB. APC mutations lead to cytokinetic failures in vitro and tetraploid genotypes in Min mice. *J Cell Biol*. 2007 Sep 24;178(7):1109-20.
290. Um JW, Min DS, Rhim H, Kim J, Paik SR, Chung KC. Parkin ubiquitinates and promotes the degradation of RanBP2. *The Journal of biological chemistry*. 2006 Feb 10;281(6):3595-603.
291. Pouligiannis G, McIntyre RE, Dimitriadi M, Apps JR, Wilson CH, Ichimura K, et al. PARK2 deletions occur frequently in sporadic colorectal cancer and accelerate adenoma development in Apc mutant mice. *Proc Natl Acad Sci U S A*. 2010 Aug 24;107(34):15145-50.
292. Prevarskaya N, Skryma R, Shuba Y. Calcium in tumour metastasis: new roles for known actors. *Nat Rev Cancer*. 2011 Aug;11(8):609-18.

293. Hanahan D, Weinberg RA. The hallmarks of cancer. *Cell*. 2000 Jan 7;100(1):57-70.
294. Pate KT, Stringari C, Sprowl-Tanio S, Wang K, TeSlaa T, Hoverter NP, et al. Wnt signaling directs a metabolic program of glycolysis and angiogenesis in colon cancer. *EMBO J*. 2014 Jul 1;33(13):1454-73.
295. Zheng J. Energy metabolism of cancer: Glycolysis versus oxidative phosphorylation (Review). *Oncology letters*. 2012 Dec;4(6):1151-7.
296. Roderick HL, Cook SJ. Ca²⁺ signalling checkpoints in cancer: remodelling Ca²⁺ for cancer cell proliferation and survival. *Nat Rev Cancer*. 2008 May;8(5):361-75.
297. Whitfield JF. Calcium, calcium-sensing receptor and colon cancer. *Cancer letters*. 2009 Mar 8;275(1):9-16.
298. Togo T. Ca(2+) regulates the subcellular localization of adenomatous polyposis coli tumor suppressor protein. *Biochem Biophys Res Commun*. 2009 Oct 9;388(1):12-6.
299. Liu W, Shen SM, Zhao XY, Chen GQ. Targeted genes and interacting proteins of hypoxia inducible factor-1. *International journal of biochemistry and molecular biology*. 2012;3(2):165-78.
300. Kuwai T, Kitadai Y, Tanaka S, Onogawa S, Matsutani N, Kaio E, et al. Expression of hypoxia-inducible factor-1alpha is associated with tumor vascularization in human colorectal carcinoma. *International journal of cancer Journal international du cancer*. 2003 Jun 10;105(2):176-81.
301. Myant KB, Cammareri P, McGhee EJ, Ridgway RA, Huels DJ, Cordero JB, et al. ROS production and NF-kappaB activation triggered by RAC1 facilitate WNT-driven intestinal stem cell proliferation and colorectal cancer initiation. *Cell stem cell*. 2013 Jun 6;12(6):761-73.
302. Yoon JC, Ng A, Kim BH, Bianco A, Xavier RJ, Elledge SJ. Wnt signaling regulates mitochondrial physiology and insulin sensitivity. *Genes Dev*. 2010 Jul 15;24(14):1507-18.
303. Meijering E, Dzyubachyk O, Smal I. Methods for cell and particle tracking. *Methods Enzymol*. 2012;504:183-200.
304. Ally S, Larson AG, Barlan K, Rice SE, Gelfand VI. Opposite-polarity motors activate one another to trigger cargo transport in live cells. *J Cell Biol*. 2009 Dec 28;187(7):1071-82.
305. Holthuis JC, Ungermann C. Cellular microcompartments constitute general suborganellar functional units in cells. *Biological chemistry*. 2013 Feb;394(2):151-61.
306. Guzun R, Kaambre T, Bagur R, Grichine A, Usson Y, Varikmaa M, et al. Modular organization of cardiac energy metabolism: energy conversion, transfer and feedback regulation. *Acta physiologica*. 2015 Jan;213(1):84-106.

307. Matsuda S, Nakanishi A, Minami A, Wada Y, Kitagishi Y. Functions and characteristics of PINK1 and Parkin in cancer. *Frontiers in bioscience*. 2015;20:491-501.
308. Fardini Y, Dehennaut V, Lefebvre T, Issad T. O-GlcNAcylation: A New Cancer Hallmark? *Frontiers in endocrinology*. 2013;4:99.
309. Mi W, Gu Y, Han C, Liu H, Fan Q, Zhang X, et al. O-GlcNAcylation is a novel regulator of lung and colon cancer malignancy. *Biochim Biophys Acta*. 2011 Apr;1812(4):514-9.
310. Yang YR, Jang HJ, Yoon S, Lee YH, Nam D, Kim IS, et al. OGA heterozygosity suppresses intestinal tumorigenesis in *Apc(min/+)* mice. *Oncogenesis*. 2014;3:e109.
311. Park MK, Ashby MC, Erdemli G, Petersen OH, Tepikin AV. Perinuclear, perigranular and sub-plasmalemmal mitochondria have distinct functions in the regulation of cellular calcium transport. *EMBO J*. 2001 Apr 17;20(8):1863-74.
312. Liu C, Hermann TE. Characterization of ionomycin as a calcium ionophore. *J Biol Chem*. 1978 Sep 10;253(17):5892-4.
313. MacLeod RJ, Hayes M, Pacheco I. Wnt5a secretion stimulated by the extracellular calcium-sensing receptor inhibits defective Wnt signaling in colon cancer cells. *American journal of physiology Gastrointestinal and liver physiology*. 2007 Jul;293(1):G403-11.
314. Ying J, Li H, Yu J, Ng KM, Poon FF, Wong SC, et al. WNT5A exhibits tumor-suppressive activity through antagonizing the Wnt/beta-catenin signaling, and is frequently methylated in colorectal cancer. *Clinical cancer research : an official journal of the American Association for Cancer Research*. 2008 Jan 1;14(1):55-61.
315. Brakeman JS, Gu SH, Wang XB, Dolin G, Baraban JM. Neuronal localization of the Adenomatous polyposis coli tumor suppressor protein. *Neuroscience*. 1999;91(2):661-72.
316. Bhat RV, Baraban JM, Johnson RC, Eipper BA, Mains RE. High levels of expression of the tumor suppressor gene APC during development of the rat central nervous system. *J Neurosci*. 1994 May;14(5 Pt 2):3059-71.
317. Lang J, Maeda Y, Bannerman P, Xu J, Horiuchi M, Pleasure D, et al. Adenomatous polyposis coli regulates oligodendroglial development. *J Neurosci*. 2013 Feb 13;33(7):3113-30.
318. Fancy SP, Baranzini SE, Zhao C, Yuk DI, Irvine KA, Kaing S, et al. Dysregulation of the Wnt pathway inhibits timely myelination and remyelination in the mammalian CNS. *Genes Dev*. 2009 Jul 1;23(13):1571-85.
319. Imura T, Wang X, Noda T, Sofroniew MV, Fushiki S. Adenomatous polyposis coli is essential for both neuronal differentiation and maintenance of adult neural stem cells in subventricular zone and hippocampus. *Stem cells*. 2010 Nov;28(11):2053-64.

320. Yokota Y, Kim WY, Chen Y, Wang X, Stanco A, Komuro Y, et al. The adenomatous polyposis coli protein is an essential regulator of radial glial polarity and construction of the cerebral cortex. *Neuron*. 2009 Jan 15;61(1):42-56.
321. Votin V, Nelson WJ, Barth AI. Neurite outgrowth involves adenomatous polyposis coli protein and beta-catenin. *Journal of cell science*. 2005 Dec 15;118(Pt 24):5699-708.
322. Koester MP, Muller O, Pollerberg GE. Adenomatous polyposis coli is differentially distributed in growth cones and modulates their steering. *J Neurosci*. 2007 Nov 14;27(46):12590-600.
323. Steketee MB, Moysidis SN, Weinstein JE, Kreymerman A, Silva JP, Iqbal S, et al. Mitochondrial dynamics regulate growth cone motility, guidance, and neurite growth rate in perinatal retinal ganglion cells in vitro. *Investigative ophthalmology & visual science*. 2012;53(11):7402-11.
324. Arrazola MS, Silva-Alvarez C, Inestrosa NC. How the Wnt signaling pathway protects from neurodegeneration: the mitochondrial scenario. *Frontiers in cellular neuroscience*. 2015;9:166.
325. Harvey A, Gibson T, Lonergan T, Brenner C. Dynamic regulation of mitochondrial function in preimplantation embryos and embryonic stem cells. *Mitochondrion*. 2011 Sep;11(5):829-38.
326. Ishihara N, Nomura M, Jofuku A, Kato H, Suzuki SO, Masuda K, et al. Mitochondrial fission factor Drp1 is essential for embryonic development and synapse formation in mice. *Nature cell biology*. 2009 Aug;11(8):958-66.
327. Alavi MV, Bette S, Schimpf S, Schuettauf F, Schraermeyer U, Wehrl HF, et al. A splice site mutation in the murine *Opa1* gene features pathology of autosomal dominant optic atrophy. *Brain : a journal of neurology*. 2007 Apr;130(Pt 4):1029-42.
328. Chen H, Detmer SA, Ewald AJ, Griffin EE, Fraser SE, Chan DC. Mitofusins Mfn1 and Mfn2 coordinately regulate mitochondrial fusion and are essential for embryonic development. *The Journal of cell biology*. 2003 Jan 20;160(2):189-200.
329. Moser AR, Shoemaker AR, Connelly CS, Clipson L, Gould KA, Luongo C, et al. Homozygosity for the *Min* allele of *Apc* results in disruption of mouse development prior to gastrulation. *Developmental dynamics : an official publication of the American Association of Anatomists*. 1995 Aug;203(4):422-33.
330. Oshima M, Oshima H, Kitagawa K, Kobayashi M, Itakura C, Taketo M. Loss of *Apc* heterozygosity and abnormal tissue building in nascent intestinal polyps in mice carrying a truncated *Apc* gene. *Proc Natl Acad Sci U S A*. 1995 May 9;92(10):4482-6.
331. Yokoyama N, Hayashi N, Seki T, Pante N, Ohba T, Nishii K, et al. A giant nucleopore protein that binds Ran/TC4. *Nature*. 1995 Jul 13;376(6536):184-8.
332. Wu J, Matunis MJ, Kraemer D, Blobel G, Coutavas E. Nup358, a cytoplasmically exposed nucleoporin with peptide repeats, Ran-GTP binding sites, zinc

fingers, a cyclophilin A homologous domain, and a leucine-rich region. *The Journal of biological chemistry*. 1995 Jun 9;270(23):14209-13.

333. Lee MW, Bassiouni R, Sparrow NA, Iketani A, Boohaker RJ, Moskowitz C, et al. The CT20 peptide causes detachment and death of metastatic breast cancer cells by promoting mitochondrial aggregation and cytoskeletal disruption. *Cell Death Dis*. 2014;5:e1249.

334. Zhou H, Zhang B, Zheng J, Yu M, Zhou T, Zhao K, et al. The inhibition of migration and invasion of cancer cells by graphene via the impairment of mitochondrial respiration. *Biomaterials*. 2014 Feb;35(5):1597-607.